

NO-A191 867

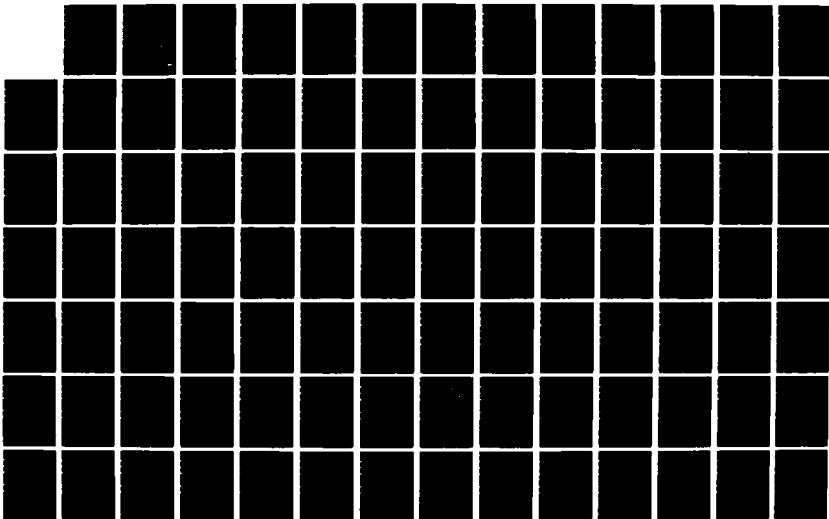
WORKING GROUP ON ICE FORCES; STATE-OF-THE-ART REPORT
(3RD)(U) COLD REGIONS RESEARCH AND ENGINEERING LAB
HANOVER NH T J SANDERSON SEP 87 CRREL-87-17

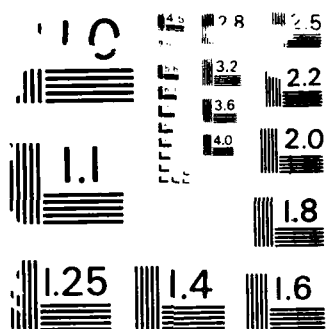
1/3

UNCLASSIFIED

F/G 8/12

NL





RESOLUTION TEST CHART
NATIONAL BUREAU OF STANDARDS-1963-A

Special Report 87-17

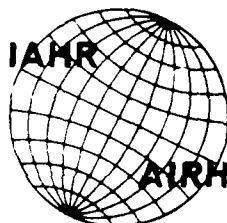
September 1987

DTIC FILE COPY

WORKING GROUP ON ICE FORCES

3rd State-of-the-Art Report
T.J.O. Sanderson, Editor

AD-A191 067



DTIC
ELECTE
FEB 01 1988
S H D

Prepared by
INTERNATIONAL ASSOCIATION FOR HYDRAULIC RESEARCH
WORKING GROUP ON ICE FORCES

Published by
U.S. ARMY COLD REGIONS RESEARCH AND ENGINEERING LABORATORY
HANOVER, NEW HAMPSHIRE



Approved for public release; distribution is unlimited.

88 1 27 173

Unclassified

SECURITY CLASSIFICATION OF THIS PAGE

REPORT DOCUMENTATION PAGE

Form Approved
OMB No. 0704-0188
Exp. Date Jun 30 1986

1a REPORT SECURITY CLASSIFICATION Unclassified			1b RESTRICTIVE MARKINGS AD-A191067	
2a SECURITY CLASSIFICATION AUTHORITY			3 DISTRIBUTION / AVAILABILITY OF REPORT Approved for public release; distribution is unlimited.	
2b DECLASSIFICATION / DOWNGRADING SCHEDULE			5 MONITORING ORGANIZATION REPORT NUMBER(S) Special Report 87-17	
4 PERFORMING ORGANIZATION REPORT NUMBER(S)			7a NAME OF MONITORING ORGANIZATION U.S. Army Cold Regions Research and Engineering Laboratory	
6a NAME OF PERFORMING ORGANIZATION Int'l. Assoc. for Hydraulic Research Working Group on Ice Forces		6b OFFICE SYMBOL (if applicable)	7b ADDRESS (City, State, and ZIP Code) 72 Lyme Road Hanover, New Hampshire 03755-1290	
6c ADDRESS (City, State, and ZIP Code)		9 PROCUREMENT INSTRUMENT IDENTIFICATION NUMBER		
8a NAME OF FUNDING / SPONSORING ORGANIZATION		8b OFFICE SYMBOL (if applicable)	10. SOURCE OF FUNDING NUMBERS	
8c ADDRESS (City, State, and ZIP Code)		PROGRAM ELEMENT NO.	PROJECT NO.	TASK NO.
		WORK UNIT ACCESSION NO.		
11 TITLE (Include Security Classification) Working Group on Ice Forces, 3rd State-of-the-Art Report				
12 PERSONAL AUTHOR(S) T.J.O. Sanderson, Editor				
13a TYPE OF REPORT		13b TIME COVERED FROM _____ TO _____	14 DATE OF REPORT (Year, Month, Day) September 1987	15 PAGE COUNT 232
16 SUPPLEMENTARY NOTATION				
17 COSATI CODES			18 SUBJECT TERMS (Continue on reverse if necessary and identify by block number)	
FIELD	GROUP	SUB-GROUP	Force (mechanics) Structures	
			Ice Underwater structures	
			Sea ice Waterfront structures	
19 ABSTRACT (Continue on reverse if necessary and identify by block number) This working group report on ice forces includes individual papers which discuss laboratory results, field measurements, instrumentation, numerical analysis, and iceberg scour. Researchers and design engineers will find this state-of-the-art report very helpful in their future work. This report should become an excellent textbook for those students who are either taking or are interested in a course in ice engineering. A more detailed abstract appears at the beginning of each individual paper.				
20 DISTRIBUTION / AVAILABILITY OF ABSTRACT <input checked="" type="checkbox"/> UNCLASSIFIED UNLIMITED <input type="checkbox"/> SAME AS RPT <input type="checkbox"/> DTIC USERS			21 ABSTRACT SECURITY CLASSIFICATION Unclassified	
22a NAME OF RESPONSIBLE INDIVIDUAL Guenther Frankenstein			22b TELEPHONE (Include Area Code) 603-646-4100	22c OFFICE SYMBOL CECRL-EI

IAHR WORKING GROUP ON ICE FORCES

3RD STATE OF THE ART REPORT ON ICE FORCES

PREFACE

The present working group on ice forces was formed in Hamburg at the last IAHR Symposium on Ice Problems, in August, 1984. It has the following members:

Ian Jordaan	(Canada)
Mauri Määttänen	(Finland)
Don Nevel	(USA)
Timothy Sanderson	(UK) - Chairman
Dev Sodhi	(USA)
Gary Timco	(Canada)
René Tinawi	(Canada)
Vitoon Vivatrat	(USA)
Egon Wessels	(West Germany)

Our principal responsibility has been to prepare a 3rd "State-of-the-Art" Report on Ice Forces. In the following pages this is presented.

We have tried wherever possible to make these review papers rather more than simply an enumeration and summary of all the papers ever written on a topic. After all, what is most valuable from each of the specialists contributing to this report, is a selective view from them of what is right, what is wrong; what is good, what is poor. As leading specialists in their individual disciplines they should be best placed to communicate to the rest of the ice community what the current state of play is in their own field: where the work is leading, which blind alleys have been followed on the way, and which avenues look most fruitful for the future. If any of us have, in so doing, given undue prominence to our own work, I apologise on our behalf.

This year's report contains contributions on a wide range of topics. Sodhi and Timco have provided contributions describing ice-structure

interaction processes, based largely on the latest advances in model ice tank experimentation. This includes a review of interaction with multiple-legged structures. A theoretical treatment of ice failure processes is given by Hallam, who assesses the status of fracture-mechanical descriptions and their ability to explain the observed behaviour of ice. In doing this she draws on a range of literature from the field of rock mechanics, which is important to ice mechanics but perhaps not as well known to us as it should be. Jordaan reviews, for the first time I believe, the status of numerical and finite-element modelling techniques as applied to ice. On the more practical side, Croasdale and Frederking review field techniques for ice force measurement. A review of iceberg impact forces is given by Nevel, and a treatment of iceberg scouring processes by Chari and Barrie. Finally, I myself have contributed a compilation of all the ice indentation data I know of, putting it onto one single (and rather crowded) pressure-area curve. Pressure-area curves have been produced at various stages during the last 5-6 years, but there now exists a wide range of important data which is no longer proprietary, and this is plotted for the first time.

I very much regret that we have been unable to include a paper from Danielewicz, Blanchet and Metge, describing the two first Hans Island research programmes. During these important programmes, full-scale forces during impact of multi-year floes were directly measured. We had hoped to include the first public release of these data in this volume, but in the event we were unable to secure industry authorisation for early release of the data from the 1981 programme. Nonetheless, the results of the 1980 programme are now available publically (Danielewicz and Metge, 1981, APOA Report No. 180), and I urge all of you who are not already familiar with it to refer to it. Because I feel that these data are so important to our understanding of full-scale interaction processes, I am taking the liberty of including with this preface a brief summary of the essential data from the 1980 Hans Island research programme.



n For	
NTIS	<input checked="" type="checkbox"/>
DTIC TAB	<input type="checkbox"/>
Unannounced	<input type="checkbox"/>
Justification	
By	
Distribution/	
Availability Codes	
Dist	Avail and/or Special
A-1	


TABLE: SUMMARY OF RESULTS FROM THE 1980 HANS ISLAND PROGRAMME

The accelerations were measured using theodolites, and probably represent averages over about 50 seconds. The impact process was correspondingly slow, lasting up to 10 minutes. Error in pressure calculations is of the order 50-100%.

Event	Floe Thickness (m)	Mass (kg) Effective	Initial Velocity (m/s)	Max. Force (MN)	Contact Area (m ²)	Average Pressure (MPa)	Remarks
A	5.6	1.7×10^{11}	0.39	214	1520	0.14	
B	5.6	1.7×10^{11}	0.26	48	930	0.05	Mean Force Only
C	5.6	1.7×10^{11}	0.11	18	400	0.05	Mean Force Only
D	4.2	8.7×10^{11}	0.28	8	800	0.01	Rotten first-year floe

To emphasise that these data should only be used with a full understanding of the circumstances under which they were collected, which may be obtained from the full report on the project. The data from the 1980 Hans Island programme, which used more sophisticated data-gathering techniques, should become available after July, 1987.

In conclusion, I hope that our report is of use to you, and I look forward to the next IAHR Symposium on Ice, in 1988.

Yours faithfully,


E. L. SANDERSON

cc: 100

See also: "Ice on Ice Forces, 1984-86"

100-100-100

REFERENCE

Danielewicz, B.W. and Metge, M. 1981. Ice Forces on Hans Island, August 1980. *AF A Project No. 180*. Available from:

Pallister Resource Management Ltd.,
105, 416 64th Avenue SE,
Calgary, Alberta, Canada T2C 2B3.

CONTENTS

	<u>Page</u>
Abstract	i
Preface	iii
 THE ROLE OF FRACTURE IN LIMITING ICE FORCES	
Abstract	1
Introduction	2
Fracture under uniform stress states	3
Uniaxial tensile fracture	3
Uniaxial compressive failure	6
Indentation fracture	16
In-plane crushing failure	17
Out-of-plane indentation failure	19
Fracture scaling laws	27
The creep fracture transition	28
Conclusions and recommendations	29
Acknowledgments	30
References	30
 ICE FORCES ON MULTI-LEGGED STRUCTURES	
Abstract	35
Introduction	36
General considerations	36
The interaction scenario	40
Design ice loads on the structure	42
Horizontal loads due to ductile indentation	42
Ice buckling	43
Dynamic ice forces	45
Vertical forces due to changes in water level	46
Prototype studies	47
Summary	49
Acknowledgments	49
References	49
 FLEXURAL AND BUCKLING FAILURE OF FLOATING ICE SHEETS AGAINST STRUCTURES	
Abstract	53
Introduction	54
Bending of floating ice sheets	54
Bending failure	59
Discrete element method	60
Sloping structure	61
Conical structures	62
Buckling of floating ice sheets	64
Experimental studies	65
Creep buckling of floating ice sheets	68
Summary	69
References	70

A PRESSURE-AREA CURVE FOR ICE	
Abstract	75
Introduction	76
Indentation Geometry	76
Data: I - Full thickness indentation	77
Laboratory tests	77
Medium-scale tests	80
Full-scale tests	80
Meso-scale models	80
Data: II - Triaxial indentation	81
Icebreakers and impact hammer	81
Discussion: Aspect ratio or scale	81
Theoretical basis for scale effects	84
Flaws	84
Non-simultaneous failure - size effect	88
Non-simultaneous failure - aspect ratio effect	90
Conclusions and recommendations	91
Acknowledgments	94
References	95
ICE SCOUR SURVEYS, STATISTICS AND FORCES	
Abstract	99
Introduction	100
Relict and recent scours	100
Mechanics of scouring	103
Scour environments and features	109
Scour rates, seabed dynamics and degradation	110
Observations of scouring events and ongoing research	111
Summary	112
Acknowledgments	112
References	114
NUMERICAL AND FINITE ELEMENT TECHNIQUES IN CALCULATION OF ICE-STRUCTURE INTERACTION	
Abstract	119
Introduction	120
Relevant ice mechanics	121
Salient aspects of ice mechanics	121
Creep and the role of plasticity theory	122
Higher strain rates and complex states of stress	125
Crushing and the shear damage process	133
Behaviour of pulverized ice	135
Behaviour of large scale ice masses	138
Numerical modelling: A critical review	139
Motivation and approach	139
Elasticity and maximum stress approaches	141
Numerical modelling of creep processes	141
Global fracture analysis	144
Damage and pulverization of ice	144
Flow of pulverized ice	146
Discrete element analysis	146
Large scale models	147
Statistical aspects	147
Conclusion	147

References	148
Appendix I: Organizations active in numerical modelling of ice masses under stress	155
FIELD TECHNIQUES FOR ICE FORCE MEASUREMENTS	
Introduction	157
Overview of methods of approach	158
In situ methods	159
General	159
Theory of ice stress sensors	161
Types and history of ice stress sensors	163
Ice strain meters	165
In situ sensors - performance data	166
In situ sensors - case histories	168
In situ sensors - comments on installation and removal	169
In situ ice sensors - the future	172
Ice forces from floe motions	172
Loads on structures	172
General	172
Ice load case studies	176
Loads on structures - comments	182
Conclusions	183
References	183
ICEBERG IMPACT FORCES	
Abstract	197
Introduction	198
Impact failure modes	198
Strength theories	199
Brittle crushing failure of ice	200
Drop ball test	203
Viscous theory	205
Comparison of theories	209
Analysis of an iceberg impacting a structure	211
Statistical analysis	214
Design criteria	215
Conclusions and recommendations	216
References	217

THE ROLE OF FRACTURE IN
LIMITING ICE FORCES

Sheila D. Hallam
Production Engineer

BP Petroleum Development Ltd., England
Britannic House, Moor Lane,
London. EC2Y 9BU

ABSTRACT

The force exerted by moving ice on an offshore Arctic structure is frequently described by a creep solution such as the reference stress method (Ponter et Al, 1983). This work is often extrapolated to higher strain rates and lower temperature regimes where the creep load bearing capacity of the material is never reached because fracture limits the ice load bearing capacity. This paper considers the ideally elastic fracture limits to ice forces and discusses how they may relate to the maximum pressures found at the transition from ductile to brittle failure.

The brittle fracture of ice under multi-axial stress conditions is considered in terms of the nucleation and propagation of cracks. Crack nucleation was found to dominate tensile failures and crack propagation to dominate compressive fracture for the grain sizes found in sea ice.

Indentation fracture mechanisms of crushing, spalling, and radial and circumferential cracking are examined. Local loads were found to be dominated by changes in the failure mechanism whereas the global load depends on circumferential flexural fractures.

Peak loads on structures will occur at the transition from creep to brittle behaviour. The relationship between this maximum and the brittle strength are discussed for nucleation and propagation controlled failures.

1. INTRODUCTION

The force exerted by ice on a structure is frequently described by a creep solution such as the reference stress method (Porter and others, 1989). The problem with using this type of approach for predicting ice loads on offshore structures is that there is no maximum load - the faster the ice moves the higher the force. Fortunately, there is another mode of failure, that of fracture, which does limit the maximum force on the structure. This maximum is illustrated by a collection of some of the available data on the strength of pure ice at small scale as a function of the strain rate (Fig. 1).

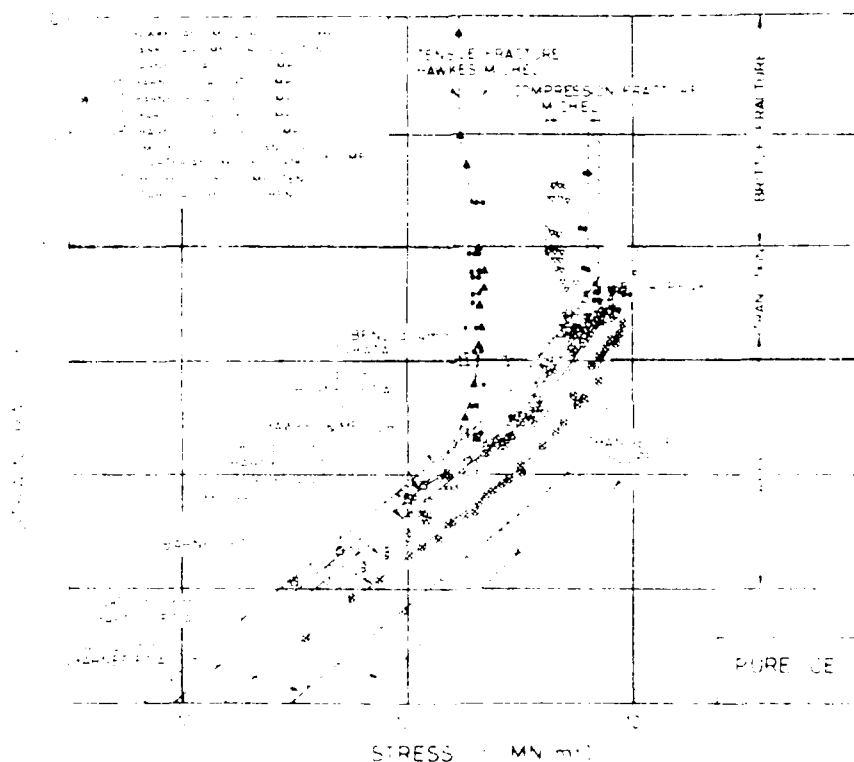


FIGURE 1. Stress-strain-rate data for pure ice at different frequencies.

The peak strength of ice occurs at the transition from creep to brittle fracture. Investigating the physics of the transition peak is difficult because it involves both fracture and creep theory. The easiest approach is to understand the truly brittle behaviour of the ice out of the transition zone, and then to study the relationship between the peak and the brittle strength.

The fracture strength of ice is very scale dependent (Sanderson, 1986). This has been attributed to factors such as geometric scaling of flaws, flaw size distributions, non-simultaneous failure and fracture mechanisms. Some of these (geometric scaling, flaw size distributions, non-simultaneous failure) are discussed in Sanderson (1986) and so will not be dealt with in detail here. Different fracture mechanisms and their associated loads are investigated and their relationship with scale effects discussed.

2. FRACTURE UNDER UNIFORM STRESS STATES

2.1 Uniaxial Tensile Fracture

Fracture in tension occurs because of the presence of flaws. For an uncracked sample of ice there are two necessary conditions for tensile fracture:

- (1) **crack nucleation** - the formation of a crack or cracks.
- (2) **crack propagation** - the stress must be sufficiently high to cause a crack to extend.

If the crack propagation stress is exceeded before the crack nucleation stress then failure is governed by the stress to nucleate a crack and the failure is very brittle. If, on the other hand, the stress to nucleate cracks occurs before the stress to propagate them, the failed ice will contain many cracks and will appear to show some ductility which is due entirely to the reduction in stiffness caused by crack nucleation. Final failure in this case is governed by the crack propagation stress.

In the case of ice with pre-existing flaws it is only the second condition that is necessary and the failure will be very brittle.

2.1.1 Crack Nucleation

Laboratory ice specimens are usually constructed very carefully such that they contain no initial flaws. This may also be the situation in the field where flaws will tend to heal and blunt in time. In these cases the nucleation condition is important.

Crack nucleation is believed to result from stress concentrations due to dislocation pile up at grain boundaries. Sinha (1982) has related crack nucleation to a critical value of the delayed elastic strain. If this is the case, then at very high strain rates and low temperatures the stress to nucleate the cracks is unlimited (Sinderson and Child, 1986). The high strain rate tensile data of Hawkes and Mellor (1972) and Michel (1978) clearly show that there is a limit to the tensile strength and this implies that cracks do indeed nucleate at high strain rates. Seng-Kiong and Shyam Sander (1985) propose an alternative crack nucleation criterion which is in close agreement to Sinha's except at high strain rates. They attribute crack nucleation to a critical tensile strain, ϵ_{nT} . So in uniaxial tension at high strain rates:

$$\epsilon_{nT} = \frac{\sigma_{nT}}{E} \quad (1)$$

where σ_{nT} is the crack nucleation tensile stress and E is Young's modulus.

Schulson and others (1964) and Lee and Schulson (1966) have conducted extensive tensile tests on ice of various grain sizes. Their results for brittle strain rates (greater than 10^{-2} /s) are presented in Fig. 2 and show a dependence on the grain size, d . The closed symbols refer to crack nucleation stresses and the open symbols to crack propagation stresses. This dependency on grain size has been questioned in the literature (Sinha, 1983) but Schulson (1984) defends these results. Indeed if we consult a classic fracture book such as Lawn and Wilshaw (1975) this classic grain size dependence in crack nucleation is normal. Including this grain size dependence into the critical strain approach gives:

$$\sigma_{nT} = \sigma_0 + \frac{\sigma_1}{\sqrt{d}} \quad (\text{or } \epsilon_{nT} = \epsilon_0 + \frac{\epsilon_1}{\sqrt{d}}) \quad (2)$$

From the tensile data at the highest strain rates we find these constants to be:

$$\sigma_0 = 5.7 \times 10^{-1} \text{ Pa}, \quad \sigma_1 = 4.6 \times 10^{-1} \text{ Pa} \cdot \text{m}^{1/2}$$

$$\epsilon_0 = 0.51 \times 10^{-3}, \quad \epsilon_1 = 0.63 \times 10^{-3} \text{ m}^{1/2} \quad (\text{where } E = 2.1 \times 10^9 \text{ Pa})$$

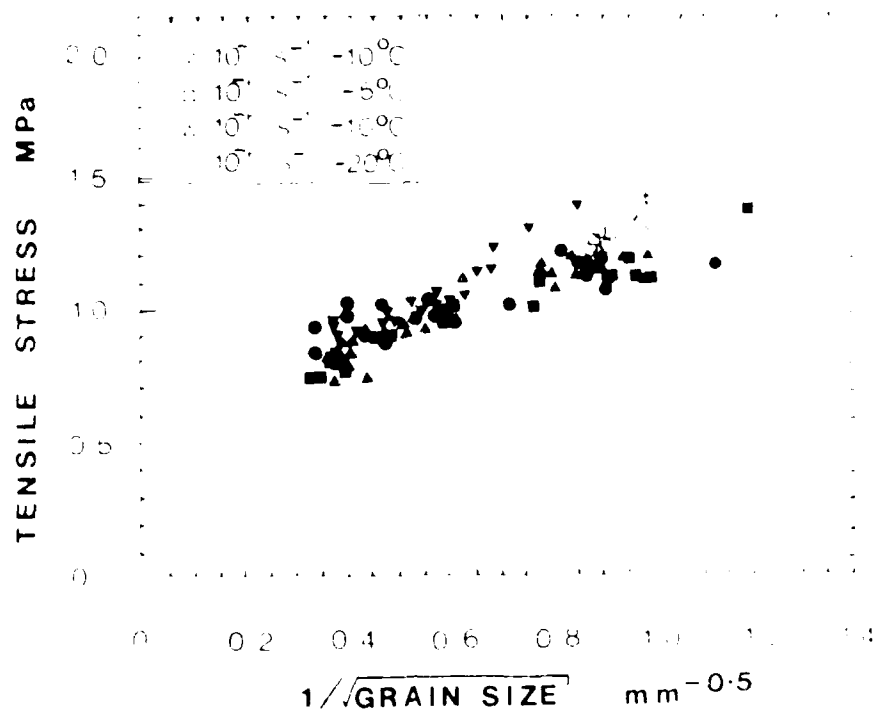


FIGURE 2 High Strain-Rate Tensile Crack Nucleation (filled symbols) and Propagation (open symbols) Stress Data as a function of Grain Size.

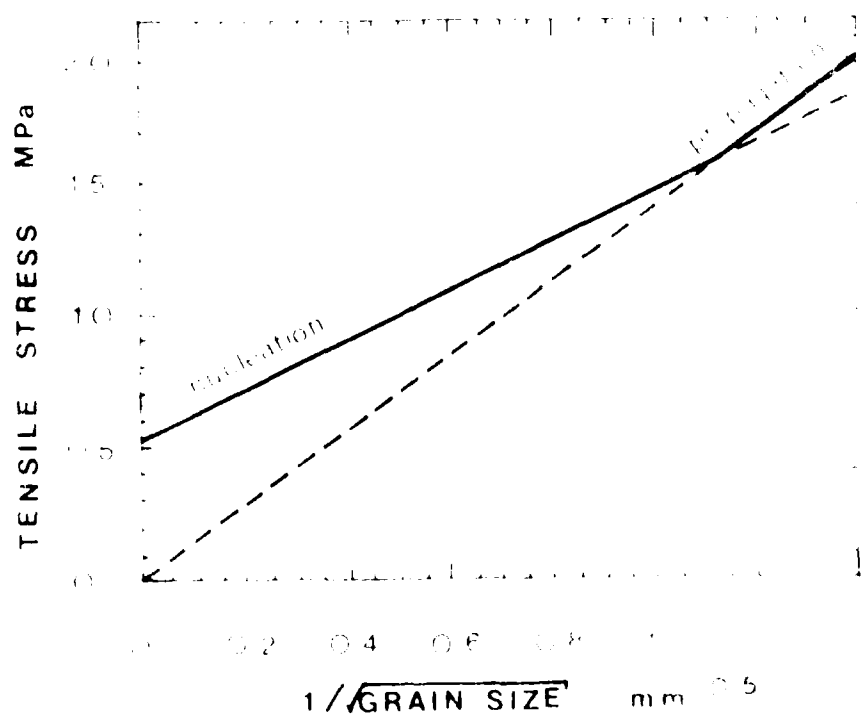


FIGURE 3 Propagated Crack Nucleation and Propagation as a function of the Grain Size.

2.1.2 Crack Propagation From an Existing Flaw

The propagation from flaws is now well understood (see, for example, Knott, 1973). The result for the propagation of a crack of length $2a$ orientated perpendicular to a uniform tensile stress σ_T is

$$\sigma_T = K_{IC} / \sqrt{\pi a} \quad (3)$$

where K_{IC} is the material property called fracture toughness which, for ice, is approximately $0.115 \text{ MPa } \sqrt{\text{m}}$. A more general form of the tensile fracture stress would be:

$$\sigma_T = Y K_{IC} / \sqrt{\pi a} \cdot f(\vartheta) \quad (4)$$

where Y is a function of the geometry of the loaded sample and $f(\vartheta)$ is a function of the crack orientation. For a material containing a population of cracks the failure will occur at the weakest link, that is, the flaw at which the fracture stress σ_T (Equation 4) is the lowest.

In the case where cracks have nucleated in the manner described previously, the length of the cracks is related to the grain size (Schulson and others 1984, and open symbols Fig. 2) giving the simple tensile crack propagation criterion:

$$\sigma_T = 0.044 / \sqrt{d} \quad \text{MPa} \quad (5)$$

The proposed tensile crack nucleation and propagation stresses (Equations 3 and 5) as a function of grain size are presented in Fig. 3.

2.2 Uniaxial Compressive Failure

Uniaxial compressive fracture can be considered in a similar way to the tensile fracture criterion. The necessary conditions for brittle fracture in an uncracked sample in compression are:

- (1) **crack nucleation** - similar to the tensile process
- (2) **crack propagation to failure** - the extension of a crack in uniaxial compression is stable and thus increasing loads are

required to make a crack extend. A crack must extend until it reaches free surfaces or until it interacts with other cracks, producing an instability.

Depending on the relative stress levels required to nucleate and extend a flaw, different types of fracture will occur that are analogous to the brittle and pseudo-ductile failures observed in tension. When pre-existing flaws are present, they need only satisfy condition (2).

2.2.1 Crack Nucleation

Compressive crack nucleation stresses at high strain rates have not been studied in detail. The onset of crack nucleation is seen as a small yield point on the stress-strain curve but its position becomes less well defined at higher strain rates (see for example Mellor and Cole, 1982). If we follow the critical tensile stress hypothesis of Seng-Kiong and Shyam Sunder (1985), cracks will form when the lateral tensile strain induced by the Poisson expansion reaches the critical level defined in Equation (2). Thus, with Poisson's ratio $\nu = 0.3$,

$$\epsilon_{nc} = \frac{\nu \sigma_{nc}}{E} = 5.7 \times 10^{-5} + \frac{3.33 \times 10^{-6}}{\sqrt{d}}$$

$$\text{or } \sigma_{nc} = 1.39 + \frac{0.082}{\sqrt{d}} \quad \text{MPa} \quad (6)$$

According to this, the stress required to nucleate a crack in compression is approximately three times that in tension in the brittle regime. It is reassuring to compare this with the apparent maximum stress to form the first crack observed in creep tests by Gold and reproduced in Sinha (1982). For columnar ice of grain size 4.5 mm the limiting stress to first cracks at high strain rates is approximately 2 MPa compared with 2.6 MPa predicted by equation (6). The low value of the initiation stress may be because of the crystal structure or because of the method of defining grain size.

2.2.2 Crack Propagation and Linkage

The stress to propagate a crack in compression is substantially higher than that in tension and the cracks will normally nucleate long before

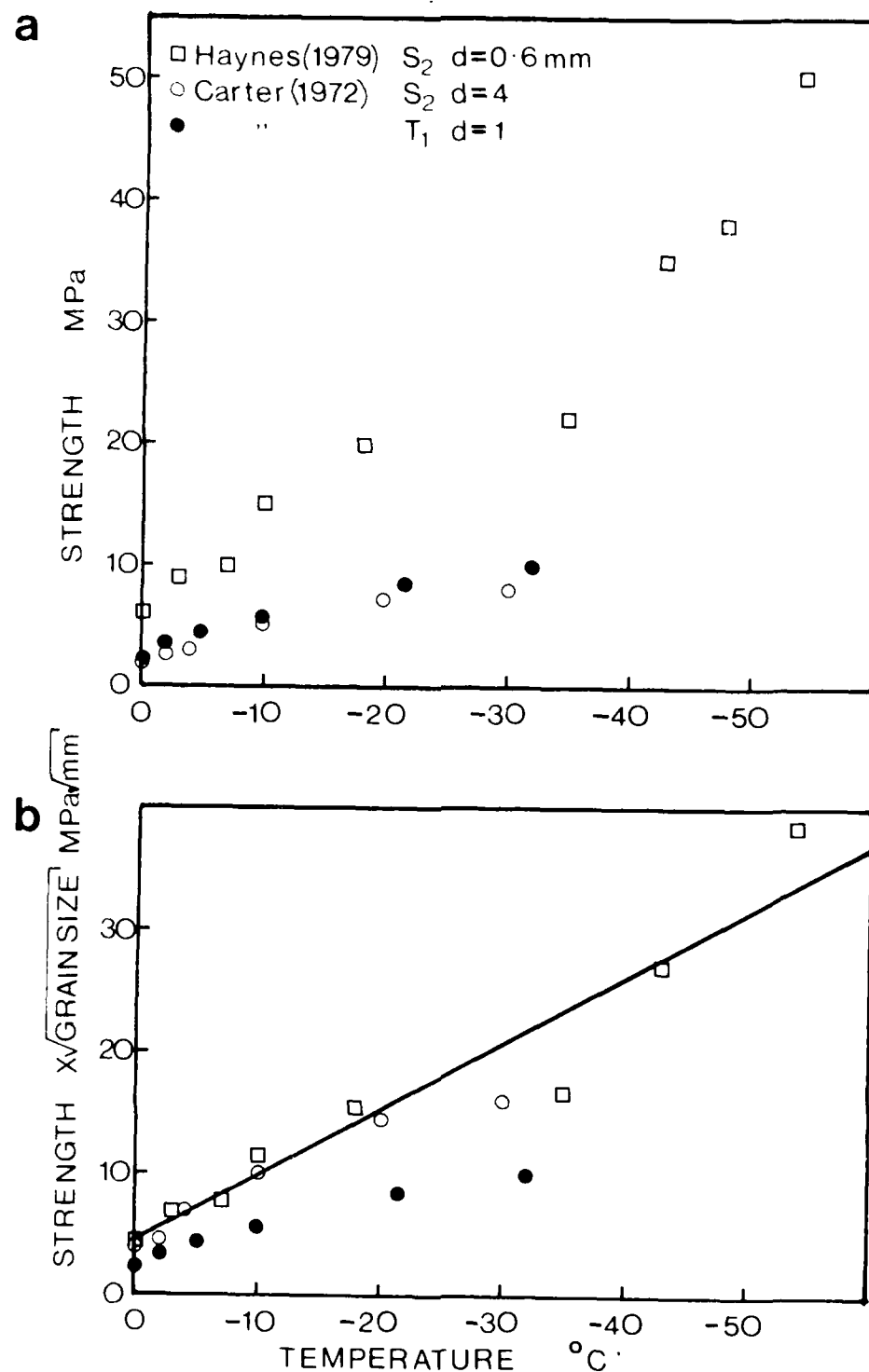


FIGURE 4 (a) with Compressive Fracture Strength Data as a Function of Temperature and
 (b) with Strength Normalised by the Inverse Square Root of Grain Size.

final failure in compression. Fig. 4a shows a summary of the compressive stress data for strain rates exceeding $10^{-2}/s$ plotted against temperature. The data are highly temperature sensitive although they are insensitive to strain rate (Fig. 1). Fig. 4b shows the same data normalised by $d^{-0.5}$. This brings the columnar data into very close agreement. This poses the following empirical equation for compressive fracture propagation:

$$\sigma_c = \frac{(\sigma_o - A\theta)}{\sqrt{d}} \quad (7)$$

where $\sigma_o = 0.14 \text{ MPa}$
 $A = 0.017$
 $\theta = \text{Temperature } (^{\circ}\text{C})$
 $d = \text{grain size (m)}$

The equations for compressive crack nucleation and propagation are plotted in Fig. 5. In the compressive case it is crack extension rather than crack nucleation which governs compressive fracture except at exceptionally large grain sizes and at temperatures close to 0°C .

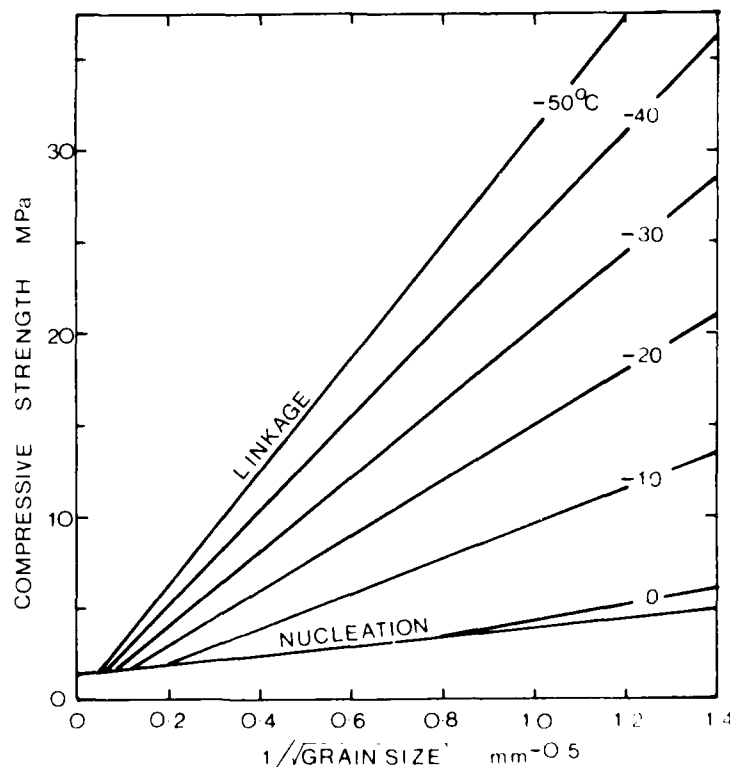


FIGURE 5 *Proposed Compressive Brittle Fracture Nucleation and Linkage Conditions at Various Temperatures as a Function of the Grain Size.*

[illegible]

the same way, the β phase is stable only at low lateral tension, γ , and is unstable at high lateral tension. However, the stability of the β phase is not affected by the lateral interaction of a population of lipid molecules that is not affected numerically by Kerut-Nasser

and Horii (1985) and analytically using damage mechanics in Ashby and Ballarín (1986). In Cooksley (1985) a very simple assumption was made for crack interaction based on the observations of experiments and this leads to a very simple compressive failure criterion

$$\frac{\sigma_c}{\sigma_{IC}} = \frac{(1+L^*)^{3/2}}{(1-L) \left[\frac{L^*}{4.33} + \frac{0.58}{(1+L^*)^2} \right]} \quad (9)$$

where L^* is the critical normalised crack extension which for a wide variety of rocks is approximately 0.5. Assuming that the cracks that nucleate in compression are the same size as those that nucleate in tension the left hand side of equation (9) is equivalent to the ratio of the compressive stress to the tensile crack propagation stress. Thus substituting from Equation 5:

$$\sigma_c = \frac{f(L^*) \times 0.044}{(1-L) \sqrt{d}}$$

$$\text{where } f(L^*) = \frac{(1+L^*)^{3/2}}{\left[\frac{L^*}{4.33} + \frac{0.58}{(1+L^*)^2} \right]} \quad (10)$$

which effectively normalises the compressive strengths by the square root of grain size. If we now compare the theoretical Equation (9) with the empirical Equation (6) we see that:

$$f(L^*) / (1-L) = 3.18 - 0.39 \mu \quad (11)$$

and thus we are drawn to the conclusion that the origin of the temperature dependency lies in the variation of the internal static coefficient of ice, μ , with temperature. If we assume that the friction coefficient is zero at -100°C (which seems entirely reasonable) then a friction of 0.86 would be necessary to explain the strength at -20°C . Making this assumption gives an empirical equation for μ :

$$f(L^*) = 3.18 \quad (\text{implies } L^* = 0.52) \quad \text{and} \quad \mu = \frac{-0.39}{3.18 - 0.39 \mu} \quad (12)$$

2.3 Multiaxial Compressive Failure

The fracture criterion can now be extended to the general stress state.

2.3.1 Crack Nucleation

This criterion can be extended to the general multi-axial stress state.

$$\epsilon_n = \sigma_3 / E - \nu \sigma_2 / E - \nu \sigma_1 / E \quad (13)$$

where σ_1 , σ_2 and σ_3 are the minimum intermediate and maximum principal tensile stresses and ϵ_n is the critical tensile strain (Equation (2)). The crack nucleation surfaces are illustrated for two common stress states in Fig. 7.

2.3.2 Crack Propagation

If a crack is subjected to confining pressure in addition to the principal compressive stress this severely inhibits crack growth. The modified version of equation (3) to account for confining pressure is

$$\frac{-\sigma_1 \sqrt{\pi a}}{K_{IC}} = \frac{(1+L)^{3/2}}{[1-\lambda-\mu(1+\lambda) - \frac{4.33}{\lambda L}] \left[\frac{L}{4.33} + \frac{0.58}{(1+L)^{1/2}} \right]} \quad (14)$$

where σ_3 is the confining pressure or the least compressive stress and λ is the ratio σ_3/σ_1 . The corresponding crack interaction equation is obtained by substituting $L = L^*$. Using the tensile crack propagation equation 5 and the empirical equations (12) gives:

$$-\sigma_1 = \sqrt{d} \frac{0.044 \times 3.18}{\{1-\lambda-\mu(1+\lambda)-2.25\lambda\}} \quad (15)$$

$$\text{where } \mu = \frac{-0.39 \theta}{3.18 - 0.39 \theta}$$

This is only valid when cracks are 'closed' under compressive normal loading and the stress to propagate a crack is more than the stress to initiate a crack ($L^*=0$). The full solution involving open cracks involves a numerical step (Cooksley, 1984) but an approximation to the

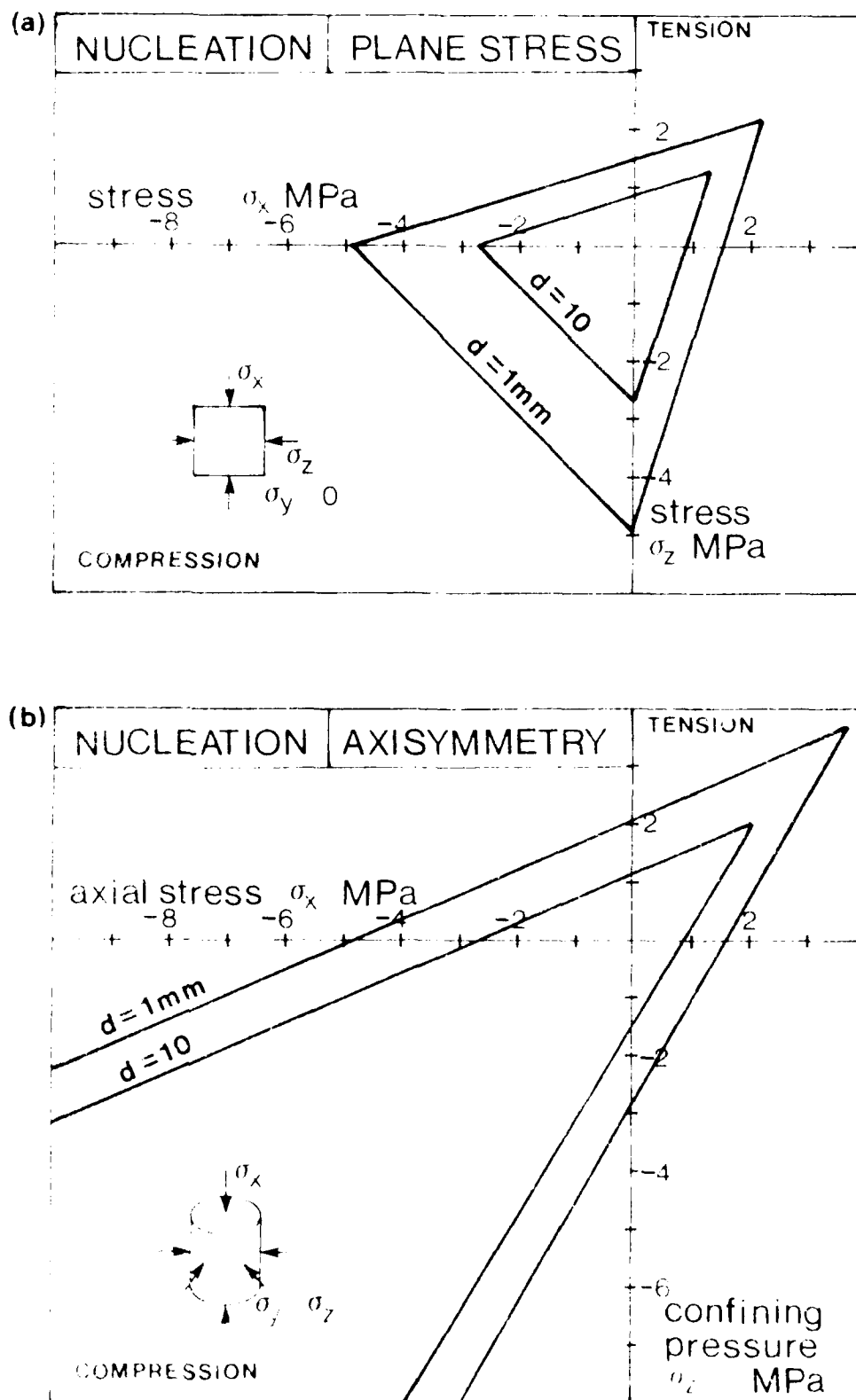


FIGURE 7 Proposed Crack Nucleation Regions for
 (a) Plane Stress and
 (b) Axisymmetry.

solution is to truncate the fracture propagation surface with the fracture initiation surface:

$$\sigma_1 = \sqrt{d} \frac{0.0759}{(1-\lambda-\mu(1+\lambda))} \quad (16)$$

where initiation refers to the formation of the wing cracks. This surface in turn is truncated by the tensile propagation controlled fracture surface:

$$\sigma_3 = 0.044 / \sqrt{d} \quad (17)$$

Examples of fracture propagation surfaces normalised by $d^{-0.5}$ and temperatures of 0° , -10° and -30°C are shown in Fig. 8 for plane stress and axisymmetric loading.

2.3.3 Post Failure Strength

After the ice has fractured in compression, the crushed ice can still carry load. This is perhaps best modelled by a Mohr-Coulomb frictional solution (Fransson and Sandkvist, 1985). The Mohr-Coulomb failure criterion can be expressed by:

$$\frac{\sigma_1 + S}{\sigma_3 + S} = f = \frac{1 + \sin\phi}{1 - \sin\phi} \quad (18)$$

where $S = c \cot \phi$

c and ϕ are the cohesive strength and the friction angle. Fransson and Sandkvist found that for fine ice the cohesive strength was so small that, for our purposes, it can be considered negligible and that $\phi = 14^\circ$. This gives:

$$\frac{\sigma_1}{\sigma_3} = f = 1.6 \quad (19)$$

It is likely that this value will increase with decreasing temperature.

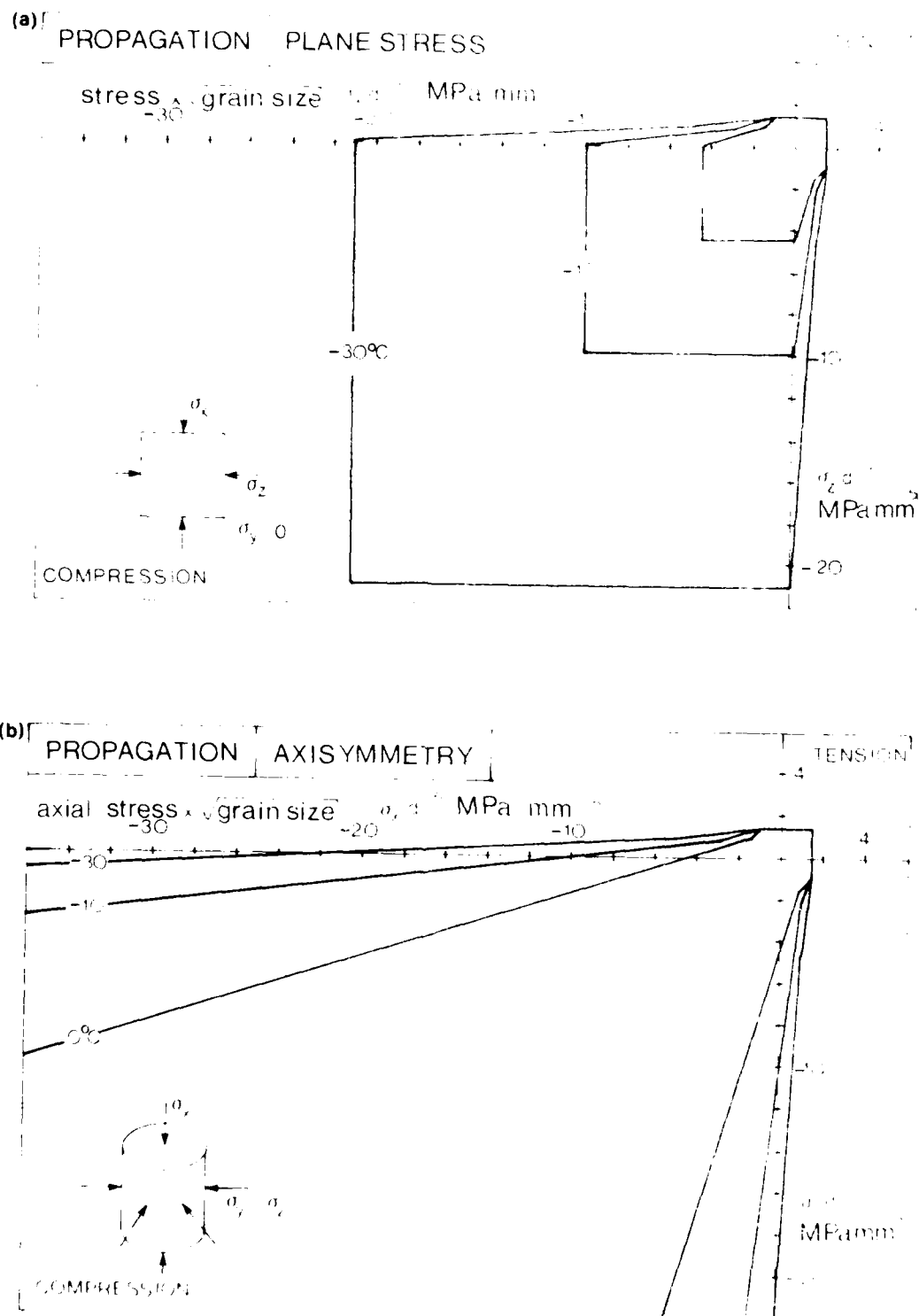


FIGURE 8 Proposed Crack Propagation Surfaces for
 (a) Plane Stress and
 (b) Axisymmetry.

3. INDENTATION FRACTURE

Two distinct types of indentation can be identified.

- I **2-dimensional indentation** - (Fig. 9a) in which indentation occurs over the full thickness of the ice sheet and the stress is biaxial.
- II **3-dimensional indentation** - (Fig. 9b) in which a limited extent of the thickness is indented. In this case the stress state is triaxial.

The first type is important in defining the global or total load on a structure and the second in defining the panel or local load.

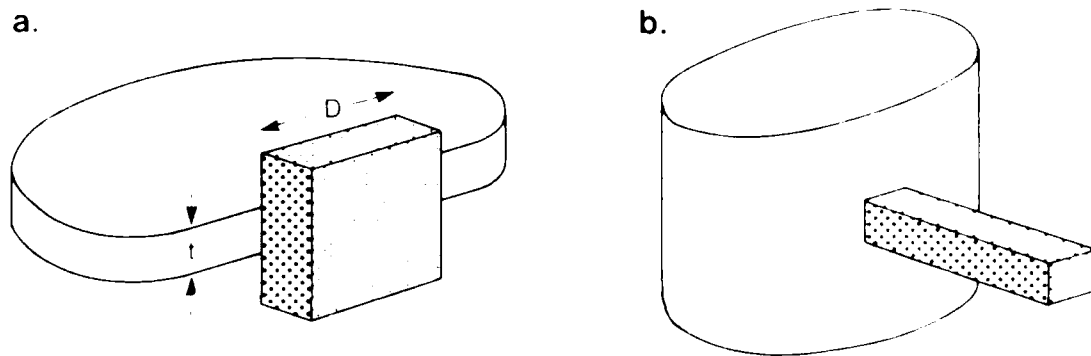


FIGURE 9 *Classification of Indentation*
(a) Type I, 2-Dimensional Indentation
(b) Type II, 3-Dimensional Indentation.

The failure of ice can also be divided into two broad categories:

- A **In-plane failure** - where the ice once fractured is not cleared from under the indenter.
- B **Out-of-plane failure** - where the ice sheet may deform or rotate out of the plane of the ice sheet.

In plane failure is likely to be dominant when failure is over areas small compared with the ice thickness. Out of plane failures can occur at larger ratios of contact width to ice thickness.

3.1 In-Plane Crushing Failure

There are many pieces of work dealing with an elastic/plastic indentation, but, in the case of ice, an increase in velocity will correspond to an increase in the yield strength. Perhaps the only truly brittle approach is of the type proposed by Ladanyi (1967). He considers the expansion of a cylinder and a sphere in an elastic/brittle material which can be used to give the solution to the type I and type II indentation problem. Fig. 10 illustrates the analysis. The zone immediately around the indenter is crushed but can carry load because of its frictional properties (Section 2.3.3). The zone far from the indenter is intact and behaves as an ideal elastic solid. In the absence of radial cracks (Fig. 10b) the extent of the crushed zone depends on the triaxial compressive strength of the material (Ladanyi uses an empirical fracture criterion developed by Fairhurst, 1964). For materials with a low ratio of uniaxial compressive to tensile strength radial cracks may form (Fig. 10a) when the circumferential stress exceeds the tensile strength. The material between the cracks then crushes in uniaxial compression.

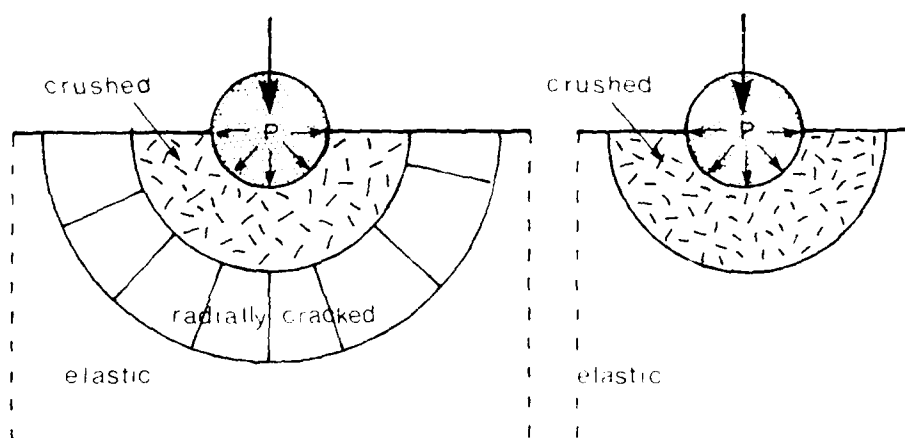


FIGURE 10 *Cavity Expansion Model*
(a) *with Radial Crack Formation*
(b) *without Radial Cracks.*

3.1.1 2-dimensional Indentation

The maximum pressure, P , for expansion of a cylindrical cavity in plane strain from the work of Ladanyi (1967) is:

With radial cracks ($\sigma_c / \sigma_T \geq 4.83$)

$$\frac{P}{\sigma_c} = 1 + \frac{2\sigma_c}{E} [1 + \nu + (1 - \nu) \ln \left(\frac{\sigma_c}{\sigma_T} + \epsilon_{av} \right)]^{-b} \quad (20)$$

where $b = \frac{f-1}{2f}$

Without radial cracks ($\sigma_c / \sigma_T < 4.83$)

$$\frac{P}{\sigma_c G} = 1 + \frac{2(1+\nu)\sigma_c G}{E} \left(\frac{\sigma_c}{\sigma_T} + \epsilon_{av} \right)^{-b} \quad (21)$$

where $b = \frac{f-1}{2f}$

and $G = \frac{1}{n+1} \left[1 - 0.25(n-1) \epsilon_{av}^{\frac{1}{2}} \right]^{\frac{1}{2}}$

Here ϵ_{av} is an average volume strain in the crushed zone during cavity expansion. Due to ignorance ϵ_{av} is normally assumed to be zero.

Fig. 11a shows the theoretical indentation pressure (normalised by the grain size) for 2-dimensional ice indentation using the uniaxial tensile and compressive propagation strengths (Equations 5 and 7) and $f = 1.6$ (Equation 19). The graph predicts an increasing indentation pressure with decreasing temperature with a step change at -1.8°C when the first radial cracks form. The absolute magnitude of the theoretical pressures are very sensitive to the frictional properties of the crushed ice.

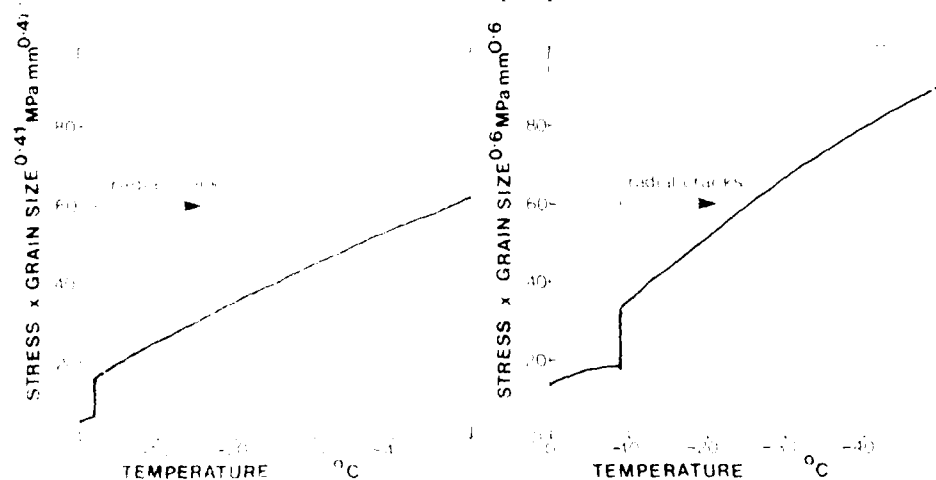


FIGURE 11 Proposed Normalised Indentation Pressures as a Function of Temperature for
(a) 2-dimensional and
(b) 3-dimensional Indentation.

3.1.2 3-Dimensional Indentation

The maximum indentation pressure, P , for this case is:

With radial cracks ($\sigma_c/\sigma_T \approx 6.64$)

$$P = \sigma_c \left(3H + \frac{1}{2} \sigma_{av} \right)^{-a} \quad (22)$$

where $a = 2/3 (1-1/f)$

$$\text{and } H = \frac{(1+\nu)\sigma_T}{E} \left(\frac{\sigma_c}{2\sigma_T} \right)^{1/2} + \frac{\sigma_c}{E} \left[1 + \left(\frac{2\sigma_T}{\sigma_c} \right)^{1/2} \right]$$

Without radial cracks ($\sigma_c/\sigma_T \approx 6.64$)

$$P = \sigma_c \left(3 + \frac{(1+\nu)\sigma_c}{2E} F + \frac{1}{2} \sigma_{av} \right)^{-a} \quad (23)$$

where a is the same as above

$$\text{and } F = \frac{2}{9(m+1)} (m-1+6.1-2/9(m-1))^{1/2}$$

Fig. 11b shows the theoretical 3-dimensional indentation pressures using the appropriate tensile and compressive uniaxial propagation strengths. The graph shows similar trends to the 2-dimensional case with the step change at the formation of radial cracks at -9°C . This is also very sensitive to the frictional properties of the crushed ice.

3.2 Out-of-Plane Indentation Failure

Certain modes of failure such as bending and spalling allow large blocks to move out of the plane of indentation. This has the effect of reducing the real area of ice contact and can lead to non-simultaneous failure (Kry, 1981; Ashby and others, 1986). These out-of-plane failures tend to occur at high D/t (aspect) ratios.

3.2.1 2-Dimensional Indentation

Timco (1986) noted failure modes for all his 2-dimensional indentation tests on laboratory columnar pure ice of grain size 1-3 mm. His results

are presented in Fig. 12 showing the zones of dominance of each failure mechanism as a function of the aspect ratio.

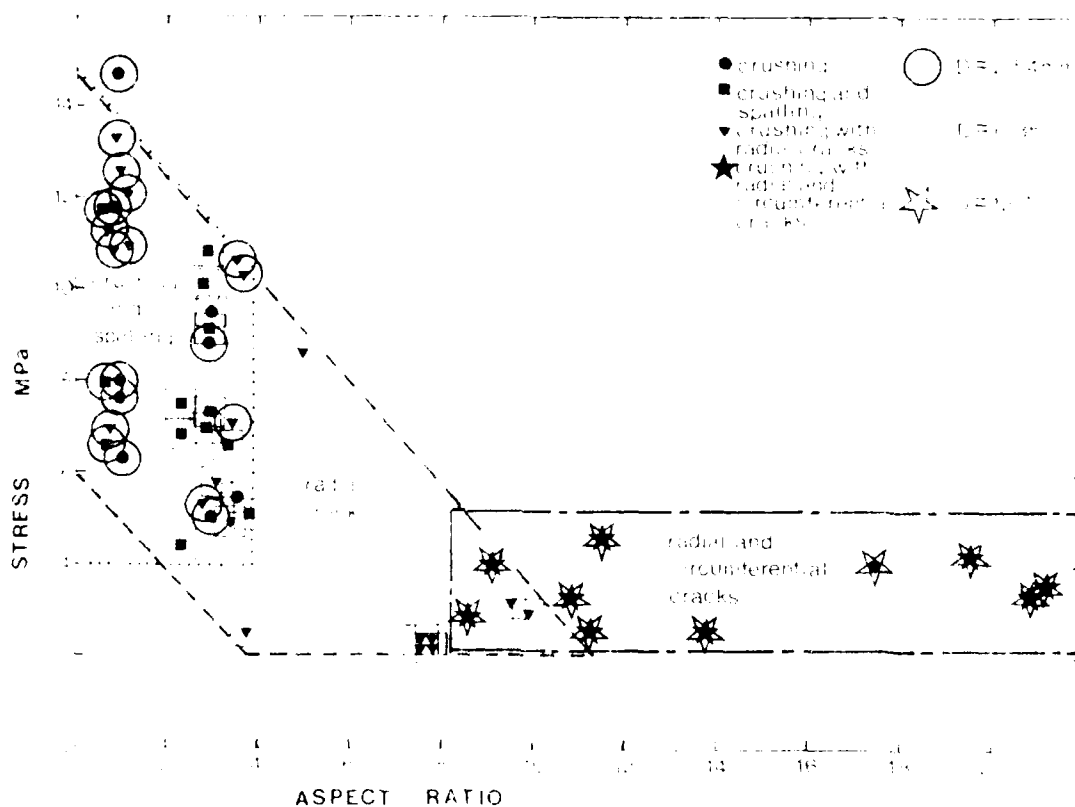


FIGURE 12 *Fracture Mode Identification Data on Pure E_T Ice Showing Regions of Dominance of Each Failure Mechanism.*

Radial Fractures

The formation of radial cracks do not of themselves lead to failure but may provide a precursor to other modes of failure, for example, the bending failure of a finger of ice between two radial cracks. The cracks generally form at very low loads. This problem has been considered by Palmer and others (1982). From their work, the load F to extend a radial crack of length c is:

$$F = \sqrt{\frac{c}{2.13}} \frac{K_{IC}}{b} \quad (24)$$

where K_{IC} is the fracture toughness, and α is a constant taken to be 0.5. Converting this to stress gives:

$$\sigma_r = \sqrt{\frac{c}{2.13}} \frac{K_{IC}}{b} \quad (25)$$

so the larger a structure the easier it is to propagate radial cracks.

Radial and Circumferential Cracks

Once radial cracks have formed, the ice between radial cracks can be analysed as a beam and the stress to cause flexural fracture can be investigated. Wierzbicki (1985) investigated the failure of a beam containing a crack of length a loaded by a force acting at one edge of the ice sheet. He found that the average stress to fracture was:

$$\sigma_f = \frac{K_{IC}}{\sqrt{a} (3Y_m - Y_p)} \quad (26)$$

where $Y_m = 1.99 - 2.47(a/t) + \dots$

and $Y_p = 1.99 - 0.41(a/t) + \dots$

If $a \ll t$ this reduces to $\sigma_f = 0.09 / \sqrt{a}$ MPa (using $K_{IC} = .115$ MPa \sqrt{m} and a is measured in metres).

A more general solution is to assume that the stress acts at an eccentricity e from the centroidal axis yielding a stress

$$\sigma_f = \frac{K_{IC}}{\sqrt{a} (6Y_m e/t - Y_p)} \approx 1.99 \sqrt{a} \frac{0.115}{(6e/t - 1)} \quad (27)$$

An alternative approach is to assume that there is no pre-existing crack but, under the applied bending moment, failure occurs by crack nucleation and that the crack, when initiated, has sufficient energy to propagate right through the ice sheet. Subtracting the average compressive stress from the surface bending tensile stress produced by the bending moment and equating to the crack nucleation condition (Equation 2) gives:

$$\sigma_f = \frac{0.51 + 0.03/\sqrt{d}}{(6e/t - 1)} \quad (28)$$

This approach has the advantage that the presence of pre-existing cracks does not have to be assumed. We have shown that for the typical grain sizes in the field, tensile fracture occurs by crack nucleation and not crack propagation.

A study of the circumferential and radial cracking failure data of Timco (1986) (Fig. 12) shows that the stress for circumferential cracking is

independent of the ice thickness which suggests a characteristic load eccentricity. The ice has an average grain size of 2 mm and a mean stress of 3.4 MPa thus $e/t = 0.22$ giving a general solution:

$$\sigma_f = (0.51 + 0.03/\sqrt{d})/0.32 \quad (29)$$

Fig. 13 compares this theoretical circumferential fracture equation with Timco's data for radial and circumferential fractures and radial fractures only. The circumferential fractures do not occur for the smaller indentors (which coincide with the lowest aspect ratios). This is presumably because the radial cracks have not grown to a sufficient length (Equation 25) to reduce the restraint on the ice plate and allow it to bend as a beam. For the large aspect ratios and large indentors (structures), the fracture strength will be limited by circumferential fractures.

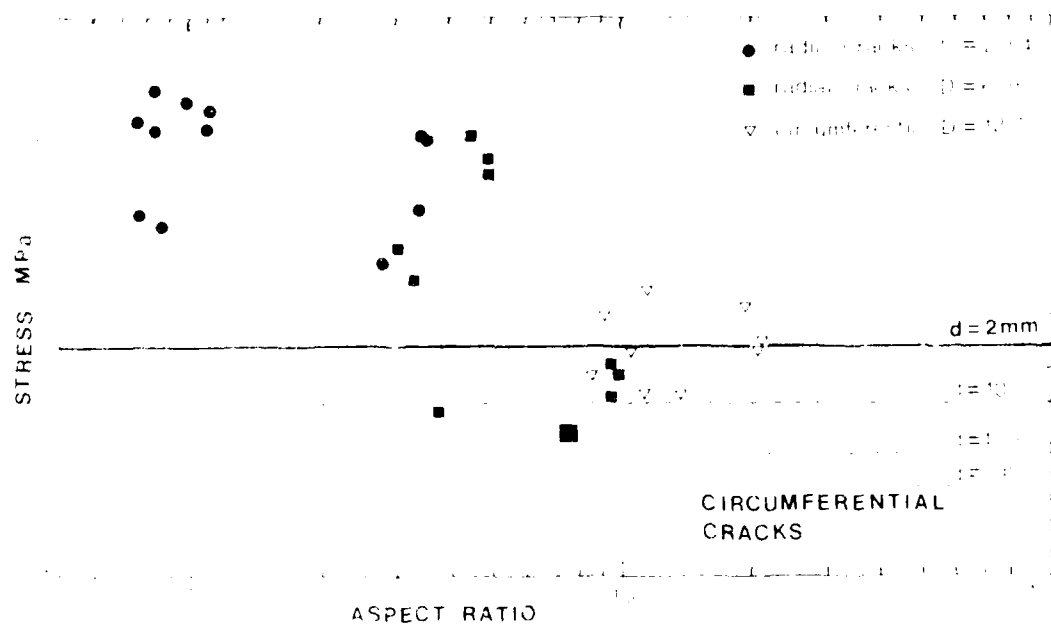


FIGURE 13 Variation of Wall Shear Indentation Fracture Stress With Indentor Diameter. Circumferential Fractures as a Function of Indentor Diameter (Equation 29).

WALL SHEAR FRACTURE

Figure 14 illustrates the process by which a crack grows parallel to the ice surface until it eventually emerges at the surface to remove a chip. Two major stages in the spalling process can be identified:

- (i) the formation of a crack with a length proportional to the ice thickness
- (ii) the extension of that crack to the surface.

The second stage of the problem has been investigated by many authors based on the work by Kendall (1978) and by Evans and others (1986). In both pieces of work, the length of the crack was found to be independent of the thickness of the ice. A drawback with this approach is that a larger force is required to initiate stage (i) than to extend the crack (stage ii). It is therefore preferable to pay attention to the formation of the initial crack.

The stage (i) spall initiation stage has been investigated by Evans and others (1984). They consider cracks being formed along the outer surface of a plastic zone. Although this theory may not be strictly applicable, we can attempt to apply it to the problem of the extension of a spall crack from a crushed zone.

Consider a cylindrical indenter of diameter D applied to a layer of thickness t such that a plastic (or crushed) zone extends to a radius b . Evans and others found that the crack length, c , extending from the zone scaled as

$$c \propto b^{5/4} (Y/K_{IC})^{1/2}$$

where Y is the yield stress for the plastic zone and K_{IC} is the fracture toughness for the brittle problem.

The radius of the plastic (or crushed) zone, b , is proportional to the diameter D^* of the indentation, $b \propto D^*$ (Evans and others 1984). It is assumed that the crack must extend until its length is of the order of the ice thickness, t , before the crack can be considered to have caused a spall (stage ii).

The total force acting when the crack has reached the surface (Evans 1981), therefore at spall formation

$$P_s \propto t^{9/5} \quad (3)$$

As the formation of a spall is controlled by force and not pressure, a spall can form from a local contact of width D^* which may be less than the total indenter diameter D . After the formation of a spall, contact could shift to another point of points leading to a progressive non-simultaneous failure. If only one failure zone (spall) was formed at any moment in time, the maximum stress on the indenter (force over the projected area) would be given by:

$$\sigma_s = Ht^{4/5}/D \quad (32)$$

where H is a constant for ice. This does not correlate well with the data from Timco (1986) shown in Fig. 14. This may be because the indenter is rectangular and not cylindrical.

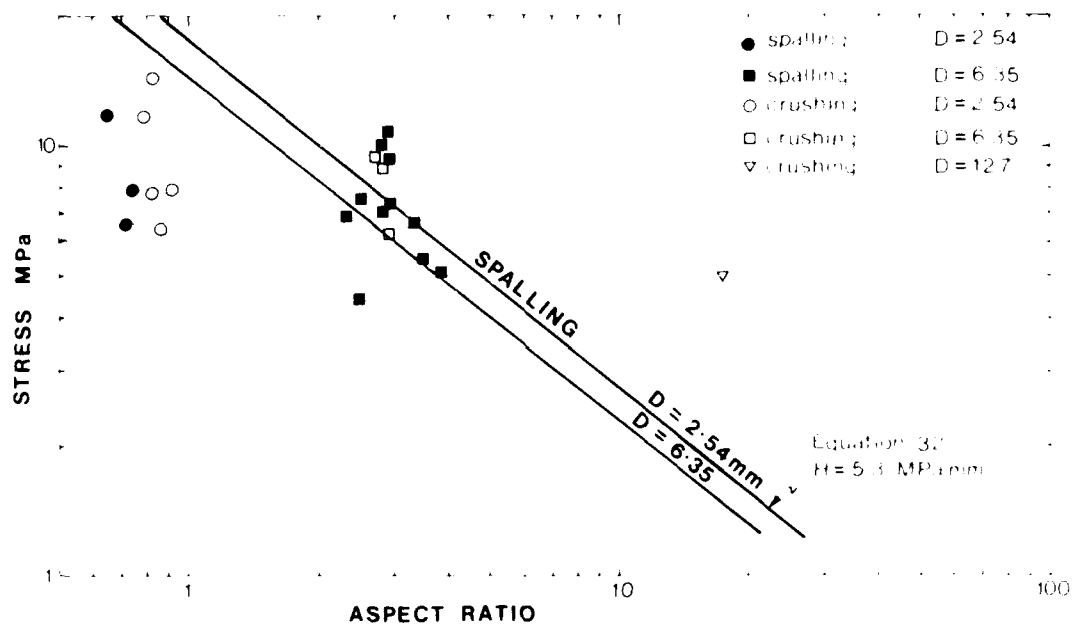


FIGURE 14 Comparison of Small Scale Spalling Indentation Data with Crushing Data and Theoretical Spalling Conditions.

Alternatively, if the indenter was rectangular and of diameter D , the radius b of the crushed zone would depend on the volume of the indent

$$b^2 \propto \delta D \text{ therefore; } c \propto (\delta D)^{5/8} \quad (33)$$

where δ is the distance indented.

Identifying the critical length of crack with the ice thickness implies that, for a given D and t , it is a critical value of δ , the indented

distance, which governs spall formation and the associated stress level is that for crushing. Fig. 14 also shows the crushing data points which occur at essentially the same stress levels as those points where spalling occurred.

Obviously, we can conclude that the understanding of spalling failure and how it may limit ice forces is far from complete, however, the importance of spalling failure on the scale of a structure may not be important as flexural failures are likely to dominate the load.

3.2.2 3-Dimensional Indentation

In this case, the contribution to load reduction that non-simultaneous failure can make is negligible. This is because the fractured ice has great difficulty in clearing from under the indenter. However, in the field, the thickness of the ice may limit the maximum local indentation load. This is because radial cracks could reach the surface of the ice allowing large flakes to spall away. As this process would repeat itself the high indentation crushing pressures would never be developed across the entire ice thickness. The types of radial cracks which may form are summarised below:

Hertzian Cone

This is the classic indentation under a blunt indenter such as a ball in very brittle materials and is summarised in Lawn and Marshall (1984). The first stage is the formation of a ring crack under the indenter which propagates to form a cone shaped crack as illustrated in Fig. 15a. The critical load for cone initiation is

$$F = Ar K_{IC}^2 / E$$

where E is Young's Modulus, A is a dimensionless constant, K_{IC} is the fracture toughness and r is the radius of the sphere. This is not dependent on the starting flaw size. This has aroused much interest because combined with the Hertzian stress relation ($\sigma \propto F/r^2$), it implies a size effect on critical stress level to initiate the cone of $1/r$.

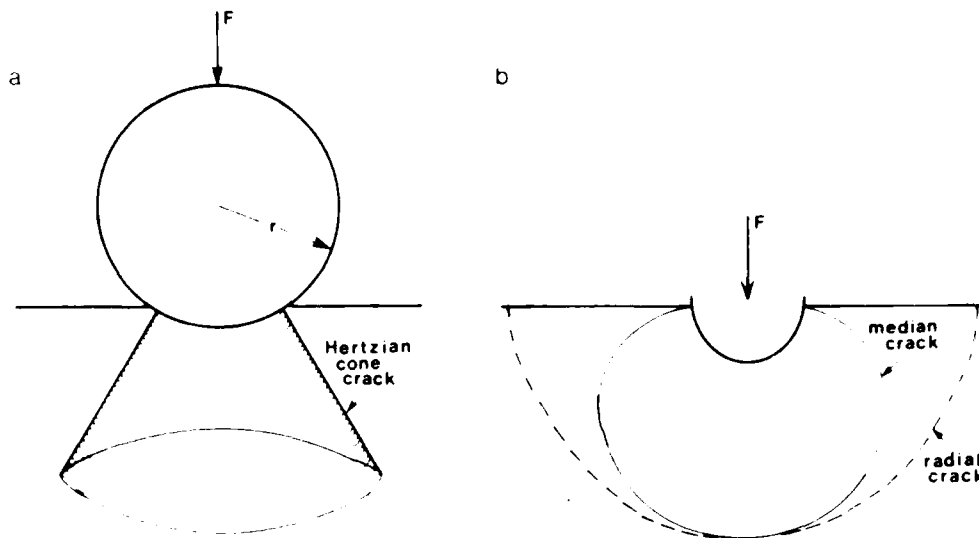


FIGURE 15 *3-Dimensional Indentation Crack Systems*
 (a) *The Hertzian Cone and*
 (b) *The Median/Radial Crack System.*

The growth of the cone crack follows a law of the form

$$F = Bc^{3/2} K_{IC}$$

where c is the crack size and B is a dimensionless constant.

Median and Lateral Cracks

Under sharp indentors and in less brittle materials localised zones of plastic deformation (or crushed zones) occur and a penny shaped crack, called a median crack may form immediately under the indenter tip (Fig. 15b). On unloading this may extend up to the surface to form radial cracks. These are of lesser importance as we are concerned with maximum loads on loading. The median crack grows according to a similar law to the Hertzian cone

$$F = Cc^{3/2} K_{IC}$$

Spalling

In both the above cases there is a crack growth process where

$$F \propto c^{3/2} \tag{34}$$

If we consider these cracks radiating from the indentation to the surface it seems reasonable that when the cracks have extended to some critical multiple of the ice thickness a block will break away and thus limit the load. Thus

$$F_s = Jt^{3/2} \quad (35)$$

where J is a constant. This might reduce the average pressure on an indentation in the same way as the 2-dimensional spalling leading to an average stress for spalling of:

$$p_s = \frac{4Jt}{\pi D^2} \quad (36)$$

where D is the diameter of the indentation. For large contact areas non-simultaneous failure would presumably occur with F_s being the force on a single contact zone.

4. FRACTURE SCALING LAWS

The indentation pressure of ice shows pronounced scale-effects. A substantial amount of the published data is presented in Sanderson (1986) on axes of log pressure against log contact area and log aspect ratio and shows how peak pressures vary as the inverse square root of contact area with some dependence on aspect ratio. The origin of the scale effects is elusive and many suggestions have been offered:

- (i) Statistical effects of flaw distributions
- (ii) Geometric scaling of flaws
- (iii) Non-simultaneous failure
- (iv) Change of fracture mechanisms

The influence of the first three have been discussed in some detail in Sanderson's paper so here we will concentrate on the last point.

At small scale, the pressure area relationship can be reproduced for ice of roughly constant thickness but the origin lies in changes of fracture mechanism induced by increasing the aspect ratio. If a large amount of data is plotted as in Sanderson (1986) these trends of decreasing pressure with aspect ratio can be lost due to the superposition of tests

with a wide variety of ice thicknesses from of order 1 mm to of order 1 m, in which the only upper limit is the crushing strength.

At large scale (and hence large aspect ratios) the radial and circumferential failure should dominate the load. The load for circumferential cracking is independent of ice thickness and probably independent of structure diameter. If we assume a typical grain size perpendicular to the lower surface in the field of 50 mm from Equation (29) the flexural pressure is 2.0 MPa. For very large aspect ratios non-simultaneous failure can occur which reduces the average stress in a statistical fashion. 2 MPa will now be the stress to fail an individual zone, which will fail over the entire ice thickness and over a width related to the spacing of the radial cracks.

5. THE CREEP FRACTURE TRANSITION

All the results so far have looked for the truly brittle solution, that is, when strain rates are sufficiently high that plasticity does not influence the strength. In reality, the stress at the transition from ductile to brittle behaviour may be higher than the brittle fracture stress. This peak is seen in uniaxial compression but not in uniaxial tension (Fig. 1).

In uniaxial tension, failure (depending on grain size) is dependent on the nucleation of cracks. At the moment of nucleation the cracks are sharp and ideal linear elastic fracture mechanics is applicable. In compression cracks nucleate long before failure which is propagation controlled. The creep field will blunt flaws and cause an apparent increase in the fracture toughness, until the ice fails by nett section creep. It seems likely that there is a simple relation between the peak stress and the brittle stress. Carter (1972) showed that its compression peak stress was approximately 1.7 times the brittle strength for a wide range of temperatures.

In other, more complicated, stress states we may postulate that if the fracture is controlled by crack nucleation (such as inflexive) the stress within the creep field has only to exceed the nucleation condition whereas, when propagation controlled (such as in indentation crushing), the stress may need to be increased by a factor of 1.7 to account for the

crack blunting process.

If progress can be made in the understanding of the transition from nett section creep to fracture it will give a simple way to convert a fracture limit to a peak pressure.

6. CONCLUSIONS AND RECOMMENDATIONS

1. The maximum force that can be exerted on a structure is limited by fracture.
2. For the large grain sizes present in sea-ice, tensile failure will be governed by the nucleation of cracks if there are no sharp pre-existing flaws.
3. Compressive Fracture will be limited by crack propagation and linkage except at temperatures close to 0°C.
4. When the failure is dominated by the nucleation of cracks then the maximum pressure occurs when the critical strain condition is exceeded within the creep field.
5. When the failure is dominated by the propagation of cracks then the peak stress will occur at the creep/fracture transition and is likely to be of order 1.7 times the brittle value.
6. Local loads on structures will be dominated by the local crushing problem and its interaction with spalling. This requires substantial investigation.
7. Global loads on structures will be dominated by circumferential (flexural) fractures and, for large aspect ratios, non-simultaneous failure.

7. ACKNOWLEDGMENTS

I thank the British Petroleum Company plc for enabling me to study in this area and permission to publish this work, and the many authors, both mentioned and unmentioned, whose research has formed the basis of this report.

8. REFERENCES

- Ashby, M.F. and Hallam, S.D., 1986. The failure of brittle solids containing small cracks under compressive stress states. *Acta Metallurgica* Vol. 34 (3), p. 497-510.
- Ashby, M.F., Palmer, A.C., Thouless, M., Goodman, D.J., Howard, M., Hallam, S.D., Murrell, S.A.F., Jones, N., Sanderson, T.J.O. and Ponter, A.R.S., 1986. Non-simultaneous failure and ice loads on Arctic structures. *Proceedings of the Offshore Technology Conference, Houston*, 399-404.
- Barnes, P., Tabor, D. and Walker, J.C.F., 1971. The friction and creep of polycrystalline ice. *Proceedings of the Royal Society (London)*, series A vol. 324, p.127-155.
- Carter, D.S., 1972. Brittle fracture of polycrystalline ice under compressive loadings. *Proceedings of the IAHR Ice Symposium Leningrad*, p.62-71.
- Carter, D. and Michel, B., 1971. Lois et mécanismes de l'apparente fracture fragile de la glace de rivière et de lac. *Université Laval, Faculté des Sciences, Département de Génie Civil, Section Mécanique des Glaces, Rapport S-22*.
- Cooksley, S.D., 1984. Yield and fracture surfaces of brittle solids under multi-axial loading. *Ph.D Thesis, Cambridge University Engineering Dept., Cambridge, England*.

- Evans, A.G., Palmer, A.C., Goodman, D.J., Ashby, M.F., Hutchinson, J.W.,
Ponter, A.R.S. and Williams, G.J., 1984. Indentation
spalling of edge-loaded ice sheets. Proceedings of the
IAHR Symposium on Ice, Hamburg.
- Fairhurst, C., 1964. On the validity of the Brazilian test for brittle
materials. International Journal of Rock Mechanics and
Mining Science. Vol. 1, p. 535-546.
- Fransson, L. and Sandkvist, J., 1985. Brash ice shear properties -
laboratory tests. Proceedings of the POAC Conference,
Narssarssuaq, Vol. 1, p. 75-87.
- Hawkes, I. and Mellor, M., 1972. Deformation and fracture of ice under
uniaxial stress. Journal of Glaciology Vol. 11 (61), p.
103-131.
- Kendall, K., 1978. Complexities of compression failure. Proceedings of
the Royal Society London, A. Vol. 361, p. 245-263.
- Kry, P.R., 1981. Scale effects in continuous crushing of ice.
Proceedings of the IAHR Symposium on Ice, Quebec.
- Ladanyi, B., 1967. Expansion of cavities in brittle media.
International Journal of Rock Mechanics and Mining
Science. Vol. 4, p.301-328.
- Lawn, B.R. and Marshall, D.B., 1984. Indentation fractography: a
measure of brittleness. Journal of Research of the National
Bureau of Standards Vol. 89 (6), p. 435-451.
- Lawn R.W. and Wilshaw, T.R., 1975. Fracture of brittle solids. 1st
Edition. Cambridge University Press, Cambridge, Chapter 2.
- Lee, R.W. and Schulson, E.M., 1986. The strength and ductility in ice
under tension. Proceedings of the 5th International
Symposium on Offshore Mechanics and Arctic Engineering,
Tokyo.

- Mellor, M. and Cole, D.M., 1982. Deformation and failure of ice under constant strain-rate. Cold Regions Science and Technology Vol. 5, p.201-219.
- Michel, B., 1978. The strength of polycrystalline ice. Canadian Journal of Civil Engineering Vol. 5 (3), p.286-300.
- Nemat-Nasser, S., and Horii, H., 1982. Compression induced non-planar crack extension with application to splitting, exfoliation and rockburst. Journal of Geophysical Research Vol. 87 (B8), p.6805-6821.
- Newman, J.C., Jr. and Raju, I.S., 1981. An empirical stress intensity factor equation for surface cracks. Engineering Fracture Mechanics Vol. 15, p.185-192.
- Palmer, A.C., Goodman, D.J., Ashby, M.F., Evans, A.G., Hutchinson, J.W. and Ponter, A.R.S., 1983. Fracture and its role in determining ice forces on offshore structures. Annals of Glaciology Vo. 4, p.216-221.
- Sanderson, T.J.O., 1986. A pressure-area curve for ice. Proceedings of the 8th International Symposium on Ice, IAHR, Iowa City, 1986, (this volume).
- Sanderson, T.J.O. and Child, A.J., 1986. Ice loads on offshore structures: The transition from creep to fracture. Cold Regions Science and Technology Vol. 12, p.157-161.
- Schulson, E.M., 1984. Does the strength of ice depend on grain size at high temperatures? Scripta Metallurgica Vol. 18, p.1439-1440.
- Schulson, E.M., and Cannon, N.P., 1984. The effect of grain size on the compressive strength of Ice. Preceedings of the IAHR Symposium on Ice, Hamburg, Vol. 1, p.29-38.

- Schulson, E.M., Lim, P.N. and Lee, R.W., 1984. A brittle to ductile transition in ice under tension. *Philosophical Magazine*, A Vol. 49 (3), p.353-363.
- Seng-Kiong, and Shyman Sunder, S., 1985. Constitutive modelling of sea ice with applications to indentation problems. Massachusetts Institute of Technology, Centre For Scientific Excellence In Offshore Engineering Report No. 3, Department of Civil Engineering Research Report No. R85-15.
- Sih, G.C.M., 1973. Handbook of stress intensity factors for research workers and engineers. Institute of Fracture and Solid Mechanics, Leigh University, Bethelhem, Pennsylvania.
- Sinha, N.K., 1982. Delayed elastic strain criteria for first cracks in ice. Symposium on the Deformation and Failure of Granular Materials, International Union of Theoretical & Applied Mechanics, Delft, p. 323-330.
- Sinha, N.K., 1983. Does the strength of ice depend on grain size at high temperatures? *Scripta Metallurgica* Vol. 17, 1269-1273.
- Timco, G.W., 1986. Indentation and penetration of edge-loaded freshwater ice sheets in the brittle range. Proceedings of the 5th International Symposium on Offshore Mechanics and Arctic Engineering, Tokyo.
- Thouless, M.D. Evans, A.G. and Ashby, M.F., 1985. Edge spalling of brittle plates. Cambridge University Engineering Department, Cambridge.
- Wierzbicki, T., 1985. Spalling and buckling of ice sheets. Civil Engineering in the Arctic Offshore, Proceedings of the Conference, Arctic '85, San Fransisco, p.953-961.

ICE FORCES ON MULTI-LEGGED STRUCTURES

G. W. Timco
Associate Research Officer

National Research Council Canada
of Canada

The determination of the forces which an ice sheet can exert on a multi-legged structure has received very little attention. This, in spite of the importance of these types of structures as docks and drilling platforms (both fixed and floating). In this paper, the types and origins of these forces are reviewed. This is done by assuming a typical platform design and determining both the total horizontal and vertical forces due to moving ice. The results of model tests are reviewed to give insight into the interaction and influence of the multiple legs on the total force on the structure. Finally, a brief annotated listing is given of the reported results of ice interacting with full scale platforms and bridge piers.

1.0 Introduction

The interaction of ice with rigid structures is a complex phenomenon in which many factors are involved. Depending on the geometry and interaction rate, any one or combination of failure modes can occur for the ice, and this governs the load on the structure. In general, the magnitude of the load depends upon the size and geometry of the structure, size and geometry of the ice features, mechanical properties of the ice, the rate of movement between the ice and the structure, rigidity of the structure, failure mode induced in the ice, environmental driving forces, degree of continuity between the ice and the structure, and inertial effects in both ice and structure. Because of this complexity, predictions of the ice loads on even the most simple-shaped structure is difficult. For a multi-legged structure, such as a drilling platform, semi-submersible, bridge pier, dock or wharf, information on ice loads is scarce. This is in spite of their importance and use in the ice-infested waters. For this type of structure it is necessary to know both the total load on the whole structure, and the loads (both in magnitude and direction) on each leg of the structure. If the legs are spaced widely apart, each may be considered as a single isolated pile and treated accordingly. However, if the legs are close together, interference effects may occur which would influence both the load on the structure and the failure mode of the ice. As such, in trying to design the optimum spacing of the legs of a multi-legged structure for strength and economy, information on both the magnitude and direction of the loads, ice failure modes and ice piece sizes are required. To date, there has been very little reported for this on full scale (prototype) structures.

In this review paper, the ice loads on multi-legged structures are reviewed. This is done in a rather unconventional way by choosing a nominal multi-legged structure design and ice conditions, and calculating various ice loads on the structure. To gain some insight into the interference effects on the ice loads and ice failure conditions, the results of model tests with multi-legged structures are briefly reviewed. Finally, a brief annotated review is given from the published literature on the ice loads on full-scale structures.

2.0 General Considerations

In order to calculate the ice loads on a structure, it is necessary to predict the failure mode of the ice. This is not always possible and several

failure mechanisms must be considered. When there are two or more competing ones, the lowest calculated ice force is usually the correct one since the ice should fail with this failure mode. To date, there has been very little information published on the ice loads (either measured or calculated) for multi-legged platforms. Because of this, the ice loads on this type of structure cannot be predicted with a high degree of confidence. In general, the approach in calculating the loads on a multi-legged structure has been to treat it as if it were composed of a number of individual piles subjected to ice loading. The loads on each leg are calculated in turn using the formulations developed in ice engineering for the situation of a single isolated pile in ice. Then, the total load on the whole structure is determined by simply summing the loads on each leg assuming some scenario of spatial and temporal variation of load on each leg. At the present time, the validity or correctness of this approach is not known. One major uncertainty in this area is to decide a priori in the treatment of the problem whether the legs of the platform can be treated individually with summing of the individual loads, or whether there is interference between them which will affect the failure mode of the ice. There is no good field information in this area and so the results of model tests are used to provide some guidance.

The ice forces on multi-legged structures have been investigated using physical modelling techniques by several authors. Many of these studies have looked at the basic physics of the interaction process of an ice sheet interacting with a row of two or more vertical piles. These tests provide insight into interference effects of the multiple legs. To date, tests of this type have been performed by Saeki et al (1978), Noble and Singh (1982), Kato and Sodhi (1983), Wessels (1983), Timco and Pratte (1985) and Evers and Wessels (1986). These papers contain a great deal of information on aspect ratio effects, rate effects, ice failure modes, etc. and the reader is referred to them for details. In general, the test results are in reasonable agreement with the following salient features:

- (1) The ice action on two legs has no interference effects if the spacing between the legs (L) is greater than six times the diameter (D) of one of the legs.
- (2) As the leg spacing decreases (for $L/D < 6$), the horizontal force on each leg in the direction of ice movement is less than that for an isolated leg under the same conditions.

- (3) Over this same range, however, the magnitude of the force on each leg in the direction perpendicular to the ice movement increases in such a way that the total force on the leg is the same as that on an isolated leg.
- (4) This mechanism causes the resultant direction of the ice loading on each single leg to change if the legs are close together. The model tests indicate that the direction of loading may deviate by as much as 12° from the direction of motion of the moving ice. Thus, when the legs are wide apart, the failure of the ice is symmetrical about each leg; whereas when the legs are close together, the failure tends to occur on one side. The proximity of the other leg causes the legs to be pushed together (see Figure 1). The resultant force on the entire platform, however, decreases with decreasing leg spacing, as the lateral components of the single leg forces compensate each other. This was confirmed by model test results on three- and four-legged platform (Evers and Wessels, 1986). The following numerical results were obtained:

The variation in the leg spacing of the four-legged platform during level ice penetrations showed the tendency that the increase in the horizontal leg forces on the entire platform from $L/D = 4.0$ to $L/D = 5.3$ was greater than the increase from $L/D = 5.3$ to $L/D = 7.3$. This is caused by the fact that at high enough values of L/D , each individual leg acts as a single independent leg. It can be expected that the resultant ice forces on the entire platform will reach an asymptotic limit at leg spacing higher than $L/D = 7.3$.

On the other hand, the variation in the leg spacing of the three-legged platform showed, as a general trend, a progressive increase in the resultant ice forces on the entire platform with increasing leg spacing. It seems that the limit where all single legs act as an individual leg is not yet reached at $L/D = 7.3$ for the three-legged platform.

The parameter study on the leg spacing of the three-legged platform as well as on the four-legged platform led to the conclusion that a minimum value of total ice force on the entire platform can be expected at a certain value of leg spacing. The value of critical leg spacing depends on the type of structure (three or four legs) as well as on the type of ice/structure interaction, i.e., level ice, ridge or pressure ice field interaction.

- (5) When $L/D > 6$, the failure of the ice is pure crushing, or crushing with radial cracks. For $L/D < 6$, tensile cracks develop in the ice such that the ice moving between the legs is broken into smaller pieces (see Figure 1). In general, the length of each ice piece is a function of the leg spacing such that it increases with increasing spacing.
- (6) For broken ice moving against the front legs of a multi-legged structure, there is a definite advantage in ice clearing and total load for a structure which has a few large diameter and widely spaced legs as compared to more numerous thinner legs. However, recent (proprietary) model tests have indicated that a closer leg spacing has an advantage in overall clearing under the structure, since the ice is broken into much smaller pieces.

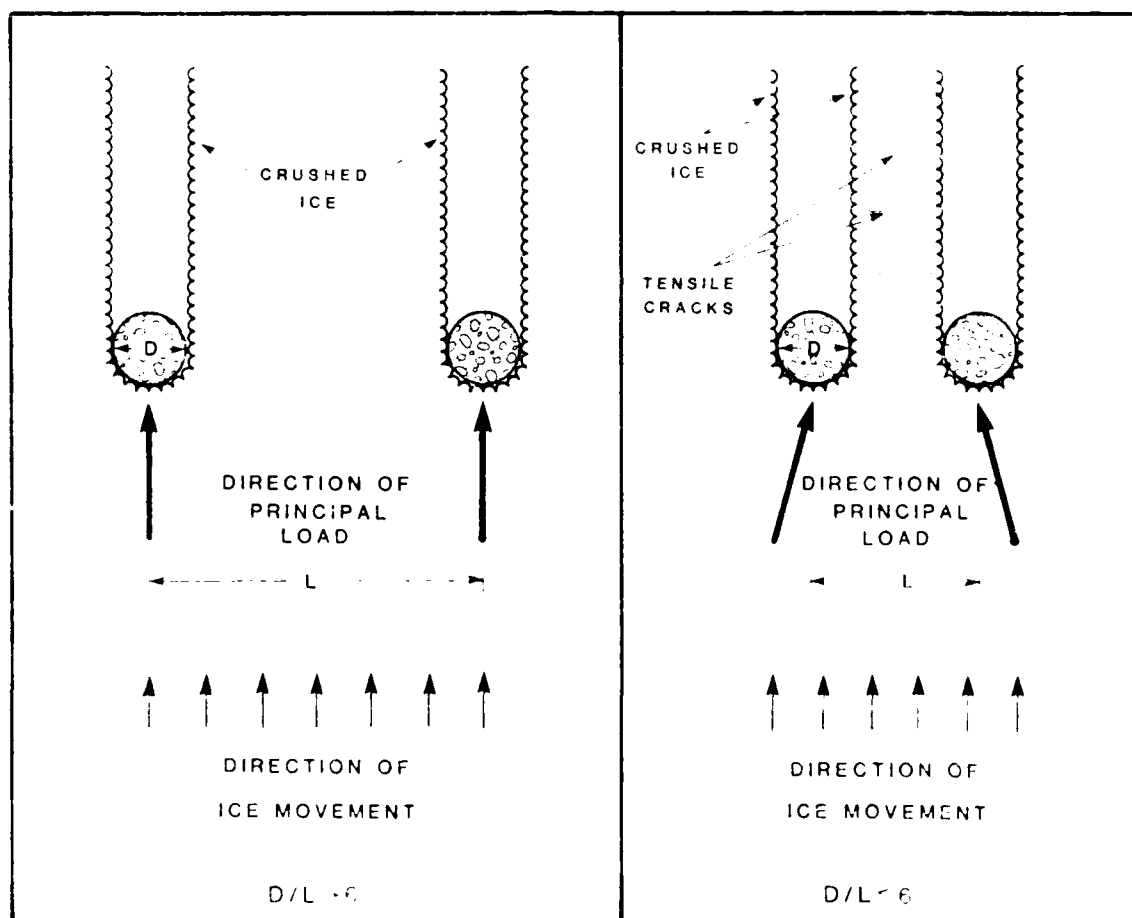


Figure 1: Ice failure modes and direction of principal loads on a multi-legged structure determined using physical modelling techniques.

(7) Model tests on complete platforms indicate that the magnitude of the load depends upon the angle of the ice movement relative to the platform legs. If, for example, the two front legs of a 4-legged platform simultaneously penetrate into the ice, the back two legs are in an ice shadow, and will not realize any appreciable load. If, however, the direction of ice movement is changed by 25° , all four legs will have ice loads on them. In this case, the back legs will experience a broken ice field and the ice may fail by bending or shearing rather than crushing. Consequently the peak loads on each individual leg do not occur simultaneously, and the maximum ice load on the total structure is less than the sum of the maximum loads on each leg if treated in isolation. The amount of reduction will depend upon the platform design and angle of ice attack. This may be investigated by model tests in ice. It should be remembered, however, that for breakout (frozen-in) conditions with complete 100% contact, simultaneous occurrence of peak loads may occur. This may increase the total force on the structure by a factor of up to 4 compared to the force during level ice penetration.

3.0 The Interaction Scenario

As an example of a multi-legged structure, we choose a 6-legged platform with a rectangular shape with overall dimensions of 30 m x 15 m with four well conductor pipes in a square array 2 m apart at the centre of the platform. The diameter of the legs and pipes are 1.0 m and 0.66 m respectively. A sketch of the hypothetical platform is shown in plan view at the waterline in Figure 2a. Assume further that this platform is to be built in 10 m of water in a region with a moving ice cover of maximum thickness 35 cm, average ice salinity 5 ‰ and minimum air temperature of -15°C (see Figure 2b).

In order to calculate the loads, representative values of the mechanical properties of sea ice are necessary. These properties depend upon many factors (see e.g. Schwarz and Weeks, 1977 or Weeks and Ackley, 1982 for a review) and so in this paper typical values are simply chosen. In the design of a structure for a specific site, however, it would be imperative to have good information on the type and extent of the ice cover at the site.

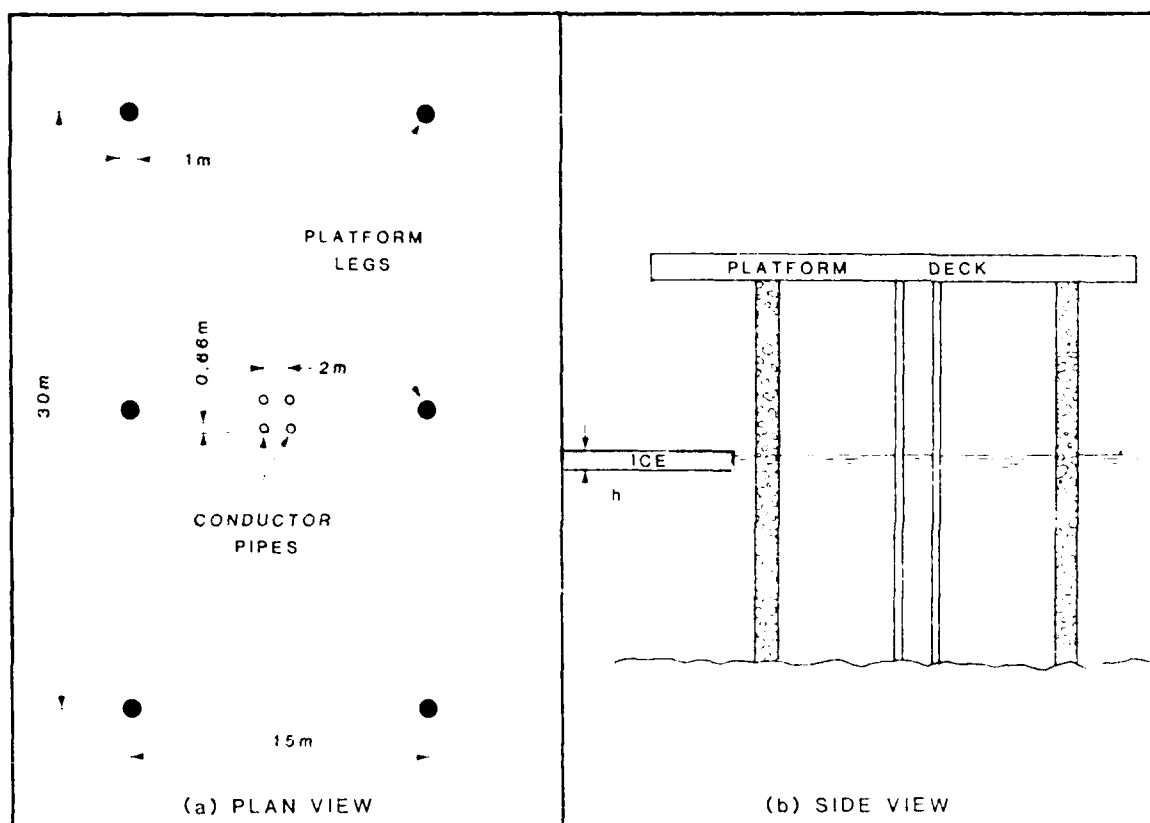


Figure 2: Schematic of the multi-legged platform used in the interaction scenario.

Since this ice is relatively thin, it will be assumed that the ice structure is granular. For these conditions, the uni-axial compressive strength (σ_C) varies with loading strain rate ($\dot{\epsilon}$) according to

$$\sigma \approx 30 \dot{\epsilon}^{0.22} \quad (1)$$

where σ is in MPa and $\dot{\epsilon}$ is in s^{-1} (Wang, 1979). At break-up, when the ice is warmer, a maximum uni-axial compressive strength at high loading rates is of the order of 2 MPa (Schwarz, 1970). Further, for the calculations, appropriate values for the flexural strength (σ_F), effective modulus (E) and characteristic length (l) are chosen to be $\sigma_F = 0.5$ MPa, $E = 3$ GPa and $l = 5.9$ m respectively.

For this situation, it is possible to use present engineering equations and results of strength measurements on sea ice to predict ice loads on the structure, as well as to illustrate the gaps in our knowledge of ice loads

on multi-legged structures. In calculating the loads on the hypothetical structure, use can be made of the model test results. For the main legs of the structure, $D/L = 15$ so each of the legs can be treated individually, neglecting interference effects. For the well conductor pipes, however, $D/L = 3.0$, so the interference effects are important. In determining the total load, the force for ice crushing for both ductile indentation and dynamic crushing will be calculated for each leg and pipe and then summed to give the maximum load on the structure. In addition to this, the load necessary for ice buckling, and the vertical ice loads due to changes in water level will be determined. In all cases, it will be assumed that there is a sufficiently large driving force on the ice to cause local failure.

4.0 Design Ice Loads on the Structure

4.1 Horizontal Loads Due to Ductile Indentation

Ice sheets in nature are in constant but very slow movement. As the ice moves, forces are exerted on isolated structures. For a platform, there are several vertical legs and conductor pipes which present conditions for ductile indentation of the ice cover. The force on one single leg or pipe can be estimated from the Korzhavin (1971) equation

$$F = k m I D h \sigma_c \quad (2)$$

where k = contact coefficient, m = shape factor, I = indentation factor, D = width of an individual leg or pipe, h = ice thickness and σ_c = uni-axial compressive strength at the loading rate of interest. For this situation we will assume frozen-in conditions (i.e. 100% contact) so $k = 1$ and for a round indenter $m = 0.9$. The indentation factor I incorporates the effects due to both the aspect ratio (i.e. structure width to ice thickness ratio) and ice anisotropy (see Figure 3). For the legs of the platform $D = 1.0$ m and $h = 0.35$ m, so $D/h = 2.9$. From Figure 3, $I = 1.2$ assuming rough (i.e. high friction) boundary conditions and granular ice. For the pipes in the platform, $D = 0.66$ m and $h = 0.35$ m so $D/h = 1.9$. From Figure 3, $I = 1.4$ for the pipes. To estimate the uni-axial strength of the ice, it is necessary to know the strain rate of the ice. The indentation of a pile in an ice sheet is a complex phenomenon in which the strain rate in the ice is high close to the indenter and decreases with distance from the indenter. It has been found that an appropriate strain rate for an isolated pile can be estimated by $\dot{\epsilon} = v/2D$ where v is the indentation velocity (Ralston, 1979). For piles in an array in moving ice, the appropriate strain rate is not known. If we assume that $\dot{\epsilon} = v/2D$ and

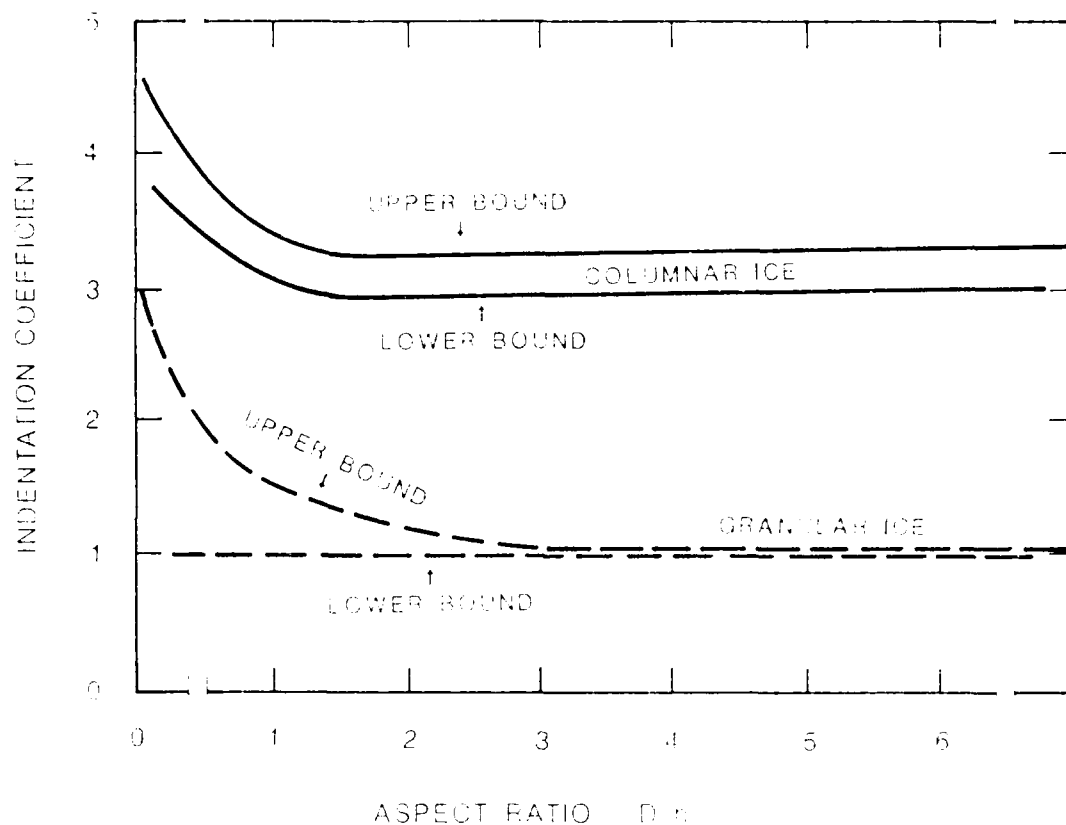


Figure 3: Indentation coefficient versus aspect ratio for columnar and granular ice (after Ralston, 1978).

movement rates of 0.3 m/hr, then, for a pile of 1 m diameter $\dot{\epsilon} = 4.2 \times 10^{-5} \text{ s}^{-1}$, and using Equation (1), $\sigma_C = 3.3 \text{ MPa}$. Then, from Equation (2), the force on a single leg is 1.2 MN. In a similar way, the load on one pipe is calculated to be 1.0 MN. In this latter case, interference effects may occur such that the pipes may be "pushed together". For the highest overall load on the platform, the individual load components should be simply summed. For this platform this yields a total load of 11.2 MN. This is the situation representing completely frozen-in conditions of the structure, and as such would give the highest peak load for this failure mode. Once the ice is in continuous movement, the load on the structure due to continuous crushing would be less than this.

4.2 Ice Buckling

Under some circumstances, especially for the case of a wide structure with a thin ice sheet, the ice can fail through buckling. This failure mechan-

ism thereby can determine the limiting load on a structure. The loads due to buckling are a function of the width of the structure, characteristic length of the ice cover, friction at the ice-structure interface, and the aspect ratio. Plots of the non-dimensional buckling loads $P/(DK\ell^2)$ are shown versus D/ℓ in Figure 4 (Sodhi and Nevel, 1980). For a multi-legged structure, there are two possible buckling scenarios; viz. buckling against a single leg and buckling against the whole structure. To estimate the buckling load, we first assume ice failure due to buckling on an individual leg. For this $D = 1$ m and $\ell = 5.9$ m (from Section 3), so that $D/\ell = 0.17$. For this ratio, assuming high friction coefficient at the ice-pile inter-

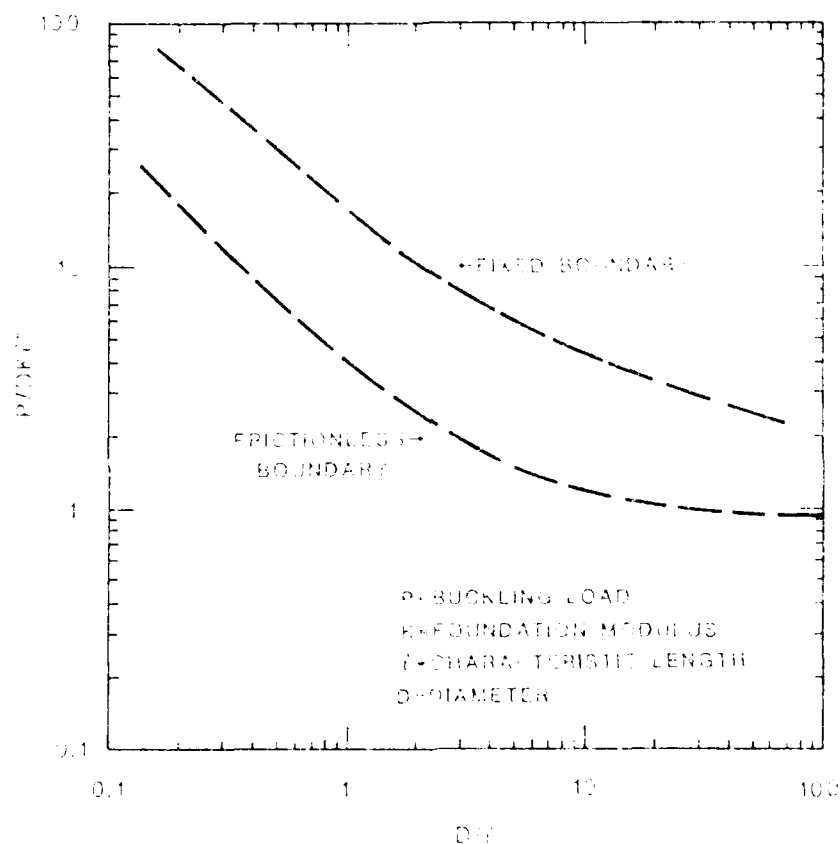


Figure 4: Buckling load versus D/ℓ for fixed and frictionless boundaries (after Sodhi and Nevel, 1980).

face, $P/(DK\ell^2) = 65$ (from Figure 4) and so $P = 22.6$ MN. This is considerably higher than the crushing load on the pile, so buckling is not probable and ductile indentation would govern the design. For the second scenario of buckling against the whole structure, the width of the structure would be 30 m, so that $D/\ell = 5.1$. From Figure 4, the buckling load for this ratio,

assuming high friction coefficient is $P/DKl^2 = 6$. Thus, for ice buckling, the load on the whole structure would be $P = 62$ MN. This is also higher than the sum of the individual loads on each leg and pipe due to crushing, so under these circumstances buckling of the ice sheet should not occur. If, however, broken ice pieces jam up underneath the platform, and then reconsolidate, this may present a situation where buckling of the parent ice sheet is the predominant failure mode. In this case, the load on the platform would be the buckling load against the full width of the structure. This clearly emphasizes the importance of minimizing this jamming through careful consideration in the design and orientation of the platform with respect to the direction of the moving ice. In this area, physical modelling tests would be very useful.

4.3 Dynamic Ice Forces

Drifting ice floes can move with considerable speed under the action of environmental driving forces, especially in spring during the ice break-up. In this case, the velocity of the ice is such that the failure of the ice occurs in the brittle or transition zone. The failure modes which may be involved are crushing, spalling, ice cracking and ice wedging. To estimate the forces involved in this process, an equation similar to Equation (2) is used except that the contact factor is included in the indentation coefficient. The equation for the ice force is

$$F = m I D h \sigma_0 \quad (3)$$

where the terms are described as in Equation (2) except for σ_0 which is a nominal strength value. We chose $\sigma_0 = 2.0$ MPa as the maximum value measured by Schwarz (1970) on warm sea ice. For this case, the indentation factor suggested by Afanasev et al. (1973) is frequently used

$$I = (5 h/D + 1)^{1/2} \quad \text{for } 6 > D/h > 1$$

$$I = 4 - 1.55 (D/h) \quad \text{for } D/h \leq 1 \quad 4.$$

For an individual leg for the platform, $D/h = 2.9$, so $I = 1.7$ and the load on a single leg due to dynamic ice crushing is 1.1 MN. In a similar way, the load on a single pipe is calculated to be 0.79 MN. This type of impact would probably not occur simultaneously on all pipes and legs. Thus the total load on the structure due to impact could be obtained through summation of the individual loads with various scenarios of the temporal and spatial distributions of the ice impacts. Model tests should give valuable information in this area for a particular platform design, both in terms of impact loads and ice jamming and pile-up beneath the structure.

4.4 Vertical Forces Due to Changes in Water Level

As water level changes through, for example, tidal action, the ice sheet adhering to a leg or pipe can deflect and exert a vertical force on it. The problem is usually approached using plate theory with the governing differential equation (Gold, 1984)

$$\Delta^4 \omega = \frac{q - K \omega}{D_i} \quad (5)$$

where ω = deflection at a given distance from the structure, q = load applied for the ice cover, K = sub-grade reaction = ρg , $D_i = Eh^3/12(1-\nu^2)$ = flexural rigidity of ice cover. Usually the treatment of the problem is in terms of the elastic solution, even though this is applicable only when the change in water level is rapid. If the water level changes are small so that no cracks occur, the analytical approach by Kerr (1978) can be used reliably for this structure geometry. In most cases, however, ice cracking will occur. For this situation there is no complete analytical model to predict the uplift forces on a multi-legged structure so it is once again necessary to treat each leg independently. One approach to the problem of an isolated pile is to treat the failure of the ice in terms of radial cracking and subsequent circumferential failure of the wedges. Based on the work of Nevel (1972), an approximate estimate of the uplifting forces on an isolated circular pile of diameter D is given by

$$P = 1.154 \sigma_f h^2 (1.05 + 2 \alpha + 0.5 \alpha^3) \quad (6)$$

where $\alpha = (D/2l)$ and σ_f is the flexural strength of the ice. For one of the legs $\alpha = 0.08$, and the vertical force is 0.09 MN. The position of the circumferential crack can be determined from Figure 5 (Christensen and Tryde, 1984). For the present case, it should occur at a distance of ≈ 3 m from the leg. Although this calculated vertical load would be appropriate in several situations, in the case of a multi-legged platform there are many uncertainties and this approach can only be used as a guide to the magnitude of the uplift forces for several reasons. First of all, it represents the elastic solution to a viscoplastic problem. Secondly, as the ice breaks in this situation, there can be flooding and refreezing such that an ice collar can form around each leg or pipe. This causes them to have a much larger effective diameter, with resulting higher vertical forces. (For example, assuming an effective diameter of $2(3 \text{ m}) + 1 \text{ m} = 7 \text{ m}$ for one leg, the calculated vertical force using Equation (6) is 0.16 MN.) Thirdly, the deformation and failure of the ice will be influenced by the proximity of the other legs and pipes in the platform, to the extent

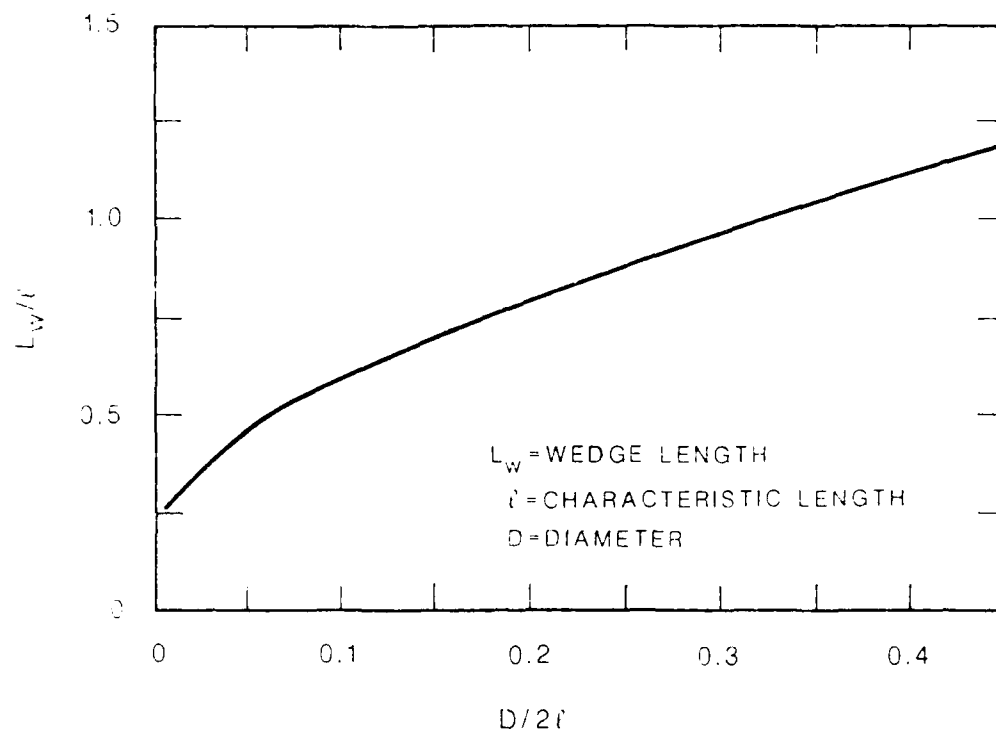


Figure 5: Wedge length versus $D/2l$ for ice failure due to uplift (after Christensen and Tryde, 1984).

that a simple summing of the loads on each individual pile may underpredict the actual total load on the structure. In those cases where interference of the ice deformation due to other structures is of concern, the best approach may be to use a finite element analysis to determine the failure mechanism (Eranti and Lee, 1981). This approach, however, is very expensive and still involves many simplifying assumptions. Thus, the magnitude of the uplift forces on a multi-legged structure cannot be easily predicted with much certainty and a great deal of work remains to be done in this area.

5.0 Prototype Studies

There have been very few reports on the ice loads or ice breaking behaviour around multi-legged structures. Because of this paucity of information and the complexity of the interaction process, it is not possible at this time to co-ordinate the results to give a consistent picture. The reports which describe the ductile indentation or dynamic impact include:

- (1) The study reported by Peyton (1968) and Blenkarn (1970) on the ice conditions and ice loads on a platform in Cook Inlet, Alaska over a

number of years. These papers report on measured prototype values and introduce the concepts and problems associated with the dynamic response of the structure.

- (2) A study reported by Schwarz (1970) on the ice loads on a marine pier in warm ice in the North Sea. In this study ice pressures up to 1 MPa were measured for weak ice.
- (3) Jizu and Leira (1981) and Wang (1983) report on the problems experienced in the Bo-hai Gulf in China by two platforms which were designed without consideration of ice effects. One platform collapsed whereas the other was unscathed. The paper outlines the forces on the platform and the problems associated with ice jamming both in front and underneath the platform.
- (4) Neill (1972), Montgomery et al. (1980) and Huiskamp (1983) report on the dynamic response and measured ice forces on bridge piers in large rivers in central Alberta. Their analysis shows that depending upon the frequency and damping characteristics of the pier and foundation, the dynamic response can exceed the static response to the peak ice force. The peak unit pressure was found to be comparable with the ice strength in compression.
- (5) The excellent review article by Neill (1976) assesses various analytical approaches, full-scale data and small-scale laboratory tests as they pertain to the estimate of forces due to impact of moving ice on piles, piers and towers.

Those reports which describe problems relating to uplift forces include:

- (6) Doud (1978) measured the uplift forces on a series of marine piles which were prone to ice-jacking caused by the vertical movement of the ice sheets. These piles were in freshwater ice.
- (7) Wortley (1984), in an engineering manual for the design of small craft harbours for ice conditions, has reported many examples of severe uplift of multi-legged piers due to ice action.
- (8) Vershinin et al. (1983) measured the uplift forces on the cylindrical supports of an offshore oil well platform due to an ice cover subjected to changes in water level. They found that the experimental values were several times higher than that computed according to the Russian Regulations Code.

6.0 Summary

In this paper, the ice forces on multi-legged structures have been reviewed. This was done by assuming a typical platform design and ice conditions and calculating the ice forces and ice behaviour (failure modes) for this situation. The results of model tests were reviewed to give insight into the interference effects between the legs. A listing of studies of ice behaviour around full-scale multi-legged structures was given. The review clearly shows that the present day level of knowledge is very unsatisfactory such that there are many uncertainties in the prediction of the ice loads on these types of structures. Much more work could be done in this, especially with regard to the leg interference effects of full platforms, the vertical loads due to tidal action, and the ice loads and ice jamming around the structure in broken pack ice.

7.0 Acknowledgments

The author would like to thank E. Wessels, R. Frederking and J.P. Mizikos for their helpful comments on an early draft of this paper.

8.0 References

- Afanas'ev, V.P. et al., 1973. "Ice Pressure on Individual Structures". Ice Physics and Ice Engineering, G.N. Yakovlev, ed., Israel Program for Scientific Translation, pp. 50-68.
- Blenkarn, K.A., 1970. "Measurement and Analysis of Ice Forces on Cook Inlet Structures". Proc. OTC, Paper No. OTC-126, Houston, TX, U.S.A.
- Christensen, F.T. and Tryde, P., 1984. "Extraction of Piles by Repeated Water-level Fluctuations". Proc. IAHR Symp. on Ice, Vol. II, Hamburg, West Germany, pp. 111-121.
- Doud, J.O., 1978. "Ice Sheet Loads on Marina Piles". J. Waterway, Port, Coastal and Ocean Div., ASCE, Vol. 104, No. WW1, pp. 11-17.
- Eranti, E. and Lee, G.C., 1981. "Introduction to Ice Problems in Civil Engineering". Dept. of Civil Eng., State University of New York, Buffalo, NY, U.S.A.
- Evers, K.H. and Wessels, E., 1986. "Model Test Study of Level Ice Forces on Cylindrical Multi-Legged Structure", Polartech 86, Helsinki, Finland, Oct. 27-29, 1986.
- Gold, L.W., 1984. "Ice Pressures and Bearing Capacity". Geotechnical Eng. for Cold Regions, O.B. Andersland and D.M. Anderson, ed., McGraw-Hill Book Comp., New York, NY, U.S.A., pp. 505-555.

- Huiskamp, W.J., 1983. "Ice Force Measurements on Bridge Piers 1980-1982". Civil Eng. Dept., Alberta Research Council Rept. SWE 83-1, Edmonton, Alberta, Canada.
- Jizu, X. and Leira, B.J., 1981. "Dynamic Response of a Jacket Platform Subjected to Ice Floe Loads". Proc. POAC 81, Vol. I, Quebec City, Canada, pp. 502-516.
- Kato, K. and Sodhi, L.S., 1983. "Ice Action on Pairs of Cylindrical and Conical Structures". U.S. Army CRREL Rept. 83-25, Hanover, NH, U.S.A.
- Kerr, A.D., 1978. "Forces an Ice Cover Exerts on Rows or Clusters of Piles Due to a Change of the Water Level". Proc. IAHR Symp. on Ice, Part I, Lulea, Sweden, pp. 509-525.
- Korzhavin, K.N., 1971. "Action of Ice on Engineering Structures". U.S. CRREL Translation TL260, Hanover, NH, U.S.A.
- Montgomery, C.J., Gerard R. and Lipsett, A.W., 1980. "Dynamic Response of Bridge Piers to Ice Forces". Can. J. Civil Eng. 7, pp. 345-356.
- Neill, C.R., 1972. "Force Fluctuations during Ice-Floe Impact on Piers". Proc. IAHR Symp. on Ice, pp. 44-50, Leningrad, U.S.S.R.
- Neill, C.R., 1976. "Dynamic Ice Forces on Piers and Piles. An Assessment of Design Guidelines in Light of Recent Research". Can. J. Civil Eng. 3, pp. 305-341.
- Nevel, D.L., 1972. "The Ultimate Failure of a Floating Ice Sheet". Proc. IAHR Symp. on Ice, Vol. I, Leningrad, U.S.S.R., pp. 17-22.
- Noble, P.G. and Singh, D., 1982. "Interaction of Ice Floes with the Columns of a Semi-Submersible". Proc. 14th Offshore Tech. Conf., Vol. IV, pp. 527-535, Houston, TX, U.S.A.
- Peyton, H.R., 1968. "Sea Ice Forces". In Ice Pressures Against Structures, compiled by L. Gold and G. Williams, NRC Tech. Memo No. 92, Ottawa, Canada.
- Ralston, T.D., 1978. "An Analysis of Ice Sheet Indentation". Proc. IAHR Symp. on Ice, Vol. I, Lulea, Sweden, pp. 13-31.
- Ralston, T.D., 1979. "Sea Ice Loads". Technical Seminar on Alaskan Beaufort Sea Gravel Island Design, Houston, TX, U.S.A., Oct. 18, 1979.
- Saeki, H., Ono T., Ozaki, A. and Abe, S., 1978. "Estimation of Sea Ice Forces on Pile Structures". Proc. IAHR Symp. on Ice, Vol. I, pp. 465-478, Lulea, Sweden.
- Schwarz, J., 1970. "The Pressure of Floating Ice-fields on Piles". Proc. IAHR Symp. on Ice, Paper 6.3, Reykjavik, Iceland.

- Schwarz, J. and Weeks, W.F., 1977. "Engineering Properties of Sea Ice". J. Glac., Vol. 19, No. 81, pp. 499-531.
- Sodhi, D.S. and Nevel, D.E., 1980. "A Review of Buckling Analyses of Ice Sheets". CRREL Sp. Rept. 80-26, Hanover, NH, U.S.A., pp. 131-146.
- Timco, G.W. and Pratte, B.D., 1985. "The Force of a Moving Ice Cover on a Pair of Vertical Piles". Proc. Can. Coastal Conf., pp. 349-362, St. John's, Nfld., Canada.
- Vershinin, S.A. et al., 1983. "Effect of an Ice Cover Frozen to the Cylindrical Supports of Offshore Oil Well Platform Subjected to Water Level Fluctuations". NRC/CISTI Tech. Translation TT-2041, Ottawa, Ont., Canada.
- Wang, Qin-jian, 1983. "A Tentative View on Ice Load Applied on Jacket Platforms in Bo-hai Gulf". Proc. POAC 83, Vol. 2, pp. 930-939.
- Wang, Y.S., 1979. "Crystallographic Studies and Strength Tests of Field Ice in the Alaskan Beaufort Sea". Proc. POAC 79, Vol. I, pp. 651-665, Trondheim, Norway.
- Weeks, W.F. and Ackley, S.F., 1982. "The Growth, Structure and Properties of Sea Ice". U.S.A. CRREL Monograph 82-1, Hanover, NH, U.S.A.
- Wessels, E., 1983. "Ice Loads on Cylindrical and Conical Offshore Structures". Lecture notes at WEGEMT VII Graduate School "Ships and Structures in Ice", Helsinki, Finland.
- Wortley, C.A., 1984. "Great Lakes Small-Craft Harbor and Structural Design for Ice Conditions: An Engineering Manual". Univ. of Wisconsin Rept. WIS-SG-84-426, Madison, WI, U.S.A.

FLEXURAL AND BUCKLING FAILURE OF
FLOATING ICE SHEETS AGAINST STRUCTURES

Devinder S. Sodhi
Research Engineer

U.S. Army Cold Regions Research
and Engineering Laboratory
72 Lyme Road
Hanover, New Hampshire 03755-1290

U.S.A.

ABSTRACT This is a review of work on bending and buckling failure of floating ice sheets, along with the forces generated during ice/structure interaction. The focus is on the work published after 1980. Estimation of ice forces as a result of bending and buckling failure of an ice sheet can be made with a fair degree of confidence when the ice/structure interaction leads to one of the two modes of failure. The problem of multimodal failure of floating ice sheets needs further study.

1. INTRODUCTION

The relative motion between an ice sheet and a structure generates forces, which are generally called ice forces. For the design of structures that are to be placed in an ice environment, the ice forces have to be estimated on the basis of environmental data and ice conditions. The design forces are generally limited to the forces required to fail an ice sheet. These forces depend upon the structure geometry (width, slope, etc.), the ice conditions (thickness, floe size, strength, etc.), and the mode of ice failure (bending, buckling, crushing, or mixed mode). The mode in which an ice sheet fails depends upon many factors, such as the ice thickness and properties, the structure width, relative velocity, and the slope of the structure.

In this review, only the bending and buckling failure of floating ice sheets will be discussed, along with the forces generated during ice/structure interaction. The focus will be on the work published after 1980, since earlier work was reported in the first state-of-the-art review by the IARR Working Group on Ice Forces on Structures (Croasdale, 1980; Sodhi and Nevel, 1980). The bending failure of ice sheets and ridges has been partially covered in the second state-of-the-art review (Sodhi and Kovacs, 1984; Krankkala and Määtänen, 1984).

2. BENDING OF FLOATING ICE SHEETS

Ice/structure interaction problems are characterized by edge loading of an ice sheet, as opposed to static or moving load on an ice sheet, where the load is generally applied vertically in the middle of an ice floe away from the boundary. Because the problem of static and moving loads on an ice sheet deserves a separate review, that subject is not included here. The problem of ice/structure interaction may be divided into two phases: initial deformation, followed by the failure of the ice sheet.

When an ice sheet is pushed against a vertical or sloping structure, the initial deformation in the ice sheet depends upon the ice behavior: elastic or inelastic. When the relative velocity between an ice sheet and a structure is high, the assumption of ice behaving as an elastic material produces good results. For low relative velocity the behavior of ice is inelastic and the failure phase of ice/structure interaction is not clearly defined. For a very high relative velocity, inertial forces

play an important role in that the failure modes of an ice sheet may differ significantly from those at low relative velocity.

The estimation of ice forces by elastic analysis is generally accomplished by determining the forces required to initiate failure. If the ice fails in brittle mode, the elasticity method generally provides a good estimation of ice forces, whereas the plasticity method yields good results for the ductile failure of ice. In plastic limit analysis, ice forces are estimated by equating the rate of work done by external forces to the rate of energy dissipation in the ice, which is assumed to have a velocity field similar to that for actual failure mode. For the buckling problem, the forces required to buckle a floating ice sheet may be obtained by conducting an elastic or viscoelastic analysis, depending on the rate of ice movement.

For elastic analysis, the differential equation that governs the transverse displacement of a floating ice sheet during an ice/structure interaction may be written as:

$$\alpha \rho h \ddot{w} + D w_{,ijjj} + N_{ij} w_{,ij} + \rho_w g w = 0 \quad (\text{for } i, j = 1, 2) \quad (1)$$

where ρ and ρ_w are the ice and water densities respectively, h is the ice thickness, α is a factor to account for the added mass of water, w is the transverse displacement of the ice sheet, D is the flexural rigidity of the ice sheet (to be discussed later), N_{ij} is the in-plane stress components, and g is the gravitational acceleration. In the above equation, the dots refer to differentiation with respect to time and the commas refer to differentiation with respect to spatial coordinates (x_1, x_2). The convention of summing repeated indices is adopted here. Factor α accounts for the inertial forces of water below the ice; its value is generally assumed to be between 1 and 2.

Equation (1) states an equilibrium between different type of vertical forces at a point (x_1, x_2) of the floating ice sheet. The first term accounts for the inertial forces, the second term the elastic forces, the third term the in-plane forces, and the fourth term the change in buoyancy forces. Depending upon the situation and problem at hand, the above equation may be simplified by excluding the first and third terms. For instance, a simple flexure problem may be analyzed by retaining only the second and the fourth terms. If in-plane forces are present, the third term should be retained to account for the contribution of in-plane forces to the equilibrium of the ice sheet. The first term, dealing with

Inertial forces, is retained only for those ice/structure interaction problems where the relative velocity is high. Further simplifications may be offered if the problem can be formulated as a one-dimensional as opposed to a two-dimensional problem, e.g. a beam on an elastic foundation (Hetenyi, 1946; Nevel, 1983).

For viscoelastic analysis, the above equation may be written to include inelastic constitutive laws relating rates of stresses and strains. Due to nonlinearities, the inelastic analyses are conducted in incremental steps, and the solution is iterated to converge at each step.

Even though an ice sheet is transversely anisotropic, it is isotropic in its horizontal plane, i.e. in the $x_1 - x_2$ plane. One single factor that influences the bending deformation of the ice sheet is the characteristic length of floating ice, defined as $L = (D/\rho_w g)^{1/4}$. Because it has a dimension of length, it is convenient to normalize the spatial coordinates with respect to the characteristic length.

The flexural rigidity is an integrated quantity defined as

$$D = \int_{-h_1}^{h_2} \frac{z^2 E(z)}{(1-\nu^2)} dz \quad (2)$$

where $E(z)$ is the modulus of elasticity at a point that is at vertical distance z from the neutral surface, ν is the Poisson's ratio, and h_1 and h_2 are the distances of the bottom and top surfaces, respectively, from the neutral surface. The neutral surface is defined as the surface where there is zero strain or stress due to bending, and its position from the top surface (h_2) can be determined from the following equation:

$$\int_{h_2-h}^{h_2} z E(z) dz = 0 \quad (3)$$

If the elastic modulus is assumed to be constant through the ice thickness, the neutral surface will be located in the middle of the ice sheet and the characteristic length can be defined as

$$L = [Eh^3/12(1-\nu^2)\rho_w g]^{1/4}.$$

The elastic modulus calculated by the use of the equation is termed the effective elastic modulus, implying that it is an approximation to integrated values. However, the elastic modulus varies across the thickness of the ice sheet because of temperature variation and other factors.

Kerr and Palmer (1972) derived a set of equations for the bending of floating ice sheets, in which they assumed a variation of elastic modulus as a result of temperature variation across the thickness of the ice sheet. They concluded that the formulations for ice sheet bending are the same as those for the corresponding homogeneous problems, if a modified flexural rigidity is used. They also gave some examples of the nonlinear stress distribution across the thickness of the ice sheet.

In a recent review of ice properties, Cox and Weeks (1985) developed a combined ice temperature-ice salinity model to generate profiles of mechanical properties for undeformed, snow-free, first-year sea ice in the Arctic Basin. The predicted profiles give composite plate properties that are significantly different from bulk properties obtained by assuming homogeneous plates. Figure 1 shows stress distribution across the thickness due to bending moment at the root of a cantilever beam. Figure 2a shows the location of the neutral surface with respect to the ice

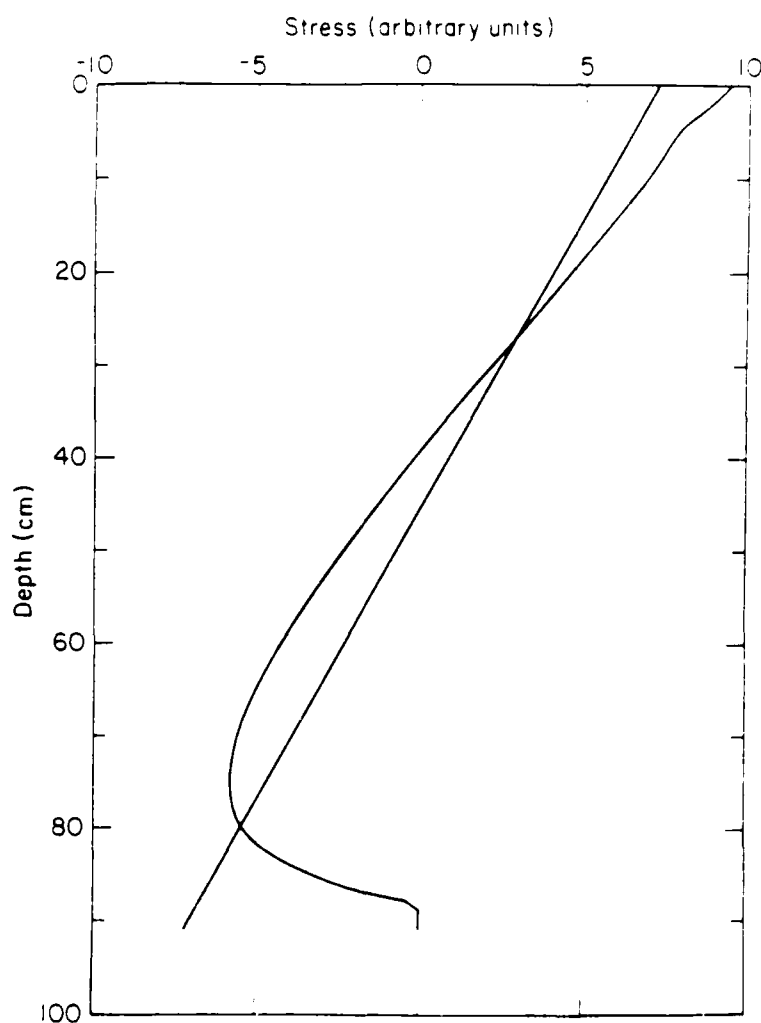


Figure 1. Comparison of stress distributions across the thickness due to bending at the root of a cantilever beam. Straight line represents a linear distribution for homogeneous, elastic material and the other line a nonlinear distribution as a result of the variation in elastic modulus (from Cox and Weeks, 1985).

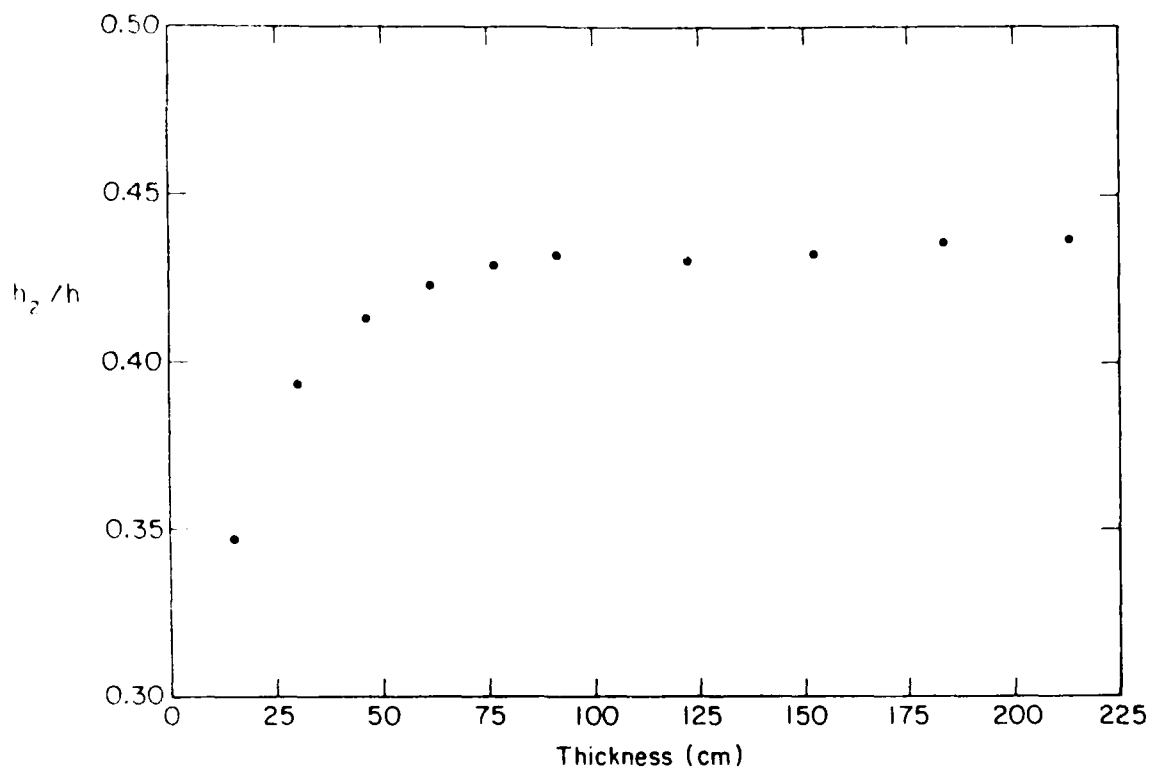


Figure 2a. Plot of dimensionless ratio h_2/h (distance of neutral surface from the top surface/total thickness) versus ice thickness from Cox and Weeks, 1985).

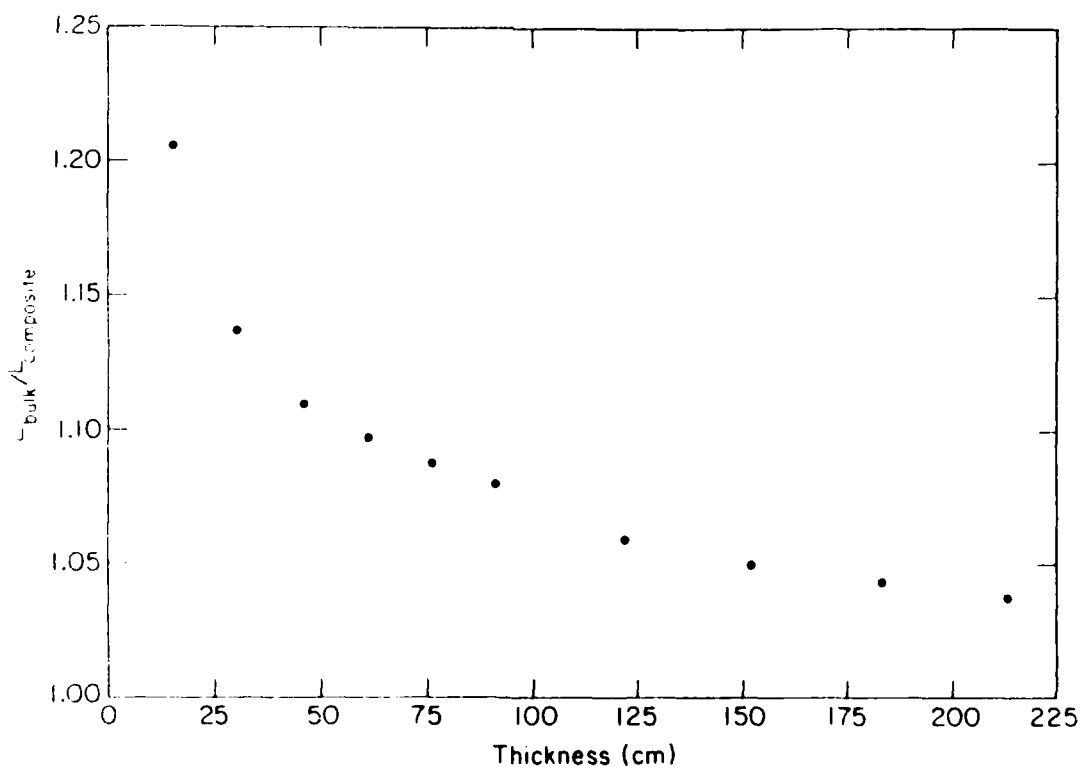


Figure 2b. Plot of the ratio of characteristic lengths assuming constant and variable elastic moduli versus ice thickness (from Cox and Weeks, 1985).

thickness. In Figure 2b, the ratio of characteristic lengths, assuming constant and variable elastic moduli, is plotted with respect to ice thickness. In addition, the failure strength profiles give maximum strengths in the interior of the sheet as contrasted with the usual assumption of maximum strength at the cold, upper ice surface. Coupled with the fact that the stress distribution during flexure of the ice sheet is nonlinear across the thickness, it becomes complicated to predict the onset of failure. Cox and Weeks also concluded that ice properties can be taken as a simple function of ice thickness and that the property profiles do not appear to be sensitive as to when a given thickness of ice started to form.

Some of the fundamental questions on flexure of saline, columnar ice are being answered through systematic laboratory tests. For example, Lainey and Tinawi (1981) found the dependence of flexural strength and elastic modulus on stress rate and temperature by conducting four-point bending tests on ice beams. Murat and Degrange (1983) conducted four-point bending tests to obtain the creep properties of sea ice. Lainey and Tinawi (1983) and Tinawi and Gagnon (1984) found that because of the anisotropy of columnar ice, shear deformation -- as opposed to bending -- contributes significantly to the long-term deformation of floating ice sheets.

3. BENDING FAILURE

Since 1980, most of the work to predict ice forces as a result of bending failure of ice sheets has been small-scale experimental studies either to verify existing theoretical results or to support new theoretical findings. In small-scale (or model) experiments, the dimensions and properties of ice sheets are reduced by a certain scale factor. These ice sheets are pushed against sloping model structures while monitoring the interaction forces. The ice forces during ice action against sloping structures can be divided into two parts: ice breaking and ice clearing. If the ice is unable to ride up and go around the structure, ice blocks accumulate in the form of a rubble field upstream of the structure. This often happens in the case of a wide structure, and the advancing ice sheet may then interact with the rubble field instead of the structure.

In model experiments involving bending failure, the ice forces are generally normalized with the product of flexural strength and the square of ice thickness. Therefore, it is appropriate to present here a few

comments on flexural strength. Though it is intended to be a measure of tensile strength, flexural strength is at best an index value. Because of the simplicity of conducting cantilever tests in situ in the laboratory, flexural strength is a useful parameter to describe the properties of ice sheets. It has been found -- both in the field and in the laboratory -- that in the case of sea ice and doped model ice, the flexural strength determined from cantilever and simple beam tests are the same (Vaudrey, 1977; Timco, 1985). This is not the case when freshwater ice is tested by these two methods: strengths from simple beam tests are greater than those from cantilever tests (Gow, 1977; Frederking and Svec, 1985) because of the stress concentration effects due to the brittle behavior of freshwater ice, which are not present for sea and model ice due to their ductile behavior.

The flexural strengths in upward and downward bending are almost equal for first-year sea ice (Vaudrey, 1977) but differ considerably for model ice. The ratio of these strengths is about 2 for urea-doped model ice; the difference is attributed to the growth of a fine-grained layer at the top (Hirayama, 1983; Timco, 1985; Yamaguchi et al., 1986). It is therefore conventional to measure the flexural strength of model ice in upward or downward bending depending on how the ice breaking takes place in a given ice/structure interaction.

Recent studies by Tozawa and Taguchi (1986) on freshwater ice specimens indicates that internal flaws have an effect on the flexural strength, which was found to decrease with the increase in specimen size (exhibiting scale effects) and was found to be distributed according to the Weibull model within each group of specimens.

A brief discussion is presented below for each group of studies related to ice/structure interaction where bending failure of the ice sheet was the primary failure mode.

(a) Discrete Element Method

Besides theoretical studies conducted in conjunction with small-scale experimental studies, the discrete element method has been a new tool to study ice/structure interaction. Yoshimura and Kamesaki (1981) presented an outline of the discrete element method and stated that a good agreement was obtained between theoretical and experimental results for the case of a cone/sheet-ice interaction. Similar claims have been made by Hocking et al. (1985a,b) who studied the interaction of ice

sheets and ridges with artificial islands and conical structures, respectively. Because this analytical tool has much to offer, we will perhaps see more results in the future as more researchers use it to analyze ice/structure interaction.

(b) Sloping Structures

Haynes et al. (1983) conducted small-scale experiments by pushing model ice sheets against narrow structures with various slope angles from the horizontal. A relationship between the non-dimensional force and the slope angle was found, as shown in Figure 3. The constant of proportionality agrees with the theoretical results of the two-dimensional analysis of Croasdale (1980). During those tests, the speed of the ice was increased steadily from 0 to 10 cm/s. Although the speed did not have any effect on the ice forces caused by the bending failure of the ice sheet, it had the dramatic effect of changing the failure mode from bending to

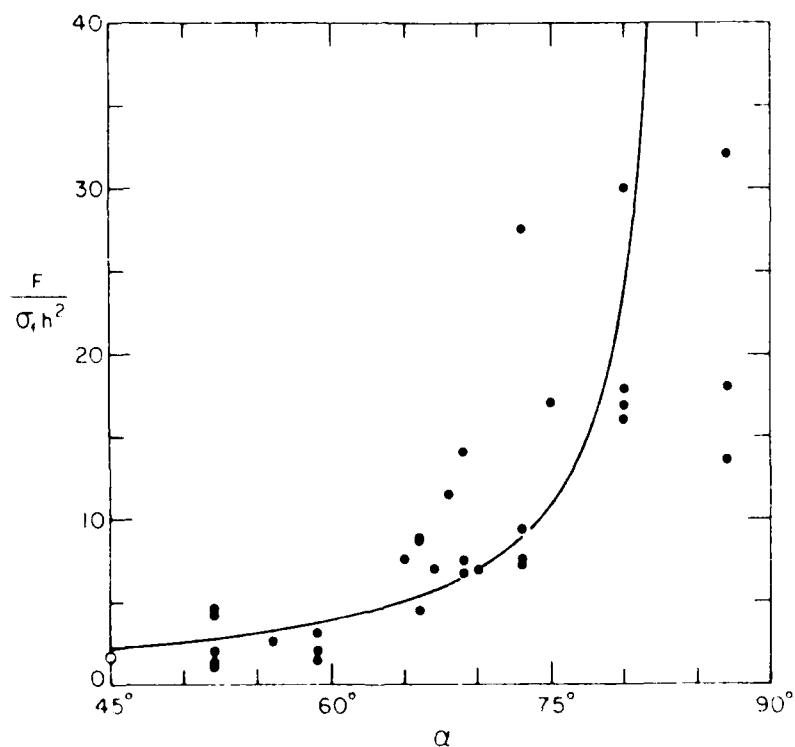


Figure 3. Plot of normalized ice force ($F/\sigma_f h^2$) on a narrow, inclined structure versus slope angle (α). Solid line is the best-fit curve through the experimental data (dots), and its equation is $F/\sigma_f h^2 = 1.78 \tan(\alpha + \phi)$, where F is the peak ice force, σ_f is the flexural strength, h is the ice thickness and ϕ the friction angle between ice and structure (from Haynes et al., 1983).

shear or crushing. The speed at which the transition in failure mode took place was found to increase with the increase in the slope angle. When the ice speed is low, the vertical forces generated during interaction are primarily caused by the weight and the elastic forces from a portion of the ice sheet near the contact area. As the ice speed increases, the kinematics of the interaction requires high acceleration of the ice sheet and water in the vertical direction during lifting, causing increased inertial forces to develop at the contact area. When the forces required to lift the ice sheet exceed the force required to cause the ice sheet failure in shear or in crushing, a transition in the failure mode takes place. Such transitions in failure mode have also been observed by others (Lipsett and Gerard, 1980; Schwarz, 1985).

An exhaustive study of ice interaction with sloping structures of different widths was conducted by Timco (1984) and Frederking and Timco (1985). They proposed that the total ice force can be divided into forces required for breaking the ice sheet, rotating the broken ice blocks, and sliding ice blocks on the structure. They obtained good agreement between the theoretical and experimental results for the individual force components, but the theoretical total force was higher than the total measured force. The discrepancy was attributed to the fact that the theoretical force was calculated by summing the peak values of each force component, when in fact it is not possible for all peak forces to occur simultaneously.

(c) Conical Structures

Many experimental studies were conducted to investigate the dependence of ice forces when a conical structure interacts with an ice sheet and a multiyear pressure ridge. Theoretical results for the above interaction were given by Ralston (1977, 1979), Abdelnour (1981), and Wang (1984).

Sodhi et al. (1985) conducted tests with a 45° upward-breaking conical structure that had diameters of 1.5 m at the waterline and 0.33 m at the top. The tests were conducted at different speeds and at two coefficients of friction. They found a good agreement between experimental and theoretical (Ralston, 1977) results for different coefficients of friction and no appreciable effect of velocity on the ice forces. On the basis of spectral analysis of the force signal, they found that the size of the initial bending failure is about one-third of the characteristic length.

Hirayama and Obara (1986) conducted a systematic series of tests with conical structures of different slopes and sizes using freshwater and urea-doped ice. Their results agreed with the experimental results of others and with the theoretical results of Ralston (1977).

Field and model studies were conducted by researchers in Finland (Määttänen and Mustamäke, 1985; Hoikka, 1985) to observe ice failure modes against a conical structure and to measure the ice forces. The model study was launched to duplicate the ice/structure interaction observed in the field. The ice forces in the field were measured by instrumenting a 10-m-diameter, 55°-slope-angle, conical structure at Kemi I lighthouse, located in the northern part of Gulf of Bothnia. The failure modes observed in the field were bending at low relative velocity and shearing/crushing at high relative velocity. Ice blocks accumulated upstream of the structure. In most model tests, this type of failure has not been observed unless the tests were conducted at high speeds (Schwarz, 1985). As Ralston (1977) developed his formulation based on observations made in model tests, its applicability may be limited to smaller conical structures where the broken ice sheet is able to clear the structure.

Abdelnour (1981) presented the results of both theoretical and experimental studies for the ice forces generated during interaction of multiyear ridges with a conical structure. Ralston (1977) had pointed out that a ridge of finite length may induce a higher ice force on a conical structure than an infinitely long ridge. Abdelnour (1981) presented expressions for the ice forces when a multiyear ridge of finite length develops "center" and "hinge" cracks. The expressions for ice forces were derived assuming elastic behavior of the ridge. Wang (1984) presented a formulation for the above problem using plastic limit analysis. He assumed different velocity fields for different lengths of ridges, in which both bending and twisting of the ridge were possible. While comparing theoretical results from elasticity and plasticity methods with those from tests with wax model ice (Abdelnour, 1981) and with natural saline ice (Verity, 1975), Wang found that the elasticity method underestimates the experimental results whereas the plasticity method overestimates them. The reason was attributed to the difference in failure criteria used in the two methods. In the elasticity method, the ridge material is assumed to be brittle-elastic, whereas for the plasticity method the ice behavior is assumed to be elastic-plastic. In

the first case, there is assumed to be no residual strength left after the failure, whereas full strength is assumed to be present while failure progresses in the plasticity method. The actual situation is in between the two assumptions.

4. BUCKLING OF FLOATING ICE SHEETS

A review of theoretical analyses was presented by Sodhi and Nevel (1980) in which only elastic buckling analyses of floating ice sheets were discussed. In elastic stability analysis, a floating ice sheet is assumed to be a beam or a plate resting on an elastic foundation — an assumption that is valid as long as the top surface of an ice sheet does not submerge below the water or the bottom surface does not emerge out of the water. For determining buckling loads, these assumptions are adequate because the deflections of an ice sheet are assumed to be small. The objective of a linear elastic stability analysis is to determine the bifurcation load when an ice sheet is pushed against a vertical structure.

Kerr (1980) showed that the buckling loads are lower for large deflections of an ice sheet than linear elastic buckling loads. While it is realized that the buckling loads are sensitive to imperfections both in terms of thickness variations and eccentricity of in-plane load, no study has been conducted to determine quantitatively the effects of such imperfections on the buckling loads.

The major contributions in this area of research since 1980 consist mainly of a few experimental studies and theoretical analyses. The experimental studies were conducted to confirm the results of earlier theoretical studies and to verify the results of dynamic and elastic buckling analyses of wedge-shaped floating ice sheets. Both elastic and dynamic buckling analyses cover the range of relative speeds of ice, with respect to structures, that can be characterized as high speeds where the behavior of ice can be assumed to be elastic. For very high speeds, the inertia of the ice sheet plays an important role in its deformation of ice sheets such that a higher order mode is induced, leading to a higher buckling load than the linear elastic buckling load. However, when the relative speed between ice and structure is very low, the ice behavior is inelastic and is best described by nonlinear creep equations. In such cases, a floating ice sheet can buckle under much lower loads than for linear elastic buckling. The amplitude of a buckled ice sheet grows

gradually with time. Although analysis of creep buckling of floating ice sheets is an important contribution, no systematic study has been conducted to determine buckling loads as a function of relative velocity and the parameters characterizing ice properties in the creep regime.

A brief discussion is presented below of the studies not included in the earlier review by Sodhi and Nevel (1980).

(a) Experimental Studies

Michel and Blanchet (1983) did indentation tests with columnar ice sheets and found that the ice sheet buckled when the aspect ratio (d/h) was high. During their tests, they had observed that two or more radial cracks would emanate from the edge of their flat indenter and that ice sheets would buckle forming a circumferential crack. The buckling loads from their tests agreed with the theoretical results of earlier studies (Sodhi and Hamza, 1977; Kerr, 1978).

Sodhi et al. (1983) conducted an experimental study to verify the results of theoretical analyses for a wide range of structure-width-to-characteristic-length ratios. In Figure 4, the results of the experi-

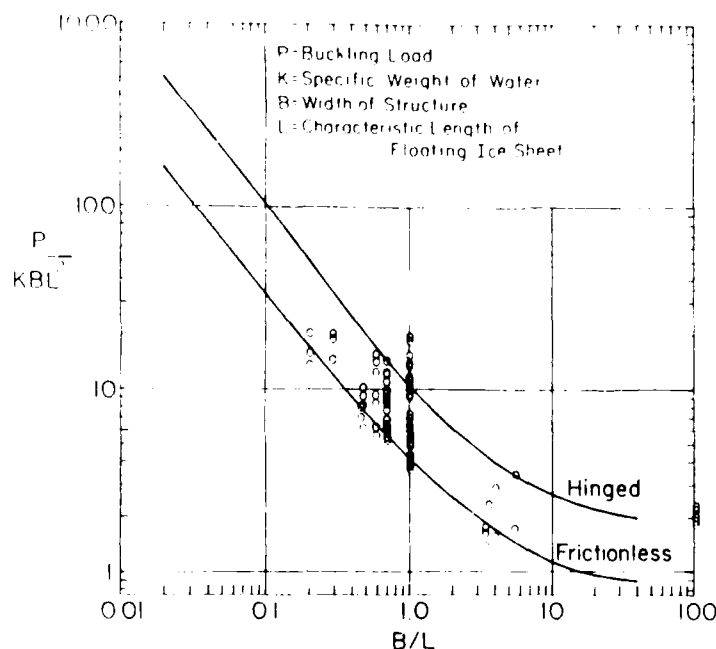


Figure 4. Comparison of experimental and theoretical buckling loads. Heavy lines: theoretical results (Sodhi, 1979); circles: experimental results (Sodhi et al., 1983).

mental study is presented in non-dimensional form. Most of the experimental data points lie between the theoretical values of normalized buckling loads for frictionless and hinged boundary conditions, which represented the extreme situations for ice/structure contact during the experiments. In those experiments, a frictionless boundary condition could be considered as one for which no frictional resistance was developed between the ice edge and the structure when the ice edge moved or deflected in the vertical direction. A hinged boundary condition would have required complete restraint of the ice sheet against vertical deflection at the line of contact with the structure. For both boundary conditions, the ice sheet was free to rotate at the edge as there was no restraining moment. Because there was no control over the boundary conditions during the experiments, the agreement between the experimental and theoretical buckling loads is considered to be good for a wide range of structure-width-to-characteristic-length ratios. However, there was considerable scatter in the data for the experiments in which the relative velocity between ice and structure was increased from 0 to 10 cm/s. In a later study, Sodhi (1983) showed both theoretically and experimentally that the dynamic buckling load of a floating ice sheet increases with the increase in relative velocity.

In subsequent experimental studies by Sodhi and Adley (1984) on wedge-shaped ice sheets, a 3-mm-thick rubber pad was glued to the structure face to induce a hinged boundary condition at the ice/structure interface. The ice edge was carefully prepared parallel to a 1.83-m-wide structure to ensure uniform contact along the whole width. The rubber pad prevented the ice edge from moving up or down, and the ice sheet was free to rotate about the line of contact. The tests were conducted at a constant relative velocity of 1 cm/s. The results of that study are shown in Figure 5 along with the results of theoretical analysis for a particular ratio of structure width to characteristic length. The overall agreement between theoretical and experimental results is good. The discrepancy between the two results may be attributed to the varying values of structure-width-to-characteristic-length (B/L) ratios in the experiments.

Using the results of Sodhi (1979), plots of nondimensional buckling loads versus wedge angle α are given in Figure 6 for different boundary conditions at the ice/structure interface and for different ratios of structure width to characteristic length (B/L).

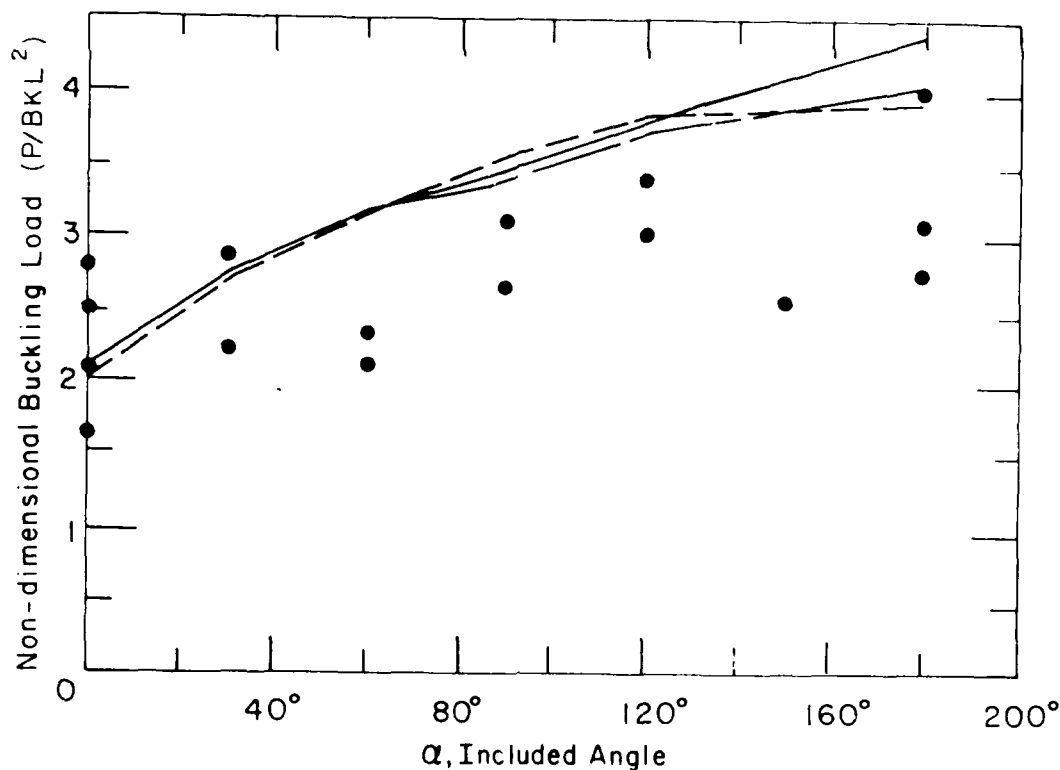


Figure 5. Plot of non-dimensional buckling load versus wedge-angle α . The solid and dashed lines represent theoretical results for a ratio of structure width to characteristic length equal to 4.3. See Figure 4 for explanation of symbols (from Sodhi and Adley, 1984).

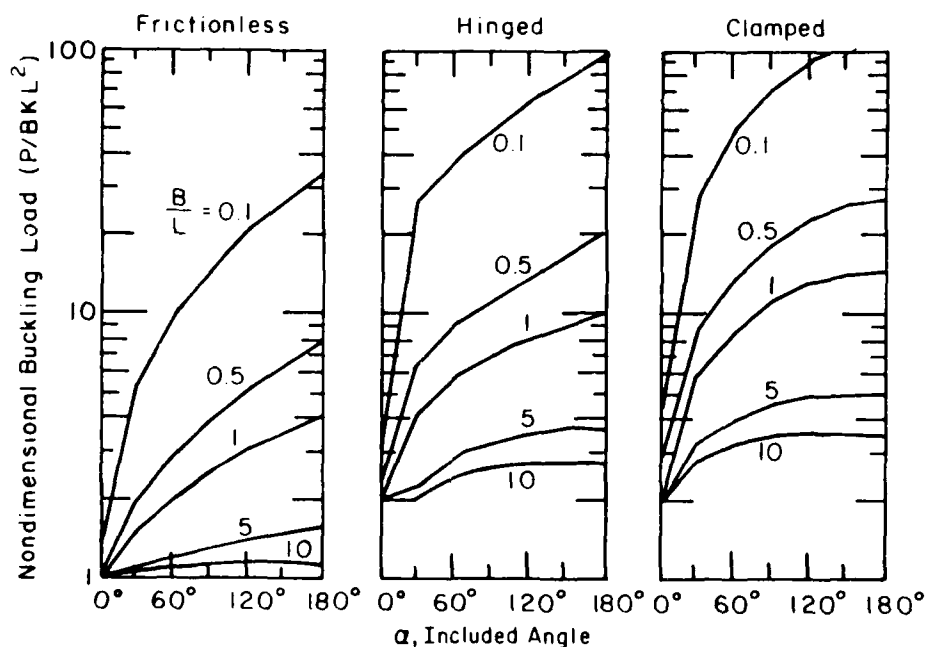


Figure 6. Plot of non-dimensional buckling load (P/BKL^2) versus included angle (α) for different boundary conditions at the ice/structure interface and for different ratios of structure width to characteristic length (B/L). See Figure 4 for explanation of symbols (from Sodhi and Adley, 1984).

When an ice sheet is pushed against two or more vertical cylindrical structures, there may be individual zones of buckling around each structure or a combined zone of buckled ice sheet across two or more structures. Kato and Sodhi (1984) conducted experiments by pushing a pair of cylindrical vertical structures through model urea ice. They found a good agreement between theoretical and experimental results when there was a single zone of buckling around each structure. However, the data for the combined mode of buckling across two structures placed near each other was consistently below the theoretical values. When the width of the buckled ice sheet was taken to be equal to the distance between centers plus the structure diameter, a good agreement was found between the theoretical and experimental results.

(b) Creep Buckling of Floating Ice Sheets

Sjölin (1984) presented a viscoelastic buckling analysis of beams and plates resting on an elastic foundation. He used the nonlinear creep power law to relate states of stress to strain rate, and the finite element method to integrate the equations with respect to time.

Sjölin (1984, 1985) presented results of a few numerical examples on beam and plate buckling. The parameters chosen for the plate on elastic foundations were somewhat similar to those for a floating ice sheet. In the example, the ice sheet has a far-field velocity of 3.75 mm/s and a thickness of 0.2 m, interacting with a 4-m-diameter structure. Although the velocity considered in this example is much less than that in any experimental study, the load between the ice sheet and the structure developed to a maximum value and remained almost constant with a slight decreasing trend with respect to maximum deflection. The nondimensional buckling load was almost close to the one from elastic buckling analysis for the same structure-width-to-characteristic-length ratio and for the same boundary condition (fixed, in this case). This suggests that when the far-field velocity is high, the resulting buckling loads are about the same value as the elastic buckling load.

Sjölin showed that creep buckling of beams on elastic foundations can take place at loads less than those for elastic buckling. Though it was not shown explicitly, it is expected that buckling of the ice sheet can also take place at in-plane loads lower than the elastic buckling load. In such cases, the deformation of the ice sheet occurs over a long time. Examples of creep buckling of the ice sheet may be found in nature



Figure 7. Photograph of a buckled ice sheet near the North Pole (89°N , 70°W) in March/April 1984 (courtesy Nordlund, 1985).

when there is steady pressure on ice sheet that is prevented by an island from drifting. Figure 7 shows a photograph of a buckled floating ice sheet (Nordlund, 1985) that was taken near the North Pole (89°N , 70°W) in March/April 1984, during the Finnish expedition to the North Pole on skis (Nordlund et al., 1985). The buckled ice sheet had an amplitude from trough to crest of approximately 1.6 m (5 ft). The following description was provided to the author by Nordlund: "The ice was very plastic at an air temperature of approximately -40°C . There were no cracks in the ice and there was no water on the ice." This description suggests that the ice sheet may have undergone creep deformation. Though ice thickness was not measured, it was thick enough to support four persons with their sledges. That a floating ice sheet can buckle to such high amplitude without cracking is noteworthy. An important point to note is that, should the far-field stress increase suddenly, such a buckled ice sheet may fail easily in continued bending or buckling, possibly starting to build a ridge.

5. SUMMARY

Most of the work related to ice forces due to the bending and buckling failure of the ice sheet has been small-scale experimental studies to verify existing theoretical results. A few theoretical studies and one or two field studies were conducted.

In bending failure, most of the work has been done on the determination of ice forces from sheet ice and ridges against conical structures.

Bending failure against sloping structures has been studied both theoretically and experimentally. When the ice velocity is high, the failure mode during the interaction of an ice sheet with a sloping structure is crushing or shear and not bending as might have been expected. There is a need to study this problem because a change in failure mode can induce forces that may exceed the intended design forces for bending failure.

In buckling failure, the results of an experimental study were reported in which overall agreement was found between buckling loads from experiments and linear buckling analysis. Later, more experimental and theoretical studies were conducted to determine dynamic buckling loads of floating ice sheets and buckling loads of wedge-shaped floating ice sheets. An important contribution was made to predict the creep buckling load. This is important because ice can deform considerably by creep under low levels of in-plane load, as observed near the North Pole. Should the in-plane force increase, it can easily lead to failure of deformed ice sheets resulting perhaps in the start of a ridge formation.

Estimation of ice forces as a result of bending and buckling failure of an ice sheet can be made with a fair degree of confidence when the ice/structure interaction leads to one of the two modes of failure. However, more work is needed to predict the forces due to multimodal ice failure.

REFERENCES

- Abdelnour, R., 1981. Model tests of multi-year pressure ridges moving into conical structures. Proceedings, IAHR Symposium on Ice, Quebec, PQ, Canada, July 27-31, Vol. II, pp. 278-749.
- Cox, G.F.N. and Weeks, W.F., 1985. On the profile properties of undeformed first year sea ice. CRREL Report prepared for the David Taylor Naval Ship R&D Center, Bethesda, MD, USA.
- Croasdale, K.R., 1980. Ice forces on fixed, rigid structures. A State-of-the-Art Report by Working Group on Ice Forces on Structures (T. Carsten, ed.) Special Report 80-26, U.S. Army Cold Regions Research and Engineering Laboratory, Hanover, NH, pp. 34-106.
- Frederking, R.G.W. and Timco, G.W., 1985. Quantitative analysis of ice sheet failure against an inclined plane. Proceedings, Fourth International Offshore Mechanics and Arctic Engineering (OMAE) Symposium, ASME, Dallas, TX, USA, Vol. II, pp. 160-169.
- Frederking, R.G.W. and Svec, O.J., 1985. Stress-relieving techniques for cantilever beam tests in an ice cover. Cold Regions Science and Technology, 11: 247-253.
- Gow, A.J., 1977. Flexural strength of ice on temperate lakes. J. Glaciology, 19(81): 247-256.

- Haynes, F.D., Sodhi, D.S., Kato, K. and Hirayama, K., 1983. Ice forces on model bridge piers. Cold Regions Research and Engineering Laboratory, Hanover, NH, CRREL Report 83-19.
- Hetenyi, M., 1946. Beams on elastic foundations. The University of Michigan Press, Ann Arbor, MI.
- Hirayama, K., 1983. Properties of urea doped ice in the CRREL test basin. U.S. Army Cold Regions Research and Engineering Laboratory, Hanover, NH, CRREL Report 83-8.
- Hirayama, K. and Obara, I., 1986. Ice forces on inclined structures. Proceedings, Fifth International Offshore Mechanics and Arctic Engineering (OMAE) Symposium, ASME, Tokyo, Japan, Vol. IV, pp. 515-520.
- Hocking, G., Mustoe, G.G.W. and Williams, J.R., 1985a. Influence of artificial island side-slopes on ice ride-up and pile-up. Proceedings, ASCE Conference Arctic '85, Civil Engineering in the Arctic Offshore, pp. 185-192.
- Hocking, G., Mustoe, G.G.W. and Williams, J.R., 1985b. Validation of CICE Code for ice ride-up and ice ridge cone interaction. Proceedings, ASCE Conference Arctic '85, Civil Engineering in the Arctic Offshore, pp. 962-970.
- Hoikkanen, J., 1985. Measurements and analysis of ice forces against a conical offshore structure. Presentation made at the Eighth International Conference on Port and Ocean Engineering under Arctic Conditions (POAC), Narssarssuaq, Greenland, September 7-14.
- Kato, K. and Sodhi, D.S., 1984. Ice action on two cylindrical structures. J. of Energy Resources Technology, 106:107-112.
- Kerr, A.D., 1978. On the determination of horizontal forces a floating ice sheet exerts on a structure. J. Glaciology, 20(82):123-134.
- Kerr, A.D., 1980. On the buckling force of floating ice plates, IUTAM Symposium on the Physics and Mechanics of Ice, Springer-Verlag, Berlin, pp. 163-178.
- Kerr, A.D. and Palmer, W.T., 1972. The deformations and stresses in floating ice sheets. Acta Mechanica, 15: 75-72.
- Krankkala, T. and M. Määttänen (1984) Methods for determining ice forces due to first- and multi-year ridges. Proceedings, IAHR Ice Symposium 1984, Hamburg, Germany, August 27-31, Vol. IV, pp. 263-287.
- Lainey, L. and Tinawi, R., 1981. Parametric studies of sea ice beams under short and long term loadings. Proceedings, IAHR Symposium on Ice, Quebec, PQ, Canada, July 27-31, pp. 607-623.
- Lainey, L. and Tinawi, R., 1983. The importance of transverse anisotropy for the bearing capacity of ice covers. Proceedings, Seventh International Conference on Port and Ocean Engineering under Arctic Conditions (POAC), Helsinki, Finland, April 5-9, Vol. 1, pp. 119-127.
- Lipsett, A.W. and Gerard, R., 1980. Field measurements of ice forces on bridge piers, 1973-1979. Alberta Research Council, Edmonton, Alberta, Canada, Report No. SWE 80-3.
- Määttänen, M. and Mustamake, E.O., 1985. Ice forces exerted on a conical structure in the Gulf of Bothnia. Offshore Technology Conference (OTC), Houston, TX.
- Michel, B. and Blanchet, D., 1983. Indentation of an S_2 floating ice sheet in the brittle range. Annals of Glaciology 4:180-187.
- Murat, J.R. and Degrange, G., 1983. Analysis of the primary flexural creep of sea ice. Proceedings, Seventh International Conference on Port and Ocean Engineering under Arctic Conditions (POAC), Helsinki, Finland, April 5-9, Vol. 1, pp. 200-211.

- Nevel, D.E., 1983. Pressure ridge forces. Proceedings, Seventh International Conference on Port and Ocean Engineering under Arctic Conditions (POAC), Helsinki, Finland, April 5-9, Vol. 1, pp. 212-220.
- Nordlund, O.P., 1985. Personal communications.
- Nordlund, O.P., Sackinger, W.M. and Yan, M., 1985. Ice features and movement north of Ellesmere Island, Canada. Proceedings, Eighth International Conference on Port and Ocean Engineering under Arctic Conditions (POAC), Narssarssuaq, Greenland, September 7-14, Vol. 1, pp. 293-304.
- Ralston, T.D., 1977. Ice force considerations for conical offshore structures. Proceedings, Fourth International Conference on Port and Ocean Engineering under Arctic Conditions, St. John's, Newfoundland, Canada, September 26-30, Vol. 2, pp. 741-752.
- Ralston, T.D., 1979. Elastic limit analysis of sheet ice loads on conical structures. Proceedings, IUTAM Symposium on Physics and Mechanics of Ice (ed. P. Tryde), Springer-Verlag, Berlin, pp. 289-308.
- Schwarz, J., 1985. Personal communications.
- Sjöblind, S.-G., 1984. Viscoelastic buckling of beams and plates on elastic foundation. Proceedings, IAHR Ice Symposium 1984, Hamburg, Germany, August 27-31, Vol. I, pp. 63-72.
- Sjöblind, S.-G., 1985. Visco-elastic buckling analysis of floating ice sheets. Cold Regions Science and Technology, 11:241-246.
- Sodhi, D.S., 1979. Buckling analysis of wedge-shaped floating ice sheets. Proceedings, Fifth International Conference on Port and Ocean Engineering under Arctic Conditions (POAC), NTH, Trondheim, Norway, August 13-18, Vol. 1, pp. 797-810.
- Sodhi, D.S., 1983. Dynamic buckling of floating ice sheets. Proceedings Seventh International Conference on Port and Ocean Engineering under Arctic conditions (POAC), Helsinki, Finland, April 5-9, Vol. 2, pp. 822-833.
- Sodhi, D.S. and Adley, M.D., 1984. Experimental determination of buckling loads of cracked ice sheets. Proceedings, Third International Offshore Mechanics and Arctic Engineering (OMAE) Symposium, ASME, New Orleans, LA, Vol. III, pp. 183-186.
- Sodhi, D.S. and Hamza, H.E., 1977. Buckling analysis of a semi-infinite ice sheet. In Proceedings, Fourth International Conference on Port and Ocean Engineering under Arctic Conditions (POAC), St. John's, Newfoundland, September 26-30, Vol. I, pp. 593-604.
- Sodhi, D.S. and Kovacs, A., 1984. Forces associated with ice pile-up and ride-up. Proceedings, IAHR Ice Symposium 1984, Hamburg, Germany, August 27-31, Vol. IV, pp. 239-262.
- Sodhi, D.S. and Nevel, D.E., 1980. A review of buckling analyses of ice sheets. A State-of-the-Art Report by the Working Group on Ice Forces on Structures, IAHR, Special Report 80-26, U.S. Army Cold Regions Research and Engineering Laboratory, Hanover, NH, pp. 131-146.
- Sodhi, D.S., Haynes, F.D., Kato, K. and Hirayama, K., 1983. Experimental determination of the buckling loads of floating ice sheets. Annals of Glaciology, Vol. 4, pp. 260-265.
- Sodhi, D.S., Morris, C.E. and Cox, G.F.N., 1985. Sheet ice forces on a conical structure: An experimental study. Proceedings, Eighth International Conference on Port and Ocean Engineering (POAC), Narssarssuaq, Greenland, September 7-14, Vol. 2, pp. 643-655.
- Tinco, G.W., 1984. Model tests of ice forces on a wide inclined plane. Proceedings, IAHR Ice Symposium 1984, Hamburg, Germany, August 27-31, Vol. II, pp. 87-96.

- Timco, G.W., 1985. Flexural strength and fracture toughness of urea model ice. Proceedings, Fourth International Offshore Mechanics and Arctic Engineering (OMAE) Symposium, ASME, Dallas, TX, February 17-21, Vol. II, pp. 199-208.
- Tinawi, R. and Gagnon, L., 1984. Behavior of sea ice plates under long-term loadings. Proceedings, IAHR Ice Symposium 1984, Hamburg, Germany, August 27-31, Vol. I, pp. 103-112.
- Tozawa, S. and Taguchi, Y., 1986. A preliminary study of scale effect on flexural strength of ice specimen. Proceedings, Fifth International Offshore Mechanics and Arctic Engineering (OMAE) Symposium, ASME, Tokyo, Japan, April 13-18, Vol. IV, pp. 336-340.
- Vaudrey, K.D., 1977. Determination of mechanical sea ice properties by large-scale field beam experiments. Proceedings, Fourth International Conference on Port and Ocean Engineering under Arctic Conditions (POAC), St. Johns, Newfoundland, Canada, September 26-30, Vol. 1, pp. 529-543.
- Verity, P.H., 1975. Small prototype cone tests, winter 1973-74. Arctic Petroleum Operator's Association, Calgary, Alberta, Canada, APOA-65.
- Wang, Y.S., 1984. Analysis and model tests of pressure ridges failing against conical structures. Proceedings, IAHR Ice Symposium 1984, Hamburg, Germany, August 27-31, Vol. II, pp. 67-76. Also Appendix to discussion of above paper, IAHR-84, Vol. III, pp. 486-491.
- Yamaguchi, E., Iwate, S., Andoh, M. and Kitazawa, T., 1986. The effects of ice-growth rate on the flexural properties of urea ice. Proceedings, Fifth Offshore Mechanics and Arctic Engineering (OMAE) Symposium, ASME, Tokyo, Japan, April 13-18, Vol. IV, pp. 293-297.
- Yoshimura, N. and Kamesaki, K., 1981. The estimation of crack pattern on ice by the new discrete model. Proceedings, IAHR Symposium on Ice, Quebec, P.Q., Canada, July 27-31, Vol. II, pp. 663-672.

A PRESSURE-AREA CURVE FOR ICE

T.J.O. Sanderson
Petroleum Engineer

BP Petroleum Development Ltd. UK
London

ABSTRACT

A wide range of published data on ice forces is presented, and peak indentation pressure is plotted as a function of (a) contact area and (b) aspect ratio. Peak pressures appear to vary inversely with square root of contact area and show some possible dependence on aspect ratio. It is difficult to account for this by arguments concerning flaws, but an explanation based on non-simultaneous failure appears promising.

1. INTRODUCTION

It is well known that as ice interacts with structures it displays a pronounced scale-effect (Kry, 1979a; Iyer, 1983; Vivatrat and Slomski, 1983; Sanderson, 1984). That is: peak pressures measured over small areas such as we test in the laboratory ($\sim 0.01 \text{ m}^2$) are higher than peak pressures over large areas such as we encounter on full-scale structures ($\sim 100 \text{ m}^2$). The first plot of pressure as a function of contact area was made by Danielewicz and Metge (1981).

Here I review a large range of published data for indentation of ice and plot it in raw form as a function of

(a) contact area

(b) aspect ratio

Both area and aspect ratio have in the literature been referred to as being responsible for a "scale-effect". They are however quite different effects, and although they may both be influential they must be distinguished.

2. INDENTATION GEOMETRY

The data plotted are for edge indentation. The tests carried out may be divided into two indentation geometries:

- I. **2-dimensional indentation** (Figure 1a), in which indentation occurs over the full thickness of an ice sample, and the stress state is biaxial.
- II. **3-dimensional indentation** (Figure 1b), in which a limited extent of the thickness is indented. In this case the stress state is triaxial.

Most tests are of type I. However, data from ice-breakers and impact hammer experiments generally fall into type II.

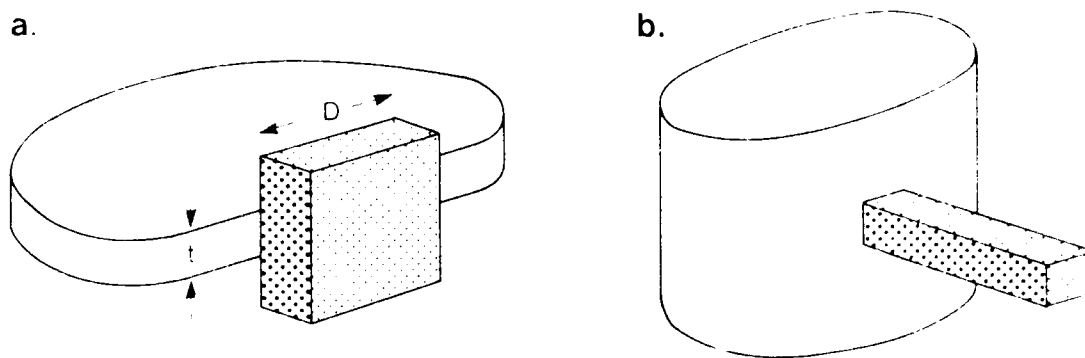


Figure 1 Two indentation geometries:

- (a) Type I, 2-dimensional edge indentation, *biaxial* stress state.
- (b) Type II, 3-dimensional edge indentation, *triaxial* stress state.

3. DATA: I - FULL THICKNESS INDENTATION

We begin with data from tests of type I, full edge indentation. The pressure-area curve for these data is shown in Figure 2. This plot shows peak pressure σ (total force P divided by contact area Dt) as a function of contact area. The data set covers a wide variety of ice types (S-2 ice, first year sea ice and multi-year ice) and a wide variety of test conditions (laboratory edge indentation, in situ jacking tests and interaction with lighthouses, offshore drilling structure and islands). None of the data are corrected in any way for temperature or salinity. Despite such indiscriminate plotting of disparate data types there is a useful general trend, as highlighted by the shaded areas in Figure 3. The data points fall naturally into 4 principal clusters, and come from the following data sources:

A. Laboratory tests

These are small-scale laboratory indentation tests performed on uniform bubble-free S-2. The data come from Hirayama and others (1974), Frederking and Gold (1975), Zabilansky and others (1975), Michel and Toussaint (1977), Kry (1979b), Michel and Blanchet (1980), and Timco (1986). They cover a range of aspect ratio (D/t) from 1.2 to 83. Note that data from Kry (1979a) are not included in

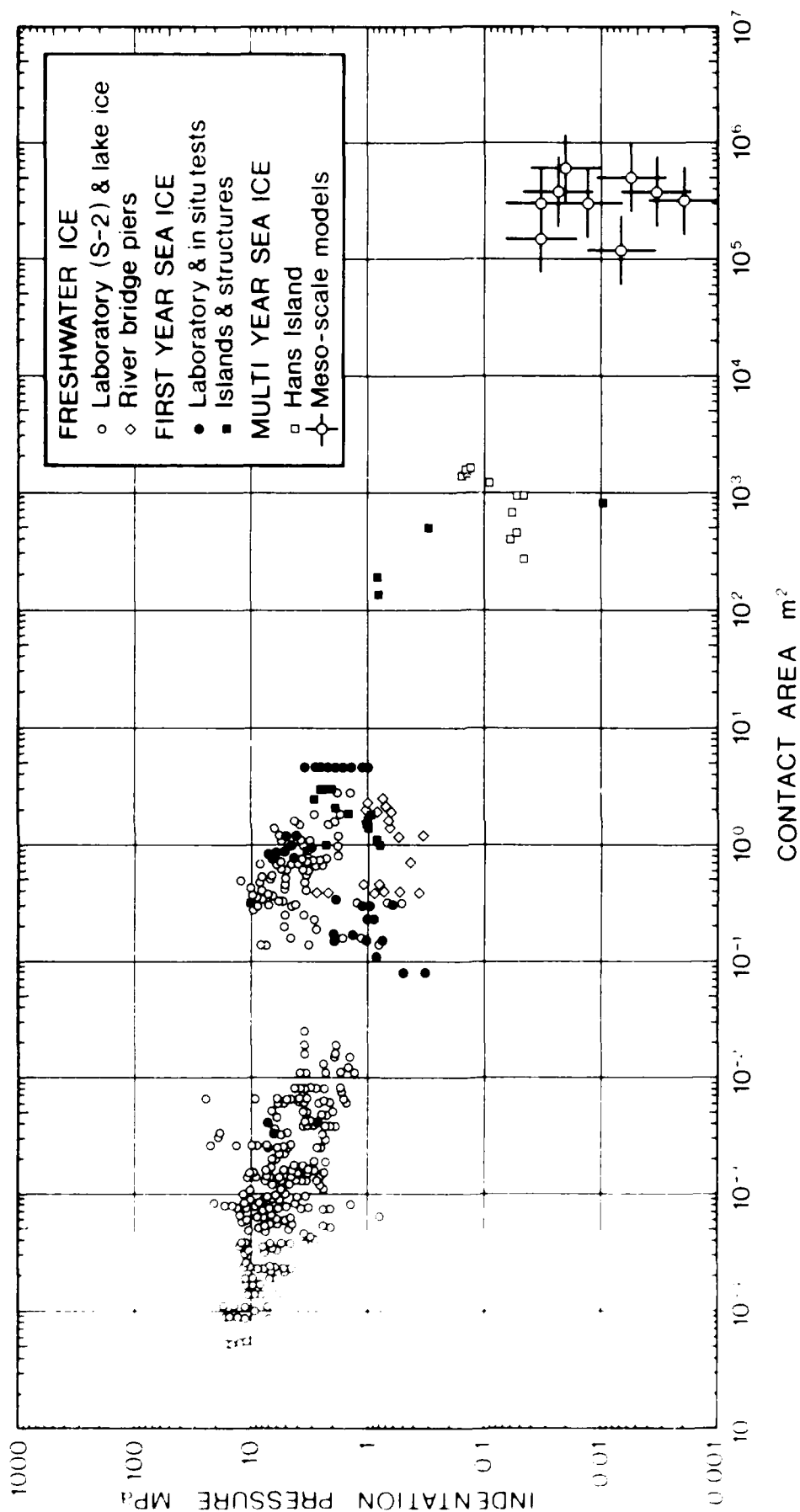


Figure 2 Plot of peak indentation pressure against contact area for type I indentation geometry. Ice types as in key.

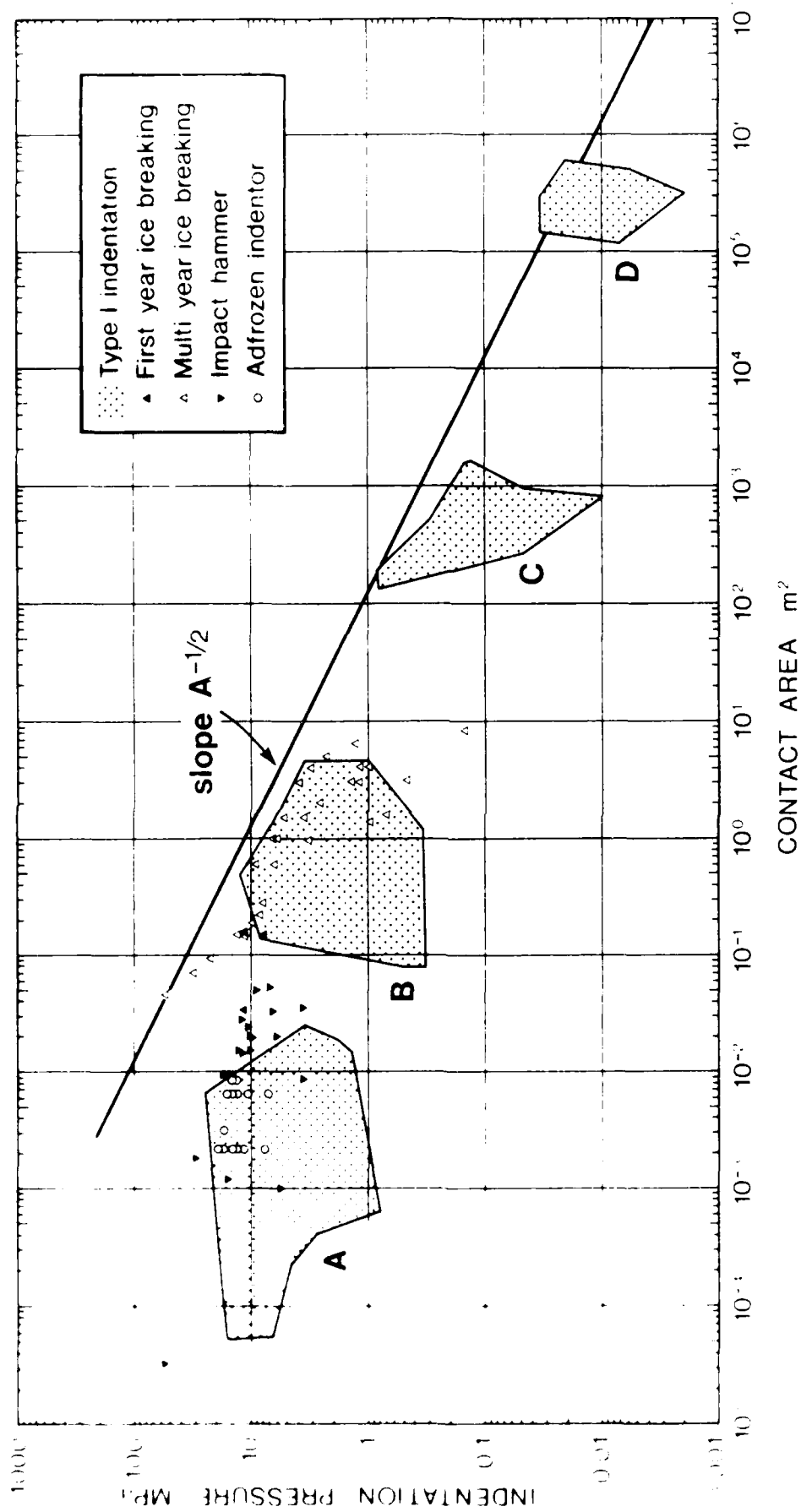


Figure 3

General trend of pressure-area curve, with data groups.

Legend:

- C: Full-scale Arctic islands and structures
- D: Meso-scale models.

Figure 2, since they were performed with ice adfrozen to the indenter. They are, however, plotted in Figure 3.

B. Medium-scale tests

These include. various in situ jacking tests performed on floating first year sea-ice, such as the "Nutcracker" tests (Croasdale, 1970, 1971), the Exxon large-scale strength tests (Lecourt and Benze, 1980, 1981) and Inoue and Koma (1985); tests on floating freshwater lake ice (Croasdale, 1971; Taylor, 1973; Miller and others, 1974; Nakajima and others, 1981); measurements on river bridge piers (Lipsett and Gerard, 1980); and sea ice data from lighthouses (Määttänen 1981; Engelbrektson, 1983) and Cook Inlet structures (Elenkarn, 1970).

C. Full-scale islands

This data group comes from Beaufort Sea artificial islands surrounded by floating first-year ice (Metge, 1976; Strilchuk, 1977; Johnson and others, 1985) and from the first (1980) Hans Island programme (Danielewicz and Metge, 1981). Data from the second and third Hans Island programmes (Danielewicz and Metge, 1982; Danielewicz and Cornett, 1984) are at present still proprietary but may of course be added to the plot as they become available.

D. Meso-scale models

In the course of modelling the large-scale dynamics of the Arctic Ocean and its ice cover it is necessary to make assumptions about the gross "compressive strength" of polar pack ice (Pritchard, 1977, 1980; Hibler, 1980a, 1980b). The models used are generally based on a grid-size of 40-125 km, in which ice movement is modelled as a function of wind and sea current. Compressive strength (load per unit length of ice cover) is a parameter which can be adjusted in order to obtain a plausible match with observed behaviour. Values obtained in this way are generally in the range $5 \times 10^4 - 10^5 \text{ Nm}^{-1}$, and refer to pack ice of highly variable thickness. In general the

mean ice thickness lies in the range 2.6 ~ 4.0 m, though it is likely that ice strength is controlled by areas of thinner ice (Rothrock, 1975). It is not clear over what distance the large-scale ice strength is effectively averaged (Croasdale, 1984) but for present purposes we shall assume a length equal to the model grid-size spacing. Thickness is assumed equal to average thickness, yielding areas of the order 10^5 m^2 . Ice strength values are plotted from Pritchard (1977, 1980), Hibler (1980a, 1980b) and Tucker and Hibler (1981). Because there is considerable doubt over the ice thickness and distance scale to which these results refer, the data points used have been plotted with error bars representing a range of a factor of 2.

4. DATA: II - TRIAXIAL INDENTATION

Tests involving icebreakers and impact hammers generally involve a degree of triaxial confinement: they are of type II, and involve geometry resembling that of Figure 1(b). Pressures measured during such tests might be expected to be higher than those of type I. Figure 3 shows a variety of such tests superimposed on the general trend of the data groups of Figure 2. The data sources are as follows:

E. Icebreakers and impact hammer

Data are included from icebreakers impacting first-year ice (St. John and Daley, 1984; St. John and others, 1984; Kujala and Vuorio, 1985) and impacting multi-year ice (Ghoneim and Keinonen, 1983; Glen and Blount, 1984; St. John and Daley, 1984; St. John and others, 1984; Edwards and others, unpublished). Results are also plotted for impact hammer tests (Glen and Comfort, 1983).

In addition, I have added to this plot the data from Kry (1979a), in which the ice was adfrozen to the indenter.

5. DISCUSSION: ASPECT RATIO OR SCALE ?

The plots of failure pressure versus contact area (Figures 2 and 3) provide an apparently clear picture of scale dependence. The addition of

points derived from icebreaker tests (Figure 3) only slightly alters the picture: as expected, at small contact areas while indenting thick multi-year ice (Glen and Blount, 1984), high degrees of confinement occur and lead to higher local pressures. In general an upper bound curve with dependence of approximately

$$p \propto A^{-\frac{1}{2}}$$

provides an empirical fit to the data, at least for contact areas exceeding 0.1 m^2 . A line of this slope is shown in Figure 3.

We see that for all tests carried out at full-scale on islands, (group C, areas exceeding 100 m^2), measured pressures have been less than 1 MPa, 10-100 times less than those at laboratory scale.

The question arises, could this instead be an effect of aspect ratio rather than size? The answer is unfortunately not clear-cut. Figure 4 shows all the data of the pressure-area curve (Figure 2) plotted instead

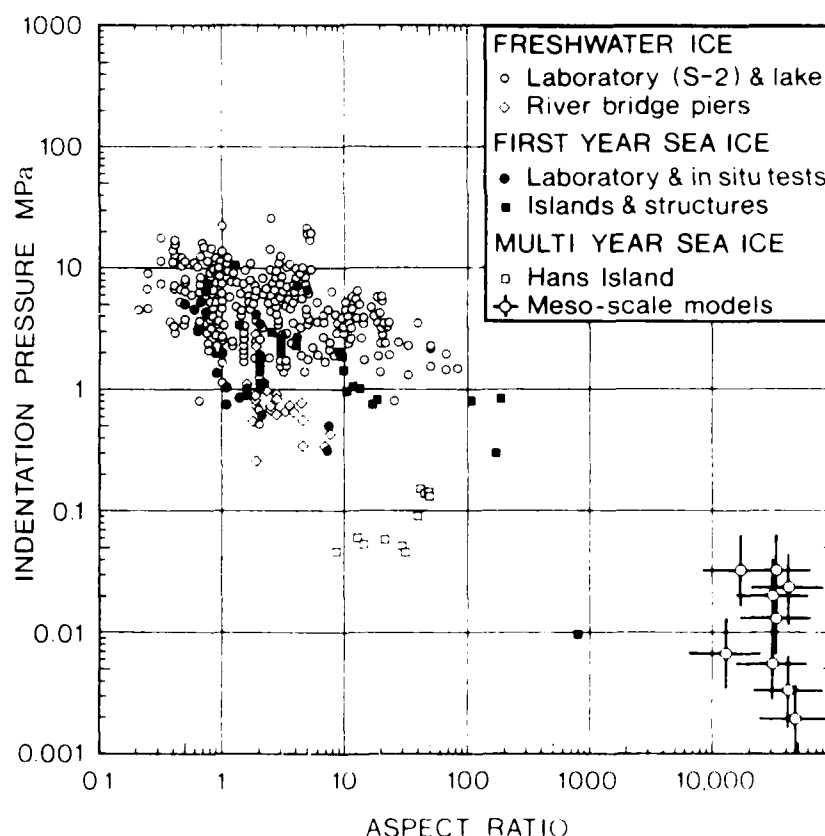


Figure 4 Plot of peak indentation pressure against aspect ratio D/t , for type I indentation geometry. Icebreaker and impact hammer data is omitted.

as a function of aspect ratio D/t . The picture is more confused than that of Figure 2, but again shows a perceptible trend, with peak pressures generally falling off with increasing aspect ratio.

It is not, however, an unambiguous dependence on aspect ratio, since the only points available for very high aspect ratio (D/t greater than 100) happen also to be points from very large size tests (areas exceeding 100 m^2). This can be seen in Figure 5, where the points of Figure 4 are subjected to the same grouping (A, B, C and D), as in Figure 3. The results from Kry (1979a) are also included. The following points emerge:

1. Data groups C and D show generally lower pressures than groups A and B, but it is ambiguous whether this is due to higher aspect ratio or to large contact area.
2. Aspect ratio is certainly not the only factor responsible for the stress reduction observed. For instance, at aspect ratio

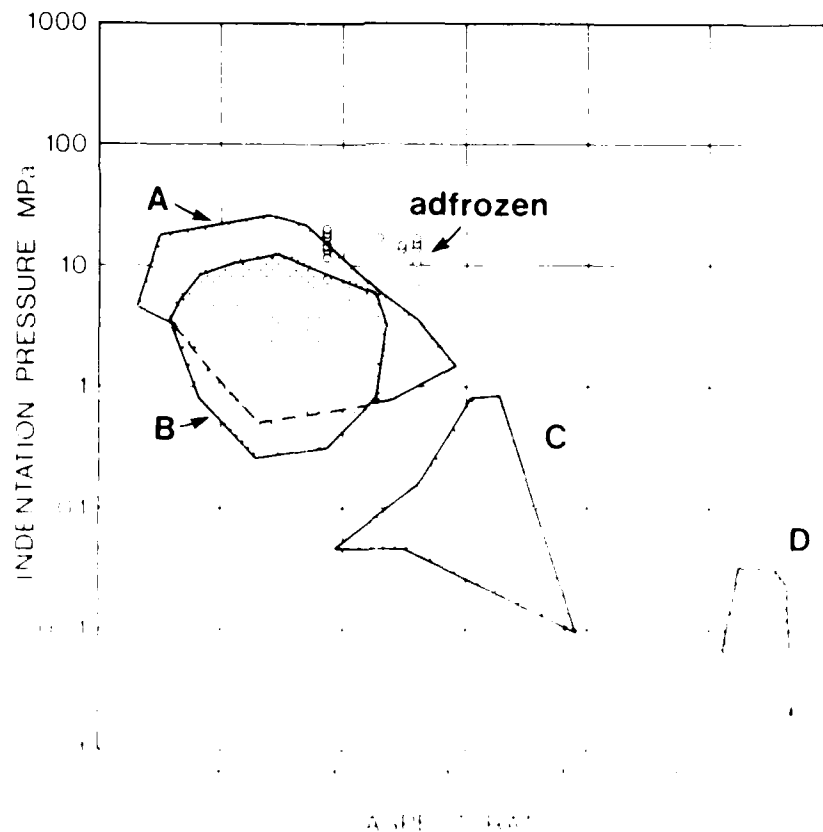


Figure 5

Indentation pressure as a function of aspect ratio for the data groups A, B, C and D, as defined in Figure 3. The results from Kry (1979a) are also included.

approximately 10, peak stresses anywhere between 0.05 MPa and 6.5 MPa are observed - and the lower stresses are generally associated with increasing contact area.

3. The data from Kry (1979a), in which ice was adfrozen to the indenter, appear not to show any dependence on aspect ratio. This is significant and lends weight, as we shall see in Section 6, to the argument that scale effects, whether as a function of size or of aspect ratio, may be due to effects of imperfect contact and non-simultaneous failure.

6. THEORETICAL BASIS FOR SCALE EFFECTS

6.1 Flaws

It is easy to call up general arguments to demonstrate why a brittle material such as ice should display a scale effect (Iyer, 1983; Sanderson, 1984; Bazant and Kim, 1985). The arguments generally concern, either explicitly or implicitly, the existence of flaws in the material, and tacitly make the assumption that flaws increase in size as sample size increases. The sample thus becomes weaker. It is worth making it perfectly clear what these assumptions are, since they are often hidden.

Consider the compressive failure of a laboratory sample of ice containing a population of flaws. The flaws may be micro-cracks, grain boundaries, or any other imperfection which is shown to behave as a flaw. The theory of compressive fracture of a flawed sample is given by Hallam (1986, this volume). For illustration let us suppose the sample to be cubic of side 1 cm, to have regular flaws of size 1 mm and a compressive strength of 1 MPa. The sample is then tested under uniaxial compression. A strength of this magnitude can be explained quite well by linear elastic fracture mechanics (Hallam, 1986).

Now consider that an identical test is performed on a sample 100 times the size. There are two simple assumptions which can be made about scaling of the sample. They are shown in Figure 6(a) and (b).

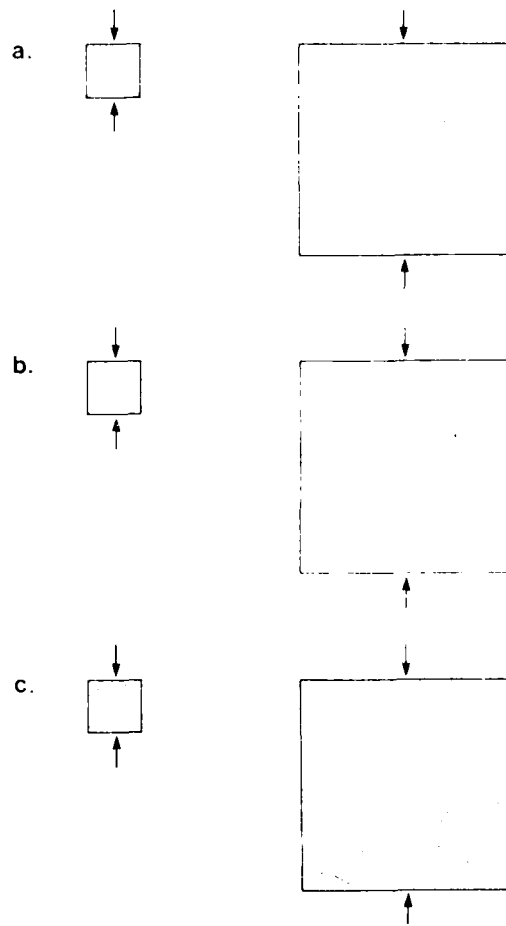


Figure 6 *Scaling assumptions: (a) Material remains uniform*
 (b) Geometric scaling of sample and material
 (c) Statistical distribution of flaws

(a) Constant flaw size

Firstly, assume that the material of which the sample is made really remains precisely the same (Figure 6(a)) and continues to contain a population of regular flaws of size 1 mm. In this case, a simple fracture mechanics analysis would show that the compressive strength remained unchanged, at 10 MPa: flaws remain the same size and so the stress required to propagate them remains the same.

(b) Geometric scaling

If, instead, the whole sample is strictly scaled up geometrically, its imperfections included (Figure 6(b)), then the larger sample will contain

flaws 100 times larger, that is, 100 mm long. In this case a fracture mechanics analysis (or indeed a simple dimensional analysis) will show that if the linear dimensions of the sample increase by a factor λ then the fracture strength will decrease by a factor $\lambda^{-1/2}$, (see, for instance, Bazant and Kim, 1985). The strength of the sample should therefore decrease by a factor of 10. Although this is a convenient demonstration of a strength reduction of the order required, it is facile to claim that it is a true explanation, for use of the geometric scaling law contains the bold physical assumption that a larger sample contains larger flaws. This may in fact be true, but if it is, it requires experimental proof and cannot just be assumed. It would in fact be most odd if doubling sample size automatically precisely doubled flaw size: it actually implies that the material has changed. Nonetheless, it is interesting to note that this explanation is still not quite sufficient to explain the observed reduction of stress with area: simple scaling would imply

$$\sigma \propto \lambda^{-1/2} \text{ or } A^{-1/4}$$

while in fact we observe approximately (as in Figure 3):

$$\sigma \propto A^{-1/2}$$

(c) Statistical effects

Another class of scaling is shown schematically in Figure 6(c). This contains the more realistic starting assumption that any material contains a statistical population of flaws of various sizes. On selecting a sample of larger size there is then a higher chance of it containing flaws from the tail-ends of the statistical distribution. There is thus a higher chance of it containing larger flaws. This argument, developed originally by Weibull (1951) is apparently powerful, but was developed principally for tensile fracture where the "weakest link" concept applies and a single controlling flaw is enough to lead to complete failure. This is not obviously true of compressive fracture. However, if compressive strength behaves in the same way we should expect strength to be a function of volume V of the form,

$$\sigma \propto V^{-1/b} \text{ or } A^{-1/2b}$$

where b is a statistical parameter characterising the flaw size distribution. In terms of area $A \propto \lambda^2$ this reduces to

$$\sigma \propto A^{-3/2b}$$

So by experiment b is of the order of 3 if the Weibull treatment is appropriate. This is consistent with values of 2-5 experimentally determined by Gold (1972).

Again, the statistical argument summarised here needs both further development and the provision of proof that flaws really do exist and behave in an appropriate statistical fashion.

It is worth looking at the approximate flaw sizes required for the argument to work:

- (i) Small-to-medium scale tests (groups A & B of Figure 3) show failure pressures of approximately 10 MPa. Assume that failure is controlled by flaws of size approximately 1-5 mm (this corresponds, for instance, to grain size).
- (ii) Large scale tests, group C, show failure pressure of approximately 0.5 MPa - a 20-fold reduction. On a simple fracture mechanics argument, this would be achieved by flaws 400 times as big, or in the range 40-200 cm. There is, however, no positive evidence that a sufficiently large number of flaws of this size do indeed exist in naturally occurring first-year and multi-year ice covers. If the argument from flaws is to be believed, the existence of these flaws needs to be established.
- (iii) Meso-scale models, group D, show strength of the order 0.01 MPa, or 1,000 times less than groups A & B. This would imply flaws of size 1-5 km. Large as this may seem, it is actually quite realistic, since on the scale of the entire Arctic Ocean, it is likely that open leads and individual floes of size several kilometres do indeed behave as flaws. Any flight across the Arctic Ocean will confirm that a sufficient number of such flaws apparently exist.

6.2 Non-simultaneous failure - size effect

Several authors have presented analyses of the statistics of non-simultaneous failure (Kry, 1980; Slomski and Vivatrat, 1983). These analyses make use of the hypothesis that large-scale failure occurs by successive fracture of independent zones (Figure 7a). The treatment is probabilistic and looks at the statistical sum of individual stress time series for a large number of zones. The statistical sum results in a "smearing" of peak stresses and the conclusion that peak stresses over a large multi-zone area should be lower than over the area of a single zone. The manner of the reduction depends on the details of the statistics used.

More recently, Ashby and others (1986) have presented an alternative approach to non-simultaneous failure which is based on a simple mechanical argument and backed up by experiments with brittle foams. As we shall see, it gives a realistic dependence on contact area. I emphasize, however, that the argument is simplistic, and makes assumptions which require experimental support. It proceeds as follows.

Consider an irregular block of thickness t in contact with an indenter of width D (Figure 7). Assume that it can be idealised as a set of cubical independent cells of dimension L . As each cell comes into contact with the indenter, assume that a distance Δ can be moved before the cell fails (this might correspond to critical displacement before flexural failure or to critical strain before crushing failure - it does not matter). Let the average force during this period of contact be F_L over the area L^2 of the cell concerned. Now, the probability, p of a particular cell area being in contact is

$$p = \Delta/L$$

(where Δ is very much less than L , so that p is small). In the total area of contact $A = Dt$, the number of cell areas n is

$$n = A/L^2 \quad (1)$$

Now simple probability theory (Ashby and others, 1986) can be used to show that the expected number of contacting cells within the area A is np

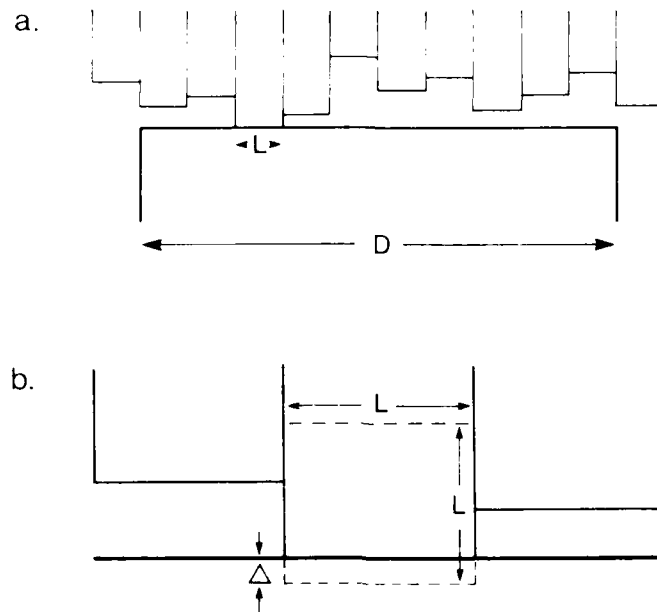


Figure 7 (a) Non-simultaneous failure

(b) Detailed geometrical assumptions and definitions for analysis by Ashby and others (1986).

and the standard deviation is approximately $(np)^{\frac{1}{2}}$. If we take the 3-standard deviation level as a reasonable extreme case, the maximum number of areas simultaneously in active contact is approximately:

$$np + 3(np)^{\frac{1}{2}} \quad (2)$$

or using equation (1) and (2),

$$\frac{A \Delta}{L^3} \left(1 + 3 \left(\frac{L^3}{A \Delta} \right)^{\frac{1}{2}} \right)$$

The total force F resulting is then

$$F = \frac{F_L A \Delta}{L^3} \left(1 + 3 \frac{L^3}{A \Delta} \right)^{\frac{1}{2}}$$

and the indentation pressure p is

$$p = \frac{F}{A} = \frac{F_L \Delta}{L^3} \left(1 + 3 \frac{L^3}{A \Delta} \right)^{\frac{1}{2}} \quad (3)$$

Notice that the second term of the equation demonstrates the observed functional dependence on the inverse square root of area.

them). Nonetheless, this does seem to present a plausible model of observed behaviour. Note that for very large contact areas, the stress levels off (here, to approximately 0.33 MPa), which is rather higher than that found in meso-scale models.

The model has, however, many shortcomings, and should not be regarded as a complete explanation. Its defects are:

1. No satisfactory physical description of the zonal failure process is given: the model is purely mechanical.
2. It is assumed that a failed zone clears perfectly, allowing a drop to zero stress.
3. The value of L has been fitted: work is needed to derive it as a function of a physical model of failure (for instance flexure).
4. The statistical approach to peak stress is arbitrary: the selection of 3 standard deviations from the mean needs justification or refinement.

6.3 Non-simultaneous failure -- aspect ratio effect

It is interesting to investigate the model of Ashby & others (1986) a little further, and investigate the possibility of aspect ratio effects.

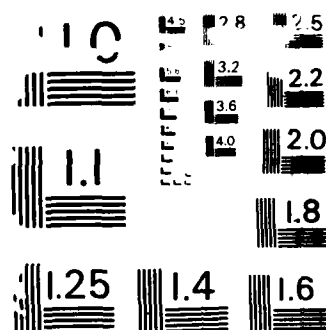
In the treatment of Section 6.2 above, we assumed that non-simultaneous failure occurred in discrete zones of size L , whose size is independent of the size of ice feature concerned. The selection of a constant value for L was quite arbitrary.

Suppose instead that zone size is a function of ice thickness. A reasonable assumption if, for instance, failure is controlled by flexural mechanism. For simplicity, put $L = t$, and assume that the distance Δ moved before failure is a constant proportion, λ , of the zone size. Assume that each cell fails at a pressure $\hat{\sigma}$, which we assume, as before, to be 15 MPa. The resulting formula, then, in terms of aspect ratio:

WORKING GROUP ON ICE FORCES; STATE-OF-THE-ART REPORT
(3RD)(U) COLD REGIONS RESEARCH AND ENGINEERING LAB
HANOVER NH T J SANDERSON SEP 87 CRREL-87-17

NL

UNCLASSIFIED



RESOLUTION TEST CHART
NATIONAL BUREAU OF STANDARDS-1963-A

$$\sigma = \hat{\sigma} \lambda \left(1 + 3 \left(\frac{t}{\lambda D} \right)^{\frac{1}{2}} \right) \quad (5)$$

or, in terms of thickness and contact area:

$$\sigma = \hat{\sigma} \lambda \left(1 + 3 \left(\frac{t^2}{A \lambda} \right)^{\frac{1}{2}} \right) \quad (6)$$

Equation (6) generates a family of pressure area curves for different values of thickness t . For illustration, four of these curves are shown in Figure 9(b), for thicknesses 0.01, 0.1, 1.0 and 10 m. They are compared with Figure 9(a) which shows data groups of the pressure area curve classified in the same manner according to thickness. It can be seen that there is a plausible resemblance between theoretical curves and the data set, but some significant departures:

1. Very high pressures (15 MPa) are predicted for thick ice (1-10 m) over areas of (1-100 m²). Such pressures have not been observed, though this may be due to absence of data.
2. Poor agreement is apparently obtained for very small areas (thickness 0.01 m and areas 10⁻⁴ - 10⁻³ m²). Predicted pressures are too low.

There is obviously room for more investigation here. Non-simultaneous failure appears to be a fruitful line of explanation, but many questions remain unanswered.

7. CONCLUSIONS AND RECOMMENDATIONS

1. Experimental evidence from a wide range of sources shows that ice failure pressure is strongly size-dependent.
2. Peak pressures appear to be proportional to approximately the inverse square root of contact area.
3. Some dependence on aspect ratio is also apparent, but aspect ratio effects alone cannot account for the scale dependence observed.

We can, for illustration, now put reasonable constants into this equation and fit it to the observed data. First, suppose $L \sim 1$ m, which is the order of size of ice fragment typically observed in the Arctic after a failure event. Secondly, assume that F_L , the force required to fail a single cell area, is 15 MN (a pressure of 15 MPa, as generally observed for data groups A & B). Now, we know that for area $A = 200$ m² the peak stress is approximately 0.8 MPa (group C). Substituting into Equation 3, we can infer that we need $\Delta = 0.02$ m, or 2 cm. This represents the distance a cell can move before failure, and 2 cm seems a reasonable value. The resulting formula is then

$$\sigma = 0.33 \left(1 + \frac{20.3}{\sqrt{A}} \right) \quad (4)$$

which is valid for $A \gg L^2$. For areas less than or equal to L^2 we expect pressure of the order of a single zone failure pressure, or 15 MPa. This resulting theoretical curve is shown in Figure 8, plotted over the data of Figure 2. Note that the treatment is not strictly valid for $A \sim L^2$.

It will be seen that it agrees well with the observed data (which is not very surprising, since it is to a large degree empirically fitted to

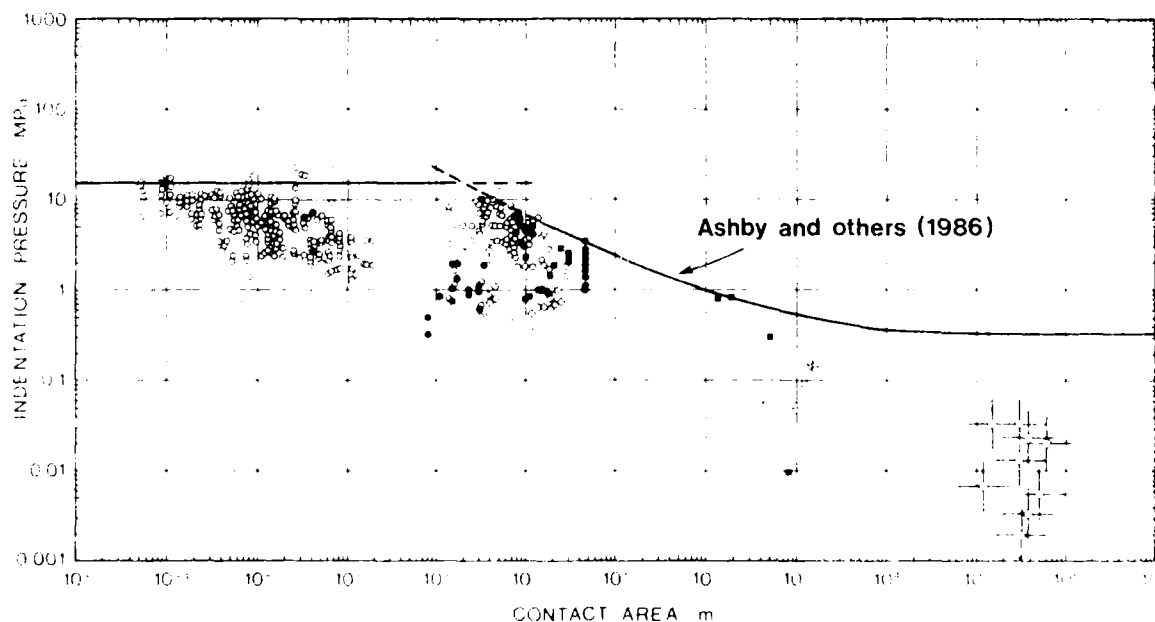


Figure 8 Theoretical curve of Ashby and others (1986), constrained to bound the observed data. The curve uses $L = 1$, $F_L = 15$ MN and $\Delta = 0.02$ m.

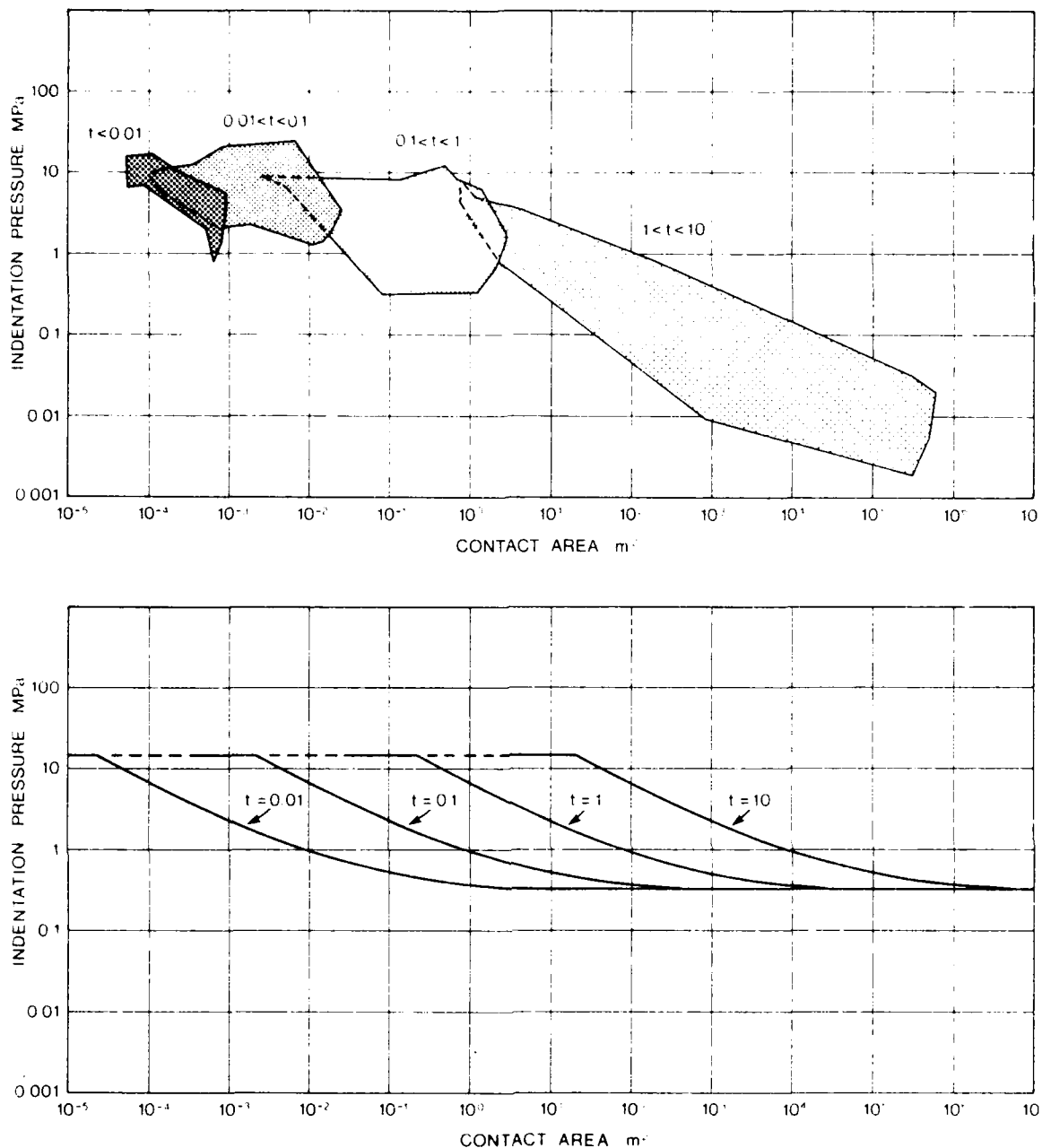


Figure 9 Aspect ratio effects:

- (a) Pressure area curve data grouped according to ranges of ice thickness.
- (b) A set of theoretical curves derived on the assumption that ice fails in units of size of the order of the ice thickness, t , in metres.

4. Arguments concerning flaws require the existence of large flaws. If the arguments are to be taken seriously, the existence of the flaws must be demonstrated.

5. A simple mechanical argument based on non-simultaneous failure provides a plausible explanation. However, it is in need of refinement and physical verification.

6. Gaps in the data set exist in two ranges of contact area:

(i) $0.01 - 0.1 \text{ m}^2$

(ii) $5 - 100 \text{ m}^2$

Experiments should be performed to fill these gaps - especially in range (ii).

7. In order to resolve the question whether size or aspect ratio is responsible for the scale effect, it is desirable to have tests performed at large size ($\sim 100 \text{ m}^2$) but low aspect ratio (1 or 2). Unfortunately this may not be technically feasible.

8. **ACKNOWLEDGMENTS**

I thank the British Petroleum Company p.l.c. for permission to publish this paper.

REFERENCES

- Ashby, M.F., and others, 1986. Non-simultaneous ice failure and ice loads on large structures, by M.F. Ashby, A.C. Palmer, M. Thouless, D.J. Goodman, S.D. Hallam, S.A.F. Murrell, N. Jones, T.J.O. Sanderson and A.R.S. Ponter. In: *Proceedings of the 1986 Offshore Technology Conference, Houston, Texas, May, 1986.*
- Bazant, Z.P., and Kim, J-K., 1985. Fracture theory for non-homogeneous brittle materials with application to ice. In: *Civil Engineering in the Arctic Offshore, Proceedings of the Conference Arctic '85*, ed. F.L. Bennett and J.L. Machemehl, San Francisco, March 25-27, 1985, p.917-930.
- Blenkarn, K.A., 1970. Measurement and analysis of ice forces on Cook Inlet Structures. In: *Proceedings of the 1970 Offshore Technology Conference, Houston, Texas, April 22-24, 1970*, OTC 1261, p.365-378.
- Croasdale, K.R., 1970. The "Nutcracker" ice strength tests. APOA Project No. 1.
- Croasdale, K.R., 1971. The "Nutcracker" ice strength tests. APOA Project No. 9.
- Croasdale, K.R., 1984. The limited driving force approach to ice loads. In: *Proceedings of the 16th Annual Offshore Technology Conference, Houston, Texas, May 7-9, 1984*, OTC 4716.
- Danielewicz, B.W., and Metge, M., 1981. Ice forces on Hans Island, August, 1980. APOA Project No. 180.
- Danielewicz, B.W., and Metge, M., 1982. Ice forces on Hans Island, 1981. APOA Project No. 181 (Restricted).
- Danielewicz, B.W., and Cornett, S., 1984. Ice forces on Hans Island, 1983. APOA Project No. 202 (Restricted).
- Edwards, R.Y., and others, Unpublished. *Ship's hull as a test instrument*, by R.Y. Edwards, W. Tam and A.M. Nawwar. Arctic Canada Ltd.
- Engelbrektson, A., 1983. Ice force design of offshore structures. In: *Proceedings of the International Conference on Offshore and Marine Technology, Gothenburg, March 1-4, 1983.*
- Frederking, R., and Gold, L.W., 1975. Experimental study of edge loading of ice plates. *Canadian Geotechnical Journal*, Vol. 12, No. 4, p.456-463.
- Choneim, G.A.M. and Keinonen, A.J. 1983. Full-scale impact tests of Canmar Kigoriak in thick ice. In: *Proceedings of the 7th International Conference on Port and Ocean Engineering under Arctic Conditions (POAC)*, Helsinki, April, 5-9th, 1983, Vol. 3, p. 329-346.

- Glen, I.F., and Blount, H., 1984. Measurement of ice impact pressures and loads onboard CCGS Louis St. Laurent. In: *Proceedings of the 1984 ASME Symposium, New Orleans, February 12-14, 1984*, Vol. 3, p.246-252.
- Glen, I.F., and Comfort, G. 1983. Ice impact pressure and load: Investigation by laboratory experiments and ship trials. In: *Proceedings of the 7th International Conference on Port and Ocean Engineering under Arctic Conditions (POAC)*, Helsinki, April 5-9th, 1983, Vol. 1, p. 516-533.
- Gold, L.W., 1972. The process of failure of columnar-grained ice. *Philosophical Magazine*, Vol. 26, No. 2, p.310-328.
- Hallam, S.D., 1986. The role of fracture in limiting ice forces. In: *Proceedings of the 8th International Symposium on Ice, IASH, Iowa City, August 18-22, 1986*, (this volume).
- Hibler, W.D., 1980a. Modelling a variable thickness ice cover. *Monthly Weather Review*, Vol. 108, No. 12, p.1943-1973.
- Hibler, W.D., 1980b. Modelling pack ice as a viscous-plastic continuum: some preliminary results. In: *Sea ice processes and models*, ed. R.S. Pritchard, Seattle and London, University of Washington Press, p. 163-176.
- Hirayama, K., and others, 1974. *An investigation of ice forces on vertical structures*, by K. Hirayama, J. Schwarz and H.C. Wu. Iowa City, IIHR Report No. 158 (University of Iowa).
- Inoue, M., and Koma, N., 1985. Field indentation tests on cylindrical structures. In: *Proceedings of the 8th International Conference on Port and Ocean Engineering under Arctic Conditions (POAC)*, Narssarsuaq, September 7-14, 1985, Vol. 2, p.555-568.
- Iyer, S.H., 1983. Size effects in ice and their influence on the structural design of offshore structures. In: *Proceedings of the 7th International Conference on Port and Ocean Engineering Under Arctic Conditions (POAC)*, Helsinki, April 5-9, 1983, Vol. 3, p.414-432.
- Johnson, J.B., and others, 1985. Kadluk ice stress measurement programme by J.B. Johnson, G.F.N. Cox and W.B. Tucker. In: *Proceedings of the 8th International Conference on Port and Ocean Engineering under Arctic Conditions (POAC)*, Narssarsuaq, September 7-14, 1985, Vol. 1, p.88-100.
- Kry, P.R., 1979a. High aspect ratio crushing tests. *APOA Project No. 93*
- Kry, P.R., 1979b. Stress distribution during continuous crushing of ice. *APOA Project No. 148*

- Kry, P.R., 1980. A statistical prediction of effective ice crushing stresses on wide structures. *Proceedings of ASCE Convention and Exposition, Portland, 14-18 April, 1980. Preprint No. 80-084.*
- Kujala, P., and Vuorio, J., 1985. On the statistical nature of the ice-induced pressures measured on board I.B. Sisu. In: *Proceedings of the 8th International Conference on Port and Ocean Engineering under Arctic Conditions (FOAC), Narssarssuaq, September 7-14, 1985. Vol. 2, p.823-837.*
- Lecourt, E.J., and Benze, D.J., 1980. Large-scale ice strength tests, 1980. *Report by ARCTEC Inc. to Exxon.*
- Lecourt, E.J., and Benze, D.J., 1981. Large-scale ice strength tests, 1981. *Report by ARCTEC Inc. to Exxon.*
- Lipsett, A.W., and Gerard, R., 1980. *Field measurements of ice forces on bridge piers, 1973-1979. Alberta Research Council Report No. SWE 80-3, Edmonton.*
- Metge, M. 1976. Ice conditions and ice defence at Netserk B-44 and Adgo P-25 during the winter of 1974-75. *APOA Project No. 66.*
- Michel, B., and Toussaint, N., 1977. Mechanisms and theory of indentation of ice plates. *Journal of Glaciology, Vol. 19, No. 81, p.285-300.*
- Michel, B., and Blanchet, D., 1983. Indentation of an S2 floating ice sheet in the brittle range. *Annals of Glaciology, Vol. 4, p.180-187*
- Miller, T.W., and others, 1974. Ice crushing tests, by T.W. Miller, A. McLatchie, R. Hedley and G. Morris. *APOA Project No. 66.*
- Määttänen, M., 1981. Experiences with vibration isolated lighthouses. In: *Proceedings of the 6th International Conference on Port and Ocean Engineering under Arctic Conditions (FOAC), Québec, July 27-31, 1981, Vol. 1, p.491-501.*
- Nakajima, H., and others, 1981. The ice force acting on a cylindrical pile, by H. Nakajima, N. Koma and M. Inoue. In: *Proceedings of the 6th International Conference on Port and Ocean Engineering under Arctic Conditions (FOAC), Québec, July 27-31, 1981, Vol. 1, p.517-525.*
- Pritchard, R.S., 1977. The effect of strength on simulations of sea ice dynamics. In: *Proceedings of the 4th Conference on Port and Ocean Engineering under Arctic Conditions, St. John's Newfoundland, 1977, p. 494-505.*
- Pritchard, R.S., 1980. A simulation of nearshore winter ice dynamics in the Beaufort Sea. In: *Sea Ice Processes and models*, ed. R.S. Pritchard, Seattle and London, University of Washington Press, p.49-61.

- Rothrock, D.A., 1975. The energetics of the plastic deformation of pack ice by ridging. *Journal of Geophysical Research*, Vol. 80, No. 33, p.4514-19.
- St. John, J.W., and Daley, C., 1984. Shipboard measurement of ice pressures in the Bering, Chukchi and Beaufort Seas. In: *Proceedings of the 1984 ASME Symposium, New Orleans, February 12-14, 1984*, Vol. 3, p.260-266.
- St. John, J.W., and others, 1984. Ice loads and ship response to ice, by J.W. St. John, C. Daley and H. Blount. *Report No. SR-1291*, Arctec Inc., Columbia and Arctec Canada Ltd., Kanata.
- Sanderson, T.J.O., 1984. Theoretical and measured ice forces on wide structures. In: *Proceedings of the 7th International Symposium on Ice, IAHR, Hamburg, August 27-31, 1984*. Vol. 4, p.151-207.
- Slomski, S., and Vivatrat, V. 1983. Selection of design ice pressures and application to impact load prediction. In: *Proceedings of the 7th International Conference on Port and Ocean Engineering under Arctic Conditions (POAC), Helsinki, April, 1983*. Vol. 2, p.909-919.
- Taylor, T.P., 1973. Ice crushing tests 1973. *APOA Project No. 52*.
- Timco, G.W., 1986. Indentation and penetration of edge-loaded freshwater ice sheets in the brittle range. In: *Proceedings of the 5th International Symposium on Offshore Mechanics and Arctic Engineering (OMAE), Tokyo, April, 1986*. (Preprint).
- Tucker, W.B., and Hibler, W.D., 1981. Preliminary results of ice modelling in the East Greenland area. In: *Proceedings of the 6th International Conference on Port and Ocean Engineering under Arctic Conditions (POAC), Québec, July 27-31, 1981*. Vol. 2, p.867-878.
- Vivatrat, V., and Slomski, S., 1983. A probabilistic basis for selecting design ice pressures and ice loads for Arctic Structures. In: *Proceedings of the 1983 Offshore Technology Conference, Houston, Texas, May 2-5, 1983*. OTC 4457.
- Weibull, W., 1951. A statistical distribution function of wide applicability. *Journal of Applied Mechanics*, Vol. 18, p.293-297.
- Zabilansky, L.V., and others, 1975. Ice forces on model structures, by L.J. Zabilansky, D.E. Nevel and F.D. Haynes. *Canadian Journal of Civil Engineering*, Vol. 2, p.400-417.

ICE SCOUR SURVEYS, STATISTICS AND FORCES

by

T.R. Chari	Faculty of Engineering & Applied Science	St. John's
	Memorial University of Newfoundland	Newfoundland
		Canada
J.V. Barrie	Centre for Cold Ocean Resources Engineering	A1B 3X5
	Memorial University of Newfoundland	

ABSTRACT

The problem of scouring by icebergs and ridge keels is of concern in the planning and design of seabed installations for the offshore oil industry. Side scan sonar surveys, observations using manned submersibles, evaluation of the geological and geotechnical properties, and mathematical and physical modelling of the scour processes are some of the methods currently used for understanding the problem of iceberg scours. The different postulations of scour mechanics and the results of observations in different geological environments are reviewed in this paper. Iceberg-seabed interactions also induce forces under the keel which create additional stresses on structures buried below the zone of maximum observed scours. This is an area of research to be pursued. A brief review is given on the ongoing DIGS (Dynamics of Iceberg Grounding and Scouring) experiments.

INTRODUCTION

Iceberg scours are observed over much of the Canadian Atlantic continental shelf. Iceberg interaction with the seabed to create linear scour marks was hypothesized by Charles Darwin (1855) and has been identified in the offshore by the development of sidescan sonar technology in the 1970's. Iceberg scour marks appear in the form of linear to curvilinear furrows and as pits, and occur over the entire eastern Canadian continental shelf from Baffin Bay to the Scotian Shelf down to water depths of greater than 700 m. These marks vary markedly in size and morphology and can occur as seabed furrows up to 200 m wide, 10 m deep and over 10 km in length.

Ice scours are formed by one of two agents which are significant in seabed disturbance - icebergs and sea ice pressure ridge keels.

Ice ridges originate from the rafting of sheets of sea ice under pressure, which produce keels of a few metres to a few tens of metres deep. These rarely exceed 40 m depth even in Arctic Ocean waters. Thus, they are significant in seabed disturbance on shallow continental shelves and in nearshore waters (Pelletier and Shearer 1972, Reimnitz and Barnes 1974, Kovacs and Mellor 1974, Wadhams 1975, Shearer and Blasco 1975, Lewis 1978, Wahlgren 1979, Vilks 1979, Reimnitz and Kempena 1982, Weeks et al 1983). On the other hand, thick glaciers and ice shelves which calve in deep waters produce large icebergs with drafts commonly in the range of 100 to 200 m (Dinsmore 1982, Hotzel and Miller 1983) or even larger (Murray 1969). These keels are the principal agents for ice-related disturbance of sediments on the offshore banks of eastern Canada (Fig. 1). The resultant scours have been defined from sidescan sonar records on the Scotian Shelf (King 1980), the western Grand Banks (King 1976), northwestern Grand Banks (Amos and Barrie 1980, Fader and King 1981, Lewis and Barrie 1981) Belle Isle Bank and the Labrador Shelf (Harris and Jollymore 1984, Gustajtis 1979, Barrie 1980, Josenhans and Barrie 1982, Syvitski et al 1983, Pereira et al 1985). On the Antarctica shelf also, similar scours are found (e.g. Orheim et al 1979, Lien 1981).

RELICT AND RECENT SCOURS

Although many scour marks are considered to be modern, many more are interpreted as being relict, dating from an earlier geological period. Their longevity is apparent from studies of ancient (Pleistocene) scours found in Norwegian Trough (Belderson et al 1973) and shelf (Lien 1983).

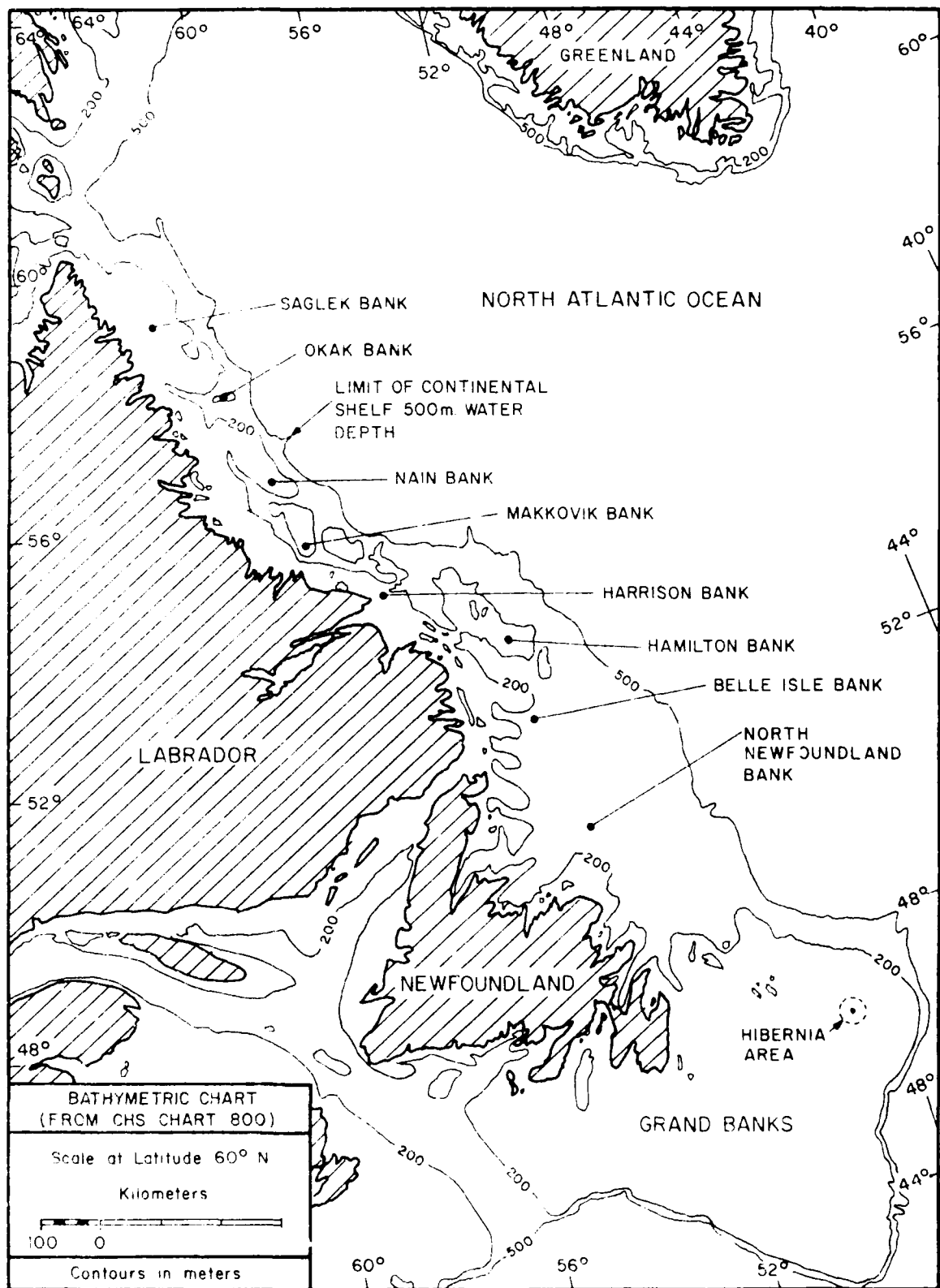


FIG. 1. CANADIAN EASTERN CONTINENTAL SHELF

in the North Sea (Stroker and Long, 1983), off the west coast of British Columbia (Claternauer and Murray 1983), on Chatham Rise off New Zealand at 43 S (Kurdass and Rad 1984), in the Beaufort Sea (Lewis 1978), in the Laurentian Channel and western Grand Banks (King 1976), on the northwestern Grand Banks (Fader and King 1981, Lewis and Barrie 1981) and on the Labrador Shelf (Gustafjis 1979, Barrie 1980, Todd 1984).

These studies demonstrate clearly that scour marks can persist for several thousands of years. Evidence also exists, however, that scours can be eroded rapidly in areas of the continental shelf exposed to dynamic sedimentological conditions (Barrie 1983).

Traditionally, floating icebergs were considered as a hazard to shipping. There have also been reported instances of damage to transatlantic submarine telecommunication cables attributed to deep-drafted icebergs scouring the ocean floor. Twenty-five such damages have been reported between 1960 and 1976 (Gustafjis 1979, Green 1984). With the recent offshore oil finds and the proposed development of the Hibernia field, scouring icebergs are a great hazard to seabed structures such as wellheads, distribution pipe lines, anchors, and mooring systems.

Icebergs not only scour the seafloor as they approach shallowing bathymetry, they also scour downslope (Barrie 1980, Woodworth-Lynas et al 1985) due to the ability to increase draft up to 50% (Bass and Peters 1984). Modern iceberg keel draft distributions show a mean maximum draft and grounding depth of 220 m (Holzel and Miller 1983). In water depths shallower than this depth, there are two principal concerns for seabed installations. Firstly, the return period or frequency of iceberg scouring for any given area, and secondly, the depth of burial below which a modern iceberg should not scour, nor will the forces transmitted by the pressure be to the buried structure.

In areas of intense scouring, stratification in the sedimentary deposits is destroyed and the resulting iceberg turbate (Vorren et al 1983) carries the area to a depth equivalent to the deepest scour. The geotechnical properties of the soil will also then be altered for bulky bottom structure production caissons. Further, the modification of bottom morphology by scour channels will affect the routing, design and construction of production pipelines (Holt 1982).

There are two independent but complementary directions in the current research on iceberg scour, one is the observation and analysis of actual scours and the other is the mathematical and physical

understanding of the mechanics of iceberg scouring.

The analysis of change in scour morphology is important for several fundamental reasons. Firstly, the dimensions of many scour marks are used in statistical analysis for determining the mean of extreme scour penetrations and for iceberg scour return periods. Morphological dimensions, such as depth and width, determined from acoustical geophysical records, will be in error due to degradation unless the processes can be quantified. Secondly, scour marks can act as benchmarks against known processes of sediment erosion. This analysis may be undertaken by examining the interrelationship of scour marks and sedimentary bedform features; subsequently, the age of a scour can be determined from the age of the bedforms. Alternatively, sediment transport can be quantified if the scour mark is of known age. These techniques are useful in examining both the modern scouring and its setting in terms of the sediment dynamic regime. Thirdly, ancient scour populations may degrade to such an extent that only residual features or turbate is left, and these are a key to their origin.

A study of the mechanics of ice-seabed interaction is necessary for estimating the maximum design burial depths for seabed installations. A mathematical analysis of the scour mechanics is also relevant in establishing the validity of the measured depths of modern scours vis-a-vis the largest icebergs observed, the geotechnical and geological properties of the seafloor, the general bathymetry, the environmental forces, and the bottom dynamics.

MECHANICS OF SCOURING

When an ice keel comes in contact with the seafloor, it may either become grounded and cease to move on, or if the environmental driving forces, dominantly currents or pressure from the surrounding sea ice can overcome seabed resistance to ploughing, the entrenched berg may continue forward to create a flat-bottomed trough that is commonly referred to as a scour.

Several hypotheses have been suggested for the mechanics of iceberg-seabed interaction and formation of scours. One such hypothesis (Chari and Allen 1972, Chari 1975) is that deepest scours will occur when the seabed has a low shear strength (Fig. 2) and the iceberg is relatively very strong. The scouring process was modelled as a up-slope ploughing phenomenon (Fig. 3) in which the soil in front is heaved up in

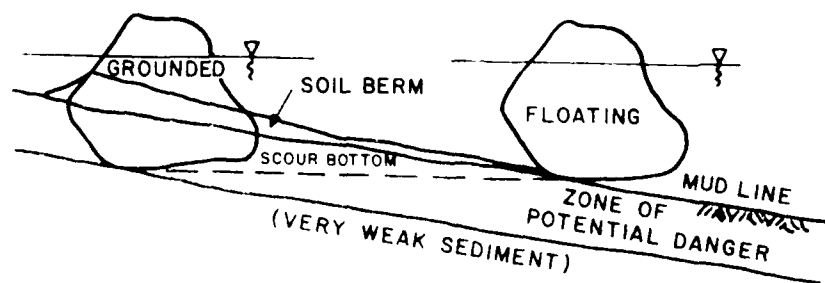


FIG. 2. HORIZONTAL PLOUGHING IN WEAK SEDIMENT

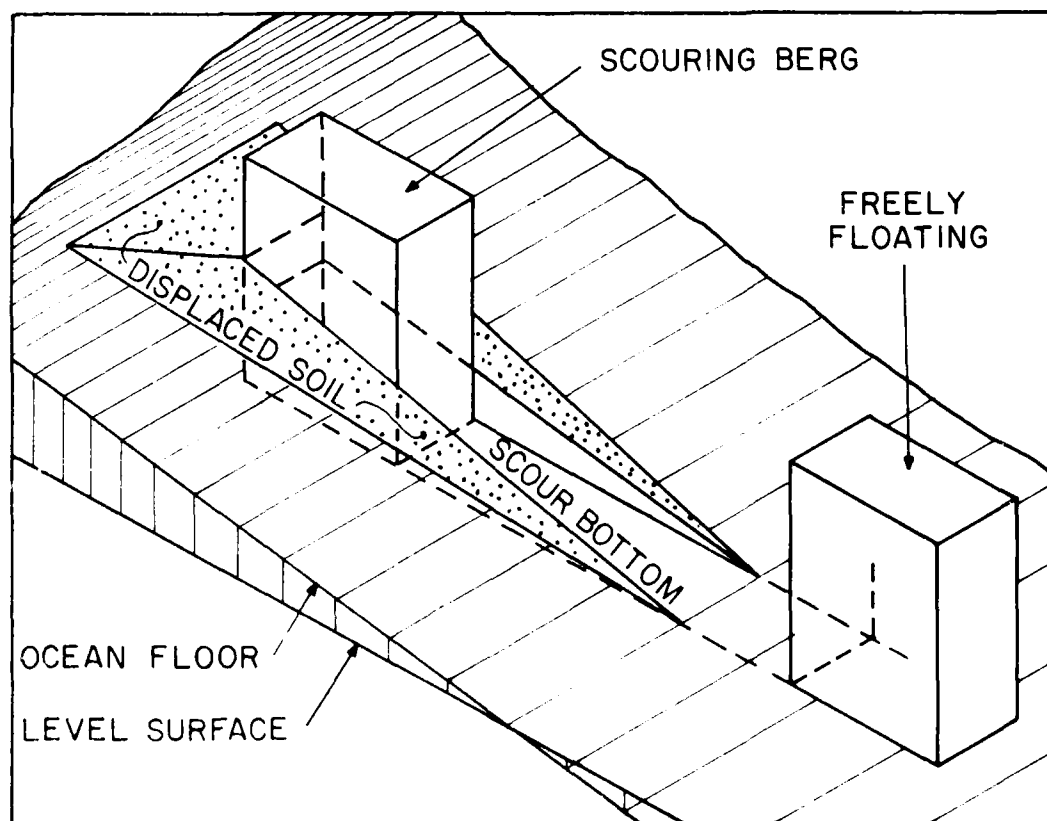


FIG. 3. MATHEMATICAL MODEL OF A SLOPE PLOUGHING

a series of passive failure rupture surfaces and displaced to the sides as the iceberg progressively moves forward. When the kinetic energy is dissipated, the iceberg becomes grounded. Several refinements have been made to the above hypothesis, to take into account the hydrodynamic drag of the currents (Chari 1979, Lopez et al 1981) and the type of seabed sediments (Chari and Peters 1981, Chari and Green 1981). A similar analytical study has been published with some refinement to the soil model and with particular reference to the sea ice keels in the Beaufort Sea (Fenco 1975, Kivisild 1981).

The above type of soil-iceberg interaction has also been extensively verified through physical laboratory models (Chari 1975, Arctec Canada 1980, Green 1984, Prasad 1985). The long flat-bottomed scour trenches observed on the seabed with raised shoulders on both sides can be easily explained by the foregoing theory. The forces transmitted into the soil by the passing keel were also estimated (Green and Chari 1981, Green et al 1983) so that seabed installations could be designed for these forces or buried below the zone of iceberg influence.

From the perspective of design engineers requiring a knowledge of absolutely safe burial depths below which a modern iceberg should not scour, this hypothesis is likely to give a satisfactory answer. Some variations of the up-slope scouring, (Fig. 4 and 5) have been discussed (Chari et al 1980), but considered as not critical for engineering design.

Side scan sonagrams and recent observations using a submersible (Barrie et al 1986) show scour features which are not always rectilinear. The physical explanation of these features is a topic of recent iceberg scour studies.

When an iceberg is drifting at a constant speed, it is in a steady-state motion. Since there is no relative velocity between the iceberg and the environmental force field around, there is no net force on the moving body. As soon as the iceberg touches the seabed there is a force resisting the forward motion of the berg. As a result of the deceleration of the iceberg, there is a relative velocity between the iceberg and the surrounding environment. Forces are thus induced (Fig. 6) such as current drag, wind drag, and ice push (if there is an icefield around). The effect of waves may be ignored, as these are secondary and negligible. For a stable iceberg which scours up-slope, the soil resistance will continually increase, the iceberg will gradually slow

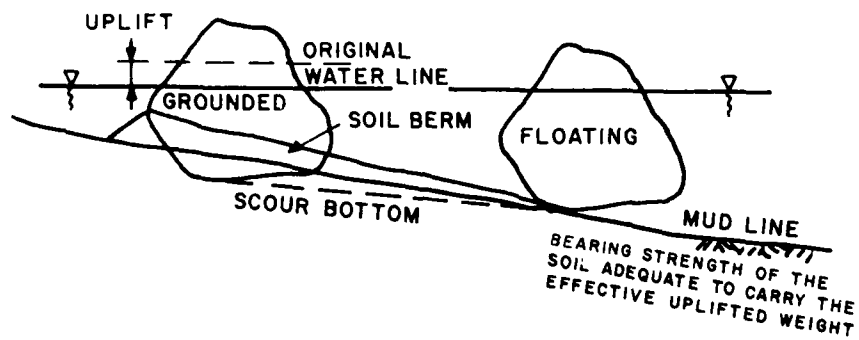


FIG. 4. LINEAR SCOURING ACCOMPANIED BY ICEBERG UPLIFT

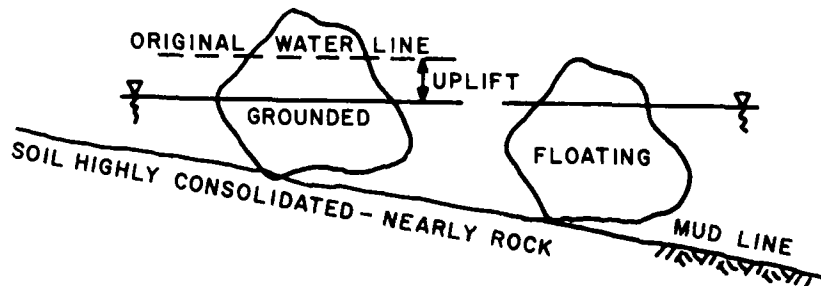


FIG. 5. ICEBERG GROUNDING ON HIGHLY CONSOLIDATED SEABED

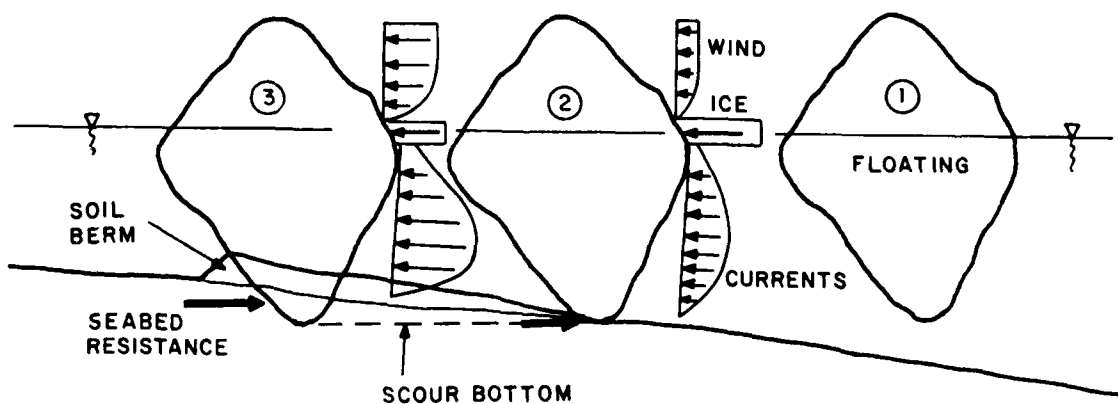


FIG. 6. ENVIRONMENTAL FORCES ON A SCOURING ICEBERG

down, and the environmental forces will also progressively increase. When the iceberg is finally grounded, the seabed resistance will be equal to the environmental forces (Fig. 7).

Icebergs continually undergo melting and assume new positions of equilibrium. If an iceberg is close to instability before contacting the seabed, it may become unstable and roll (Fig. 8) over as soon as the seafloor offers resistance. Such an iceberg could create a deep pit, and get grounded. If the kinetic energy of the iceberg is large and the depth of initial seabed penetration is small, the iceberg would move forward after creating a pit (Chari and Prasad 1986). The resulting feature would be a scour trench of finite length, with a pit at the head of the scour track.

Sometimes, parts of an iceberg break off along natural cleavage planes in the process of melting. Such icebergs may roll over and the resulting draft of the iceberg may increase by as much as 50% (Bass and Peters 1984). Those icebergs could also cause pits on the seafloor (Clark et al 1986) or a pit accompanied by a scour track.

The dynamic process of roll over by an unstable iceberg is complex. Before the iceberg reaches a new equilibrium, it will be subjected to vertical harmonic motions. Thus, an iceberg which causes a deep pit as soon as it overturns, may follow through causing a relatively shallow, long and flat scour track (Fig. 8). Several other hypotheses can be postulated for a rolling iceberg based on the above concept to explain down-slope scours, pit chains, and other variations and combinations thereof. For design purposes, iceberg pits are localized events and have to be assessed from statistical evaluation of actual observations and supported by other data such as iceberg sizes, geotechnical properties of the seabed, and other environmental factors in that location.

The assumption of an infinitely strong iceberg is appropriate for purposes of evaluating the depth below which the seabed will not be disturbed. However, icebergs have planes of natural cleavage along which failure often occurs. If the seabed resistance is greater than the iceberg strength along its planes of weakness, it is likely that the iceberg will break and float freely, after leaving a segment of the iceberg grounded. Such a process has been discussed by Clark et al (1986).

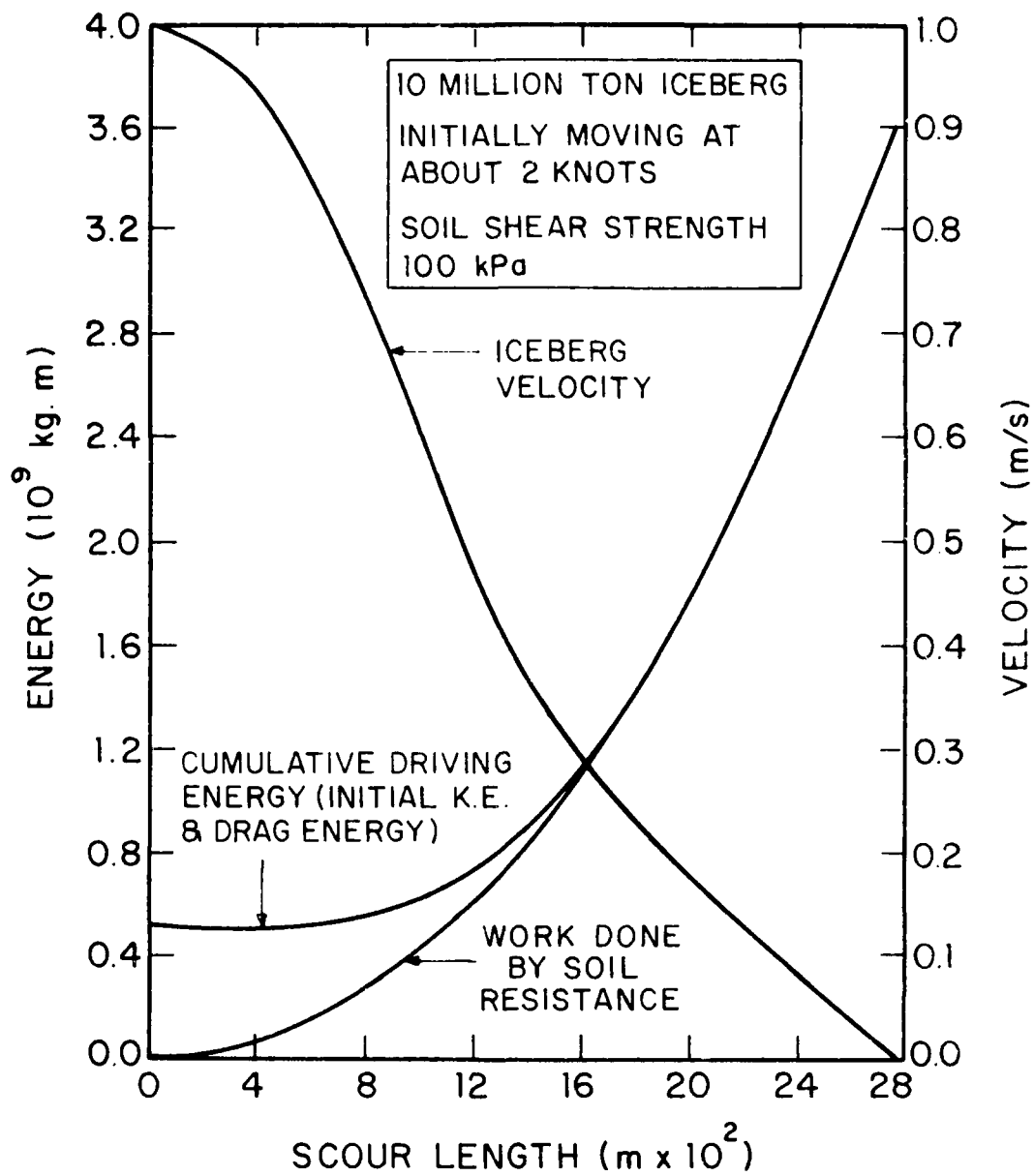


FIG. 7. ENERGY EXPENDED BY A SCOURING ICEBERG

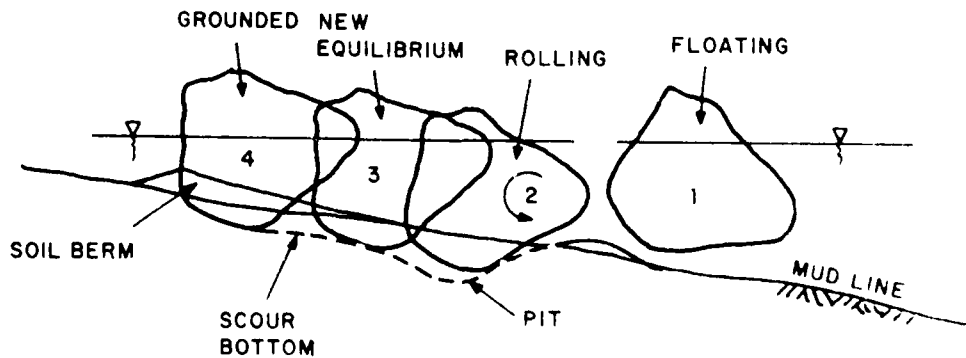


FIG. 8. MECHANICS OF PIT FORMATION, ACCOMPANIED BY A LINEAR SCOUR PROFILE

The processes of ice scour formation in the Beaufort Sea by sea ice pressure ridge keels are somewhat similar to those discussed earlier. However, the predominant driving force is the moving sea ice cover while the ocean currents are considered to be the major factor in the Labrador Sea.

SCOUR ENVIRONMENTS AND FEATURES

Three distinctive environments of iceberg scours have been defined from regional geophysical surveys and submersible observations for the eastern Canadian Atlantic shelf (Barrie 1983). These environments reflect different soil types which are partially a result of different surficial sediment origins.

Scour marks in stiff clays have been observed to have steep rims (berms or embankments), with slope angles up to 60° and scour penetration depths up to 6 m and greater. Submersible observations off Cumberland Sound in Baffin Bay (MacLean 1982) have demonstrated the nature of these steep-sided deeply-penetrated scours. Another area where similar geomorphological scour relief occurs is southern Saglik Bank in the Labrador Sea (Barrie 1980, Todd 1984, Josenhans et al 1985, Gilbert and Barrie 1985). Iceberg scours on the seabed of southern Saglik Bank above 170 m water depth cover 70-100% of the entire seabed surface. The predominantly long, linear to curvilinear scour marks occur with average penetration depths of 3 m, widths of 30 m and lengths of several kilometres.

Scour marks development in bouldery material are characterised by concentrations of large boulders in the rims associated with a finer matrix of gravel and sand in the troughs. The reliefs of such marks are from 1 to 4 m and slope angles are up to 15° (Lewis et al 1982). Submersible observations in this type of environment have been made in areas of the northeast Newfoundland shelf (Syvitski et al 1982) and from areas of Hamilton Bank on the southern Labrador Shelf (Collins and Diemand 1982). Typically, the sediments in these regions are silty sands which are poorly sorted and contain a high percentage of boulders, cobbles and pebbles.

Scour marks developed over areas of thin surficial cover, over semi-consolidated or consolidated bedrock or hard till, show concentrations of boulders, cobbles, pebbles and sand in their rims and have a relief of only 1 to 2 m, with slope angles of 5° or less (Barrie 1983).

examples are Makkovik Bank (Josenhans and Barrie 1982, Gilbert and Barrie 1985) where thin sands overlie a consolidated till (Josenhans et al 1985) and the northwestern Grand Banks (Fader and King 1981, Lewis and Barrie 1981) where a thin Quaternary section of sand and gravel overlies Tertiary sediments (Barrie et al 1984). Iceberg scours in both areas have average widths of 35 m and penetration depths usually less than 2 m. Iceberg pits and pit chains are as common as linear scours in this environment. Some appear overdeepened, a result of subsequent soil failure (Barrie et al 1986).

SCOUR RATES, SEABED DYNAMICS AND DEGRADATION

The iceberg scour record for the foregoing three model environments is representative of the geological history of the region since the last glaciation; it also indicates the extent to which both relict and modern sedimentary processes affect the areas. The dimensions of the scours in the three cases are consistent with the scour hypotheses discussed earlier for those geotechnical environments.

The number of modern scour events varies with water depth and location. Woodworth-Lynas et al (1985) predict a grounding/scouring rate for Saglek Bank of 4.3% and for Makkovik Bank 3.3% of all bergs in one season based on iceberg observations from drilling platforms. Iceberg scouring rates on the Grand Banks drop to less than 1% (d'Apollonia and Lewis 1985). Josenhans and Zevenhuizen (1984), using a series of oriented bottom photographs along a 6 km transect show a well-defined 'fresh' keel mark cut through a lag gravel into the underlying muddy sand and gravel (diamict) substrate of Makkovik Bank. Similar observations were made on transects of Nain and Saglek Banks (Josenhans and Zevenhuizen 1984), suggesting that present-day scouring is, indeed, a frequent occurrence within the shoal areas (i.e. 85-200 m). Using rough calculations based upon the above scour frequency for Saglek Bank, Woodworth-Lynas et al (1985) predict that 110 million m³ of seabed material is reworked by this process each year. This is reduced greatly on the Grand Banks of Newfoundland.

Although iceberg scour longevity is apparent over most of the shelf, recent scours are degraded rapidly by the bottom dynamics of some of the areas. The cohesiveness and physical properties of sediments also significantly influence the scour preservation potential.

Barrie (1983) demonstrated that wave induced sediment transport is one of the most effective agents in scour degradation. Barnes and Reimnitz (1979) also observed the significance of waves in conjunction with currents in eroding ice scour ridges in the Beaufort Sea as did Kobayashi (1982) in the southern Beaufort Sea.

Consequently, in water depths less than 160-180 m, the character of the seabed is a product of the excavation and reworking of the seabed by icebergs, and the removal of excavated material and incorporation of it into the sediment transport budget. In areas where scour mark obliteration by bottom currents exceeds the excavation by iceberg ploughing, the seafloor (as seen from sidescan sonar records) will appear to show little evidence of iceberg impact thus falsely suggesting a low incidence of iceberg grounding. Conversely where the obliteration rate is low, for the same number of groundings, many well-preserved scour marks will appear on the seabed, which can be misinterpreted to indicate a higher rate of incidence. Estimates of the rate of iceberg groundings, from seafloor observations must carefully consider, therefore, the modern sediment dynamics. A mathematical model to determine populations of iceberg scour depths (Gaskill et al 1985) requires an input relating to the quantitative values of scour infill rates.

OBSERVATIONS OF SCOURING EVENTS AND ONGOING RESEARCH

Although iceberg scour marks on the continental shelf are attributed to iceberg interaction with the seabed, as defined above, few observations of an iceberg making contact with the seabed and creating an identifiable scour have been documented in the literature. In many cases, known groundings have been related indirectly to an iceberg scour that has been detected by acoustical geophysical means subsequent to the scour event.

An example of direct observation is a blocky iceberg code-named Caroline (Lewis and Barrie 1980) (Fig. 9) which was established as being grounded on the shoal area of Saglek Bank in August, 1979 during continuous iceberg tracking using the radar on CSS HUDSON (Fillon 1979). The berg grounded in 118 m of water, the inferred draft. The iceberg appeared to have been ploughing a singular and finally double keeled scour towards the east with an average scour depth of less than 0.5 m and a maximum scour width of 45 m (Fig. 9). The scour occurred in an area of overconsolidated till (Unit 3A) with overlying patches of sand (Josenhans

et al 1985). The double keeled scour converged eventually at the end of the scour track, demonstrating the possible rotation of the scouring iceberg. The scour was resurveyed in 1982 (Fig. 9) using the same BIO 70 kHz sidescan sonar. An iceberg scour such as this provides a benchmark from which change in scour morphology can be monitored. If a new scour in similar soil types can be further examined by use of a manned submersible, direct observations of both scour formations can be made and compared. In August 1985, the PISCES IV submersible off the MV PANDORA II provided such an opportunity.

During the Dynamic Iceberg Scouring and Grounding Experiment (DIGS) (Lewis et al 1985, Josenhans et al 1985), the Caroline scour was relocated and a new scour was identified cross-cutting it. Both scours were examined from the PISCES IV submersible. The 1979 scour had undergone considerable modification by currents and macrobenthos. Results from this major program will be published in the near future.

Further work on mathematical and physical modelling is also in progress to estimate the forces below the scour due to keel pressures during scouring.

SUMMARY

The type of scour features formed on the seafloor depend on the geological, geotechnical, and environmental phenomena. Observations of existing scour marks show qualitative correlation between those variables. Further coordinated research to quantify the measurements should lead to refined estimates for purposes of design of seabed installations.

ACKNOWLEDGMENTS

The authors acknowledge the continued support provided by Dr. C.F.M. Lewis and several of his colleagues at the Bedford Institute of Oceanography in the various field programs. Funding for the theoretical and laboratory studies was provided through research grants from the Natural Sciences and Engineering Research Council of Canada. Thanks are due to Miss Moya Grouchy for organizing and typing this paper.

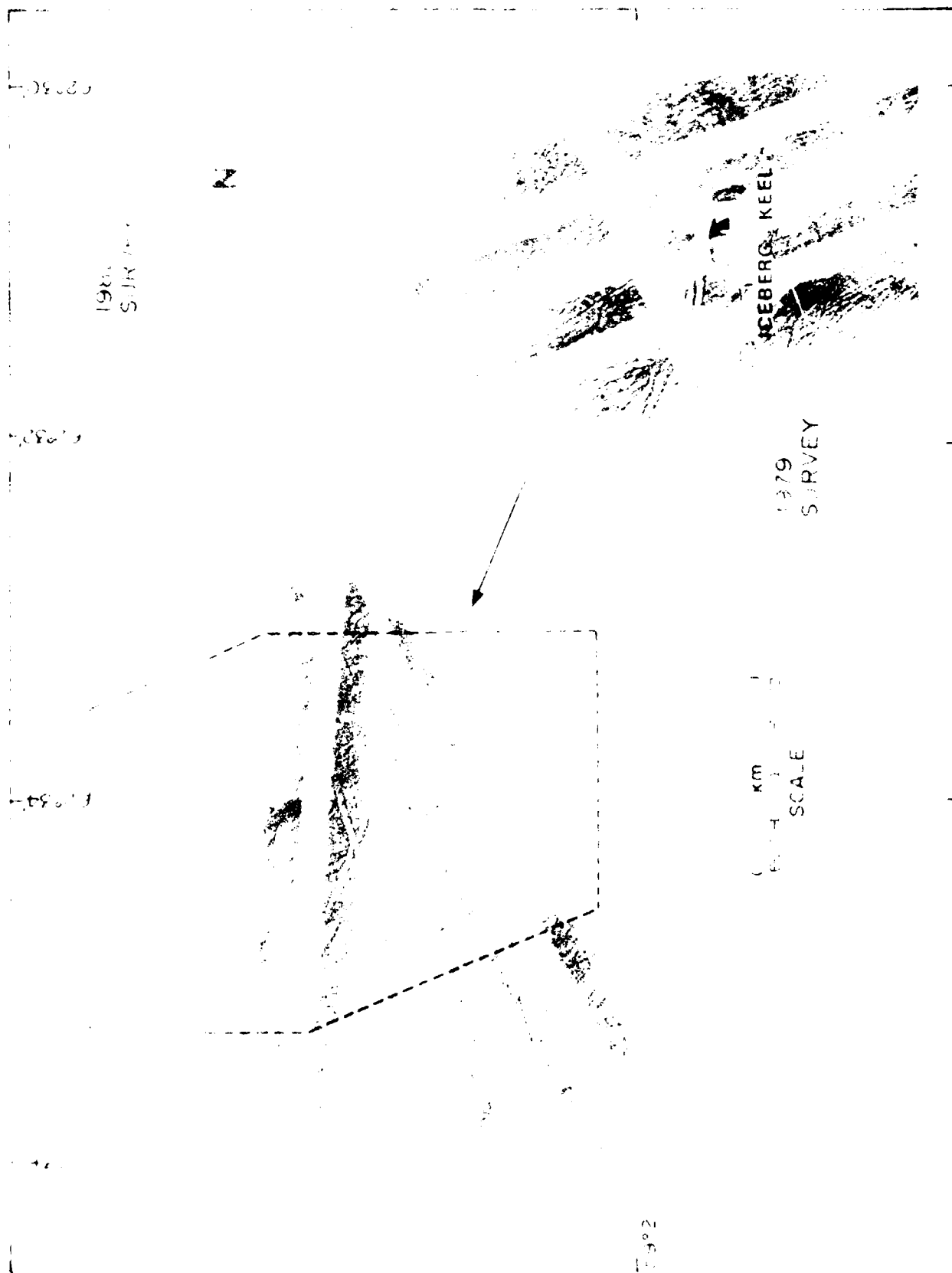


FIG. 9. OBSERVATIONS OF "CAROLINE SCORER", 1979 AND 1980 SURVEY.

REFERENCES

- Amos, C.L. and Barrie, J.V. (1980): "Hibernia and Ben Nevis Seabed Study - POLARIS V Cruise Report", June 1980, C-CORE Data Report 80-17, 40 p.
- Arctec Canada Limited (Abdelnour, R. and Lapp, D.) (1980): "Model Tests of Sea Bottom Ice Scouring", APOA Project No. 150, Report to Arctic Petroleum Operators Association.
- Barnes, P.W. and Reimnitz, E. (1979): "Ice Gouge Obliteration and Sediment Redistribution Event", 1977-1978, Beaufort Sea, Alaska, USGS Open File Report 79-848, 22 p.
- Barrie, J.V. (1980): "Iceberg/Seabed Interaction (Northern Labrador Sea)", Annals of Glaciology, Vol. 1, pp. 71-76.
- Barrie, J.V. (1983): "Sedimentary Processes and the Preservation of Ice Scours on the Eastern Canadian Continental Shelf", The 7th International Conference on Port and Ocean Engineering under Arctic Conditions (POAC), Vol. 4, Helsinki, Finland, pp. 635-653.
- Chari, T.R. and Peters, G.R. (1981): "Estimates of Iceberg Scour Depths", Proceedings of the Symposium on Production and Transportation Systems for the Hibernia Discovery, St. John's, Newfoundland, pp. 178-188; 432-455.
- Chari, T.R. and Prasad, K.S.R. (1986): "Analytical and Experimental Modelling of Iceberg Scours and Pits", Third Canadian Conference on Marine Geotechnical Engineering, St. John's, Newfoundland, June 1986.
- Chari, T.R., Peters, G.R. and Muthukrishnaiah, K. (1980): "Environmental Factors Affecting Iceberg Scour Estimates", Cold Regions Science and Technology, Vol. 1, pp. 223-230.
- Clark, J.I., Landva, J., Collins, W.T. and Barrie, J.V. (1986): "The Geotechnical Aspects of Seabed Pits in the Grand Banks Area", Third Canadian Conference on Marine Geotechnical Engineering, St. John's, Nfld., June 1986.
- Collins, W.T. and Diemand, D. (1983): "Norploy '82 Cruise Report", August 1982, C-CORE Cruise Report 83-4, 31 p.
- d'Apollonia, S.J. and Lewis, C.F.M. (1985): "A numerical model for calculating long term frequency and spatial distribution of iceberg grounding events", ESRF Ice Scour Workshop, Calgary, Alberta (in press).
- Darwin, C.R. (1865): "On the Power of Icebergs to make rectilinear, Uniformly-Directed Grooves Across a Submarine Undulatory Surface", London, Edinburgh, and Dublin Magazine and Journal of Science, Vol. 10, pp. 96-98.
- Dinsmore, R.P. (1972): "Ice and its Drift into the North Atlantic Ocean", International Commission for the Northwest Atlantic Fisheries Special Publication No. 8, pp. 89-128.

- Fader, G.B. and King, L.H. (1981): "A Reconnaissance Study of the Surficial Geology of the Grand Banks of Newfoundland", Current Research Part A, Geological Survey of Canada, Paper 81-1A, pp. 45-81.
- Fenco Consultants Limited (1975): "An Analysis Study of Ice Scour on the Sea Bottom", APOA Project No. 69, 165 p.
- Fillon, R.H. (1979): "Cruise Report No. 79-019 CSS HUDSON", August 9-26, 1979, Bedford Institute of Oceanography, 20 p.
- Gaskill, H., Nicks, L. and Ross, D. (1985): "A Non-deterministic Model of Populations of Iceberg Scour Depths", Cold Regions Science and Technology (in press).
- Gilbert, G.R. and Barrie, J.V. (1985): "Provenance and Sedimentary Processes of Ice Scoured Surficial Sediments", Labrador Shelf, Canadian Journal of Earth Sciences, Vol. 22, pp. 1066-1079.
- Green, H.P. (1984): "Geotechnical Modelling of Iceberg-Seabed Interaction", M.Eng. Thesis, Memorial University of Newfoundland, St. John's, Newfoundland, 165 p.
- Green, H.P. and Chari, T.R. (1981): "Sediment Compaction Below Iceberg Scour Furrows", Oceans '81 Conference Record, IEEE-MTS Conference, Boston, pp. 223-227.
- Green, H.P., Reddy, A.S. and Chari, T.R. (1983): "Iceberg Scouring and Pipeline Burial Depth", the 7th International Conference on Port and Ocean Engineering under Arctic Conditions, Helsinki, Finland, Vol. 1, pp. 280-288.
- Gustajtis, K.A. (1979): "Iceberg Scouring on the Labrador Shelf, Saglek Bank", C-CORE Technical Report 79-13, Memorial University of Newfoundland, St. John's, Newfoundland, 89 p.
- Harris, I. McK. and Jollymore, P.G. (1974): Iceberg Furrow Marks on the Continental Shelf Northeast of Belle Isle, Newfoundland. Canadian Journal of Earth Sciences, Vol. 11, pp. 43-52.
- Hotzel, I.S. and Miller, J.D. (1983): "Icebergs; Their Physical Dimensions and Presentation and Application of Measured Data", Annals of Glaciology, Vol. 4, pp. 116-123.
- Josenhans, H.W. and Barrie, J.V. (1982): "Preliminary Results of Submersible Observations on the Labrador Shelf", Geological Survey of Canada Current Research, Part B, pp. 269-276.
- Josenhans, H.W. and Zevenhuizen, J. (1984): "Seafloor Dynamics on the Labrador Shelf", Symposium on Sedimentology of Shelf Sands and Sandstones, Abstract, p. 80.
- Josenhans, H.W., Klassen, R.A. and Zevenhuizen, J. (1985): "The Lateral Distribution, Physical Properties, and Quaternary History of the Labrador Shelf Sediments", Canadian Journal of Earth Science (in press).

- Johnson, M.A., Barrie, J.V., Woodworth-Lynas, C.M.F. and Parrott, D.R. (1980): "Field - Observations of Iceberg Grounding and Scouring: Observation of Iceberg Scour Marks by Manned Submersible", Proceedings Arctic Workshop, Bedford Institute of Oceanography, pp. 9-11.
- Johnson, M.A. (1981): "Relict Iceberg Furrows on the Laurentian Channel and Western Grand Banks", Canadian Journal of Earth Sciences, Vol. 13, pp. 1061-1092.
- Johnson, M.A. (1984): "Aspects of Regional Surficial Geology Related to Site Investigation Requirements - Eastern Canadian Shelf", Offshore Site Investigations, Ardus, D.A. (ed.); Graham and Trotman, London, pp. 1-6.
- Johnson, M.A. (1981): "Use of Mathematical Models to Estimate Ice Scour", Conference on Canadian Offshore Drilling and Downhole Technology (1981), Edmonton, Alberta, pp. 68-76.
- Kobayashi, N. (1982): "Sediment Transport on a Gentle Slope due to waves", ASCE Journal of the Waterway, Port, Coastal and Ocean Division, Vol. 108, WW3.
- Krass, A. and Mellor, M. (1974): "Sea Ice Morphology and Ice as a Geological Agent in the Southern Beaufort Sea", The Coast and Shelf of the Beaufort Sea, Reed, J.C. and Sater, J.E. (eds.); Arctic Institute of North America, Arlington, Va., pp. 113-161.
- Krumm, H.F. and Rad, U. (1984): "Underwater Television and Photography Observations, Side-Scan Sonar and Acoustic Reflectivity Measurements of Phosphorite-rich Areas and Chatham Rise (New Zealand)", Geol. Jb, 101, pp. 59-89.
- Lewis, G.F.M. (1978): "The Frequency and Magnitude of Drift-Ice Groundings from Ice-Scour Tracks in the Canadian Beaufort Sea", The 4th International Conference on Port and Ocean Engineering Under Arctic Conditions, St. John's, Newfoundland, Vol. 1, Memorial University of Newfoundland, pp. 568-579.
- Lewis, G.F.M. and Barrie, J.V. (1980): "Ice Scour Studies on the Labrador Shelf", Proceedings of the Workshop on Research in the Labrador Coastal and Offshore Region, Goose Bay, Labrador, Newfoundland Institute of Cold Ocean Science, Memorial University of Newfoundland, pp. 264-265.
- Lewis, G.F.M. and Barrie, J.V. (1981): "Geological Evidence of Iceberg Groundings and Related Seafloor Processes in the Hibernia Discovery Area of Grand Banks, Newfoundland", Symposium on Production and Transportation Systems for the Hibernia Discovery, St. John's, Newfoundland, pp. 146-177.
- Lewis, G.F.M., MacLean, B. and Falconer, R.K.H. (1980): "Iceberg Scour Abundance in Labrador Sea and Baffin Bay: A Reconnaissance of Regional Variability", Proceedings of the First Canadian Conference on Marine Geotechnical Engineering, Calgary, Alberta, pp. 79-94.

- Leis, C.F.M., Josenhans, H.W., Fader, G.B., MacLean, B., d'Appollonia, S. and Barrie, J.V. (1982): "The Distribution and Shape Variability of Iceberg Scour Marks on Canadian Continental Shelves", Joint Oceanographic Assembly, Poster Abstracts, Vol. 2, Halifax, Nova Scotia, p. 40.
- Lien, R. (1981): "Seabed Features in the Blaaenga Area, Weddel Sea, Antarctica", The 6th International Conference on Port and Ocean Engineering under Arctic Conditions (POAC), Vol. II, Quebec, pp. 706-716.
- Lien, R. (1982): "Ice Age Plough Marks a Hazard to Pipelines in Northern Seas", Offshore Engineer, May, p. 79.
- Lien, R.L. (1983): "Iceberg Scouring on the Norwegian Continental Shelf", Proceedings of the Offshore Technology Conference, Houston, Texas, Vol. 3, pp. 41-48.
- Lopez, R., Chari, T.R., Moore, E., Peters, G.R. and Zielinski, A. (1981): "Hydrodynamic Effects of Iceberg Gouging", Cold Regions Science and Technology, Vol. 4, No. 1, pp. 55-61.
- Luternauer, J. and Murray, J.W. (1983): "Late Quaternary Morphologic Development and Sedimentation, Central British Columbia Continental Shelf", Geological Survey of Canada, Paper 83-21, 38 p.
- MacLean, B. (1982): "Investigations of Baffin Island Shelf from Surface Ship and Research Submersible in 1981", Geological Survey of Canada. Current Research, Part A, Paper 82-1A, pp. 445-447.
- Murray, J.F. (1969): "The Drift, Deterioration and Distribution of Icebergs in the North Atlantic Ocean", CIM Special Vol. 10, The Ice Seminar, pp. 3-18.
- Orner, G., Glen, J.W., Adie, R.J., Johnson, D.M., Homer, D. and MacQueen, A.D. (1979): "Plough Mark in the Weddel Sea", Journal of Glaciology, Vol. 23, p. 402.
- Pelletier, B.R. and Shearer, J.M. (1972): "Sea Bottom Scouring in the Beaufort Sea of the Arctic Ocean", Twenty-fourth International Geological Congress, Montreal, pp 251-261.
- Prasad, K.S.R. (1985): "Analytical and Experimental Modelling of Iceberg Scours", M.Eng. Thesis, Memorial University of Newfoundland, St. John's, Newfoundland, 170 p.
- Reinartz, E. and Barnes, P.W. (1974): "Sea Ice as a Geologic Agent on the Beaufort Sea Shelf of Alaska", The Coast and Shelf of the Beaufort Sea, Reed, J.C. and Sater, J.E. (eds.); Arctic Institute of North America, Arlington, Virginia, pp. 301-353.
- Reinartz, E. and Kempema, E. (1982): "Dynamic Ice-Wallow Relief of Northern Alaska's Nearshore", Journal of Sedimentary Petrology, Vol. 52, pp. 451-461.

- Shearer, J.M. and Blasco, S.M. (1975): "Further Observations of the Scouring Phenomena in the Beaufort Sea", Current Research Part A, Geological Survey of Canada, Paper 75-1A, pp. 483-493.
- Stoker, M.S. and Long, D. (1984): "A Relict Ice-Scoured Erosion Surface in the Central North Sea", Marine Geology, Vol. 61, pp. 85-93.
- Syvitski, J.P.M., Fader, G.B., Josenhans, H.W., MacLean, B. and Piper, D.J.W. (1983): "Seabed Investigations of the Canadian East Coast and Arctic Using PISCES IV", Geoscience Canada, Vol. 10, pp. 59-68.
- Todd, B.J. (1984): "Iceberg Scouring on Saglek Bank, Northern Labrador Shelf", M.Sc. Thesis, Dalhousie University, 166 p.
- Vilks, G. (1979): "The Holocene Marine Environment of the Beaufort Shelf", Geological Survey of Canada Bulletin, 303 p.
- Vorren, T.O., Morten, H., Edvardsen, M. and Hanson, O.W.L. (1983): "Glaciogenic Sediments and Sedimentary Environments on Continental Shelves; General Principles with a Case Study for the Norwegian Shelf", Glacial Deposits in North West Europe, 1983.
- Wadhams, P. (1975): "Sea Ice Morphology in the Beaufort Sea", Beaufort Sea Technical Report No. 36, Canada Department of Environment, Victoria, British Columbia, 66 p.
- Wahlgren, R.V. (1979): "Ice Scour Tracks in Eastern MacKenzie Bay and North of Pullen Island, Beaufort Sea", Current Research, Part B, Geological Survey of Canada, Paper 79-1B, pp. 51-62.
- Weeks, W.F., Barnes, P.W., Rearic, D.M. and Reimnitz, E. (1983): "Statistical Aspects of Ice Gouging on the Alaskan Shelf of the Beaufort Sea", U.S. Army Corps of Engineers, CRREL, Report 83-21.
- Woodworth-Lynas, C.M.T., Simms, A. and Rendell, C.M. (1985): "Iceberg Grounding and Scouring on the Labrador Continental Shelf", Cold Regions Science and Technology, Vol. 10, pp. 163-186.
- Yalin, M.S. (1963): "An Expression for Bedload Transportat on", ASCE, Journal of the Hydraulics Division, Vol. 89 (HY3), pp. 221-250.

NUMERICAL AND FINITE ELEMENT
TECHNIQUES IN CALCULATION OF
ICE-STRUCTURE INTERACTION

Ian J. Jordaan

Det norske Veritas
(Canada) Ltd.
Calgary, Alberta

Canada

ABSTRACT

Better understanding of the mechanics of ice has led to increased demands for improved computational methods. To put this into perspective, current trends in ice mechanics are reviewed. These relate principally to creep, global (tensile) fracture as well as compression fracture (crushing). The need for numerical methods (finite element, discrete element, finite difference) is discussed in the light of the review of mechanics of ice, as well as the boundary conditions for the ice feature. Analyses carried out in past studies and current work at various institutions are reviewed. These include applications of elasticity, plasticity, creep (reference stress), fracture and damage mechanics. Future research needs are reviewed: these include studies of fracture, as related to splitting of ice features, spalling and flexural failure, as well as crushing. The latter can be studied by means of damage mechanics as well as viscoplastic analyses, which are reviewed and discussed. Viscoplastic analysis of crushed ice cannot be carried out using failure surfaces for the virgin ice: new techniques are required, requiring flow formulations and Eulerian coordinates. There is a need for integration of the various aspects with mechanical models based on the **actual** processes involved in large and small scale experiments.

1. INTRODUCTION

Many branches of engineering are concerned with the response of ice to stress: this may be aimed at ice load estimation or the response of ice as an engineering material, for example, in terms of its bearing capacity. The key to more accurate estimation of ice response lies in the implementation of realistic ice mechanics in analytical methods. This is particularly true in the estimation of ice loads for offshore structures: the motivation is similar to the use of hydrodynamics for wave loads on ships and structures.

The main emphasis in the present paper is on the analysis of floating ice masses, such as multi-year floes, and their interaction with offshore structures. At the same time, some consideration is given to bearing problems, ride-up and large-scale analysis of sea, ice and surroundings.

At the previous IAHR conference, Sanderson (1984) considered wide structures, with the width (D) being several times greater than the ice thickness (T). Typically, an Arctic exploration structure may be 100 m wide and multi-year ice is about 5 m thick on average giving a D/T ratio of 20. A monopod structure might yield a value of, say, 2. Such ratios are attained in the laboratory, but the scale is up to three orders of magnitude less. For several reasons, the most important being the brittleness of ice, it is not possible to scale these results, without a detailed appreciation of the mechanics of ice particularly during the process of interaction with a structure.

To pursue briefly the question of scaling noted above, it is useful to introduce the idea of average ice pressure on the structure, defined so that the force on a structure, F, is given by:

$$F = \sigma_a \cdot A \quad (1)$$

where A = contact area and σ_a = average ice pressure. The value of σ_a might be as high as 10 MPa for laboratory indentation and as little as 1 MPa for full scale impacts of natural multi-year sea ice on structures with lateral dimensions of the order of 100 m (based on Hnatiuk and Felzien, 1986, and other sources).

In comparing laboratory and field data, the scale effect represented by one to two orders of magnitude can be readily identified if not explained by using values of σ_a , as above. Often σ_a is interpreted as a "crushing strength": "crushing" covers a multitude of factors: splitting, flexural failure, spalling, as well as pulverizing and subsequent clearing of pulverized ice.

The concept of average ice pressure can also be interpreted as an energy per unit volume (Laskow, 1982). The power P of energy dissipation or transformation at the face of a structure, i.e. $P = \underline{F} \cdot v$, where v is the relative velocity of ice and structure yields the following:

$$P = \sigma_a A dv/dt = \sigma_a dV/dt \quad (2)$$

where V is volume, for the case where force and velocity are in the same direction and magnitude of force is given by Eq. (1): dV/dt is the volume of ice penetrated per unit time. The quantity σ_a then has the units of energy per unit volume.

Such general considerations of average ice pressure and energy are useful to put values into a practical format: an explanation of the 10 - 100 factor relating σ_a in the small and the large can only be obtained by studying the mechanical processes. As far as analytical studies are concerned, it will be suggested that the complexity of ice behaviour, including variation of its properties with stress history, combined with the variability of ice properties and geometry in nature, dictates the use of numerical methods for its analysis. The endpoint may well be in terms of a practical format such as the value of σ_a to use in design.

2. RELEVANT ICE MECHANICS

2.1 Salient Aspects of Ice Mechanics

There are many manifestations of the behaviour of ice that lead to a picture that is at first confusing: this complexity becomes apparent in reviews such as Michel (1978). Interpretation is

sometimes difficult and, in particular, the fact that ice is extremely brittle, points to the need for methods of analysis more advanced than conventional continuum theories. First, the salient points are identified and then interpreted in terms of observed behaviour of small and large scale specimens.

Ice is an elastic, creeping solid, yet it is extremely brittle, one of the most brittle materials on earth. It forms as an anisotropic crystal, and if these are aligned so that the crystal c-axes are in the horizontal plane (for example) in an ice sheet, the response of a specimen from the sheet will be anisotropic, although the sheet may be a plane of elastic symmetry if the c-axis directions are randomly oriented in the horizontal plane. If the c-axes are randomly oriented in space, the ice may be treated as isotropic; such granular ice, as it is termed, is strictly speaking statistically isotropic. Anisotropic response for elasticity and creep of solids is well understood and documented both for classical mechanics as well as in the case of numerical analysis. These aspects are therefore not of major concern (in terms of their ability to be analyzed), and consequently will not be stressed in the following.

As mentioned earlier, ice is extremely brittle as is evidenced by the extremely low fracture toughness and strain energy release rate. The latter value is of the order of $1 - 2 \text{ J/m}^2$, similar to the value for glass. The result of this extreme brittleness is a propensity to fracture, and for stable microcracking to be a common occurrence in compressive states, leading to disintegration or pulverization of ice.

All of the above phenomena will now be discussed in further detail with numerical analysis in mind.

2.2 Creep and the Role of Plasticity Theory

One might consider plasticity theory as a simplification, or special case of creep. If the "flow" takes place at a distinct yield point (stress level), and happens rapidly, then creep can be replaced by "plastic flow". There is no evidence that this is the case for ice; Pounder (1965) pointed this out and the most widely accepted

creep law for ice is that proposed by Sinha (1978), given here in terms of the uniaxial creep compliance, for loading at $t = 0$.

$$J(t) = \frac{1}{E} + \frac{1}{E_k} (1 - e^{-At^B}) + Ct^n \quad (3)$$

In this, E = elastic modulus, and E_k , A , B , C , and n are constants.

It is attractive to represent this in terms of a rheological model (Figure 1); this is strictly correct for the elastic and viscous terms, but the delayed elastic term - the second term on the right hand side of Eq. (3) - cannot strictly be derived on the basis of viscoelastic theory. The power " B " in t^B in the exponent is the reason for this. Other models were reviewed recently by Ashby and Duval (1985) and there appears to be scope for other formulations.

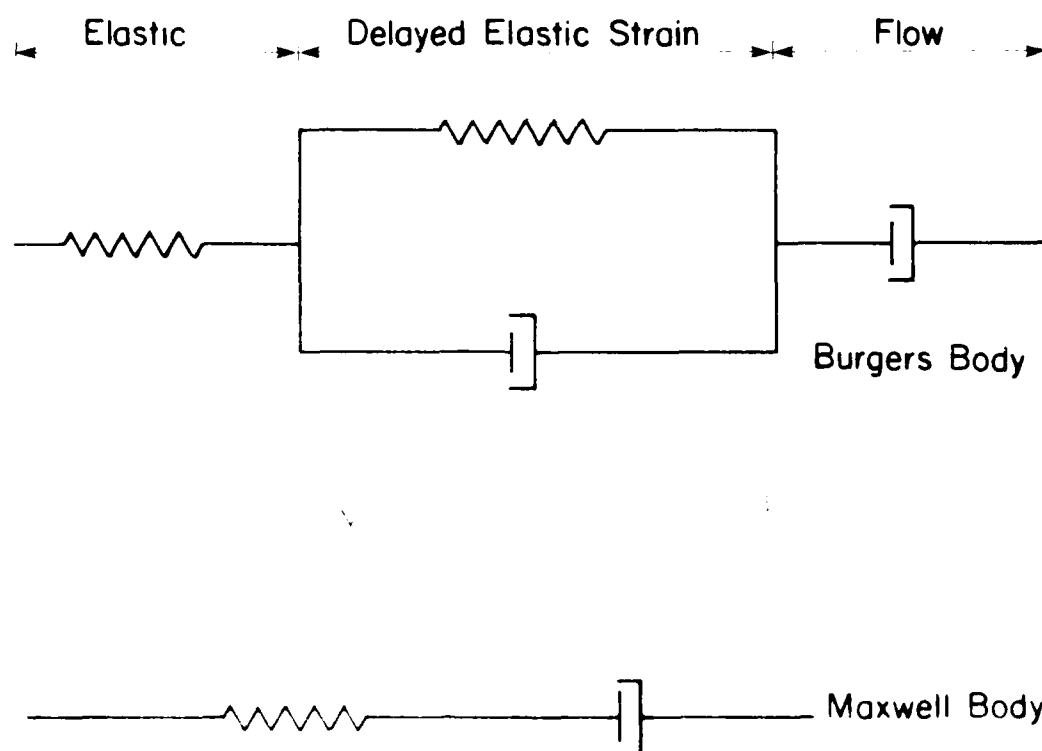


Figure 1. Viscoelastic Models for Ice

It is an interesting fact that a class of models of the kind

$$\dot{\epsilon}(t, \tau) = J_1[\dot{\psi}(t) - \dot{\psi}(\tau)] \quad (4)$$

where $\psi(\cdot)$ represents a function or "reduced time" that accounts for a range of effects, including non-linearities of stress-strain relationships, can be derived from general constitutive theories (Shapery, 1964). These can be put into stress-strain relationship of the kind:

$$\epsilon(t) = \int_0^t J_1[\dot{\psi}(t) - \dot{\psi}(\tau)] \frac{d\sigma}{d\tau} d\tau \quad (5)$$

which is of the form of a Boltzmann superposition model, even though non-linearities are included. Models of this kind, and their use in modelling ice, are reviewed in Jordaan (1986).

The form of model just described is at the same time extremely convenient from the point of view of numerical modelling, since computer storage of the entire stress-strain history is not necessary: only current values are needed. Thus, substantial computer savings can be attained.

Glen's law - the third term of Eq. (3) - comes into the category just described, with

$$\dot{\epsilon}(t) = \int_0^t (1/\eta(\sigma)) d\sigma$$

where $\eta(\sigma) = c\sigma^{n-1}$ is the viscosity of the non-linear dashpot, at the instant in time when the stress σ is applied.

It is often appropriate to neglect primary creep (or even elasticity) if secondary creep dominates. The lower part of Figure 1 shows the simple Maxwell model which can be used to solve a variety of practical problems.

As noted earlier, there is no clear threshold stress for creep and this is illustrated in Figure 2, where some curves based on constant strain rate have been calculated. The "yield" plateaux are not unique and depend on the strain rate. These results are confirmed by many experimental data sets.

There is no method known to the writer of replacing a creep analysis with a plastic one and obtaining a rigorously correct result. The reference stress method (Ponter et al., 1983) provides an approximate method. As noted in the introduction, the rate at which the force F on the structure does work is the power $P=Fv$ if v is in the direction of F and this may (in the absence of other "work" terms) be equated to the rate at which work is dissipated in the ice, i.e.

$$P = \int \sigma_{ij} \dot{\epsilon}_{ij} dV \quad (6)$$

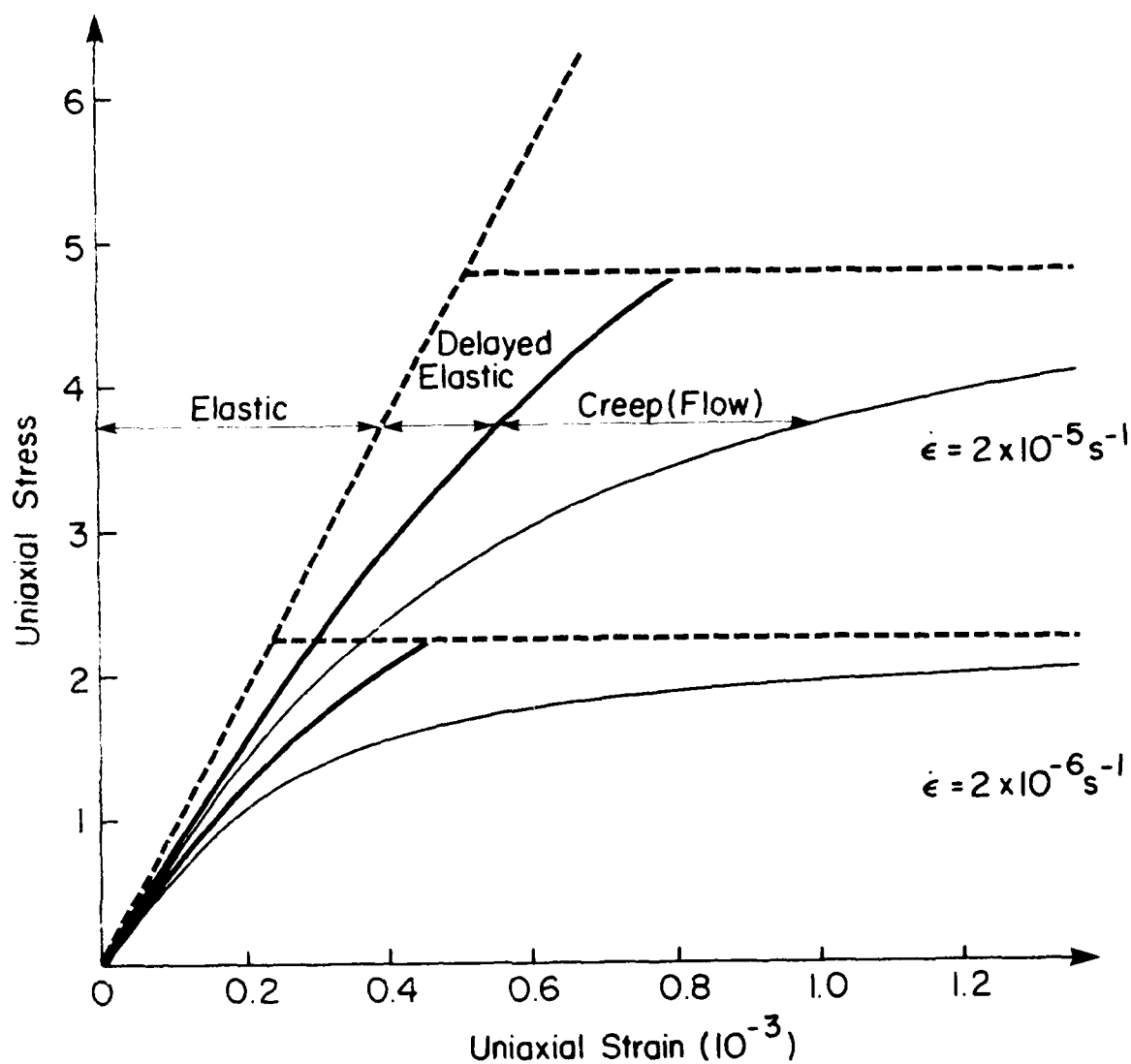
where σ_{ij} is the stress at any point, ϵ_{ij} is the associated strain and V is volume. This may be written as:

$$P = \sigma_R \dot{\epsilon}_R V_R \quad (7)$$

where σ_R is the reference stress at reference strain rate $\dot{\epsilon}_R$. By an appropriate choice of σ_R , $\dot{\epsilon}_R$ and V_R , a plastic solution can be obtained for the steady state case where F is constant. This is not a rigorous analogy and is only a convenient approximate solution method, requiring elasticity or plasticity solutions as a basis. It does not imply that creep and plastic solutions in general give similar answers, only that similar results can be obtained by the choice of parameters. This choice is by no means arbitrary.

2.3 Higher Strain Rates and Complex States of Stress

Although ice creeps at any stress state or level, apart from purely hydrostatic states, it is usually dominated by the propensity to fracture. Figures 3-5 illustrate the overall picture. Under tensile states of stress, the critical flaw will propagate at a stress given by $\sigma_c = \sqrt{(EG_c)/(\pi a)}$ where E = elastic modulus, G_c = energy requirement per unit area of crack, and is essentially a material



$E = 9500 \text{ MPa}$; $T = -10^{\circ}\text{C}$

Creep Laws Used : $\epsilon_d = 2 \frac{\sigma}{E} (1 - \exp(-(At)^B))$

$$\dot{\epsilon}_f = C \sigma^3$$

$C = 1.76 \times 10^{-7} \text{ s}(\text{MPa})^{-3}$; $A = 2.5 \times 10^{-4} \text{ s}^{-1}$; $B = 0.34$

Figure 2. Various Creep Relationships and Plasticity Approximations. Plastic Yield Plateaux Vary with Strain Rate

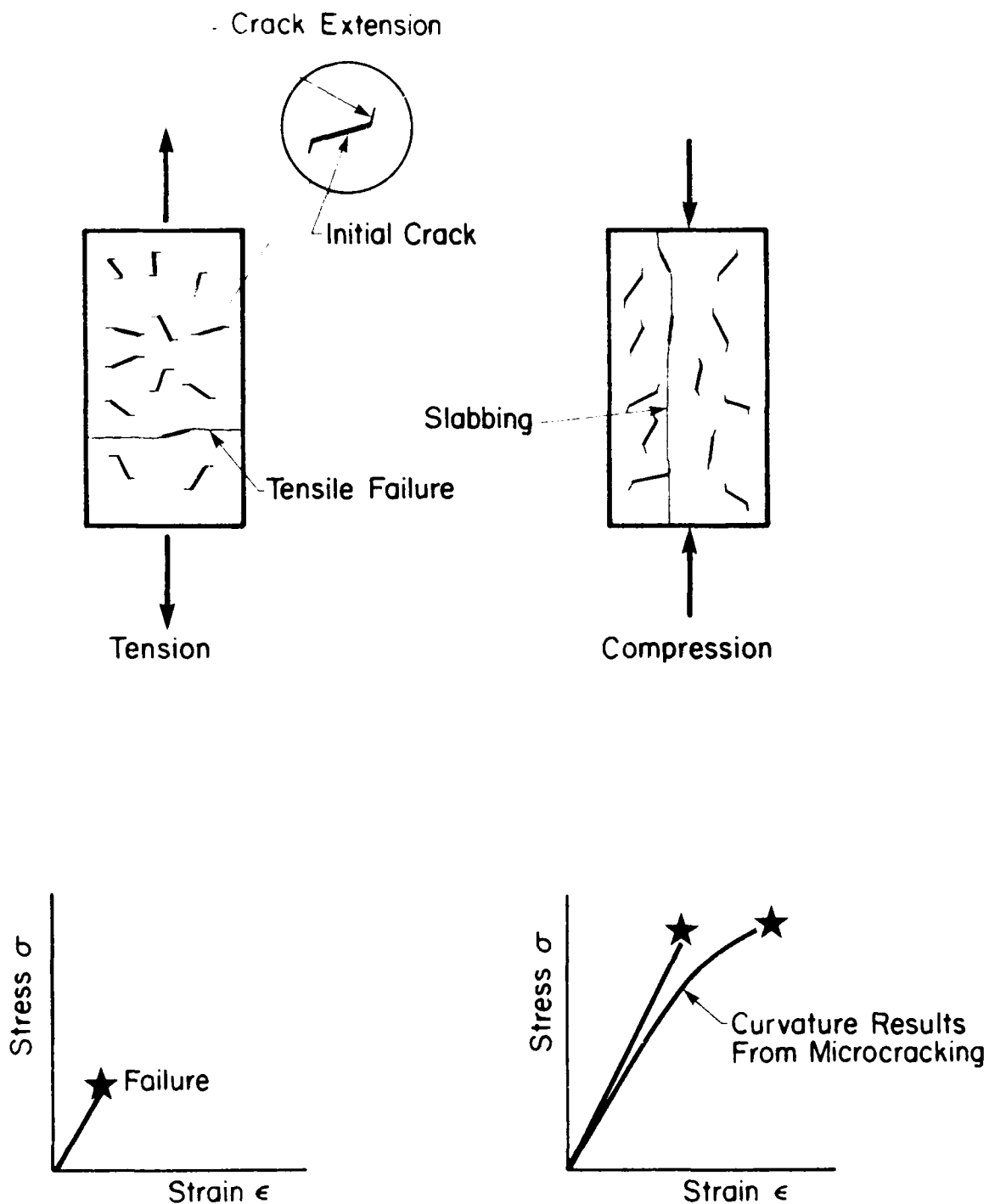


Figure 3. Response to Uniaxial Stress at Higher Strain Rates:
Under Tensile Stress the Dominant Flaw Propagates,
and Under Compression Stable Microcracking
Followed by "Slabbing" Occurs

constant (for a given stress state) and a = half the crack length. The value of G_c is determined by experiment and depends on the stress state, which affects the ease with which a crack will propagate; see for example Sih (1973). The critical flaw will have the combination of length and orientation which gives the lowest value of σ_c for all cracks in the sample of material in the body under consideration (at lower stresses, the material will creep without fracture). Generally the critical crack will propagate right through the specimen, leading to failure.

Under compression, cracks are somewhat less prone to propagate completely through the specimen. Some microcracking generally occurs before failure. The phenomenon of "slabbing" is observed at higher strain rates; this is seen in most brittle materials such as concrete, sulphur, glass and ice. A single crack propagates right through the specimen, parallel to the direction of loading. This is also seen in quite large scale tests (Wang and Poplin, 1981).

Figure 4 illustrates schematically the stress-strain response of ice in compression, as it relates to a variety of phenomena. The figure is based on results in the literature and the key features as regards the material response are also illustrated. As the strain rate increases, pure creep becomes less important, microcracking is observed and the curves and the tests are often terminated by cracks that extend vertically from the top to bottom of the specimen, the "slabbing" phenomenon as noted above (Ashby and Hallam, 1986).

The imposition of compressive states of stress can be appreciated by writing the stress and strain tensors, σ_{ij} and ϵ_{ij} respectively as:

$$\sigma_{ij} = p\delta_{ij} + s_{ij} \quad (8)$$

$$\epsilon_{ij} = e_v\delta_{ij} + e_{ij} \quad (9)$$

where p = $1/3 \sigma_{ii}$ = volumetric stress,
 s_{ij} = deviatoric stress,
 e_v = $1/3 \epsilon_{ii}$ = volumetric strain,
 e_{ij} = deviatoric strain, and
 δ_{ij} = Kronecker delta.

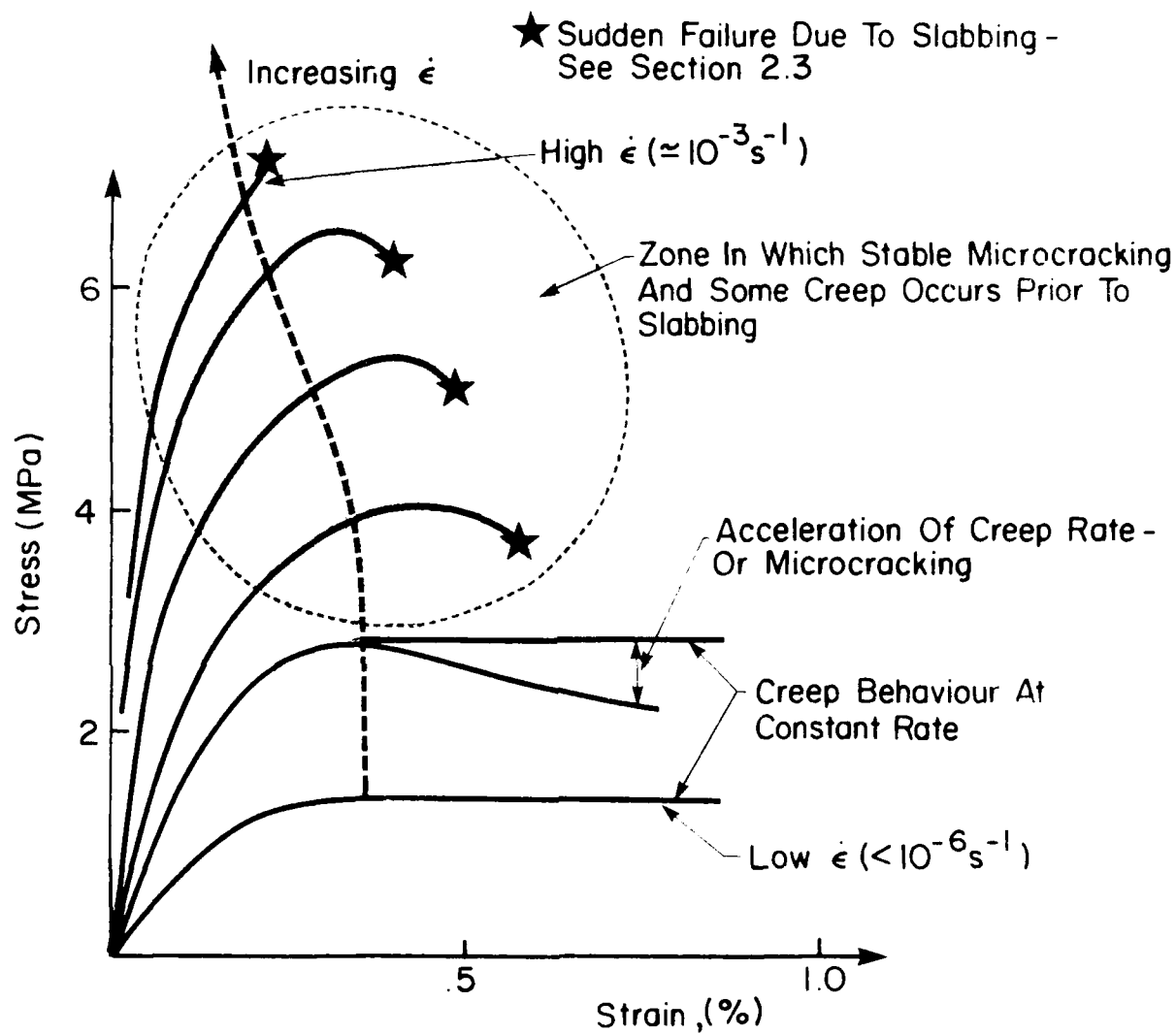


Figure 4. Shape of Uniaxial Compressive Stress-Strain Curves at Constant Strain Rate, as Related to Creep, Microcracking and Slabbing

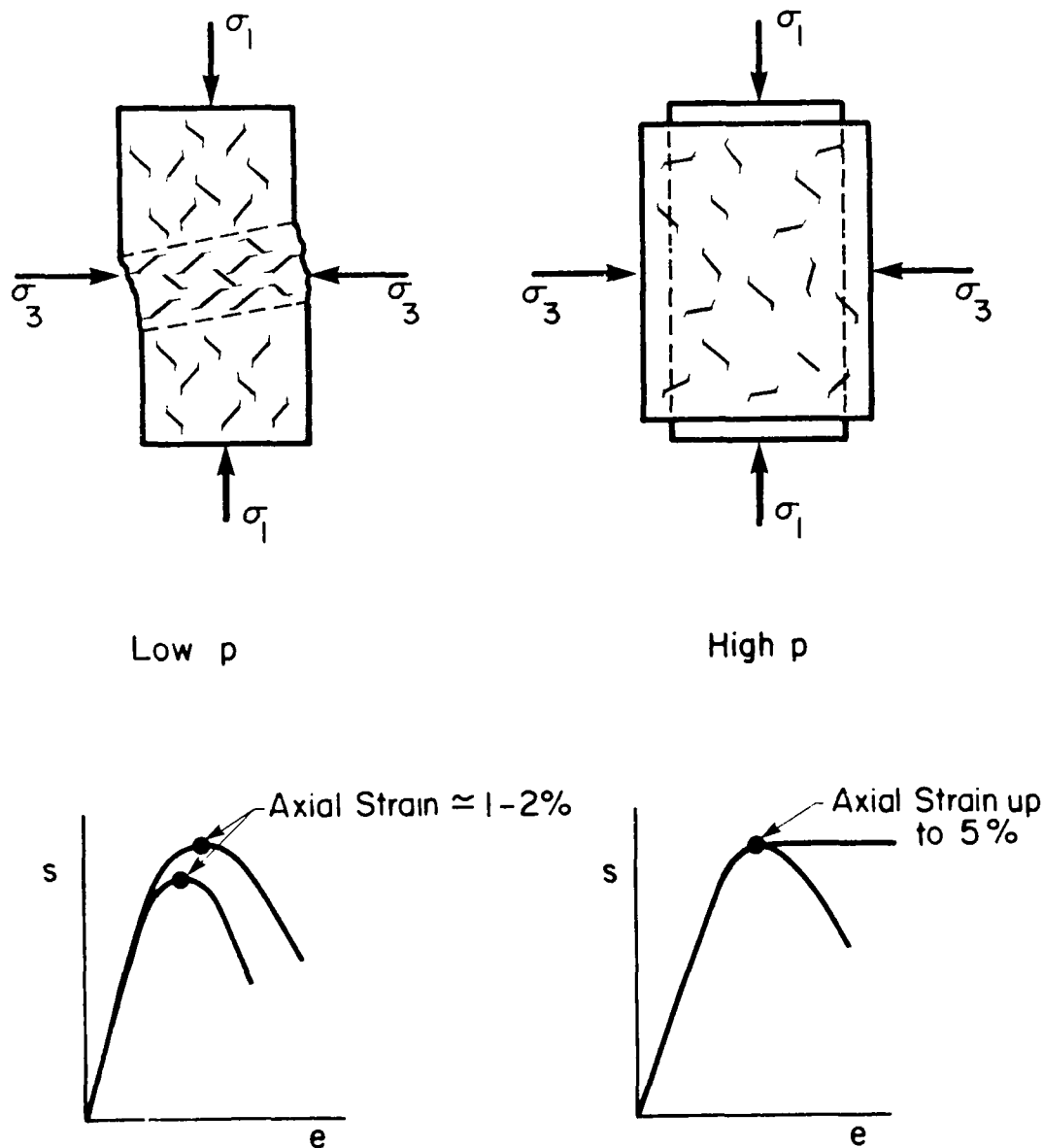


Figure 5. Behaviour Under Multi-Axial Compression and Related Deviatoric Stress-Strain Relationships Based on Ashby and Hallam (1986); At low hydrostatic stresses p the microcracks extend in shear and lead to a "shear" damage process whereas at high values of p , the microcracks become stabilized and only creep is observed.

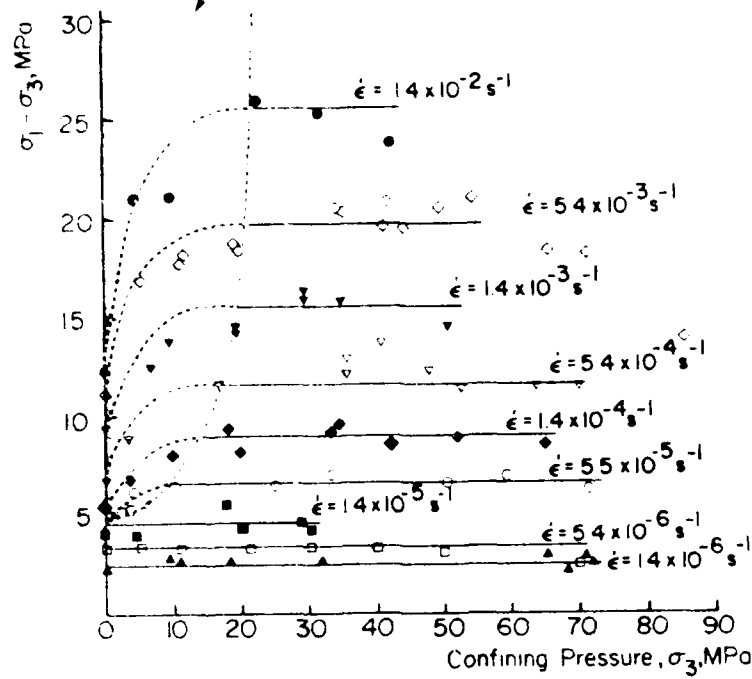
The imposition of a deviatoric stress state proportional to $(\sigma_1 - \sigma_3)$ is obtained by tests on cylinders under lateral confining pressure σ_3 (Figure 5). The results are illustrated in the figure in schematic form. At low p (and σ_3), cracks extend in a shear mode in a stable manner progressively damaging the ice; this crack propagation is suppressed at higher values of p , and creep will prevail.

This response is illustrated by the experimental results of Jones (1982). In an interesting and well-conceived set of experiments, cylindrical specimens with constant σ_3 (as described in the preceding paragraph) were subjected to constant strain rate in the axial direction. The resulting values of $(\sigma_1 - \sigma_3)$ were measured and the curves of stress versus strain included creep curves and other curves of the type illustrated in Figures 4 and 5, depending on the strain rate and the value of p . It is interesting to analyze these results with regard to the effect of strain rate. The following is consistent with the interpretation of Jones (1982), but somewhat more attention is given to the role of creep.

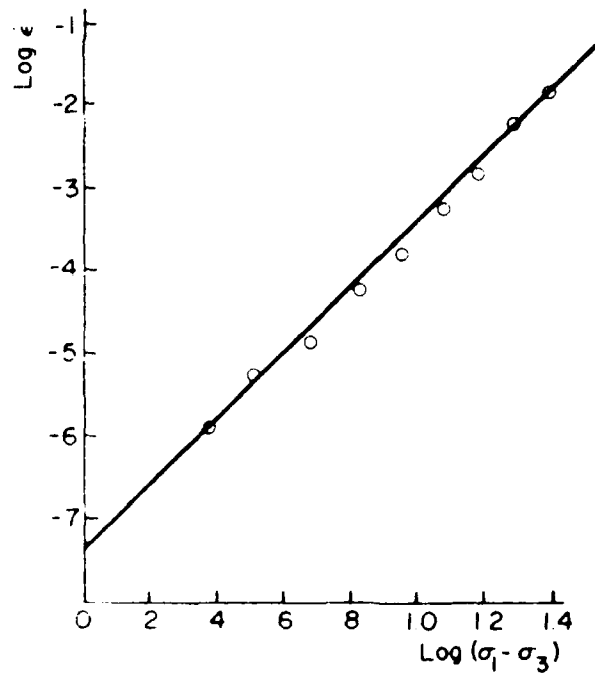
The first important point to be considered is that the imposition of a stress state $\sigma_1 > (\sigma_2 = \sigma_3)$ results in a value of $p = (\sigma_1 + 2\sigma_3)/3$ and $s_{12} = 2(\sigma_1 - \sigma_3)/3 = -2s_{31}$. In other words, the deviatoric stress is proportional to $(\sigma_1 - \sigma_3)$. If creep is independent of p , and directly related to $(\sigma_1 - \sigma_3)$, then the curves of $(\sigma_1 - \sigma_3)$ (at constant strain rate) versus strain will be independent of σ_3 . This is confirmed by the maximum values of $(\sigma_1 - \sigma_3)$ at various values of σ_3 given in the paper by Jones as shown in Figure 6(a). The one exception is the response at combinations of higher strain rates and low σ_3 , attributed to the spread of microcracks. This zone is shown as shaded in Figure 6(a).

It is interesting to observe that the peak values of stress in Figure 6(a), taken from non-shaded areas, i.e. those which are attributed to a creep response, can be considered to correspond to steady state secondary creep. At this stage in the stress strain curve, $\dot{\epsilon} = k\sigma^n$ and $\log \dot{\epsilon} = \log k + n \log \sigma$. These are plotted in Figure 6(b) and a reasonable straight line is obtained corresponding to $n = 3.8$. There is some evidence of lower values of $(\sigma_1 - \sigma_3)$ at high values

Zone of Low Hydrostatic Pressure p
 Shear Damage Process (Fig 5) is Applicable



(a)



(b)

Figure 6. (a) Experimental Results of Jones (1982) show the dominant creep behaviour except for shaded area
 (b) determination of n in $\dot{\epsilon} = K\sigma^n$

of σ_3 in Figure 6(a): this is not very conclusive and in addition, the main area by practical importance is the left half of Figure 6(a).

The conclusion of this section is that creep analysis is appropriate for low strain rates and also at higher strain rates with confining pressures sufficient to suppress the propagation of microcracks. There appears to be little scope for plasticity-based yield criteria under these conditions. The occurrence of microcracking under moderate compression is an area of great practical concern since this is the principal mechanism involved in the "ice crushing" process.

2.4 Crushing and the Shear Damage Process

Under moderate confining pressures, it has been observed that shear cracks form and aggregate and result in failure (Ashby and Hallam, 1986). This has also been observed in other materials (Resende and Martin, 1984). Because most practical cases of ice-structure interaction involve moderate confining pressures, this process is regarded as being most important in practice.

Visual evidence supporting the shear damage process has been obtained. Figure 7(a) shows a photograph of cracks forming under an indenter (Timco 1986; Tomin et al, 1986). The stress state is close to plane stress, i.e. moderate confinement, and can be approximated by the Michell solution, see Timoshenko and Goodier (1970, p. 104), for stress field resulting from uniform pressure across the indenter. Figure 7(b) shows the orientation of the planes of maximum shear, based on the Michell solution, which match closely the orientation of the cracks in Figure 2(a).

It is important to recognize that the shear planes in Figure 7(a) are not slip lines as evidenced in plasticity. As the process continues, the cracks link up until discrete pieces of ice attain the ability to move relative to each other. In plasticity theory, slip lines are not associated with damage, and in this sense, the **progressive degradation of the material is quite different from plasticity**, since it leads to disintegration of the material.

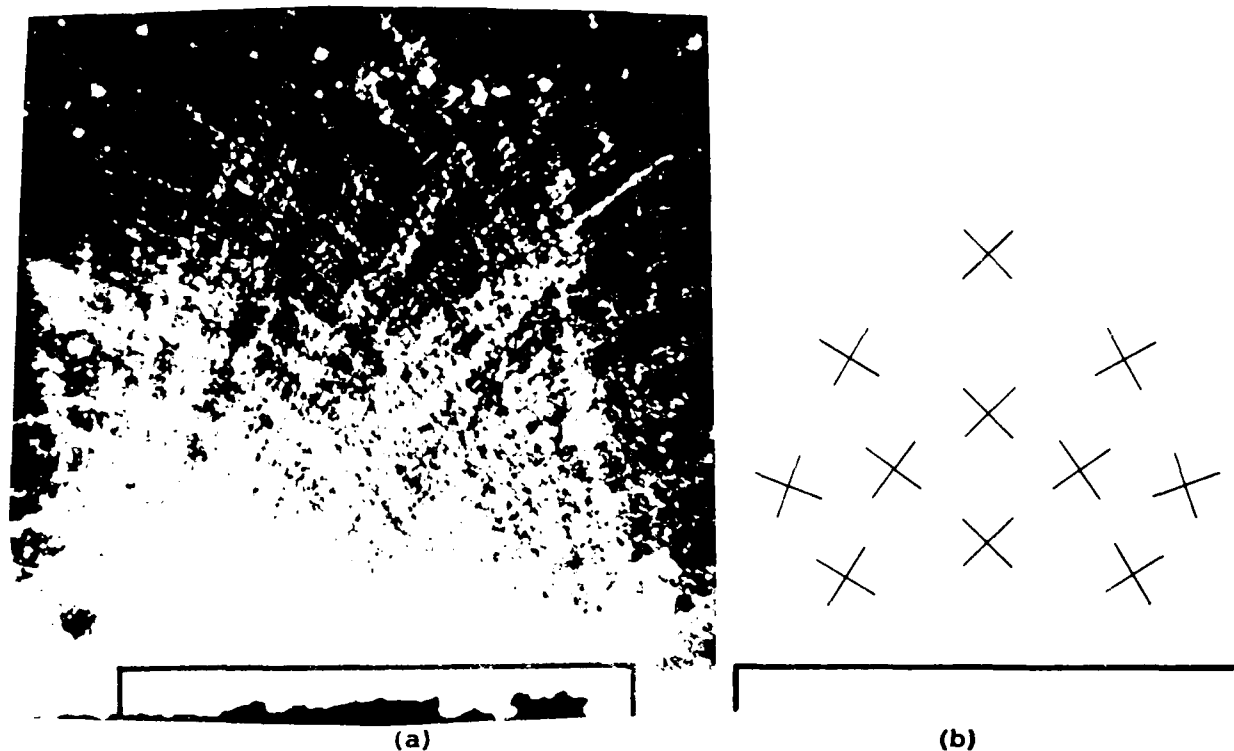


Figure 7. Process of Shear Damage in Ice

A reasonable way to analyze the process of progressive damage is to take a continuum mechanics approach. The study of individual crack propagation is important for understanding the underlying phenomena but quickly results in an intractable situation when considering the myriad of relatively stable cracks in the compression zone. The continuum analysis mentioned above focusses instead on the overall changes to the elastic response caused by the system of microcracks in the material. (We concentrate here on the effect of the elastic behaviour: creep damage theories (Leckie, 1978) can also be considered, but they are beyond the present scope. They would consider the effect of damage on elasticity and creep.)

If one removes the elastic stiffness in **shear**, one is left with a group of particles that can slide over each other. The latter behaviour can be treated as a viscous flow phenomenon (see next section).

With regard to the degradation of elasticity, the process envisaged is shown in Figure 8. The material exhibits a strain-softening curve, resulting from the extension and proliferation of the micro-crack system. Upon unloading, a reduced elastic modulus results from

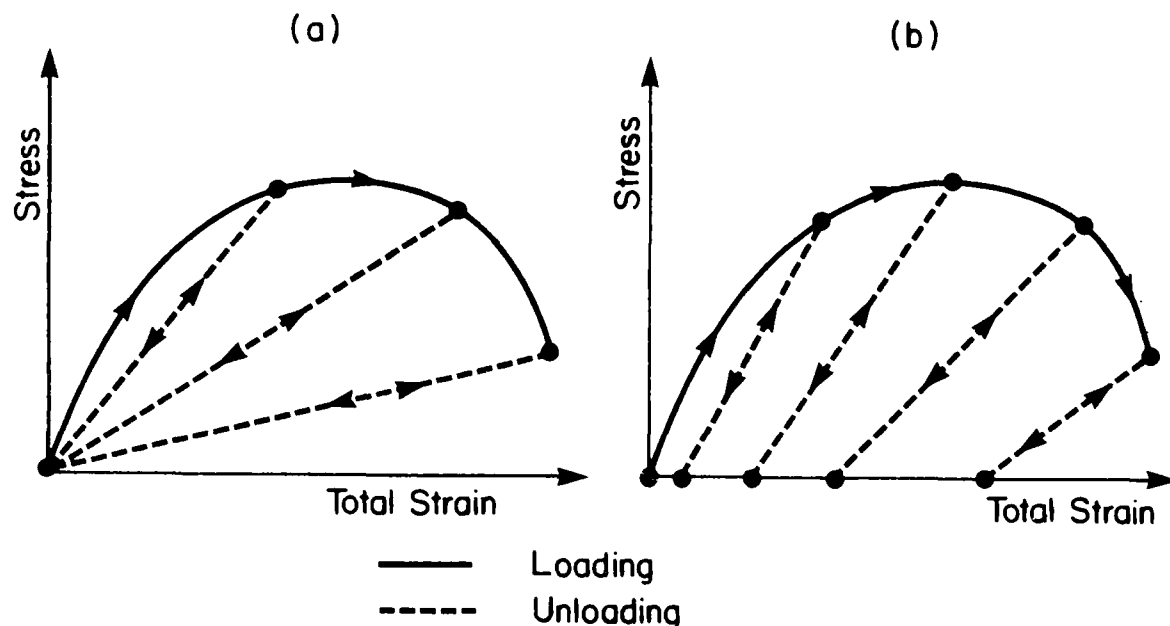


Figure 8. Process of Progressive Damage

(a) With Memory of Origin

(b) Damage Accompanied by the Development of Permanent Strains

the same cause. Finally the material has effectively no elastic stress resistance and particles can move relative to each other. There are other effects such as dilatational behaviour of the cracked ice that should be accounted for, but they are considered to be of less importance. Application of damage mechanics to ice is in its infancy.

The implementation of damage mechanics in continuum analysis is difficult to conceive as a closed form solution technique, but it may be achieved by numerical analysis which provides an excellent ongoing method for improving theories. Closed form approximations are expected to result at a later stage.

2.5 Behaviour of Pulverized Ice

The clearing of ice around a structure or obstacle is important, and can be achieved in several ways:

1. creep of ice around the structure at low strain rates;
2. rotation and movement of large pieces of broken ice, resulting from global (tensile) fractures; and
3. "flow" of crushed ice.

The present section deals with the third of these. One can think of a distortional "energy" of disintegration (Figure 9), which results in the virgin material being transformed into a pulverized "flowing" material also illustrated in Figure 9.

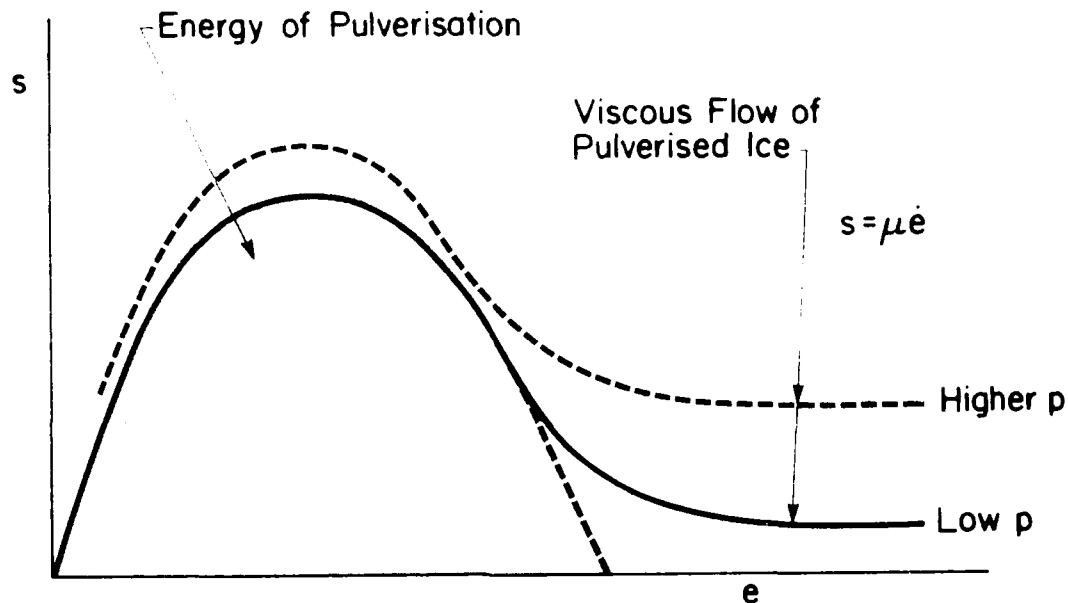


Figure 9. Shear Stress-Strain Curves With Possible Effect of Hydrostatic Pressure p Illustrated

Kurdymov and Kheisin (1976), in analyzing a set of dropped ball tests, proposed a "flow" method of analysis. Figure 10 shows the geometry of the ball and the viscoplastic layer of crushed ice, next to the ball with a thickness h . There are some challenging aspects that must be considered in putting this analysis in the context of solid mechanics applied to ice, as summarized in the preceding section. The most important of these is the question of Eulerian versus Lagrangian coordinates. Before addressing this, we shall review the basic theory.

The idea of Kheisin and his co-workers was to treat the ice as a viscous fluid. Taking up this idea, we write the deviatoric stress as a function of the rate of deformation tensor D_{ij} , i.e.

$$s_{ij} = \phi_{ij} (D_{kl}) \quad (10)$$

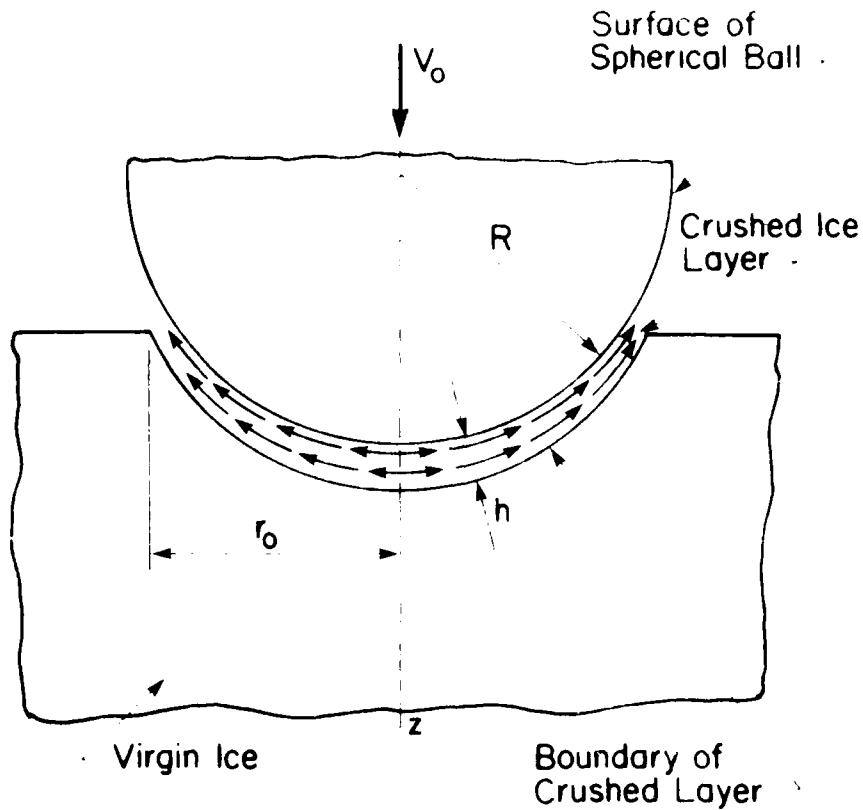


Figure 10. Viscoplastic Layer of Crushed Ice Under the Ball (after Kurdymov and Kheisin, 1976)

where $\phi_{ij}(\cdot)$ is a nonlinear function. Equation (10) represents a fluid obeying Stoke's law; if the function $\phi(\cdot)$ is linear we have a Newtonian fluid:

$$s_{ij} = K_{ijkl} D_{kl} \quad (11)$$

It is of great interest to note at this point that a problem in elasticity exists, that is completely equivalent to that of the Newtonian fluid; this is the problem of Hooke's law:

$$s_{ij} = G_{ijkl} e_{kl} \quad (12)$$

where G is the shear modulus and e (as before) the deviatoric (shear) strain. One has, perforce, to treat the material as incompressible -

which is a suitable assumption for the viscous material. We will proceed with further consideration of the rate of deformation tensor D_{ij} of equation (11); it is the symmetric part of the velocity gradient tensor $\partial v_i / \partial x_j = D_{ij} + E_{ij}$ (Note that x is a spatial coordinate). the skew-symmetric component E_{ij} is concerned with rotations and does not enter into the stress-strain relations. the important point is that D_{ij} is the material derivative of the Eulerian infinitesimal strain tensor, i.e. $D_{ij} \equiv d\epsilon_{ij}/dt$.

The problem of crushed ice can be treated initially as one of slow viscous flow:

$$\frac{\partial p}{\partial x_i} - F_i \rho - \mu \nabla^2 v_i = 0. \quad (13)$$

In this equation, p is pressure, F_i is a body force in direction i , μ = coefficient of viscosity and $\nabla^2 (\cdot) = \text{Laplacian}$.

Inertia terms have been neglected, and simple rough calculation shows this to be reasonable: the vertical distance travelled by ice particles after observed indentations and impacts is of the order of metres or less and this can be compared to the energy in the process, which turns out to be many orders of magnitude greater than inertial energy. Nevertheless, further study of this point can be undertaken with established techniques.

In conclusion of this section, it may be stated that a viscoplastic "flow" solution technique is an excellent starting point for the problem of clearing of crushed ice. It leads itself to numerical analysis and does **not** correspond in any way to plasticity of the virgin material.

2.6 Behaviour of Large Scale Ice Masses

Floating sea ice forms and deforms, melts, consolidates, contains brine pockets, flaws and cracks and is highly irregular in thickness and geometry. All of these factors cry out for numerical modelling,

and this is supported by the kinds of phenomena observed in large scale impacts. The Hans Island experiments have shown several of the effects but general observation of the Arctic shows phenomena such as ridge-building. Figure 11 illustrates some of these in a general way. Large scale splitting has certainly been observed; non-simultaneous failure is observed on wide structures (Kry, 1976) and flexural failures - Figure 11(c) - are observed even in the case of multiyear floes. The phenomena just noted all call for a statistical treatment: weakest link theories (Weibull, 1951; Maes, Jordaan and Baldwin, 1986) as well as statistical averaging as proposed by Kry have their role.

3. NUMERICAL MODELLING: A CRITICAL REVIEW

3.1 Motivation and Approach

Computer analysis has become a technique that is used when standard methods cannot be used because of the complexity of implementing them. The need for numerical modelling becomes evident when consideration is given to the following:

- (i) the complex behaviour of ice, particularly its disintegration and subsequent "flow", result in spatially varying mechanical properties.
- (ii) the irregular shape, geometry and boundary conditions of ice in the field.
- (iii) the random distribution of flaws in sea ice and icebergs.
- (iv) the fact that flow of crushed ice and its clearing implies a flow (Eulerian) approach as against a Lagrangian approach for "solid" ice mechanics.

Some research groups have been particularly active in numerical modelling and they are identified in Appendix 1.

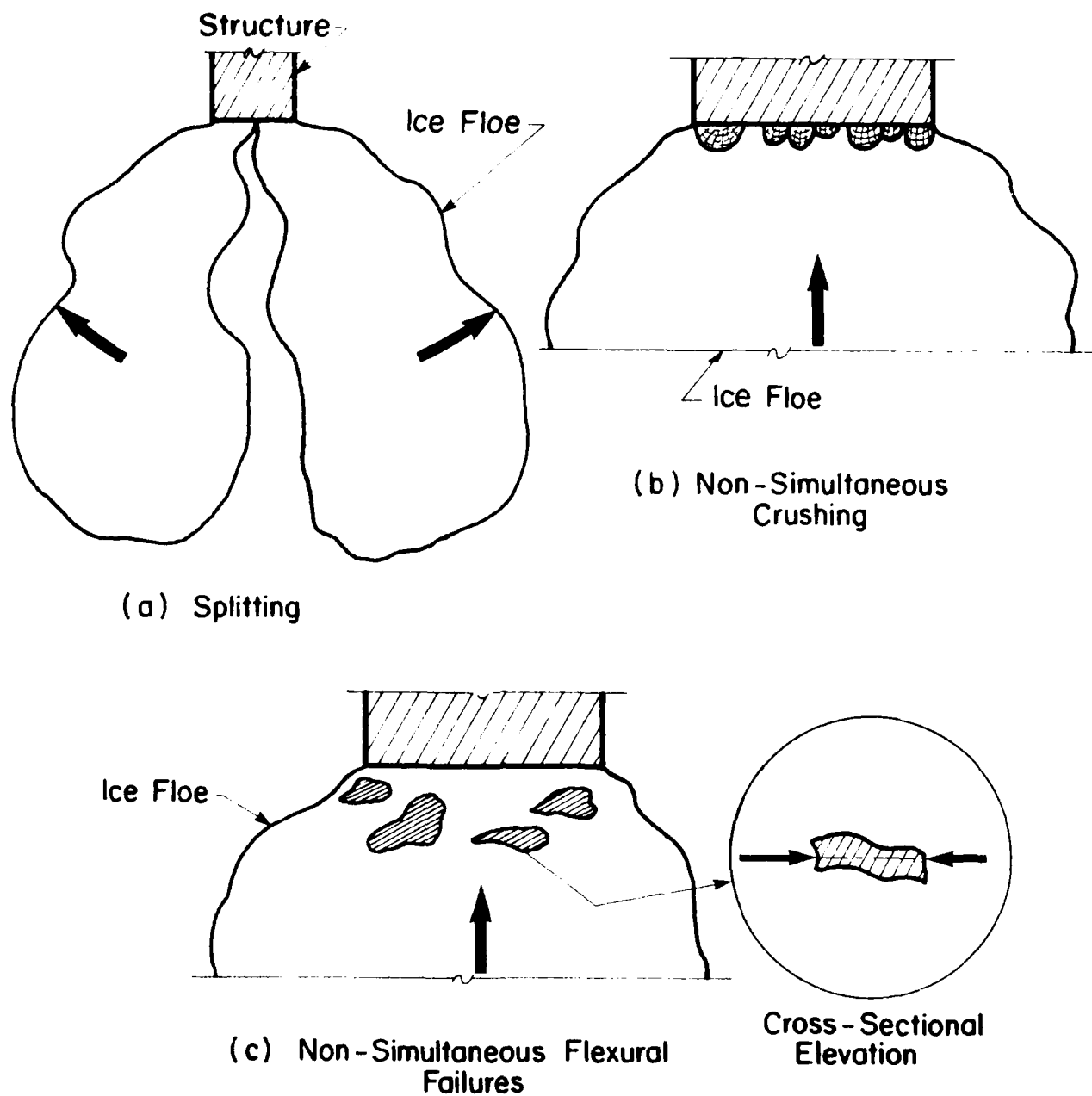


Figure 11. Some Phenomena Observed in Large Scale
Impacts of Floes and Structures (Schematic)

3.1 Elasticity and Maximum Stress Approaches

For rapid loading, ice response can be characterized by linear elasticity. An interesting finite element analysis of ice sheets, taking into account anisotropy, was presented by Riska (1980). Along with this analysis, failure criteria were proposed to deal with columnar ice. These were used to give maximum stress combinations at failure and good agreement with measured values was obtained. The author proposed more detailed analysis of the failure process - and this is in accord with the thrust of the present report.

Other numerical elastic analyses include the work of Sodhi and Hamza (1977), who conducted a finite element analysis of ice sheets (plates on elastic foundation). The emphasis here was on buckling phenomena.

3.2 Numerical Modelling of Creep Processes

Creep will be the dominant process only at very low strain rates; fractures and crushing are observed even at rates of movement found in landfast ice. Bearing problems in which ice is used as a structural material supporting load, represent an area where creep analysis is most important.

One of the earliest studies was one of the flow of large ice masses, e.g. glacial ice (Emery and Mirza, 1980). In this, finite elements were used to simulate flow behaviour (creep); basal sliding as well as discontinuities were also simulated using special elements.

An interesting analysis of creep buckling of floating ice sheets was carried out by Sjolind (1984) based on the power-law creep term of Eq.(3), i.e. $\dot{\epsilon} = C\sigma^n$.

The reference stress method was used to solve the indentation problem for ice (Ponter et al, 1983). A finite element solution was used to obtain "input" solutions for the method. Various values of n in a power-law creep formulation were investigated. The method provides an attractive method for obtaining a range of approximate

closed form results from a limited number of finite element runs, and has been used in practical studies of ice-structure interaction (e.g., Nessim, et al, 1986).

Bruen and Vivatrat (1984) and Vivatrat, Chen and Bruen (1984) used a power-law stress-strain relationship similar to those just discussed with $n \approx 3$ for low strain rates and $n \rightarrow \infty$ higher rates ($> 3 \times 10^{-4} \text{ s}^{-1}$). The method of analysis was based on a bound theorem of creep analysis and required the definition of a velocity field as shown in Figure 12(a). Higher strain rates were account for by considering lines of constant strain rate - the circles in Figure 12(b). Within the fractured and crushed zones, the boundaries of which are given by the circles, different energy dissipation mechanisms are operative. The results show an increasing effective ice pressure with velocity, with a reduction of the pressure due to the fracture, and crushing mechanisms. It is considered that the method is very promising: a more direct linkage of energy dissipation to the processes of damage and flow of crushed ice (Sections 3.4 and 3.5) would be advantageous.

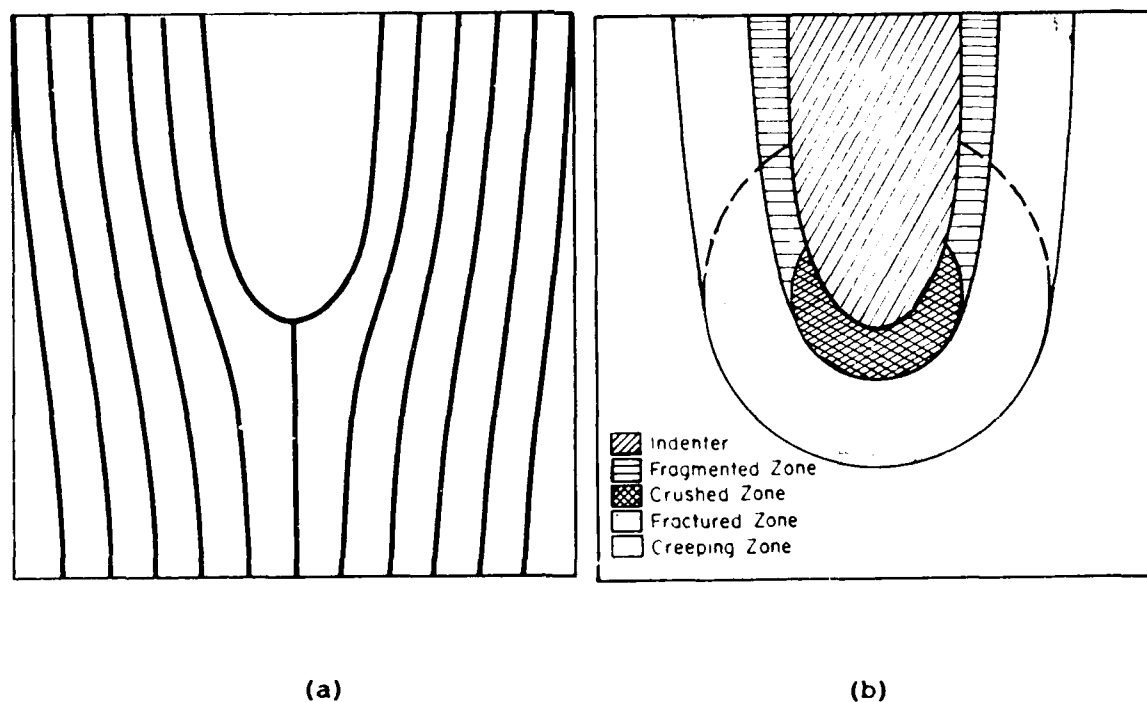


Figure 12. Bruen and Vivatrat's Velocity Field Approach

In the context of the above method, it should be noted that a finite element analysis of creep in ice has been developed (Chehayeb et al, 1985) and compared to upper bound solutions based on velocity fields as well as to other solutions.

It was pointed out earlier that bearing problems pose an important area where creep solutions can be of use. Figure 13 shows a result obtained by the writer's team as an illustrative example. It is based on elastic response with power-law creep, using the finite element program ABAQUS.

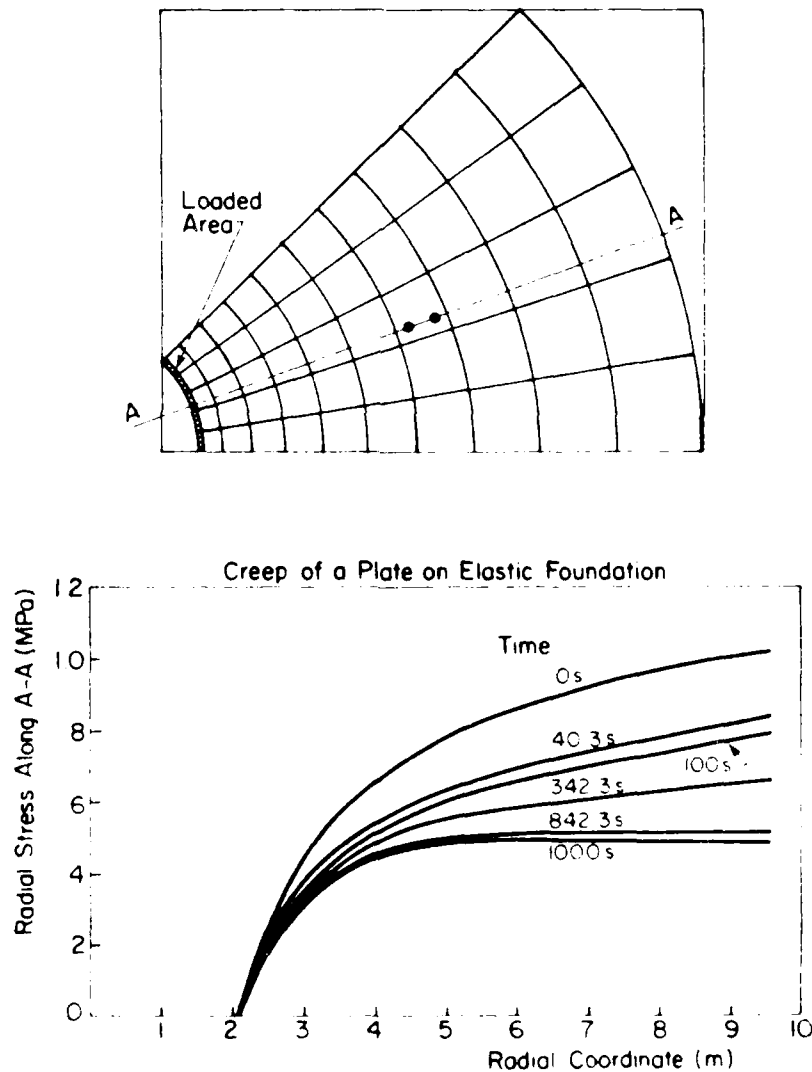


Figure 13. Time-Dependent Bearing Analysis of a Floating Plate: Arc Opposite Loaded Edge is Fixed. Power-Law Creep With $n = 3$ Considered

3.3 Global Fracture Analysis

Global fracture is characterized by propagation of a single crack and a small number of cracks in zones of tension. This kind of event can lead to substantial load reduction by the splitting of ice features and the subsequent creation of additional degrees of freedom. In icebreaking activities, this is of major significance.

One of the first calculations of this kind was presented by Palmer et al (1983). It was clear that further numerical work was needed in order to calculate more general situations, and the use of an incremental approach to propagation of cracks in large floes was used (Hamza and Muggeridge, 1984).

The use of energy release can be also accomplished by the use of the J-integral (Parks, 1977) using finite elements leading to results for general geometries, both of the crack and the ice feature. This approach has been pursued by Tomin et al (1985) and a typical mesh around a crack in an indenter problem is shown in Figure 14. In this analysis, the crack length is incremented, and in effect the strain energy released is compared to the energy requirement per unit area of the crack.

Plasticity and creep effects at the crack tip can be included in the J-integral method, but are not usually of significance - or rather, the effect can be included in the energy requirement with linear elastic methods used for the energy release.

The use of fracture mechanics in bow form analysis and optimization is of great potential importance, and should be pursued in investigations of Arctic Shipping. The phenomenon of slabbing needs to be clarified further from a scientific standpoint as regards the mechanisms involved.

3.4 Damage and Pulverization of Ice

As pointed out earlier (Sections 2.3 and 2.4), the most important damage is in states of moderate compression. This was recognized by

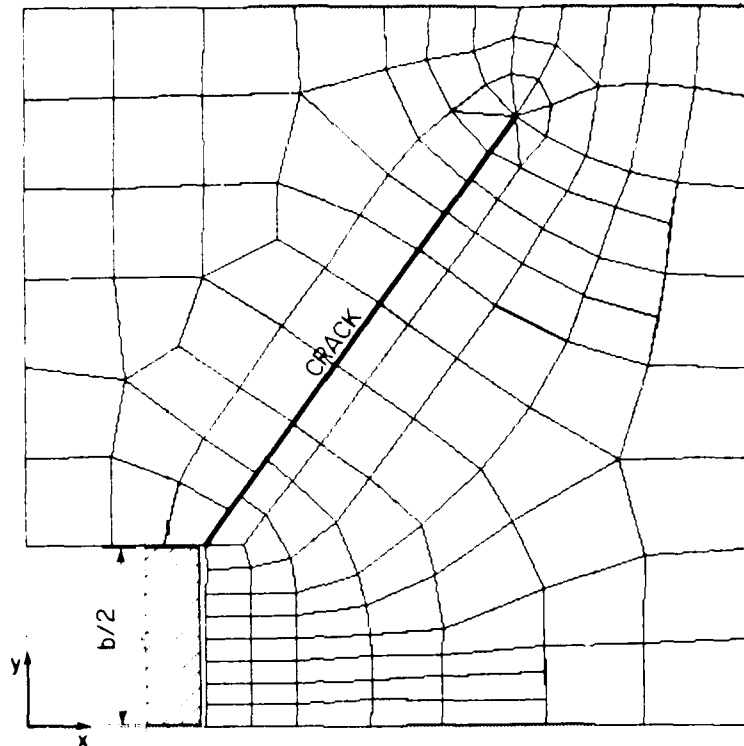


Figure 14. Close-up View of the Local Mesh Around the Large Crack

Ting and Sunder (1985) who applied damage mechanics to sea ice with a parameter D varying from 0 (no damage) to 1 (fully damaged). They applied this to the delayed elastic and viscous flow terms in the creep equation: degradation of elasticity was therefore only partly taken into account. Analyses such as those of Bazant and Kim (1985), applied to tensile states, should be assessed in light of the fact that ice damage is important in states of moderate compressive stress. The latter approach was based on the blunt crack band theory, which could be extended to other states of stress.

A point that has not been recognized sufficiently is the process of shear damage. As pointed out in Section 2.4, this leads to eventual pulverization and indeed a crushed material that flows - but without the rigidity of the virgin material. Shear damage has been analyzed with regard to rock masses (Resende and Martin, 1984) and was applied to ice by Corneau et al (1986). The degrading stress-strain relationship was of the kind illustrated in Figure 8(b).

3.5 Flow of Pulverized Ice

One does not have the luxury in ice mechanics of stopping the analysis at a convenient point since one is not usually "designing" the ice feature. In Section 2.5, the work of the Russian researchers was discussed and the fact that pulverized ice will flow around an object (at higher strain rates) was pointed out. The approach of these workers has been followed by Brown et al (1986). An extension of this analysis based on the elastic-viscoelastic analogy described in Section 2.5, using finite element methods, has been given by Corneau et al (1986). This gives Eulerian solutions (flow through the mesh) based on the analogy mentioned. An analysis using finite differences and the computer program PISCES has been outlined by Kivisild and Iyer (1978).

3.6 Discrete Element Analysis

Discrete elements differ from finite elements in that the movement of each element is followed during the interaction simulation. The discrete elements can separate along their boundaries, so that discontinuities can be modelled.

The method was applied to ice problems by Yoshimura and Kamesaki (1981). It has formed the basis of the program CICE, developed by Hocking and his co-workers (Williams et al, 1985; Hocking et al, 1985). This program has been calibrated against a wide set of experimental and field results. To give a flavour of the results, Figure 15 shows a cross-sectional plot of ice pieces during an interaction.

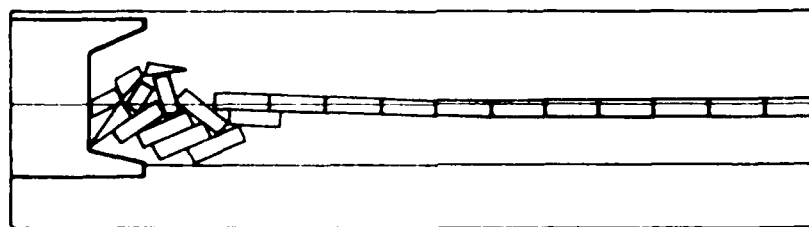


Figure 15. Discrete Element Analysis of Interaction of Ice Floe and Structure

A variety of failure criteria are available, however, to simulate the break-up of ice pieces. It is considered that a more detailed analysis of fracture, taking into account existing cracks and flaws, would make the calibration more effective. This could be achieved by calibration with FE models of the kind described earlier (Section 3.3). Also, the "book-keeping" involved in following individual ice pieces in analyses of crushing would become excessive. A separate "flow" analysis (Section 3.4) would be a possibility in this regard. The method is, however, ideally suited for problems involving ride-up and pile-up.

3.7 Large Scale Models

The dynamics and thermodynamics of sea ice cover is studied to determine the extent, thickness distribution and velocity field of the ice. Work in this area has been surveyed by Sodhi (1984) and will not be dealt with in further detail here. The point might be made that most analyses include viscoplastic constitutive relations for ice and that fracture and damage are not modelled.

3.8 Statistical Aspects

One of the more important potential uses of numerical methods is to study statistical aspects of ice mechanics. This work is in its infancy: A recent study by Maes et al (1986) shows some results which are illustrated in Figure 16.

4. CONCLUSION

It is tempting to describe the field of numerical analysis of ice as a "Tower of Babel" of conflicting approaches - as one distinguished researcher once described the field of ice mechanics. Yet there is an urgent need to continue with a variety of approaches, so as to respond to the complexity of ice behaviour. At the very least, numerical analysis provides an ongoing tool for learning about the mechanics of ice: and indeed, many of the studies summarized have done that. High-speed computers provide the opportunity to perform analyses that were not conceivable even one or two decades ago. These tools can be

taken several steps forward and used in obtaining practical results. For instance, the analysis of global fracture processes could be carried out with the methods described using the J-integral: this could be used for bow form analysis, for example, with the present stage of technology. Joint analytical (numerical) and experimental work would be invaluable in general in advancing the state-of-the-art.

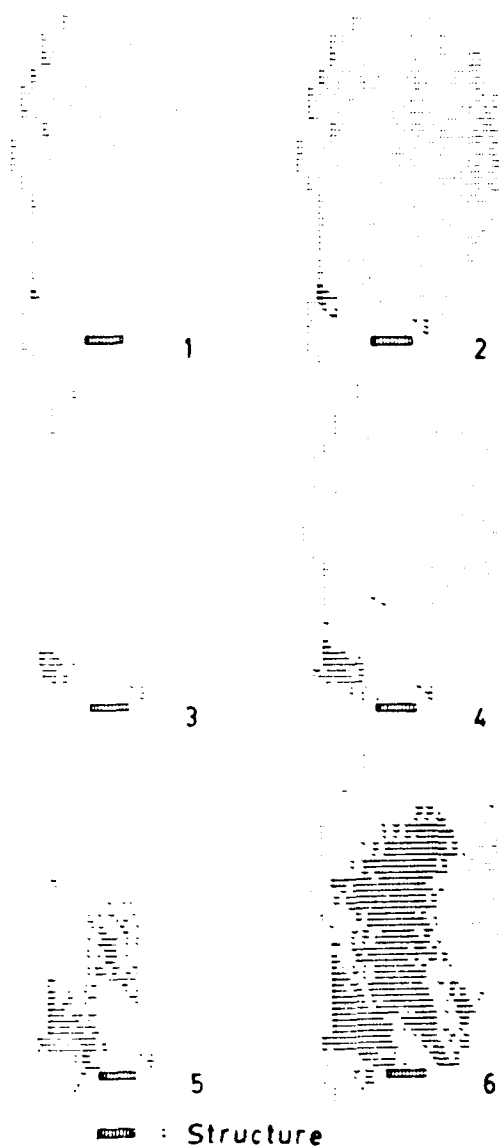
It may seem a truism to state that in making this advance, it is important to model realistically the behaviour of ice. Yet there are still analyses that are proposed that describe ice as a "plastic" material in the sense of a classical continuum mechanics approach. Other approaches have analyzed ice as a set of nonlinear springs without specifying how the stiffnesses are obtained.

The following aspects need particular attention:

- damage process in the small, and in the large;
- ice clearing, flow of pulverized ice, Eulerian formulations;
- statistical effects, local bending (buckling) of imperfect sheets, spalling, non-simultaneous failure; and
- fracture mechanics for large ice features as found in the field.

References

- Ashby, M.F. and Hallam, S.D., 1986. The Failure of Brittle Solids Containing Small Cracks Under Compressive Stress States. *Acta Metallurgica*, Vol.34, No.3, pp. 497-510.
- Ashby, M.F. and Daval, P., 1985. The Creep of Polycrystalline Ice. *Cold Regions Science and Technology*, Vol.11, pp. 285-300.



Loads on the structure :

1 : 2.2 MN/m	2 : 2.8 MN/m
3 : 3.3 "	4 : 3.9 "
5 : 4.4 "	6 : 5.0 "

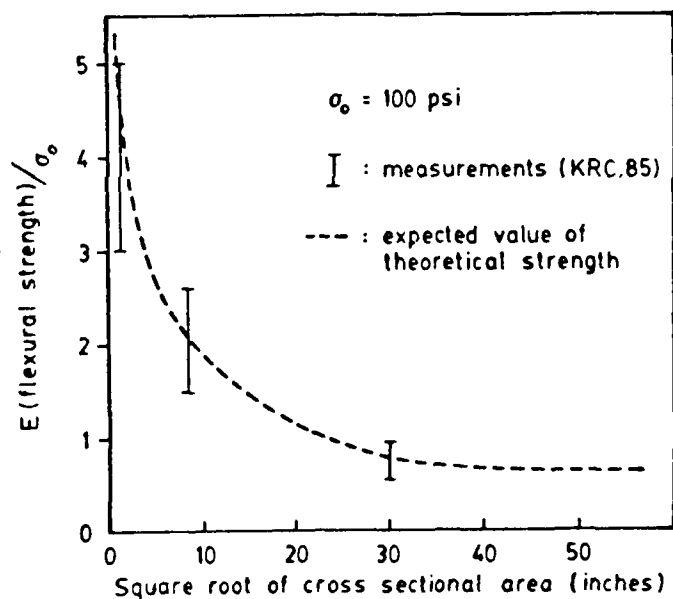


Figure 16(a). Finite Element Analysis of Progressive Breakup of Floe Against Structure, Shaded Areas Showing Damaged Areas;

(b) Statistical Result Showing Size Effect Relationship

(from Maes et al, 1986)

- Bazant, Z.P. and Kim, J.K., 1985. Fracture Theory for Non-homogeneous Brittle Materials with Application to Ice. Proceedings, ARCTIC 85, Civil Engineering in the Arctic Offshore, ASCE, March, pp. 917-929.
- Brown, T.G., et al. 1986. Ice-Structure Interaction Global and Local Loads. Proceedings, Fifth OMAE Symposium, Vol.IV, ASME, pp. 555-560.
- Bruen, F.J. and Vivatrat, V., 1984. Ice Force Prediction Based on Strain-Rate Field. Proceedings Third OMAE Symposium, ASME, 1984, pp. 275-281.
- Chehayab, F.S., Ting, S.K., Sunder, S.S. and Connor, J.J., 1985. Sea Ice Indentation in the Creeping Mode. Proceedings, OTC, Vol. 4, pp. 329-341.
- Cormeau, A., Jordaan, I.J. and Maes, M., 1986. Development of a Model for Progressive Damage in Ice. Report by Det norske Veritas (Canada) Ltd., prepared for Public Works Canada.
- Cormeau, A., Jordaan, I.J., Nessim, M. and Tomin, M., 1984. Ice-Structure Interaction: A Fundamental Energy-Based Approach. Proceedings, IAHR Symposium on Ice, Vol.III, pp. 161-174.
- Emery, J.J. and Mirza, F.A., 1980. Finite Element Method Simulation of Large Ice Mass Flow Behaviour. IUTAM Symposium, Copenhagen 1979, Springer-Verlag, pp. 82-92.
- Hamza, H. and Muggeridge, D.B., 1984. A Theoretical Fracture Analysis of the Impact of a Large Ice Floe with a Large Offshore Structure. Proceedings, Third OMAE Symposium, ASME, Vol. III, pp. 291-297.
- Hnatiuk, J. and Idzien, E.G., 1986. Performance of Beaudril's New Beaufort Sea Drilling System. Proceedings, Fifth OMAE Symposium, Vol.IV, pp. 183-191.

- Hocking, G., Mustoe, G.G.W., and Williams, J.R., 1985. Dynamic Global Forces on an Offshore Structure from Multi-year Ice Floe Impacts. Proceedings, ARCTIC '85 Conference, ASCE, San Francisco, March, pp. 202-210.
- Hocking, G., Mustoe, G.G.W., and Williams, J.R., 1985. Influence of Artificial Island Side-Slopes on Ice Ride-Up and Pile-Up. Proceedings, ARCTIC '85 Conference, ASCE, San Francisco, March, pp. 185-192.
- Jones, S.J., 1982. The Confined Compressive Strength of Polycrystalline Ice. Journal of Glaciology, Vol. 28, No. 98, pp. 171-177.
- Jordaan, I.J., 1986. Constitutive Theories for Creep and Implications for Numerical Analysis, With Special Emphasis on Ice. In preparation.
- Kivisild, H.R. and Iyer, S.H., 1978. Mathematical and Physical Modelling of Ice. Proceedings, IAHR Symposium, Lulea, Sweden, Part 1, pp. 379-291.
- Kry, P.R., 1976. Effect of Structure Width on the Stresses from Continuously Crushing Ice. Imperial Oil Report No. IPRT-SME-76, Calgary, Alberta.
- Kurdyumov, V.A. and Kheisin, D.E., 1976. Hydrodynamic Model of the Impact of a Solid on Ice. Prikladnaya Mekhanika, Vol. 12, No. 10, pp. 103-109.
- Laskow, V., 1982. Ship-Ice Interaction Models. SNAME, Arctic Section, Calgary, Alberta.
- Leckie, F.A., 1978. The Constitutive Equations of Continuum Creep Damage Mechanics. Phil. Transactions Royal Society, London, A288, pp. 27-47.

- Maes, M., Jordaan, I.J., Cormeau, A. and Baldwin, J., 1986. Probabilistic Theories for the Failure of Sea Ice. International Conference on Ice Technology, MIT, Boston.
- Michel, B., 1978. Ice Mechanics. Les Presses de L'Université Laval, Québec.
- Nessim, M.A., et.al., 1986. Probability Based Design Criteria for Ice Loads on Fixed Structures in the Beaufort Sea. Report, Det norske Veritas (Canada) Ltd.
- Palmer, A.C., et.al., 1983. Fracture and Its Role in Determining Ice Forces on Offshore Structures. Annals of Glaciology, Vol. 4, pp. 216-221.
- Parks, D.M., 1977. The Virtual Crack Extension Method for Nonlinear Material Behaviour. Computer Methods in Applied Mechanics and Engineering, Vol. 12, pp. 353-364.
- Ponter, A.R.S., et.al., 1983. The Force Exerted by a Moving Ice Sheet on an Offshore Structure. Part I: The Creep Mode. Cold Regions Science and Technology, Vol. 8, pp. 109-118.
- Pounder, E.R., 1965. The Physics of Ice. Pergamon Press.
- Pulkkinen, E.A., 1985. The Creep Analysis of Ice Forces by the Finite Element Method. Proceedings, POAC 85, Vol.1, pp. 138-150.
- Resende, L. and Martin, J.B., 1984. A Progressive Damage 'Continuum' Model for Granular Materials. Computer Methods in Applied Mechanics and Engineering, Vol. 42, pp. 1-18.
- Riska, K., 1980. On the Role of Failure Criterion of Ice in Determining Ice Loads. Technical Research Centre of Finland (VTT), Ship Laboratory Report 7, Espoo.

- Sanderson, T.J.O., 1984. Theoretical and Measured Ice Forces on Wide Structures. Proceedings, IAHR Symposium, Hamburg, Vol.IV, pp. 151-207.
- Schapery, R.A., 1964. Application of Thermodynamics to Thermomechanical, Fracture and Birefringent Phenomena in Viscoelastic Media. Journal of Applied Physics, Vol. 35, No. 5.
- Sih, G.C., 1973. Introductory Chapter: A Special Theory of Crack Propagation. In Mechanics of Fracture, Methods of Analysis and Solution of Crack Problems, Ed. G.C. Sih, Noordhoff.
- Sinha, N.K., 1978. Short-Term Rheology of Polycrystalline Ice. Journal of Glaciology, Vol.21, pp. 457-473.
- Sjolind, S-G., 1984. Viscoelastic Buckling of Beams and Plates on Elastic Foundation. IAHR Ice Symposium, 1984.
- Sjolind, S-G., 1985. Viscoelastic Buckling of Floating Ice Sheets. Cold Regions Science and Technology, Vol. II, pp. 241-246.
- Sodhi, D.S., 1984. Computational Mechanics in Arctic Engineering. Proceedings, CSCE Specialty Conference in Computer Methods in Offshore Engineering, Halifax, N.S., pp. 351-374.
- Sodhi, D.S. and Hamza, H.E., 1977. Buckling Analysis of a Semi-Infinite Ice Sheet. Proceedings POAC 77, Memorial University of Newfoundland, St. John's, Newfoundland, pp. 593-604.
- Timco, G.W., 1986. Indentation and Penetration of Edge-Loaded Freshwater Ice Sheets in the Brittle Range. Proceedings Fifth OMAE Symposium, Vol. IV, ASME, pp. 444-452.
- Timoshenko, S.P. and Goodier, J.N., 1970. Theory of Elasticity. 3rd Edition, Mc-Graw-Hill.

- Ting, S.K. and Sunder, S.S., 1985. Constitutive Modelling of Sea Ice with Applications to Indentation Problems. Massachusetts Institute of Technology, CSEOE, Research Report No. 3.
- Tomin, M.J., Cheung, M., Jordaan, I.J., and Corneau, A., 1986. Analysis of Failure Modes and Damage Processes of Freshwater Ice in Indentation Tests. Proceedings Fifth OMAE Symposium, Vol. IV, ASME, pp. 453-460.
- Tomin, M.J., Corneau, A. and Jordaan, I.J., 1985. Development of Analytical Models Related to Experimental Work on Ice-Structure Interaction. Det norske Veritas (Canada) Ltd., Report submitted to Public Works Canada.
- Vivatrat, V., Chen, V. and Bruen, F.J., 1984. Ice Load Prediction for Arctic Nearshore Zone. Cold Regions Science and Technology, Vol. 10, pp. 75-87.
- Wang, Y.S. and J.P. Poplin, 1981. Large Scale Ice Strength Tests, 1980. Exxon P.R.C. 23PR81.
- Weibull, W., 1951. A Statistical Distribution Function of Wide Applicability. Journal of Applied Mechanics, Vol. 18.
- Williams, J.R., Hocking, G., and Mustoe, G.G.W., 1985. The Theoretical Basis of the Discrete Element Method. Int. Conf. on Advances in Numerical Methods in Eng., Univ. of Swansea, U.K.
- Yoshimura, N. and Kamesaki, K., 1981. The Estimation of the Crack Pattern on Ice by the New Discrete Model. IAHR Symposium on Ice, Quebec.

APPENDIX 1

ORGANIZATIONS ACTIVE IN NUMERICAL MODELLING OF
ICE MASSES UNDER STRESS

Applied Mechanics Inc.

Frank Bercha and Associates

Massachusetts Institute of Technology

University of Oulu

U.S. Army Cold Regions Research and Engineering Laboratory

Det norske Veritas (Canada)

Brian Watt and Associates

FIELD TECHNIQUES FOR ICE FORCE MEASUREMENTS

K.R. Croasdale	Esso Resources	Calgary
Frontier Section Head	Canada Ltd.	Alberta, Canada
 R. Frederking	 National Research	 Ottawa
Senior Research Officer	Council of Canada	Ontario, Canada

1.0 Introduction

Efforts expended on analytical solutions for ice forces and on laboratory testing of ice are of limited value unless full-scale observations and calibrations of ice structure interaction are also available. Without real-world experience and measurements it is doubtful if any substantial progress could have been made in understanding the physics of ice-structure interaction, and in developing workable engineering methods.

In recognition of the importance of obtaining actual measurements of ice forces, engineers have for a long time been developing measurement techniques. Many bridge piers, lighthouses and docks have been instrumented. More recently, the artificial islands and caisson structures being used for exploratory drilling in the Arctic Ocean have been the subject of ice-interaction measurements. In addition, natural features such as small rock islands have been used as substitutes for real structures in order to study ice-structure interaction in environments where no man-made structures yet exist.

In addition to providing a key to better predictions, it is important to recognize that the field measurement of ice forces is also an important element of operational safety procedures. As engineers and operators recognized the uncertainty inherent in ice force predictions, especially in new environments (which were not always well-known), it became apparent that a real-time indicator of the force levels on a structure (and/or its response) could be a vital element in operational safety.

Therefore, from the time of the early artificial drilling islands it has been quite common to link ice force instrumentation to operational alert procedures. Alert procedures have been described elsewhere, (Wright and Weaver, 1983) but briefly, as ice forces and/or structure deformations reach certain predetermined levels, operational procedures on the island are modified on a real-time basis. A typical extreme operational response would be to secure the well and evacuate all but a skeleton crew. Such situations have been rare, but they have occurred. Obviously they are costly modifications to an already costly operation. When ice force measurement devices are linked to such operational procedures then of course it is of paramount importance that the ice force measurements (and their interpretation) are reliable and reasonably accurate.

Observation and measurements of ice-structure interaction have been conducted worldwide, but because of the background and experience of the authors, this review paper will focus primarily on techniques developed and applied in North America, especially in Canada. It should be emphasized however that the international scientific and engineering community has contributed significantly to this topic; although it was in Canada where most of the new techniques for arctic structures were applied first.

1.0 Overview of Methods of Approach

When ice pushes against a structure a force is generated. According to Newton's Law, the force is equally and oppositely applied to both the structure and the ice. Therefore to measure the interaction force we have a choice of measuring either the response of the structure, or the response of the ice. This distinction broadly categorizes the two fundamental approaches, namely;

- in situ measurements on the ice,
- structural response measurements.

Each approach has its advantages and disadvantages, ideally both methods should be used together, but in some situations only one of the approaches will be feasible.

For example, in dynamic ice situations where the ice is continuously moving, it is preferable to instrument the structure, because in situ instruments on the ice will quickly move by the structure. On the other

hand, once the ice around a structure has become landfast (and subject to relatively small movements) it will often be preferable to instrument the ice surrounding the structure, (especially if the structure is an artificial island surrounded by a grounded rubble field and therefore difficult to instrument for global ice loads).

For discrete ice features, such as isolated multi-year floes or icebergs, measurements of the deceleration and motions of the ice as it interacts with the structure can be used to deduce the global ice forces.

On a structure we have the choice of either measuring the actual ice pressures at the ice line, or measuring the global response of the structure. Neither approach is simple, and both methods have their difficulties when the structure is large and has redundant load paths. Ice pressure panels at the ice line have the advantage that local variations in ice pressure can also be measured. But unless a continuous band of load panels is placed around the structure (an expensive proposition on a large structure), considerable interpolation and extrapolation is required in order to predict global forces from a limited number of local ice pressure readings. Also, sloping structures are not amenable to this form of instrumentation for global forces.

Internal strain gauging of structural elements is often a popular method, but interpretation usually requires either a full-scale calibration or a reliable structural analysis.

Another approach is to use soils instrumentation (e.g. total pressure cells, slope indicators, piezometers etc.) either in the foundation or interior fill. The major drawback of this approach is that under service loads, the response of the soil is often too small to be measured reliably.

3.0 In Situ Methods

3.1 General

Superficially it would seem to be a relatively simple matter to measure in situ stresses in an ice sheet. Why not simply measure strain and convert to stress using a value of modulus for ice? Alternatively why not install in the ice a hydraulically filled flat jack connected to

a pressure transducer and measure the pressure as the ice is stressed? Both of these approaches are simple, and have been used with other materials including soils and rock; what are the issues relating to their use in ice?

First, in ice, the simple conversion of strain to stress is fraught with difficulty, because ice is not a linear elastic material. Ice is a material close to its melting point and therefore exhibits creep. When ice is loaded with a constant stress it initially deforms elastically (i.e. if the load is removed the strain returns to zero) but after a few minutes (or less) the ice creeps. Initially there is a primary creep phase in which the strain rate is decreasing with time. This phase is followed by a secondary creep phase in which the strain rate is constant, and finally there is a tertiary creep phase in which the strain rate increases to failure. These different creep regimes make the interpretation of a simple strain measurement extremely difficult, especially since the elastic and creep deformation characteristics vary with ice temperature, crystallography, salinity and stress level. In fact, it is generally recognized by proponents of strain meters that ice stress can be interpreted sensibly only when the ice is in secondary creep. In that phase, there is a unique relationship between strain rate and stress according to Glen's law

$$\dot{\epsilon} = A\sigma^n \quad (1)$$

where $\dot{\epsilon}$ is strain rate; σ is stress, n is equal to about 3, and A is a coefficient depending on ice characteristics such as temperature, salinity and crystal structure. Thus, strain meters, according to the theory of ice deformation, may be useful only to measure loads applied long enough for secondary creep to be established (about 45 minutes or more).

The use of strain meters will be discussed later. At this point, it is interesting to note that historically, because of perceived difficulties in relating ice strain to stress, ice engineers have pursued the concept of an in situ stress sensor which would be insensitive to varying ice deformation characteristics resulting from creep and to the effects of

varying ice properties such as temperature, salinity and crystal structure.

3.2 Theory of ice stress sensors

There are problems associated with insertion of a sensor into an ice sheet and interpretation of the results. First, an inclusion in an ice sheet can lead to a disturbance of the stress field such that the stress experienced by the sensor is different from the stress in the sheet had the sensor not been there. This problem has been addressed by several investigators (Metge et al, 1975; Templeton, 1981; Chen, 1981) and elastic theories have been developed which relate sensor stiffness and geometry to the modulus of the surrounding material.

Typical results from this theory of inclusions are reproduced in Fig. 1. The results show obviously that the ideal sensor should have the same modulus or stiffness as the ice. So why not build sensors according to such a specification? The problem, discussed earlier, is that the relationship between stress and strain (modulus) for ice is complex and there is no unique value. Ice modulus varies with temperature, salinity, crystal structure and, because of creep, with time of loading. Therefore the ideal sensor should read the ice stress regardless of the modulus of the surrounding ice. How can this be achieved?

The first attempt to rationalize sensor design was described by Metge et al (1975). A wide thin sensor was proposed with sufficient stiffness that as the effective ice modulus varied, the ratio between ice stress on the sensor and stress in the ice remained constant. As can be seen from Fig. 1, this should result in an inclusion factor (stress ratio) remaining close to 1.0. This then would be the ideal sensor form, and it is the reason why several sensors of this type have appeared.

The equation for Figure 1 is of the form: (Chen, 1981)

$$\frac{\sigma}{\sigma_1} = \frac{(E_1/E) + (H/2D)(N/E)}{(E_1/E) [1 + (H/2D)(N/E)]} \quad (2)$$

Where σ is the undisturbed stress in the ice

σ_1 is the average stress felt by the sensor E_1

E_1 is the elastic modulus of the sensor

- D is the width or diameter of the sensor in a direction perpendicular to the stress
- H is the thickness of the sensor in the stress direction
- N is a property of the ice such that it is analogous to the subgrade reaction.

Chen recommends that the value of N/E be taken as 1.0 based on both theoretical and experimental examination of the problem. Thus equation (2) reduces to

$$\frac{\sigma}{\sigma_1} = \frac{(E_1/E) + H/2D}{(E_1/E)(1 + H/2D)} \quad (3)$$

This equation is very similar to the one proposed by Metge et al (1975) and yields a graphical result very similar to Figure 1.

Templeton (1981) provided a very thorough analysis of the embedded ice sensor problem and confirmed the use of an equation similar to (3). He also examined the effects of differential thermal expansion and the effects of transverse pressure (biaxial stress), and developed equations for their effects. He concluded that their effects on sensor accuracy could be minimized by maximizing the width-to-thickness ratio, i.e. using a thin wide sensor.

Despite this sound theoretical and practical basis for thin wide sensors, others have developed symmetrical cylindrical sensors. These have the advantage of biaxial capability and can usually be inserted into an augered hole.

The theory of biaxial cylindrical sensors has been developed and reported on by Cox and Johnson (1983). Their analysis yields, for a very stiff sensor, a value of $\sigma_1/\sigma = 1.5$ which is the same result as given by equation (3). Therefore, a stiff cylindrical sensor should have an inclusion factor of about 0.67 to obtain values of undisturbed ice stress. However, interpretation is not simple, because of the biaxial nature of the gauge. Readers are referred to the report of Cox and Johnson (1983) for the full theoretical treatment.

Even if we can accurately measure ice stress at discrete points in an ice sheet pushing against a structure, a remaining problem is that of converting these readings into a global load on the structure. A typical deployment of stress sensors in the ice around a structure is shown in Figure 2 (Netserk F-40, instrumented by Esso Resources Canada Ltd. in 1976). The theoretical approach to the problem is to calculate stress fields in the surrounding ice, match the readings from the stress sensors to the theoretical stress fields, hence to deduce the global load on the structure.

Initial application of this approach assumed elastic properties for the surrounding ice; more sophisticated approaches assume elasto-plastic ice properties and/or take into account modifications to the stress distribution due to ice creep. Wang and Ralston (1983) examined the radial stress distribution in an ice sheet pressing against a circular cylinder (with a frictionless boundary condition). A typical result of their analysis (Fig. 3) shows that a simple elastic analysis gives a good approximation for radial stress decay. Furthermore it shows that if a stress sensor is placed at a distance of one structure radius away from the structure typically it will measure about 60% of the ice pressure acting at the ice structure interface.

Naturally given adequate resources, the placing of several sensors along radial lines out from the structure would be desirable in order to confirm and/or calibrate such theoretical predictions.

It should be noted also that variation in ice modulus and thickness and the presence of cracks can seriously affect the prediction of global loads on the structure from in situ sensor readings.

3.3 Types and history of ice stress sensors

The first in situ ice pressure sensor (known to the authors) was developed at the University of Alaska in the early seventies (Nelson, 1975). The University of Alaska sensor was a small stiff sensor based on a strain-gauged metal cylinder. About the same time, the National Research Council in Ottawa developed a small soft sensor based on a thin-walled metal cylinder (Frederking, 1980).

Esso Resources Canada contracted the University of Alaska to install some of its sensors around some of the early artificial islands in the Beaufort Sea. Difficulties in interpretation of a small stiff sensor led Esso to develop the wide thin soft sensor which was subsequently used quite extensively by Esso around its islands (Metge et al, 1975).

The Esso sensor was later improved upon by Exxon who maintained the geometry of the Esso sensor but redesigned it internally to achieve better linearity and a different stiffness (Templeton, 1979; Chen, 1981).

During the late 1970's and early 1980's, a large variety of sensors started to appear. The original Esso design was again used as the basis for the MEDOF panel used by Dome around the Tarsiut island (Pilkington et al, 1983). Oceanographic Services developed a small cylindrical hard sensor which could be installed in a hole cored in the ice sheet (Johnson and Cox, 1980). ARCO Oil and Gas Company developed a sensor based on the flat jack principle (McBride, 1981). More recently, Arctec Canada has built a thin wide metal sensor called the Hexpack (Graham, et al, 1983). Other Canadian companies have developed both biaxial and panel type sensors as well as hydraulic disk types.

In terms of generic types, most of the above sensors can be considered to fall into two broad categories;

- thin wide sensors with a stiffness close to that of ice, and
- small stiff sensors

In a category of its own is the ARCO hydraulically filled disc, which is thin in relation to its diameter, but is small (about 4 inches in diameter) in relation to the ice thickness.

The thin wide panel sensors are generally arranged to measure the ice stress through the full ice sheet thickness. Their sensing elements can be wired-up to give either the average compressive stress through the thickness or the ice stress at various levels through the ice thickness.

Obviously small sensors can only measure stress over a small area, therefore, several may be needed through the ice sheet thickness in order to obtain an integrated stress for load. Thin wide sensors can usually

measure stress only in one direction, small cylindrical sensors can measure the principal stresses and direction. Of course any uniaxial sensing unit can be arranged in a rosette to enable principal stresses at a point to be measured.

3.4 Ice strain meters

Surface strain meters for use on sea ice have been in use for over a decade. Goodman (1980) describes their history and technical details. The original design was based on an invar wire and could typically resolve strain to 10^{-8} . Moore and Wadhams (1980) describe a rod strain meter which is generally more robust and portable than the wire gauge but with less resolution (10^{-7}).

Strain meters have been used to study the response of ice floes and icebergs to wave action (Goodman et al, 1980) and to conduct strain measurements in floating ice platforms (Anderson and Perry, 1980). Prodanovic (1978) describe a steel rod strain meter which was used to study strains in the land fast ice in the Alaska Beaufort Sea. More recently strain meters have been used on ice around structures in order to estimate ice forces. British Petroleum have pioneered this latter application (Goodman 1983; Sanderson et al, 1983; Frederking et al, 1984).

Strain meters have certain advantages over stress meters,

- they are easily deployed
- they do not disturb the ice stress

On the other hand, they have certain disadvantages,

- they measure only surface strain, bending strains may mask the compressive strains of interest
- their interpretation requires an intimate understanding of how strain rate relates to ice stress for different kinds of ice at various temperatures and salinities.

It is beyond the scope of this paper to present the theory for the interpretation of strain meters. The reader is referred to Sanderson (1984) for more details.

For additional discussion of various sensor types and their history refer to 4th Report of Working Group on Testing Methods in Ice, IAHR (1984).

3.5 In situ sensors - performance data

During the development and application of in situ ice sensors, a variety of tests have been performed to establish sensor characteristics and their response in controlled load environments. Basic performance data required for all sensors is a calibration of output against applied stress. For most sensors this is easily done in a loading press. Such tests also will indicate any fundamental problems such as non-linearity and hysteresis which could adversely affect their interpretation. Tests conducted in a sensitive test machine can also give the stiffness of the sensor which may be required to interpret the results using inclusion theory.

Calibration and testing of an ice sensor in a press is relatively simple, but does not confirm whether the sensor behaves as expected when it is contained in an ice sheet. Therefore, tests of sensors in ice under controlled load conditions are very important in establishing confidence in their readings. Until recently few tests of this nature have been performed. The exceptions were tests conducted on the Esso panel (Trofimenkoff, 1977), tests conducted on the Exxon panel (Chen 1981), tests conducted by Frederking (1980) on a cylindrical sensor and tests conducted on a biaxial cylindrical sensor (Johnson and Cox, 1980; Cox, 1984). The latter tests were conducted in the laboratory using both saline and fresh water ice under both uniaxial and biaxial stress conditions. Laboratory testing of this sensor was feasible because of its small size (5.72 cm diameter). Typical results from these tests showed good agreement between applied and measured stresses (within 15%), a resolution of about 20 kPa, and a temperature sensitivity of about 5 kPa/°C.

In a recent experiment, ten sensor types were tested in a large outdoor ice basin under controlled load conditions (K.R. Croasdale and Associates Ltd, 1984; Croasdale et al, 1986). The ice sheet was approximately 0.7 m thick, 50 m long and 30 m wide. Loads up to 1400 kN were applied at one end and reacted against an instrumented structure 3 m wide at the other end. The sensors were placed in the ice in front of the structure analogous to how they might be used in the field in an ice sheet surrounding a structure. The overall goal of the research project

was to evaluate how well sensors of various types could predict the forces on a structure, for both short- and long-term loads.

Twenty two separate tests were conducted at a variety of load levels. For most of the tests, most of the sensors yielded an output which generally tracked quite well the applied load on the structure. For each load plateau tested, the output from each sensor was converted to an average pressure across the reaction structure assuming an elastic stress distribution in the ice sheet.

For each sensor it was then possible to present the results as actual pressure on the structure (obtained directly from the load cells supporting the reaction structure) against predicted pressure on the structure obtained from the sensor reading. Results obtained for a typical panel-type sensor are shown in Figure 4. The panel measured the average ice stress through its thickness. Where small sensors (e.g. hydraulic disks) were used these were arranged in a rosette at two levels in the ice sheet. The average of the outputs from the two levels was used to obtain the results shown in Figure 5. Results obtained from the stiff cylindrical bi-axial sensor are shown in Figure 6. The slightly greater scatter obtained from this sensor is most likely due to the problem of using the measured stress as the average through the ice thickness. It was recognized that in some of the later tests, bending was induced in the ice sheet due to tilting back of the reaction structure. This bending of the ice sheet, although not detectable to the eye, also severely affected the use of the strain meters to predict loads on the structure.

In general, the experiment showed that in situ ice stress sensors of various generic types did respond as expected. For example, the panel-type sensors had inclusion factors close to 1.0, which did not change significantly with the time of applied load, i.e. creep. The experiment also indicated that for those sensors which were operational, the average percentage difference between the actual load on the structure and that obtained from the sensors readings was better than about 30%. Sensors which sampled at various levels in the ice sheet showed that a redistribution of stress through the ice sheet thickness did occur under long term loads, presumably due to creep. These results

emphasize the need to measure ice stress at more than one level through its thickness.

3.6 In situ sensors - case histories

The exploratory drilling islands which were built in the shallow waters of the Beaufort Sea commencing in 1973 provided a major incentive for the development and application of in situ ice stress sensors. Artificial islands are not easily instrumented for ice forces, especially if they become (as most do) surrounded by a grounded ice rubble field. Under these circumstances, about the only feasible method of deducing ice forces is to install in situ sensors in the ice surrounding the island and grounded rubble.

Initial efforts were based on a small hard sensor developed at the University of Alaska (Nelson and Sackinger, 1976). In addition, Esso's research department in Calgary, which was responsible for the monitoring of the early island, developed a thin wide soft sensor designed to penetrate the full ice thickness. These were usually arranged to measure radial stresses applied to the island (Figure 2). They were usually hard-wired back to a central data acquisition system on the island. Soils instruments, such as slope indicators and piezometers, were often also installed at a site, as well as devices to measure relative movement between the ice and the island.

Table 1 is an extension of a similar table originally prepared by Sanderson (1984). It summarizes the applications of in situ ice sensors (to measure ice forces) which has occurred in the Canadian Arctic from 1974 to the present. As Table 1 indicates, the first five islands were all instrumented in a similar fashion using Esso panels. The data gathered provided confirmation of design criteria and insights into ice structure interaction processes. As well, the instruments were linked to a real-time ice alert and ice defence system, which provided comfort to both the operating staff, management, and regulators, especially as islands were being built in ever increasing water depths.

Results from these early ice force monitoring projects are contained in the original company reports which are now available through APOA (see Table 1). Sanderson (1984) refers to the results and provides a brief

bending in the ice sheet which also induced cracking of the ice. The bending and cracking of the ice made comparison between sensors rather difficult.

The instrumentation of the Esso caisson retained island has been described by Hawkins et al (1983). At both sites where the caisson has been deployed (Kadluk and Amerk - see Table 1), in situ ice sensors have been deployed also. Results from the in situ sensors are reported by Johnson et al (1985), Croasdale (1985), Sayed et al (1986). At the Amerk location ice panels were placed in the refrozen ice rubble surrounding the caisson. The objective of the program was to investigate load transfer through the grounded ice rubble to the steel caisson. The results of the work indicate that at low load levels (i.e. 250 kPa applied at outside edge of rubble), all the load appears to be transferred to the underwater berm via the grounded ice rubble, and the caissons see no load.

Results from the monitoring of the SSDC at Uviluk and other locations have not been published yet.

One other application of in situ sensors which is in its early stages (and is referred to in Table 1) is to measure the driving forces in the pack-ice. In the context of ice forces, the incentives for such measurements was discussed by Croasdale and others in 1984. A project on the topic financed by the Government of Canada (proposal - Croasdale, 1985) led to a trial deployment of sensors in a multi-year floe in the southern Beaufort Sea in April 1986. The sensors had been specially designed for the low stress expected, and extensively cold room tested prior to field deployment. The results from the program will be published in 1987.

3.7 In situ sensors - comments on installation and removal

Panel-type sensors are usually installed using long-bladed chain saws. The thicker the ice the more difficult this operation becomes. Ice up to about 1 m thick is usually no problem, ice thicker than 1.5 m presents quite a challenge. Even though panel sensors are thin, they are thicker than a normal chain saw blade and it is usually necessary to make two parallel cuts about 10 cm apart. Care should be taken to avoid breaking

discussion of an event during which ice stresses up to 1.0 MPa were measured. Interpreted average stress across the island width was 1.2 MPa.

In 1981 the Tarsiut caisson island was constructed in 22 m of water. It was a significant departure in design from the dredged islands built to that time. Therefore it was decided to invest heavily in instrumentation for both operational safety and research purposes. The two seasons of data gathering at Tarsiut are referred to in Table 1 and have been discussed by Sanderson (1984), and Pilkington et al (1983). Note that the Medof panel is based on the internal design of the original Esso panel but uses the volume change of a fluid to indicate strain (the original Esso sensor measured capacitance). Also note that the Tarsiut second-season program utilized surface strain meters as a method of estimating total loads on the island (Sanderson, 1984). No results from the Tarsiut monitoring programs have yet been published but Pilkington et al (1983) notes that "The strain-gauged flat jack panels (on the structure) and the Medof panels (in-situ) provided the best ice load information, and generally, reasonable agreement was noted between these instruments where they could be compared."

Adams Island is a small natural rock island at the north end of Baffin Island. It was chosen by the National Research Council of Canada as a site to conduct ice interaction research. In situ instruments, both stress meters and strain meters were used. Details of the programs and results are given by Frederking et al (1984 and 1986). A typical output from one of the biaxial stress sensors is shown as Figure 7. Maximum principal compressive stress measured in the ice was about 350 KPa. (The ice was land-fast, with movements up to 300 mm/day and a strong tidal cycle).

The Nanisivik Dock on Baffin Island was also a site where in situ instruments were deployed during the winter of 1983/84 (see Table 1). Four different types of stress sensor and one strain meter were used. The overall objective of the program was to compare results from a variety of sensors installed at the same location. The results are described by Croasdale (1985). In general, compressive stresses in the ice around the dock were low. There was a strong tidal cycle causing

through to water until the full slot perimeter has been cut as deep as possible (dry slots are easier to cut than wet slots, especially in extremely cold weather).

If a chain saw is not available a slot can be made using a continuous line of augered holes, broken between if necessary, using an ice chisel. Where a major installation of ice panels is planned around a structure, a tractor equipped with a ditching blade is well worth having, and will save considerable labour. Slots can also be cut with steam or hot water, which incidentally, is the preferred method of panel removal.

Panel-type sensors should never be placed closer together than about 2 m. It is important to perform final checks on the sensor operation and to take zero readings prior to installing the sensors in their slots (recognizing that the temperature of the sensor lying on the ice will usually be colder than when it is frozen in). Freeze-in stresses will often be recorded by sensors (typically up to 350 kPa), but they are usually relieved by creep over a period of the first few days of operation of the sensor.

Smaller cylindrical and disk-type sensors (say less than 10 cm diameter) can be installed in augered holes. This operation of course is much easier. In this case the depth of the holes can be set less than the ice thickness and the sensors flooded from the top. The only advantage is to be able to use fresh water rather than saline water when operating on sea ice. Experience indicates that under typical winter arctic conditions the choice of sea water or fresh water as a backfill material is not critical. Under warm conditions, fresh water is preferred in order to avoid the low modulus associated with warm saline ice. Under relatively warm conditions the freezing-in process can be accelerated by using a pack of dry ice at the surface and by putting back the ice cuttings into the augered hole after sensor installation.

In situ calibrations of ice sensors have been attempted using thin flat jacks inserted into slots close to the sensors. Results from these calibrations are often ambiguous because of uncertainty about the actual stress distribution induced in the ice by the flat jack. For sensors which are temperature sensitive it is usually necessary to install a

thermistor string close to the sensor through the ice thickness. Sensors should be installed in a flat and even area of the ice sheet, away from any cracks which may already be in the ice. If it is not possible to install a rosette of stress sensors, then a strain meter rosette on the ice surface near the stress sensor may be very helpful in interpretation of the stress readings.

3.8 In situ ice sensors - the future

The technology of ice stress sensors is now reasonably well developed. Sensors of various geometries ranging from thin wide panels to small stiff cylindrical sensors appear to function satisfactorily. Remaining problems are;

- improving installation and removal procedures especially for remote applications;
- development of a sensor which does not have to be frozen-in (for summer multi-year floe impact studies either by ships or against structures);
- reducing sensor costs (so that they can be abandoned if necessary);
- further work on low stress range sensors for pack ice force measurements (work on this has already started; Croasdale, 1985).

4.0 Ice Forces from Floe Motions

Another approach to measuring ice forces during ice-structure interaction is to deduce the ice forces from floe motions during an impact. Such an approach was used at Hans Island in 1980, 1981 and 1983. At Hans Island the decelerations of multi-year floes impacting the island were measured. By also estimating the mass of the floes, the ice forces acting between floe and island were deduced. These experiments have been described by Metge et al (1981) and Danielewicz et al (1983). Readers are referred to these references for a detailed discussion of the technique.

5.0 Loads on Structures

5.1 General

Where structures are placed in ice-covered waters an opportunity is presented for direct measurement of ice loads. Generally this can be accomplished by one of three fundamental approaches: (i) measure strains, deformations or movements of the structure itself, (ii) addition

of load sensing panels to the structure, and (iii) in cases of dynamic loads, measure accelerations of the structure, which, when combined with a knowledge of the dynamic response of the structure, allows loads to be determined. All three, but particularly the first two approaches generate information relevant to both local and global ice loads.

The first direct measurements of ice loads were on hydraulic structures such as bridge piers, dams and lighthouses. Measurements were carried out in the Soviet Union, United States of America, Germany, and Canada prior to 1970. In the past decade and a half, efforts have concentrated on measurements on offshore structures in marine environments. As indicated in the introduction, this review will concentrate on more recent experience in North America. Each of the three measurement approaches will now be considered in general. The remainder of this chapter will contain a number of case studies, critical comments and a concluding statement on the current status and future directions.

5.1.1 Structural measurements

The structure itself can be used as a transducer by measuring strain in components of the structure, relative deformations between parts of the structure, or absolute movements of the structure. In all cases some form of calibration is needed to convert the measurements into ice loads. Conversion can be accomplished by analytical calculations or by physical load calibration tests. Analytical calibrations require an accurate description of the geometry of the components of the structure, the nature of the interconnections between the components, and the constitutive relations for the materials from which the components are constructed. In large steel or reinforced concrete structures such analytical expressions generally exist since they are used in design. However they require adaptation to make them suitable for load predictions. When such expressions can be derived with adequate accuracy, point loads or load distributions can be deduced from strain or deformation measurements in the structure. Ambiguities in interpretation may arise due to redundancies in the load paths between load application points and strain gauge locations. Analytical calculations also are required to optimise the location of instrumentation.

Alternatively, physical calibration tests can be done, i.e. known loads or load distributions are applied to the structure and the resulting strains or deflections are measured. Physical calibrations potentially are more accurate provided that the nature of the actual ice load is correctly anticipated. However, physical calibrations are expensive to perform and have a limit on how far they can be extrapolated. Ideally a combination of physical and analytical calibrations should be used.

The actual type of transducer used in this type of measurement includes strain gauges or displacement transducers. Strain gauges are bonded to parts of the structure which are expected to have high sensitivity and accurate response to the anticipated loads. Similarly, displacement transducers, pendulums, borehole inclinometers or laser beams have been used to measure relative displacements between different parts of a structure. Surveying instruments including laser ranging devices are used to measure absolute displacements of the structure.

5.1.2 Add-on transducers

Load sensing panels have been placed on or in the outer surface of structures to measure ice loads. These are special purpose instruments which are designed or adapted to directly measure ice loads. In essence they consist of some sort of plate or panel to collect ice load and a load measuring transducer. The collector panel can vary in size from a few millimeters to a few meters. The load measuring transducer can have several levels of sophistication; i.e. measure total normal loads, shear loads and load distributions. They can provide information on global loads, local loads and pressure-area distributions.

Load or pressure panels are a more direct way of measuring ice loads than structural measurements, but bridging effects (similar to the well known problem of in situ transducers) present problems. It is necessary to match the stiffness and surface characteristics of the transducer to those of the structure. This task is not trivial. If the sensor is stiffer than the surrounding structure it will tend to shed ice, and if it is more compliant it will tend to shed load. Ice is neither elastic nor a simple fluid, but is viscoelastic, so the distribution of pressure is complex. It is desirable that appropriate calibrations be used when using ice.

No theory, similar to that for in situ transducers, has been developed for the design and placement of force or pressure transducers on structures subject to ice loads. Graham et al (1983) have suggested criteria, which, while developed for soils, could in the absence of any other guidelines, be applied for ice. The following criteria might be applied: (i) for a diaphragm type pressure sensor under a uniform pressure the ratio of diaphragm diameter to centre deflection should exceed 2000 at rated pressure, (ii) for a rigid plate transducer the ratio of diameter to deflection should exceed 10,000 at rated load. This is a subject which requires further work.

One class of transducer includes small circular diaphragm types which use strain gauges or pressure gauges to measure ice pressures on their sensing surface. The sensing surface is generally mounted flush with the structure surface. The other class of transducer uses a large panel with some type of load cell sandwiched between it and the structure. The load cells employ strain gauges or hydraulic pressure transducers as sensing elements.

5.1.3 Accelerometers

In the case of dynamic loading it is possible to use accelerometers to measure the dynamic response either of components or the total structure. Knowing the dynamic characteristics of the structure, dynamic ice loads can be determined from acceleration measurements. The dynamic equation of equilibrium and

$$m \ddot{x} + c \dot{x} + kx = F \sin \omega t \quad (5.1)$$

where m , c and k are the mass, damping and stiffness parameters, respectively, of the structure, x is the displacement of the structure from its equilibrium position, \dot{x} is the velocity, and \ddot{x} is the acceleration of the structure at time t . With a knowledge of the mass m , damping c , stiffness k , displacement x , and the structure equation of motion (5.1) can be calculated. With the knowledge of the structure equation of motion (5.1) and the displacement x , the acceleration \ddot{x} can be calculated. This is the acceleration of the structure. The acceleration of the structure is the acceleration of the structure. The acceleration of the structure is the acceleration of the structure.

physical calibrations can be carried out whereby a known load is applied to the structure and the dynamic response measured. From the dynamic response a transfer function can be derived which allows dynamic forces to be calculated from measured accelerations.

0.2 Ice load case studies

As mentioned in the introduction of this chapter there have been a number of projects to measure ice loads on structures. A partial inventory of such projects, together with some of their salient features is presented in Table 2. In selected instances more detailed information follows.

0.2.1 bridge piers

Work on bridge piers has shown that simple load measuring systems, noses or piles hinged below the water line and supported by a load cell above the water line, are most reliable. They only produce information on total loads, however, such systems can be made relatively stiff and rugged to obtain ice loads independent of the measuring system characteristics. The piers themselves may have a natural frequency in the range of the applied ice loads. Therefore it is important to know the dynamic characteristics of the pier so that true ice forces can be interpreted, free of any resonant condition. Whatever type of ice load measurement is made, it is highly desirable that realistic physical vibration tests be carried out. This is particularly so in the case of frame loading.

0.2.2 lightpiers

Techniques for measurement of ice forces on lightpiers are similar in many respects to those of bridge piers. An additional approach which was developed for lightpiers is to measure the acceleration response of the pier to ice loads. Combining the accelerations with the structure characteristics, as discussed in section 0.1.3., ice forces can be calculated. The major problem with measurements on lightpiers is maintenance. It has been necessary to have reliable self-contained instrumentation systems on the pier combined with either a telemetry system for transferring data to a shore station or a recording system on the pier with sufficient capacity to last throughout the measuring period, which could be up to 3 or 4 months.

5.2.3 Petroleum exploration structures

Tarsiut

Tarsiut is the location of a concrete caisson retained island in the Beaufort Sea. It comprises 4 sand-filled caissons which in turn enclose a sand-filled core. The structure is about 100 m across at the water line and has a vertical outer surface. The caissons are 10 m high and rest on a berm which comes to within 6 m of the water surface. The structure was extensively instrumented to measure ice loads (Pilkington et al, 1983) both for operational safety reasons and for future design. See Figure 8 for a schematic presentation of instrumentation locations.

Instrumentation comprised sensors to measure loads on the outer face, strain gauges embedded in the concrete and geotechnical sensors in the foundation and core. The strain gauges were of a weldable type and were attached to the steel reinforcing rods in the concrete. Gauge locations were selected on the basis of finite element calculations which also provided calibration coefficients for converting the measured strains to ice loads. From the distribution of gauges it was possible to establish load distributions and global loads. In spite of the care taken in the installation of gauges and cables, only a third of the gauges were operational at the beginning of the measurement program. Fortunately there was sufficient redundancy that useful results could still be obtained. A system of four 4 m by 4 m flat jack panels was attached to the outside of the east caisson (see Fig. 8 for locations). The outer face of each panel was a 89 mm thick steel plate to ensure that applied ice loads were uniformly distributed to the 16 flat jacks behind each panel. Pressure transducers measured the flat jack pressures.

Circular load cells were mounted in 880 mm diameter recesses in the north caisson. The sensing face was supported on shear bars or spiral coil hydraulic hoses. For more details on the characteristics of these transducers see Graham et al (1983). The shear bar transducers had a number of desirable features (low temperature coefficient, no creep and high stiffness). The spiral coil transducers had less desirable features but were inexpensive. Unfortunately a storm in the autumn led to water entering these gauges and making a number of them inoperable. Finally eight 50 mm diameter microstud gauges were installed in one of the flat

jack panels to measure local pressures. These were a diaphragm type of pressure gauge.

Experience over the winter 1981/82 showed that the embedded strain gauges and flat jacks provided consistent and reasonable ice load information. Inclinometers provided qualitative confirmation of major ice loading events and quantitative information for operational purposes.

Single Steel Drilling Caisson

The SSDC is a converted super tanker which has undergone extensive modifications to adapt it for use as a support structure for year-round exploratory drilling in the Beaufort Sea. The structure is 162 m long, 53 m wide, and 25 m high and is designed to rest in a water depth of 9 m. A submarine berm is constructed to achieve this water depth. All sides are vertical at the water line. This structure was usually surrounded by a small grounded rubble field.

A total of 16 1×2 m Medof panels was attached to the outer hull of the bow, port side and stern in side-by-side pair arrays. There were also two flat jacks on the bow and a number of shear bar panel sensors on the starboard side. The shear bar panels had sensor areas 0.5×0.5 m, 1×1 m and 1×2 m. They were arranged in arrays so that vertical ice pressure distributions and an indication of pressure-area relations could be obtained. Bulkheads were also strain-gauged. The shear bar transducers performed well under dynamic ice loads. A critical feature in the installation was the protection of the electrical cables from the ice pressure panels. They ran up the outside of the hull, and although protected behind steel angles, still were subject to damage due to supply boats impacting on them.

Caisson Retained Island

The CRI is an eight-segment octagonal-shaped steel structure. It is about 118 m across on the flats, 12 m high and the outer face is inclined (60° from the vertical). A central core 92 m across is filled with sand. Instrumentation consists of sensors for ice loads on the outer surface of the caisson, strain gauges on structural elements of the caisson and geotechnical sensors in the sand core and under the foundation (Hawkins

et al 1983). A schematic of the layout of the sensors is shown in Figure 9.

Ice force sensors on the outer surface comprise three different sizes and types. The smallest, microcells, are 165 mm in diameter. They are a temperature compensated strain-gauged diaphragm type. Four clusters of 4 sensors are mounted on the north quadrant of the caisson at the water line. They measure point or local ice loads and have high load capacity and short response time. The sensors are mounted flush with the caisson surface. The next type of sensor is an 815 mm diameter maxicell. These sensors measure pressure in a spiral coiled hydraulic tube sandwiched between two steel plates. It is effectively a load cell with an equivalent capacity of 7 MPa. Because of its construction it does not have a short response time. A total of 8 of these sensors are mounted on the southern half of the caisson. They are supported by structural stringers and are flush with the surface. The third type of sensor is a shear bar type with a load sensing surface 2.1 m high by 0.5 m wide. Strain gauged shear bars sense the normal component of the ice load applied to them. Nine of these sensors are deployed around the northern half of the caisson. For more details on the specifications of these sensors see Graham et al (1983). The internal structure of the caissons is instrumented with 156 weldable strain gauges. The locations were determined from a finite element analysis which also provided a means for interpreting the ice loading from the measured strains.

Geotechnical sensors are used to measure the response between the caisson and the sand and foundation. The instrumentation comprises total pressure cells, pore pressure cells and inclinometers.

Lo (1985) presented a method for calculating global ice loads from the UEL from strain measurements on web frames. The global loads calculated were considered to be accurate to within 20%. The local load distribution across a span (2.9m) was found to be very much a function of the ice modulus due to bridging effects. Discussed in section 3.1.2. Results from measurements with the microcell on shear bar panels could resolve this question of bridging but none are given.

Molikpaq

The Molikpaq is a bottom founded steel caisson structure designed for year-round use in the Beaufort Sea. It is 89 m across at the water line and encloses a sand-filled core. The exterior surface is sloped at 1:10 from the vertical. The structure has been deployed in water depths exceeding 20 m which places it in an area of moving ice most of the winter. Consequently no protective rubble field forms around the structure.

An extensive array of sensors is installed on the structure to help assure operational safety as well as to provide collecting data for analysis purposes (Rogers et al 1986). The instrumentation includes Medot ice load panels on the outer surface of the structure, strain gauges on various internal elements of the caisson, extensometers to measure global distortion of the caisson, accelerometers, piezometers, total pressure cells to measure interaction pressures between the base of the caisson and the soil foundation, inplace inclinometers to measure relative deformations of the sand core, and video cameras to document the structure failure modes. The Medot panels (1.1×2.7 m) are a total load type of panel, i.e. they sense the total ice load on them. The contact area of the ice on the panel had to be estimated in order to determine the effective ice pressure. The panels are deployed in several horizontal arrays which allows local load distributions and shear stresses to be determined.

The Medot panel is a sandwich of two steel plates (inner about 3 mm and outer about 1 mm) with a central piezometric button. The panels are mounted on the surface and filled with a fluid medium of the solution. Load is applied to the panel causing the button to compress and the internal pressure to rise and the gauge, thus change of volume causes the fluid to move to the gauge and a change in pressure to the panel to change. A pressure transducer is attached to the gauge to measure the hydrostatic head of the fluid. The change in pressure is related to the response as estimated by the following equation:

where ΔP is the change in pressure, ΔV is the change in the volume of the fluid, ΔV_c is the change in the volume of the caisson, ΔV_s is the change in the volume of the sand, ΔV_w is the change in the volume of the water, and ΔV_a is the change in the volume of the air.

of the ballast water in the ballast tanks of the caisson. In this way a known physical load could be generated to verify the response of the strain gauges.

The strain gauges, Medof panels and out-of-round distortion of the caisson have produced consistent predictions of global ice loads. Because of the absence of a rubble field the ice loading has a strong dynamic character. The accelerometers and strain gauges gave similar results indicating ice loading frequencies in the range 0.5 to 4 Hz.

5.2.4 Measurements on ships

Techniques used to measure ice loads on ships provide another source of experience which can be examined. They are similar to those used on structures, so are of definite interest. A number of studies carried out and some of their features are enumerated in Table 2. The following discussion will focus briefly on the techniques used.

The first category of technique to be examined is that of "add-on" transducers to measure loads or more correctly average pressures. One example is a 10 mm diameter strain gauged diaphragm pressure sensor mounted flush with the hull of the "Louis St. Laurent". The sensors are small and an array is needed to produce useable results, however they do require a means by which spacial and temporal variations of local ice pressures can be studied. Another is the "Varsta" gauge which uses the hull plating with a circular stiffening ring and supports welded to the hull to form a plate. The stiffening ensured that the "sensor element," 100 mm in diameter, acts like a circular plate rigidly supported around its circumference. A displacement transducer measures the deflection of the plate although strain gauges have also been used. It has the advantage of not requiring any holes through the hull plating. This technique has been used on a number of ships in the Baltic and produces useful results. A recent interesting application is the installation of 12 sensors mounted to the bow area of the "Leinster". Each plate has a central transducer supported on four pillars which allow not only the measurement of pressure, but also the magnitude and direction of the force exerted by the ice. The technique has produced good

The other approach is to apply strain gauges to the structural frame elements of the vessel which, together with a finite element analysis, allows ice loads to be determined. Both total loads and load distribution can be determined. As with structures, the location of the gauges is critical. The anticipated ice loading has to be simulated in order to interpret the strain results. Global loads are generally interpreted by treating the hull girder as a beam in bending. Another approach to obtain load distribution information as well as total loads is to measure shear strain difference between upper and lower ends of a frame and interpret it with a load influence coefficient matrix generated with a finite element analysis. These techniques have been successful.

5.3 Loads on structures - comments

The load measuring instrumentation which has been most successful has been the large panel type of transducer having a contact area in the order of 1 m^2 . These large panels can be made quite rugged. The results they produce can be used successfully to predict total loads acting on a structure. Smaller transducers have produced useful information on local ice loading on ships but apparently have not been of much use in the case of large structures. In the case of any type of panel type transducer, large or small, there is still a need for a better theoretical understanding of the "bridging" phenomenon.

The same limitations are highly desirable for all loading cases, i.e., large or small vessels, strain gauging of the structure, or dynamic loading. Where possible, particularly in the case of small ice pressure transducers, physical simulations should be performed with ice as the loading medium.

In operations with offshore exploration/exploitation structures direct measurement of the structure is of equal or more interest than load. In these structures, large strain gauges and displacement transducers are not available to measure all three components of the structure pressure field in the structure.

Any load and instrumentation which is applied to a structure must be rugged and reliable. It must be designed to protect instrumentation capable of measuring in water and in air. As always, good planning,

care, attention to detail and "good luck," are necessary components to a successful program.

6.0 Conclusions

Field techniques for ice force measurements have been the subject of a number of major studies over the past decade. Extensive instrumentation is now available, both in the form of transducers and data loggers. An adequate theoretical basis is available in most cases for interpreting results. Our understanding of ice forces on structures is still, however, incomplete. Every opportunity must, therefore, be taken to use the techniques available to measure and observe ice/structure interaction phenomena.

REFERENCES

- Anderson, K.G. (ed.) 1983. Tarsiut Island research programme 1982-83. APOA Project No. 198. (Proprietary).
- Anderson, K.G. and Perry, C. 1980. Strain measurements in floating ice platforms, Workshop on Sea Ice Field Measurements, St. John's Newfoundland, C-CORE Report 80-21. pp. 33-53.
- Blenkarn, K.A. 1970. Measurement and analysis of ice forces on Cook Inlet structures. 2nd Annual Offshore Technology Conference, Houston, Texas, April 22-24, 1970. OTC paper 1261, Vol. 2, pp. 365-378.
- Chen, A.C.T. (1981) Ice Pressure Sensor Inclusion Factors. A.S.M.E. Petroleum Division, Journal of Energy Resources Technology, Vol. 103, No. 1, March 1981, pp. 82-86.
- Comfort, G., and Noble, P. 1979. "Ice Trials to Evaluate Low Friction Coating on CCGS Louis S. St. Laurent", Arctec Canada Report 357C-4, October, 1979.
- Cox, G.F.N. and Johnson, J.B. 1983. Stress measurements in ice. CRREL Report 83-23.
- Cox, G.F.N., 1984. Evaluation of a biaxial ice stress sensor. IAHR Ice Symposium Hamburg 1984, Vol. 2, pp. 349-361.
- Croasdale, K.R., Graham, B.W., Comfort, G. and Marcellus, R.W. 1986. Evaluation of ice pressure sensors and strain meters in a large test basin. Submitted to IAHR Ice Symposium, Iowa City.

- Croasdale, K.R. 1985. Ice Investigations at a Beaufort Sea Caisson.
Report produced for National Research Council of Canada by
K.R. Croasdale & Associates Ltd.
- Croasdale, K.R. and Associates Ltd. 1984. Evaluation of ice pressure
sensors and strain meters in a large ice test basin. Research
Report of AOGA Project 253.
- Daley, C. St. John, J.W., Seibold, F. and Bayley, I. 1984. Analysis
of extreme ice loads measured on USCGC Polar Sea, SAME Transactions,
Vol. 92, pp. 241-252.
- Danys, J.V. 1975. Offshore installations to measure ice forces on the
lightpier in Lac St. Pierre. 9th International Conference on
Lighthouses and Other Aids to Navigation, Ottawa 1975. Paris,
International Association of Lighthouses Authorities.
- Danielewicz, B.W., Metge, M. and Dunwoody, A.B. 1983. On estimating
large scale ice forces from deceleration of ice floes. VTT
Symposium 38, 7th International Conference on Port and Ocean
Engineering Under Arctic Conditions, Helsinki, Finland, Vol. 4,
pp. 537-46.
- Engelbrektson, A. 1978. Dynamic ice loads on a lighthouse structure.
Proceedings 4th International Conference on Port and Ocean
Engineering under Arctic Conditions, Sept. 26-30, 1977. St. John's,
Newfoundland, Vol. 2, pp. 730-740.
- Frederking R.M.W., Sayed, M., Hodgson, T., and Berthelet, W., 1985. Ice
force results from the modified Yamachiche Bend Lightpier, winter
1983-84. Proceedings, of Canadian Coastal Conference, 1985, Aug.
13-16, St. John's, Newfoundland. pp. 319-331.
- Frederking, R. Wessels, E., Maxwell, J.B., Prnsenberg, S. and
Sayed, M., 1986. Ice pressures and behaviour at Adams Island,
winter 1983/84. Canadian Journal of Civil Engineering,
V. 13(2), pp. 140-149.
- Frederking, R. 1980. A Tubular Transducer of In-situ Stress Measurements
in Ice. Proceedings of Workshop on Sea Ice Field Measurements, St.
John's, Newfoundland, C-CORE Report 80-21., pp. 165-192.
- Frederking, R.M.W., Sayed, M., Wessels, E., Child, A.J. and
Bradford, D. 1984. Ice interaction with Adams Island, winter
1982-83. Proceedings IAHR Ice Symposium, Hamburg, Vol. 3.
pp. 187-201.

- Gaida, K.P., J.R. Barnes, and B.D. Wright 1983. Kulluk-An Arctic Exploratory Drilling Unit, OTC paper 4481 Offshore Technology Conference, Houston, Texas, May 1983, Vol. pp. 337-346.
- Ghoneim, G.A.M., and Keinonen, A. 1983. Full scale impact tests of Canmar Kigoriak in very thick ice. 7th Interantional Conference on Port and Ocean Engineering under Arctic Conditions, Helsinki, Finland, Vol. 3, pp. 329-346.
- Goodman, D.J., Wadham, P., and Squire, V.A., 1980. The flexural response of a tabular ice island to ocean swell. Arnals of Glaciology, Vol. 1, pp. 23-27.
- Goodman, D.G. 1980. Surface strain measuring instruments for use on sea ice. Workshop on Sea Ice Field Measurements, St. John's, Newfoundland, C-CORE Report 80-21. pp. 75-96.
- Goodman, D.J. 1983. Ice load instrumentation for Arctic Offshore Structures. Proceedings of the 7th International Conference on Port and Ocean Engineering under Arctic Coditions, Helsinki, April 1983, Vol. 4, pp. 703-704.
- Graham, B.W., Chabot, L.G., and Pilkington, G.R. 1983. Ice Load Sensors for Offshore Arctic Structures. Proceedings 7th International Conference on Port and Ocean Engineering under Arctic Conditions, Helsinki, Finland, Vol. 4 pp. 547-562.
- Hawkins, J.R., James, D.A. and Der, C.Y. 1983. Design, construction and installation of a system to measure environmental forces on a caisson retained island. 7th International Conference on Port and Ocean Engineering under Arctic Conditions, Helsinki, Finland. Vol. 4, pp. 770-779.
- IAHR, 1984, 4th Report of Working Group on Testing Methods in Ice, IAHR Ice Symposium, Hamburg, Vol. 4 pp. 1-41.
- Johnson, J.B., Cox, G.F.N., and Tucker III, W.B. 1985. Kadluk ice stress measurement program. 8th International Conference on Port and Ocean Engineering under Arctic Conditions. Narsarsuaq, Greenland Sept. 7-14, 1985, Vol. 1, pp. 88-100.
- Johnson, J.B. and Cox, G.F.N. 1980. The OSI Ice Stress Sensor. Workshop on Sea Ice Measurement, St. John's, Newfoundland, C-CORE Report 80-21 pp. 193-207.
- Määttänen, M. 1978. Ice-Force measurements at the Gulf of Bothnia by the Instrumented Keml 1 Lighthouse, Proceedings 4th International

- Conference on Port and Ocean Engineering under Arctic Conditions,
Sept 26-30, 1977. St. John's, Newfoundland. Vol 2. pp. 730-749.
- McFadden, T., Haynes, D., Burdick, J. and Zarling, J. 1981. Ice force
measurements on the Yukon River bridge. Proceeding ASCE
Specialty Conference, The Northern Community, April 8-10, 1981,
Seattle, Washington, pp. 749-777.
- Metge, M., Strilchuk, A., and Trofimenkoff, P., (1975). On Recording
Stresses in Ice. In IAHR 1975 Ice Problems Symposium
Proceedings, Hanover, N.H., pp. 459-468.
- Metge, M., Danielweiser, B. and Moore, R. 1981. On measuring large
scale ice forces: James Island 1980. 11th International Conference on
Port and Ocean Engineering under Arctic conditions, Quebec, V.Q.,
pp. 629-642.
- Metge, M. 1976. Ice conditions and ice defence at Netsok Bay and
Algoa Bay during the winter of 1974-75. APDA Project No. 1-75-1.
- Metge, M., Pilkington, S.S., Stralberg, A.O., Blanchet, L. 1980. A new
sensor for measuring ice forces on structures. 1st Annual Conference on
Ice Engineering, 1980, Vol. 4, pp. 14-21.
- Motgomery, G.L., Smith, S., and Upsett, A.W., 1980. Dynamic
response of marine piers to ice forces. Canadian Journal of Civil
Engineering, Vol. 7, No. 2, pp. 948-956.
- Moore, R., and Williams, P., 1975. Recent developments in structural
design. Workshop on Structural Measurement, St. John's, New Brunswick,
Canada September 1-3, 1975.
- Nelson, W., and Metge, M., 1975. Ice resistance of netsok bay. The ice engineer
and architect, Vol. 1, No. 1, Winter Edition, pp. 198-205.
- Parkinson, C. 1977. International conference on problems under Arctic
conditions, Quebec, Canada, pp. 1-8, 1977.
- Rosen, H., 1976. Ice Force Measurements on Structures Using
Impedance. Proceedings of the 1976 ASCE Specialty Conference on
Arctic Engineering.
- Selby, M., and Nelson, W.M., 1976. Ice stress measurements at Algoa
and Netsok Islands. 11th International Conference on Arctic
Engineering.
- Smith, M., Smith, M., Roscoe, N., and Johnson, M. 1975. Model and
field experiments for development of ice resistant offshore
structures. 11th Annual Offshore Technology Conference, Houston,
Texas, May 2-7, 1975. Paper 3750, Vol. 4, pp. 31-34.

- Pilkington, R., Blanchet, D. and Metge, M. 1983. Full-scale measurements of ice forces on an artificial island. VTT Symposium 38, 7th International Conference on Port and Ocean Engineering under Arctic Conditions, Helsinki, Finland, Vol. 4, pp. 818-834.
- Prodanovic, A., 1978. Field Ice Strain Measurements, IAHR Ice Symposium, Lulea, Sweden, Aug 7-9, 1978, Part 1, pp. 151-164.
- Riska, N., Nappin, J., and Viorin, J. 1983. Ice load and pressure measurements on board I.S. Sisu. 7th International conference on Port and Ocean Engineering Under Arctic Conditions, Helsinki, Finland, Vol. 4, pp. 108-109.
- Saunders, B.L., Harris, E.A., Seto, V.W. and Metge M. 1986. Performance report of the Workshop, while deployed at Tarsiat p-45. Third Annual Marine Geotechnical Conference, St. John's, 11-13, June 1986. Lulea, Sweden, U.L. and Beili, C.R., 1968. Determination of actual forces on bridge piers due to moving ice. Proceedings 1968 Congress of Canadian Road Association (now Roads and Transportation Association of Canada), Toronto, Canada, pp. 1-74.
- Schmidtson, L.B., 1984. Theoretical and measured ice forces on wide structures. Presented at IAHR Ice Symposium, Hamburg, Vol. 4, pp. 101-107.
- Simpson, J. L., Gill, A.J., Duckworth, R. and Westermann. P.H. 1984. Local ice load programme, Tarsiat Island, 1983. Report by BP Petroleum Development Ltd. (Proprietary).
- Sizer M., Cassile N.R., Frederking R. 1986. Ice stress measurements in a rubble field surrounding a caisson-retained island. Presented to International Conference on Ice Technology, MIT, Cambridge, Mass, June 10-12, 1986. McBride, E.J., 1981 "Ice Stress Sensor Program", Exxon Oil and Gas Company, Plano, Texas.
- Schwartz, J. 1977. The pressure of floating ice fields on piles, International Association for Hydraulic Research, Proceedings 1st Ice Symposium, Reykjavik, Iceland. pp. 6.3.1-6.3.-12.
- Schwartz, J. and Müller, L., 1985. Eisbrechetechnische Expedition mit PFS Polarster - Ziele und erste Ergebnisse. Statuseminar des BMFT Entwicklungen in der Schiffstechnik, 31 Okt. 1985. Hamburg, pp. 134-163.
- Semeniuk, A. 1977. Ice pressure measurements at Arisa 1-1. Report No. 9-42. APDA Project No. 122-1.

NO-A191 067

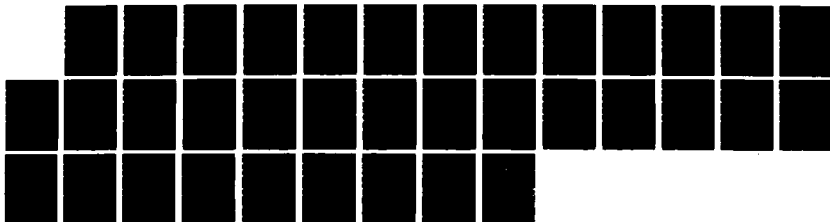
WORKING GROUP ON ICE FORCES; STATE-OF-THE-ART REPORT
(1RD)(U) COLD REGIONS RESEARCH AND ENGINEERING LAB
HANOVER NH T J SANDERSON SEP 87 CRREL-87-17

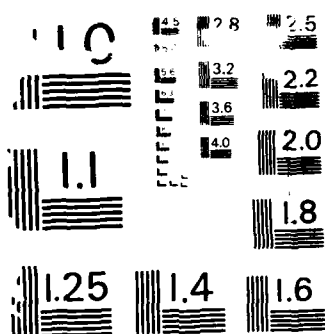
3/3

UNCLASSIFIED

F/G 8/12

NL





COPY RESOLUTION TEST CHART
NATIONAL BUREAU OF STANDARDS-1963-A

- Sodhi, D.S., Kato, K., and Haynes, F.D. 1983. Ice force measurements on a bridge pier in the Otauquechee River, Vermont. CRREL Report 83-20 December 1983, Hanover, N.H.
- Strilchuk, A.R. 1977. Ice pressure measurements, Netserk F-4-, 1975-76. APOA Project No. 105-1.
- Templeton III, J.S. 1981. Analysis for an embedded ice pressure sensor. Journal of Energy Resources Technology, Vol. 103. No. 1, March, pp. 87-95.
- Templeton, J.S. 1979. "On Measurement of Sea Ice Pressures". In POAC 1979 Conference Proceedings, Trondheim, Norway, Vol. 1, pp. 73-88.
- To, N.M. 1985. A method of calculating the global ice load on Esso's caisson retained island at Kadluk. 8th International Conference on Port and Ocean Engineering under Arctic Conditions, Greenland, Vol. 2, pp. 667-676
- Trofimenkoff, P.N. 1977. Ice pressure sensor calibrations 1976. Imperial Oil Ltd. APOS Project 105-2.
- Wang, Y.S. and T.D. Ralston, 1983. Elastic-Plastic Stress and Strain Distributions in an Ice Sheet Moving Against a Circular Structure. Proceedings of 7th International POAC, Technical Research Centre of Finland, Helsinki, 1983, Vol. 2, pp. 940-951.
- Wright, B.D. and Weaver, J.S. 1983. Tarsiut winter alert monitoring. 15th Annual Offshore Technology Conference, May 2-5, 1983, Houston OTC paper 4518, Vol. 4, pp. 61-66.
- Weaver, J.S. and Berzins, W. 1983. The Tarsiut island monitoring program. 15th Annual Offshore Technology Conference, Houston, Texas, May 2-5, 1983. OTC paper 4519, Vol. 2, pp. 67-74.
- Wetmore, S.B. 1984. Concrete Island Drilling System; Super Series. (Super CIDS). 16th Annual Offshore Technology Conference, Houston, Texas, May 7-9, 1984. Vol. 3, pp. 215-226.

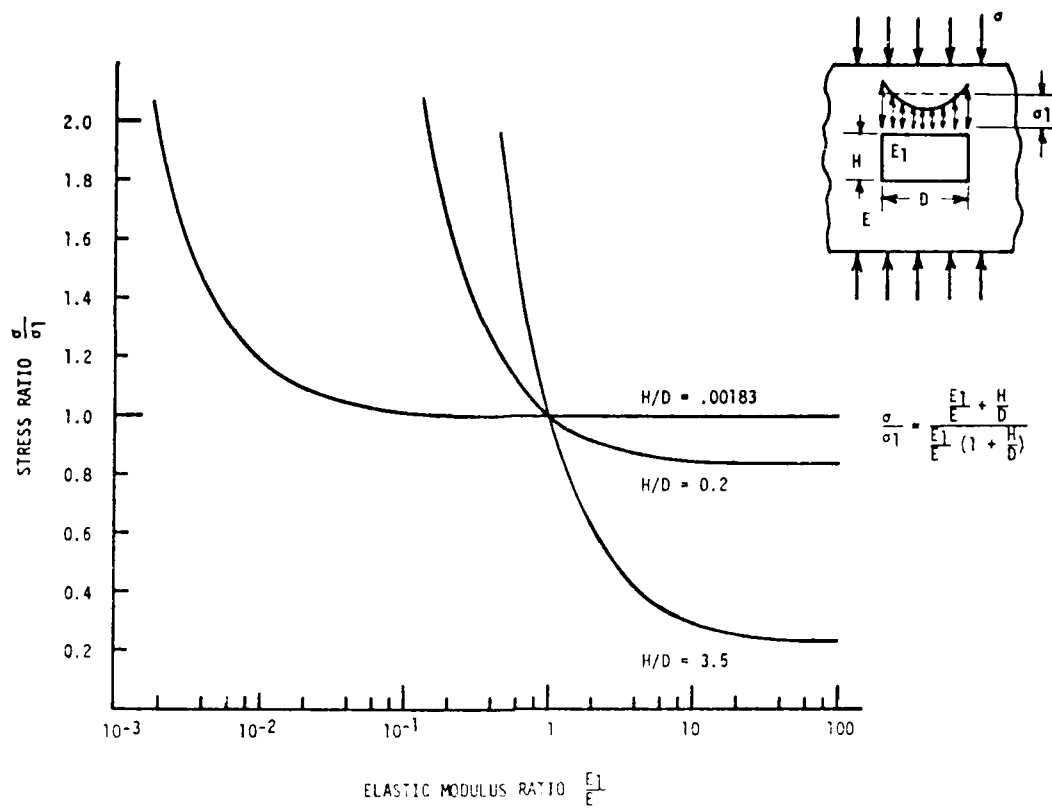


FIGURE 1
INCLUSION FACTORS FOR IN-SITU STRESS MEASUREMENTS
(AFTER METGE ET AL., 1975)

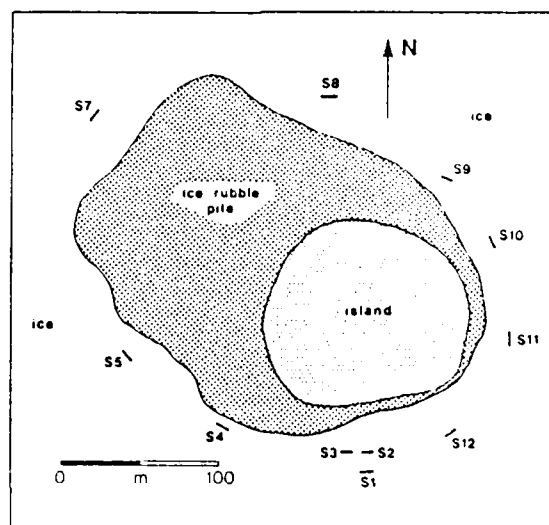


FIGURE 2
LOCATION OF STRESS SENSORS AROUND NETSERK F-40
(AFTER SANDERSON, 1984)

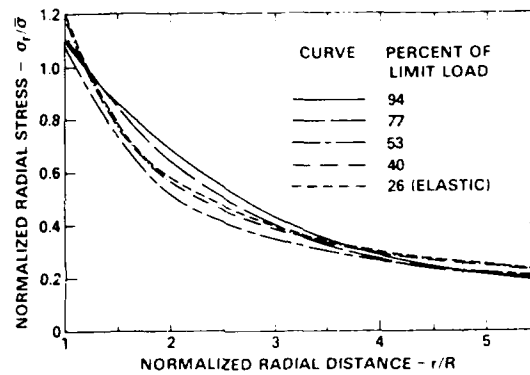


FIGURE 3
DISTRIBUTIONS OF RADIAL STRESS AS IT
DECAYS WITH DISTANCE FROM A CIRCULAR
INDENTOR (AFTER WANG AND RALSTON, 1983)

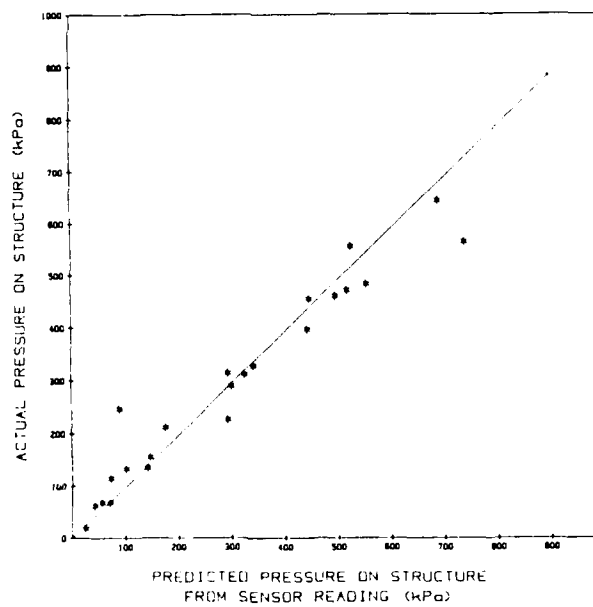


FIGURE 4
RESULTS FROM ICE STRESS PANEL IN LARGE
SCALE ICE BASIN TEST
(AFTER CROASDALE ET AL., 1984)

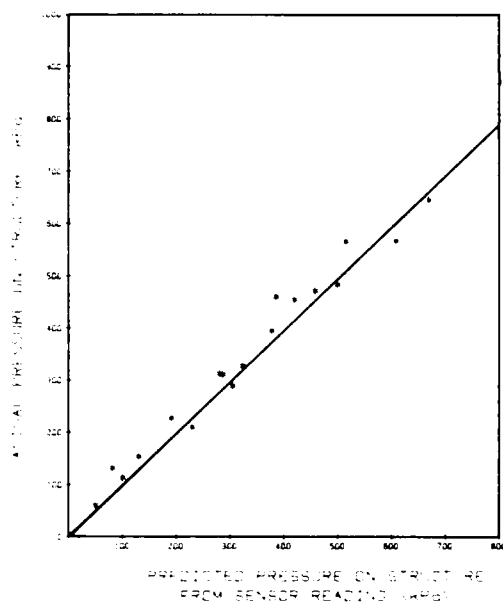


FIGURE 5
RESULTS FROM HYDRAULIC DISK ICE
SENSOR IN LARGE SCALE ICE BASIN
TESTS (AFTER CROASDALE ET AL., 1984)

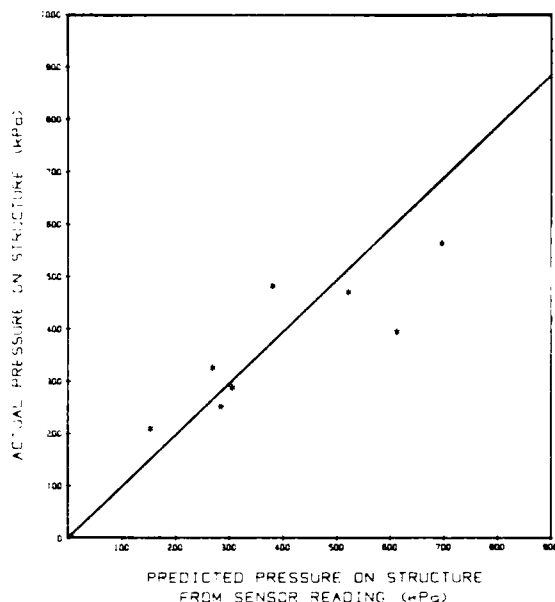


FIGURE 6
RESULTS FROM CYLINDRICAL BIAXIAL
SENSOR IN LARGE SCALE ICE BASIN TESTS
(AFTER CROASDALE ET AL., 1984)

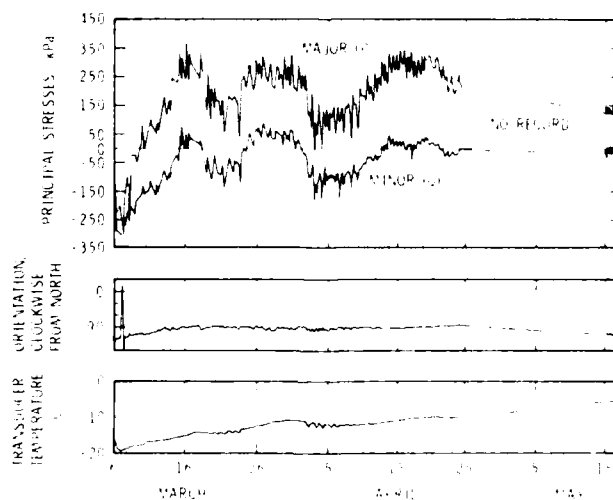


FIGURE 7
RESULTS OF BIAXIAL ICE STRESS MEASUREMENTS
AT ADAMS ISLAND (AFTER FREDERKING ET AL.,
1985)

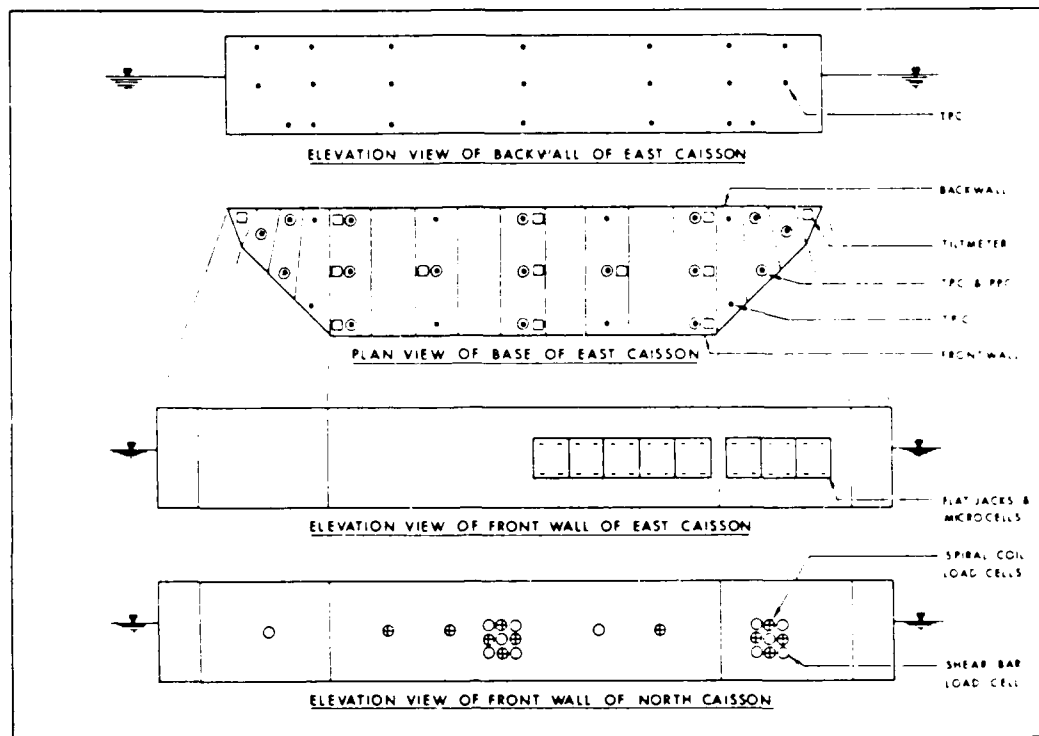


FIGURE 8
LAYOUT OF CAISSON INSTRUMENTATION AT TARSUUT (AFTER WEAVER AND BERZINS, 1983)

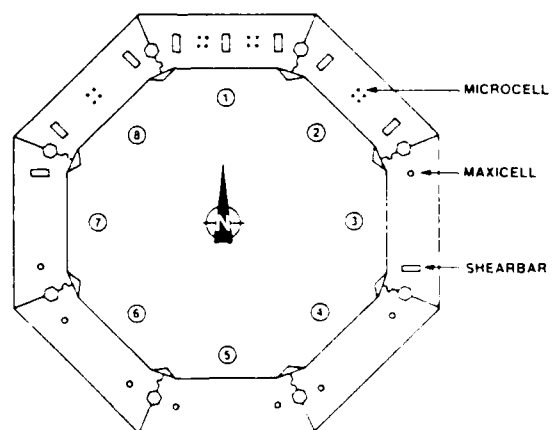


FIGURE 9
ICE FORCE SENSOR LOCATIONS ON CAISSON
RETAINED ISLAND (AFTER HAWKINS ET AL.,
1983)

TABLE 1 APPLICATION OF IN-SITU METHODS FOR ICE FORCE MEASUREMENTS IN CANADIAN ARCTIC
(After Sanderson, 1984)

SITE	DATE	WATER DEPTH (M)	COMPANY OR AGENCY	IN-SITU METHOD	OTHER INSTRUMENTATION	SOURCE
Adgo P-25 (Artificial Island)	1974/75	2	Eso (Imperial)	-U of Alaska small cylindrical stress sensors -Eso thin wide stress sensors	-soils instruments -wire/reel ice movement devices -meteorology	APDA 104: Metge (1976) Nelson and Sackinger (1976)
Netsen South B-44 (Artificial Island)	1974/75	4.5	Eso (Imperial)	-Eso thin wide stress panels (20)	-soils instruments -wire/reel ice movement devices - meteorology	APDA 104: Metge (1976)
Netsen North F-40 (Artificial Island)	1975/76	7	Eso (Imperial)	-Eso thin wide stress panels (13)	-soils instruments -wire/reel ice movement devices -meteorology	APDA 105: Strilchuk (1977)
Kannerk J-42 and Annak L-30 (Artificial Island)	1976/77	8 and 8.5	Eso (Imperial)	-Eso thin wide stress panels	-soils instruments -ice movement -meteorology	APDA 122 Semeniuk (1977)
Tarsiat N-44 (Caisson Island)	1981/82	22	Gulf; Dome and B.P.	-Medof panels -6P strain meters	-soils instruments -strain gauges on caissons -load panels on caissons -meteorology	APDA 197 Pilkington and others, (1983)
Uviluk P-66 (Single Steel Drilling Caisson)	1982/83	31	Dome/Canmar	-Medof panels	-soils instruments -strain gauges and load panels on structure -meteorology	(in preparation)
Multi-year Floe in pack ice of Beaufort Sea	1986	30cm	K.R. Croasdale and Associates Ltd. supported by Canadian Govt and Gulf Canada	-2 arrays of specially designed low stress range sensors	-Argos buoy for position and movement of floe	Croasdale (1984 and 1985)

Tarsut N-44 (Caisson Island)	1982/83	22	Gulf; BP and ARCO	-Medof panels -BP strain Meters -ARCO hydraulic stress panels	(As above)	APOA 198 Anderson (1983) Sanderson (1983)
Adams Island	1982/83	10	National Research Council of Canada, HSVA' BP	-IRAD stiff biaxial stress sensors -BP strain meters	-strains by survey -meteorology, tides currents	Frederking et al (1984)
Adams Island	1983/84	10	National Research Council of Canada, HSVA	-IRAD biaxial stress sensors -Terrascience (IDEAL) stress panel	-strains by survey and wireline -meteorology, tides currents	Frederking et al (1986)
Nadluk (Caisson retained Island)	1983/84	14.5	Esso; CRREL	-IRAD biaxial stress sensors -Exxon stress panels	-soils instruments -strain gauges and load panels on caissons -meteorology, ice movement	Johnson et al (1985)
Nanisivik Dock Baffin Island	1983/84	13	Public works Canada	-Four different types of stress sensors -One strain meter	-tides -meteorology	Croasdale (1985)
Amerk O-09 (Caisson Retained Island)	1983/84	26	National Research Council; US Dept. of Interior; Esso	-Exxon panels -Hexpack panels -Ideal panel -CMEL Biaxial stress sensor	-strains by survey -soils instruments -strain gauges and load panels on caisson -meteorology	Croasdale (1985); Sayed et al (1986)

TABLE 2 CASES OF ICE FORCES MEASUREMENTS ON STRUCTURES

SITE	DATES	COMPANY OR AGENCY	METHOD/INSTRUMENTATION	SOURCE
a) Bridge Piers Hondo, Alberta	1967-present	Alberta Research Council and Alberta Highways	bridge pier with special nose section hinged at bottom and supported by load cell at top; 2.3m ϕ 23° from vertical added accelerometers.	Sanden and Neill (1968) Montgomery et al (1980)
Pembridge, Alberta	1969-present		bridge & pier with special pile hinged at bottom and supported on load cells at top; 0.86m ϕ vertical; ice thickness 0.5m	
Eider River Estuary Germany	1967-69	Technical University of Hanover	Array of 50 load cells covering contact surface 1.5m high of 0.6m diameter pile, ice thickness 0.4m	Schwarz (1970)
Yukon River, Alaska	1977-80	Cold Regions Research and Engineering Lab and University of Alaska	5-1.5m x .5m wide plates supported on a strain gauge beam to measure ice load on nose of pier, 2-1.8m x 1.8m plates supported on load cells to measure total ice load, accelerometers	McFadden et al (1981)
Ottawaquechee River, Vermont	1982	Cold Regions Research and Engineering Lab.	4-0.56m x 1.22 panel supported on load pier, panels cover 2.5m vertical range of V-shaped pier	Sodhi et al (1983)
b) Light Piers Yamichiche, Quebec	1975-present	Transport Canada and National Research Council	Load panels supported on load cells; ice thickness 0.6m	Danys (1975) Frederking et al (1985)
Kemi I, Finland	1975-77	University of Oulu	relative deformations of pier, 200 mm pressure sensing plates and accelerometers	Mänttinen (1978)
Norströmsgrund, Sweden	1972-present	VBB Consulting	Forces calculated from records of 4 accelerometers	Engelbrektson (1978)
c) Petroleum	Exploration and Production		Structures	
Cook Inlet, Alaska	1963-69	Pan American Petroleum Corp.	Strain gauges on structural members, 0.9m ϕ ; accelerometers; ice thickness 1.1m	Blenkarn (1970)
Saroma lagoon, Japan	1976-80	Mitsui	strain gauges inside 2.5m cylinder cantilevered from sea bottom to measure horizontal and vertical ice loads.	Oshima et al (1980)
Tarslut	1981-83	Gulf/Canmar	Ice pressure measuring panels of various sizes, strain gauges internal to structure, soil pressure cells, piezometers and inclinometers	Pilkington et al (1983) Weaver and Berzins (1983)

SSOC	1982-84	Canmar		
CR1	1983-85	Eso Resources Canada	Ice pressure sensors, strain gauges on internal structure, piezometers and inclinometers	Hawkins et al (1983)
Molikpaq	1984-present	Gulf Canada Resources	Ice pressure panels, strain gauges, accelerometers, displacement transducers, piezometers and inclinometers	Rogers, et al (1986)
Super CDS	1984-present	Global Marine	Ice pressure panels, strain gauges in structural elements, piezometers and inclinometers	Wetmore (1984)
Kulluk	1983-85	Gulf	Ice loads monitored from loads measured in anchor lines	Gaida et al (1983)
d) Ships Sisu, Finland	1977-82	Technical Research Centre of Finland	"Varsta" ice pressure gauges and strain gauges on frames	Riska et al (1983)

Louis S. St Laurant, Canada	1977-80	Canadian Coast Guard/Arctec Canada	15mm ϕ ice pressure transducers. Strain gauges on frames	Comfort & Noble (1979)
Canmar Kigoriak, Canada	1980-83	Canmar	"Varsta" ice pressure gauges, strain gauges to measure shear and bending ice frames, webs and plating.	Ghonein & Keinonen (1983)
M.V. Arctic, Canada	1978-86	Canartic and Transport Development Centre	Weldable strain gauges on frames and plates.	Neth et al (1983)
Polar Sea, USA	1983	U.S. Coast Guard and Maritime Administration	strain gauging of frames to measure load distribu- tions over 10m ² area.	Daley et al (1984)
Polarstern, Germany	1984-85	Hamburg Ship Model Basin	Normal and 2 shear loads (in 2 orthogonal directions) on a 1m ² area plate supported on load cells; strain gauges on frame	Schwarz and Müller (1985)

☆U.S. GOVERNMENT PRINTING OFFICE:1986-601-816-0

ICEBERG IMPACT FORCES

Donald E. Nevel

Conoco Inc.

U.S.A.

ABSTRACT

A state-of-the-art review is presented for iceberg impact forces on offshore structures. A detailed description is given of the expected brittle crushing failure of the ice. Since no iceberg impacts have been observed, the description was obtained from laboratory and field impact tests. Various strength theories are discussed. The drop ball test is analyzed for the constant strength and viscous strength theories, and it is concluded that the results do not significantly differ. Therefore, the simpler constant strength theory is recommended for use. A review of the literature showed that there is very little published data on the brittle impact strength of ice, particularly in regard to the so-called size effect. There are some proprietary data in the oil industry.

A review is given for the analysis of an iceberg impacting a structure. The resulting deformation and motion of the iceberg, structure, and soil influence the interaction force. A review of the literature suggests that ice crushing, local contact shapes, and iceberg rotation are the more significant factors. A simplified equation is developed to account for the horizontal rotation of the iceberg.

Since the iceberg parameters can vary over wide ranges, it is recommended that each parameter be described by a probability of exceedance distribution. A numerical method is described to obtain the probability of exceeding the impact force.

The design ice force should then be selected by a return period or the probability of exceeding the force for a given time period. The over turning and torsional moments on the structure can be similarly selected.

INTRODUCTION

This paper gives a state-of-the-art review of iceberg impact forces on offshore structures. This problem is important for the design of offshore structures in areas of drifting ice islands in the Beaufort Sea and icebergs along the eastern Canadian coast. The oil industry is considering offshore structures in these areas. This review considers icebergs impacting rigid structures sitting on the seabed. In-depth discussions are presented for the iceberg impact strength, the overall interaction between the iceberg and the structure, and methods for statistically describing the impact force. Areas that have not been included are iceberg impacts with the seabed or underwater berms, iceberg impacts with floating or moored structures, and the influence of iceberg management, such as destruction and towing, on the frequency of collisions.

IMPACT FAILURE MODES

When a drifting iceberg impacts an offshore structure, the impact force depends upon the mode of failure and the associated ice strength. Since iceberg failure modes during impact have not been observed, possible failure modes are discussed by considering what is reasonable to expect. Possible modes of failure are crushing, splitting, and bending. The crushing mode is the most reasonable to expect. The splitting mode might occur for smaller icebergs after some crushing has occurred. In this case the splitting would limit the maximum crushing force. The bending mode could occur if the iceberg were shaped like a beam or plate. Icebergs along eastern Canada are typically globular in shape rather than shaped as a beam or plate.

The crushing mode of failure can be classified according to the depth of penetration and speed of impact. Deep penetrations produce different failure mechanisms than shallow penetrations. For offshore structures, we envision shallow penetrations because of the bluntness of the structure. There has been some work performed on ice impacts with deep penetration, particularly for high speeds, but this work is not applicable here and therefore was not considered.

For shallow penetration, there could be two failure modes depending upon the speed of impact. For slow speeds, a ductile-type failure will occur where the crushing strength is rate dependent because of the creep and flow of the ice. For speeds slow enough to create ductile failures, the iceberg does not have enough kinetic energy to create large impact forces. For fast speeds, a brittle-type failure will occur. These two failure modes are demonstrated in Figure 1 by the different force signatures as obtained by Kitami et al. [29]. Kitami's data were obtained using sea ice and a similar behavior is expected for iceberg ice. The transition

speed between ductile and brittle failure depends upon temperature, and it is estimated to be about one centimeter per second.

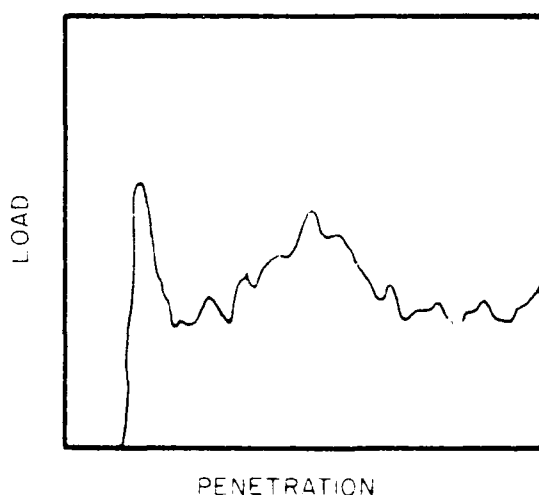


Figure 1a. Fast Brittle Failure

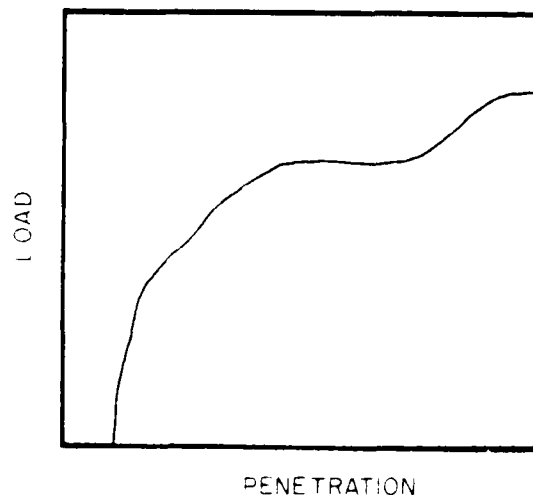


Figure 1b. Slow Ductile Failure

STRENGTH THEORIES

Numerous strength theories have been suggested for ice impact failure. The simplest and most frequently used is the "constant strength" theory. This theory assumes that the contact pressure between the ice and structure is uniform over the contact area and is constant during the impact. Variations of this theory can be considered where the crushing pressure is a function of velocity or strain rate, porosity or density, temperature, crystalline structure, and size or contact area. The velocity or strain rate dependencies which have been proposed [10,11,40,42] are those obtained from ductile modes of failure which have not been verified for brittle modes of failure. If the strength is velocity dependent, it should be determined from brittle modes of failure, not the ductile mode which primarily reflects the creep of the ice.

The strength is commonly considered a function of the contact area. Several authors [11,42] derive this function from the aspect ratio (width of structure divided by ice thickness). This aspect function was empirically developed from experiments of cylinders indenting ice sheets at slow speeds where the presence of the top and bottom free surfaces of the ice sheet influence the failure load. This is not applicable for brittle crushing of icebergs, and therefore, this approach is questionable.

For a crushing strength, the energy per unit volume of crushed material has been proposed by some authors [2,23,26,27]. This is called "specific energy." Specific energy, in principle, is

a different strength criteria. However, if the volume of penetration is used for the specific energy, the specific energy is equivalent to the constant strength criteria.

Brittle fracture theory considers the nucleation and propagation of cracks. Crushing of the ice involves many cracks and breaking of the ice pieces into smaller particles. The crushing process of the ice is too complicated to be described by brittle fracture theory. The brittle fracture theory is used to estimate splitting of ice floes[10]. A similar approach can be used to estimate the splitting of icebergs. For icebergs, the main problem is the estimation of the tensile stresses near the crushed contact zone since the crack propagates from this zone. It is probably dependent upon the damage and local geometry created by the crushing process.

The shear strength criterion can be applied to ice failure. Shear failure can occur in uniaxial and multiaxial compression. The shear strength is represented by failure surfaces in the principal stress space. The shear strength of ice is associated with the amount of internal damage of the ice. As the ice is loaded, internal cracks occur. With increased cracking, the ice can flow along maximum shear lines causing collapse and failure. The shear strength is a function of either the hydrostatic stress or the normal stress on the shear plane. Generally the shear strength is associated with ductile modes of failure, but could also be applied to brittle modes. For the broken and pulverized zone of ice that occurs during impact in the brittle failure mode, a viscous theory has been proposed by Kheisin et al.[24,31]. This theory will be elaborated on later in the paper.

Although strain failure theories have been proposed for some types of ice problems, the application of a strain failure to the iceberg impact problem has not been proposed.

Hertzian contact stresses are associated with deformation of the contacting bodies, not the strength of the materials. Khrapaty and Berezovskii[25] have extended the Hertzian idea to estimate contact stresses as a function of penetration.

BRITTLE CRUSHING FAILURE OF ICE

Based on laboratory and field tests, a detailed description of the brittle failure of a blunt object impacting a large ice mass will be given. Since conventional testing machines are not fast enough, drop ball tests have been used. In these tests, a weight with a spherical surface is dropped on a solid ice surface. These tests were first performed by Pounder and Little[39] in 1959. Later Kheisin and his coworkers[22,23,24,31,33] used larger spheres with an accelerometer. Drop ball tests have also been performed by Timco and Martin[45], Tsurikov and

Veselova[46], and Khrapaty and Tsuprik[26,27]. Detailed failure descriptions have been given in References 22 and 27. Other impact tests have been performed by Lavrov[32], Riska[41], Glen and Comfort[18], and El-Tahan et al.[15,16]. In order to simulate iceberg impacts, a large mass impacting at velocities up to a few meters per second is required. Because of the difficulty of handling a large mass, Benoit et al.[6] used hydraulic rams to simulate drop ball tests whose final contact areas were as large as 3 square meters.

After reviewing the available descriptions, the brittle failure of a blunt object impacting a large ice mass can be summarized as follows. Upon initial impact, the virgin unbroken ice at the contact becomes pulverized. A set of concentric conical cracks and a set of radial cracks form as shown in Figure 2[26]. The pressure of the pulverized layer spalls out the surface ice pieces adjacent to the indenter. Part of the pulverized ice layer is expelled. If the energy is sufficient, the penetration continues with the contact area becoming larger.

Underneath the pulverized ice, the uncracked ice has a rough surface. As the indenter continues to penetrate, it makes contact with the high points on this surface, pulverizing each point in turn, and continues to expel the pulverized ice. Forces are required to pulverize the high points as well as to expel the pulverized ice. The typical pressure time history is shown in Figure 3 which is from El-Tahan et al.[16]. Note the high initial pressure obtained as compared to later pressures.

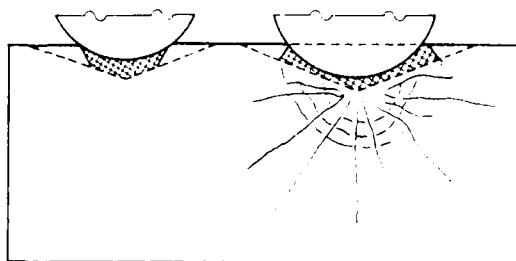


Figure 2. Impact Damage of Ice

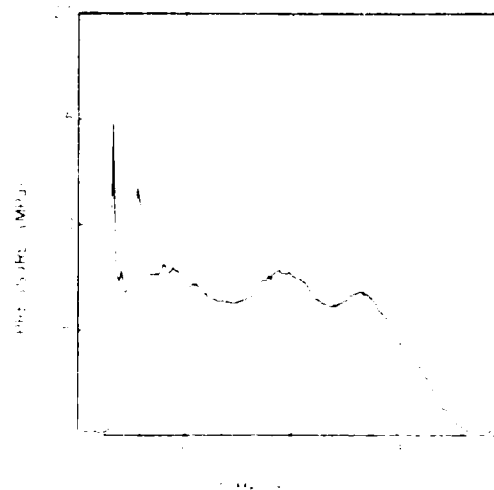


Figure 3. Ice Pressure During Impact

The sudden drop of pressure indicates brittle failure of the high points on the contact surface and a sudden increase in pressure indicates making contact with a high point.

For large contact areas, typical force time records show many sudden changes typified by this brittle failure. This indicates that the dominant force is associated with brittle fracture of

the high points on the ice surface rather than the expelling of the pulverized ice which should show as a smoother force time record.

As a result of this failure process, the average contact pressure on the indenter is extremely high upon initial contact, fluctuates rapidly, and decreases as the contact area grows. Whether the average pressure continues to decrease beyond the range of the available test data is an interesting question. The answer will depend upon the roughness of the newly created ice surface. Nevel[38] and Ashby et al.[3] have previously discussed the concept of a decrease in the ice strength with contact area caused by nonuniformity of contact created by the failure itself.

From the above discussion, one can conclude that the design strength for iceberg impacts should be obtained from tests with realistic initial velocities and large contact areas. The tests which best meet these criteria are those performed in the field on an iceberg by Benoit et al.[6] for an initial velocity of 10 cm/sec and a final contact area of 3 m², but the test results are proprietary. Other impact tests were performed in the laboratory on iceberg ice by El-Tahan[15,16]. These tests had a temperature of -5°C, an initial velocity of 2 m/sec, a final contact area of about 10 cm², and produced a strength of about 17 MPa. This high strength is probably due to small contact areas.

Kheisin et al.[23] performed drop ball tests on a freshwater lake with velocities ranging from 0.6 to 4.0 m/sec. Contact areas were not reported, but because steel hemispheres of 156 and 300 kg were used, the contact area must have been much larger than those of El-Tahan. Kheisin obtained average strengths of 8 and 3 MPa for air temperatures of about -10°C and -3°C, respectively. The results showed that the strength was independent of the velocity.

Khrapaty et al.[2,26,27] performed tests similar to Kheisin on sea ice. The strength depended upon temperature. By replotting his data and fitting a curve by eye, his results can be expressed as $\sigma = 6.5 e^{+5 T}$, where σ is the strength in MPa and T is the temperature in degrees centigrade. At a temperature of -10°C, the strength was about 6 MPa. Khrapaty also found the strength independent of velocity. The results from other drop ball tests[39,45,46] and impact tests[18,32,41] are not discussed here because these tests were not performed on iceberg ice and were of limited contact area.

The uniaxial compressive strength of iceberg ice has been measured by El-Tahan et al.[15,16] and by Gammon et al.[17]. At a temperature of -5°C and a strain rate of 10⁻³ sec, El-Tahan found an average strength of 7.4 MPa while Gammon found 5.3 MPa. Many icebergs along the coast of eastern Canada are calved from Greenland glaciers. Kovacs et

al.[30] measured the uniaxial compressive strength of Greenland glacier ice at a temperature of -25°C and a strain rate of about 10^{-3} sec. The results of the dense ice ranged from 6 to 12 MPa. Earlier Butkovich[7] found the uniaxial strengths for Greenland ice to be from 3 to 8 MPa at a temperature of -5°C and much slower strain rates. The relation between uniaxial compressive strength and drop ball strengths have not been established, but results seem to be of the same order of magnitude.

The conclusions made from these results are (1) the impact strength for iceberg ice is in the range of 6 to 10 MPa and probably decreases as the area of contact becomes larger, (2) the impact strength is independent of speed in the range of 0.6 to 4.0 meter/sec. and (3) the impact strength depends on the temperature of the ice. The in situ temperature of icebergs has been measured by Diemand[12] and can be as cold as -10°C within one meter of the iceberg's surface.

DROP BALL TEST

The drop ball test will be analyzed using the constant strength theory and the viscous strength theory. A comparison will be made between these theories including their specific energies.

Consider a rigid sphere of radius R and mass M dropped from a height H onto a semi-infinite ice mass. The potential energy at the time of release, MgH , is equal to the kinetic energy at the time of contact, $\frac{1}{2} MV_o^2$, where g is the gravitation constant and V_o is the velocity of the sphere at the beginning of impact. Most of this energy will be expended by crushing the ice, and a small amount may remain with the sphere after impact.

Both Yen et al.[47] and Likhomanov and Kheisin[33] have experimentally determined the coefficient of restitution of steel balls dropped on ice. They show that the coefficient of restitution decreases with increases of mass, velocity, and temperature. For warm fresh-water ice, a 300-kg steel ball with an initial velocity of 1.4 meters per second produced a 0.10 coefficient of restitution. With much larger masses, the coefficient of restitution should become very close to zero. Hence we will neglect elastic strain energy of the ice and assume that energy is expended by crushing the ice as given by

$$\frac{MV_o^2}{2} = \int_0^{Z_o} F dZ \quad (1)$$

where F is the force, Z is the penetration distance, and Z_o is the final penetration distance.

The constant impact strength theory assumes that the contact pressure is uniform over the contact area and is constant with time during the impact. Figure 4 shows a uniform pressure p

acting over an area A . The pressure acting in an arbitrary direction x or y on the projected areas are

$$p_x = \frac{F_x}{A_x} = \frac{p A \sin \theta}{A \sin \theta} = p \quad (2a)$$

and

$$p_y = \frac{F_y}{A_y} = \frac{p A \cos \theta}{A \cos \theta} = p. \quad (2b)$$

Hence the pressure on a projected area is the same as on the contact area.

Hence the force F can be written as

$$F = \sigma A \quad (3)$$

where σ is the impact crushing strength, and A is the projected contact area. For a sphere, this area equals $\pi(2RZ - Z^2)$ where R is the radius of the sphere. For small penetrations, we can neglect Z^2 and the area becomes

$$A = \pi 2RZ. \quad (4)$$

Substituting Equations (3) and (4) into (1), we integrate and solve for the final penetration distance to obtain

$$Z_o = \left(\frac{M V_o^2}{\sigma \pi 2R} \right)^{1/2}. \quad (5)$$

The force during impact can be expressed as

$$F = \frac{M V_o^2}{Z_o} \left(\frac{Z}{Z_o} \right) \quad (6)$$

and it reaches its maximum value at $Z = Z_o$. The local pressure p equals the nominal pressure q and is equal to the impact crushing strength σ throughout impact. The dynamic equation is

$$M V \frac{dV}{dZ} = -F \quad (7)$$

where V is the instantaneous velocity of the sphere. Substituting Equation (6) into (7) and integrating, we obtain the velocity

$$\frac{V}{V_o} = \left[1 - \left(\frac{Z}{Z_o} \right)^2 \right]^{1/2}. \quad (8)$$

Expressing V as a time derivative of z , and integrating Equation (8), we obtain the time, t

$$t = \frac{Z_0}{V_0} \arcsin (Z/Z_0). \quad (9)$$

The total impact time T at $z = z_0$ is

$$T = \frac{\pi Z_0}{2 V_0}. \quad (10)$$

The specific energy ϵ is defined as the energy dissipated in crushing the ice divided by the volume of crushed ice. The volume of penetration is $\pi Z^2 (R - Z/3)$ for the drop ball test. For small penetrations, we neglect the $Z/3$ term to obtain

$$\epsilon = \frac{M (V_0^2 - V^2)}{2 \pi R Z^2}. \quad (11)$$

Substituting Equation (8), we get

$$\epsilon = \frac{M V_0^2}{2 \pi R Z_0^2} \quad (12)$$

which is constant throughout the impact. The strength σ obtained from Equations (3), (4), and (6) is also equal to Equation (12), and in this case the constant strength and specific energy are the same.

VISCOUS THEORY

The viscous theory assumes that a crushed ice layer forms between the structure and the unbroken ice and that this layer flows in a viscous manner. Kheisin et al.[24,31] developed a method for solving the equations for this problem following the method used in lubrication between bearings. This solution for the rigid sphere impacting ice will be rederived and expressed in a way which can be compared to constant strength theory.

At any instant during the impact of a rigid sphere on ice, we assume that a crushed ice layer of thickness h has developed. We assume that this layer is thin when compared to the radius of the contact area r_0 . A sketch of this layer is shown in Figure 5. At the interface between the crushed and uncrushed ice, $z = h$, we assume that the radial velocity u and the vertical velocity w are zero. At the interface between the rigid sphere and the crushed ice, $z = 0$, we assume that the shear stress τ is zero and that the vertical velocity is the instantaneous velocity V of the sphere. At the perimeter of the crushed layer $r = r_0$, we assume that the pressure is zero.

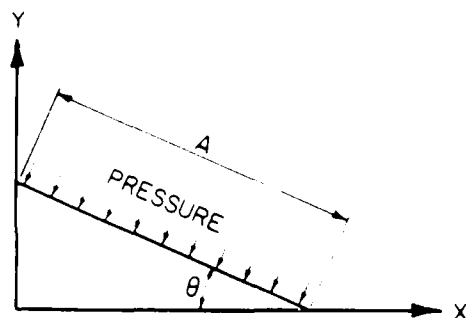


Figure 4. Pressure on Contact Area

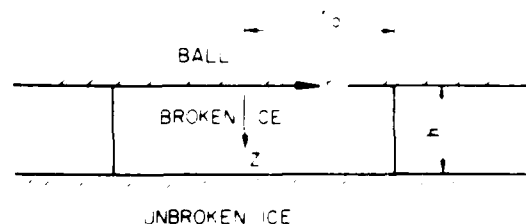


Figure 5. Viscous Ice Strength Model

We will assume that the layer of crushed ice behaves as an incompressible viscous fluid. In the Navier-Stokes equation which describes this fluid motion, we shall neglect the body forces due to gravity and the acceleration forces. The forces due to pressure and viscous flow will be retained. For axial symmetric flow in cylindrical coordinates r and z , the Navier-Stokes equations are

$$\frac{\partial p}{\partial r} = \mu \left[\frac{\partial^2 u}{\partial r^2} + \frac{1}{r} \frac{\partial u}{\partial r} + \frac{\partial^2 u}{\partial z^2} \right] \quad (13a)$$

$$\frac{\partial p}{\partial z} = \mu \left[\frac{\partial^2 w}{\partial r^2} + \frac{1}{r} \frac{\partial w}{\partial r} + \frac{\partial^2 w}{\partial z^2} \right] \quad (13b)$$

where p is the pressure, μ is the viscosity, u and w are the velocities in the r and z directions, respectively.

In order to solve these equations, we assume that the radial velocity is independent of r , $u = u(z)$, and that the vertical velocity w is zero everywhere except at $z = 0$ where it is equal to V . Equation (13b) becomes

$$\frac{\partial p}{\partial z} = 0 \quad (14a)$$

which says that the pressure is independent of z . Equation (13a) becomes

$$\frac{\partial p}{\partial r} = \mu \frac{\partial^2 u}{\partial z^2} \quad (14b)$$

The boundary conditions for this equation are $u = 0$ at $z = h$ and $\tau = \mu \left(\frac{\partial u}{\partial z} + \frac{\partial w}{\partial r} \right) = 0$ at $z = 0$. Since $w = 0$, the last boundary condition becomes $\frac{\partial u}{\partial z} = 0$. Integrating Equation (14b) with respect to z and using these boundary conditions, we get

$$u = \frac{1}{2\mu} \frac{\partial p}{\partial r} (z^2 - h^2). \quad (15)$$

We consider the incompressibility of the crushed layer by equating the downward flow of material from the sphere's movement $\pi r^2 V$ to the radial flow $\int_0^h 2\pi r u dz$ to obtain

$$h^3 dp = - \frac{3}{2} \mu V r dr \quad (16)$$

In order to solve this equation, we must know the thickness h of the crushed ice layer. Kheisin assumed that the pressure p is proportional to h by the equation $p = kh$ where k is a constant. Although other assumptions can be made, we will proceed with Kheisin's assumption because of its simplicity. Then Equation (16) becomes

$$p^3 dp = - \frac{3}{2} \mu k^3 V r dr \quad (17)$$

whose solution is

$$p = [3 \mu k^3 V (r_o^2 - r^2)]^{1/4} \quad (18)$$

where the boundary condition $p = 0$ at $r = r_o$ has been used.

Integrating the pressure over the contact area and dividing by the contact area πr_o^2 , we obtain the nominal pressure q of

$$q = \frac{4}{5} [3 \mu k^3 V r_o^2]^{1/4} \quad (19)$$

Dividing the pressure p by the nominal pressure q , we obtain

$$\frac{p}{q} = \frac{5}{4} \left[1 - \left(\frac{r}{r_o} \right)^2 \right]^{1/4} \quad (20)$$

which shows that the maximum pressure is at the center and is 1.25 times the nominal pressure.

The total contact force is the nominal pressure times the area which is

$$F = \frac{4}{5} \pi (3 \mu k^3)^{1/4} V^{1/4} r_o^{5/2} \quad (21)$$

The equation of motion for the sphere during impact is the same as before and is given by Equation (7).

Using Equation (21) and $r_o^2 = 2RZ$ where Z is the penetration of the sphere, Equation (7) can be integrated. Using the boundary condition $V = V_o$ when $Z = 0$, we get the velocity V during impact to be

$$\frac{V}{V_o} = \left[1 - \left(\frac{Z}{Z_o} \right)^{9/4} \right]^{4/9} \quad (22)$$

where the final depth of penetration Z_o is

$$Z_0 = \left(\frac{45}{28\pi} \right)^{4/9} \frac{M^{4/9} V_0^{7/9}}{(3\mu k^3)^{1/9} (2R)^{5/9}} \quad (23)$$

Equation (22) can be integrated to get the time t as a function of the penetration distance Z

$$\frac{V_0 t}{Z_0} = \int_0^Z \frac{1 - (Z/Z_0)^{9/4}}{(Z/Z_0)^{5/4}} dx \quad (24)$$

The total impact time T is

$$T = 1.6778 Z_0 / V_0 \quad (25)$$

The specific energy ϵ during impact is given as before by Equation (11) and, using Equation (22) becomes

$$\epsilon = \epsilon_0 \frac{1 - [1 - (Z/Z_0)^{9/4}]^{8/7}}{(Z/Z_0)^2} \quad (26)$$

where the specific energy at final penetration ϵ_0 is given by Equation (12) with Z_0 defined in Equation (23)

Using Equations (22) and (23), the force from Equation (21) becomes

$$F = \epsilon_0 A_0 \frac{9}{7} \left(\frac{Z}{Z_0} \right)^{5/4} [1 - (Z/Z_0)^{9/4}]^{1/7} \quad (27)$$

where the final contact area $A_0 = 2\pi R Z_0$.

The maximum force occurs at

$$\frac{Z}{Z_0} = \left(\frac{35}{44} \right)^{4/9} = 0.9033 \quad (28)$$

which corresponds to $V_0 t / Z_0 = 1.12$. The maximum force F_m is

$$F_m = \epsilon_0 A_0 0.9026 \quad (29)$$

The average force F_a during impact is

$$F_a = \epsilon_0 A_0 0.5 \quad (30)$$

Dividing the force of Equation (27) by the contact area $2\pi R z$, the nominal pressure q is

$$q = \epsilon_0 \frac{9}{7} \left(\frac{Z}{Z_0} \right)^{1/4} [1 - (Z/Z_0)^{9/4}]^{1/7} \quad (31)$$

The maximum nominal pressure occurs at

$$\frac{Z}{Z_0} = \left(\frac{7}{16}\right)^{4/9} = 0.693 \quad (32)$$

which corresponds to $V_0 t Z_0 = 0.755$. The maximum nominal pressure q_m is

$$q_m = \epsilon_0 \frac{9}{7} \left(\frac{7}{16}\right)^{1/9} \left(\frac{9}{16}\right)^{1/7} = \epsilon_0 1.0803. \quad (33)$$

The average nominal pressure during impact is

$$q_m = \epsilon_0 \frac{4}{7} \int_0^1 X^{-4/9} (1 - X)^{1/7} dx \quad (34)$$

which when integrated gives $q_m = 0.9420 \epsilon_0$.

COMPARISON OF THEORIES

We now compare the constant strength theory to the viscous theory for the rigid sphere dropped on the ice. For an initial velocity V_0 , the theories are compared by assuming the same Z_0 which is experimentally measured. Equations (5) and (23) give the relation between Z_0 and the constant strength and viscosity, respectively. The initial velocity V_0 , final penetration Z_0 , final contact area $A_0 = 2\pi R Z_0$, and final specific energy $\epsilon_0 = MV_0^2/\pi 2R Z_0^2$ are used to make the solutions dimensionless. Figures 6, 7, 8, and 9 show the velocity V/V_0 , the force $F/\epsilon_0 A_0$, the specific energy ϵ/ϵ_0 , and the average pressure q/ϵ_0 as a function of the penetration Z/Z_0 for the two theories. Figure 10 shows the penetration Z/Z_0 as a function of the time $V_0 t Z_0$ for the two theories. Figure 11 shows the pressure p/q as a function of position r/r_0 for the two theories. Table 1 shows a comparison of key values for the two theories.

TABLE 1
THEORY COMPARISON OF DROP BALL TEST

	<u>Constant</u>	<u>Viscous</u>
Max. Sp. Energy	ϵ_0	$1.026 \epsilon_0$
Maximum Force	$\epsilon_0 A_0$	$0.903 \epsilon_0 A_0$
Average Force	$0.5 \epsilon_0 A_0$	$0.5 \epsilon_0 A_0$
Time of Impact	$1.57 Z_0/V_0$	$1.678 Z_0/V_0$
Max. Pressure q	ϵ_0	$1.080 \epsilon_0$
Ave. Pressure q	ϵ_0	$0.942 \epsilon_0$
Max. Pressure P	q	$1.25 q$

Although there are some differences, these results show that they are not great. Therefore, it seems reasonable to use the simpler constant strength theory rather than the more complicated viscous theory.

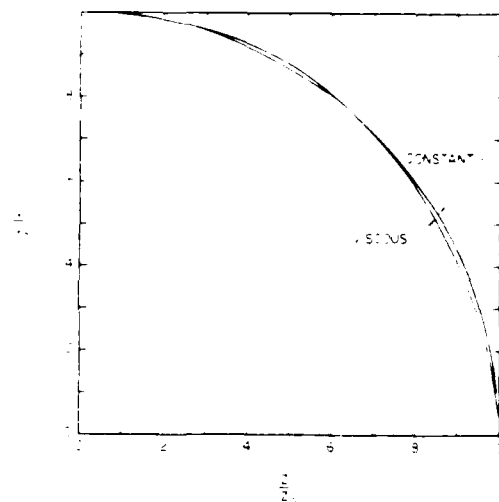


Figure 6. Velocity Versus Penetration

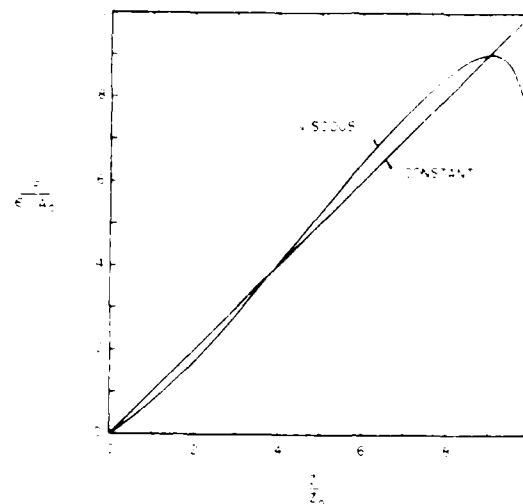


Figure 7. Force Versus Penetration

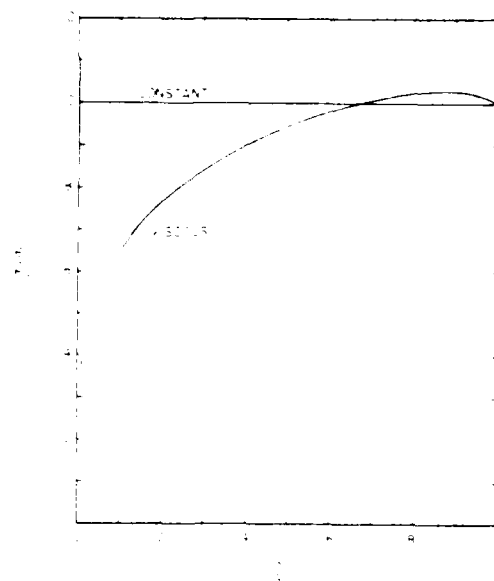


Figure 8. Specific Energy Versus Penetration

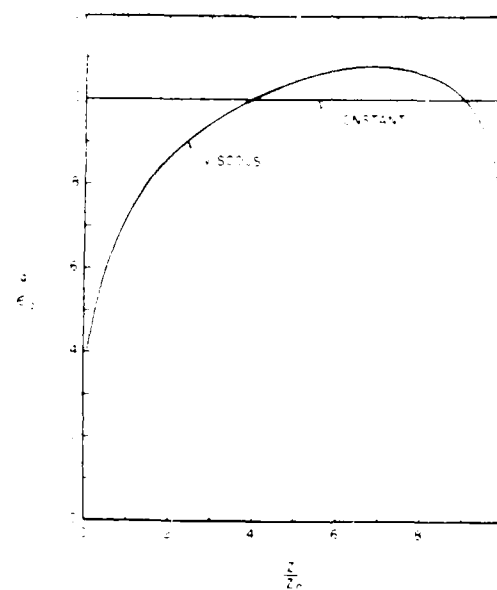


Figure 9. Nominal Pressure Versus Penetration

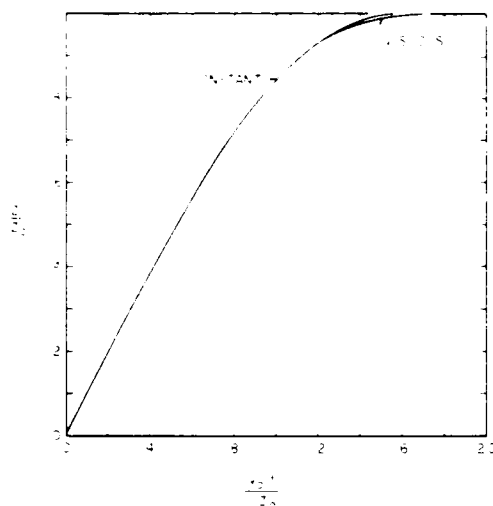


Figure 10. Penetration Versus Time

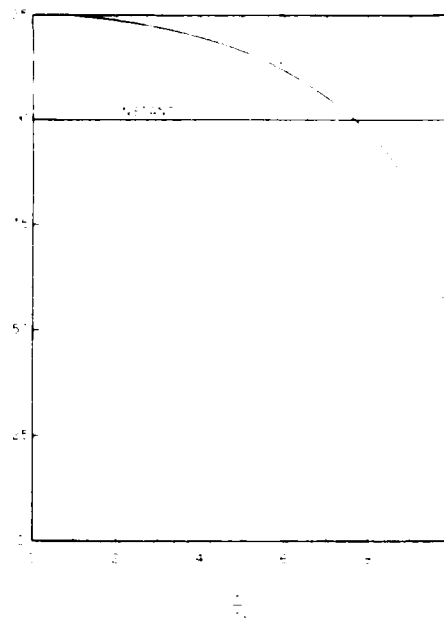


Figure 11. Pressure Versus Contact Radius

ANALYSIS OF AN ICEBERG IMPACTING A STRUCTURE

The dynamics of an iceberg impacting a structure must be analyzed in order to calculate the interaction force. The motions, whether rigid or deformable, of all elements should be considered, but motions that are small are usually neglected in order to simplify the problem.

The simplest analysis only considers the crushing of the ice and the linear motion of the iceberg. In addition, the iceberg's deformation[35], the iceberg's rotation[4,42], the rigid body motion of the structure[11,20,40], the deformation of the structure[40], and the deformation of the soil[11,20,40] have been considered. The water forces are included through added mass factors, and sometimes through damping factors, which are applied to the iceberg and structure. For impacts whose contact surfaces are not perpendicular to the direction of motion, the possibility of the iceberg sliding along the surface should be considered.

The equations of motion for each body are used along with the initial conditions. The boundary conditions at the contact is specified in terms of the brittle crushing strength and possible iceberg sliding. The resulting nonlinear equations of motion are solved numerically by time stepping from the initial condition. A predictor-corrector method[1] is recommended for the time stepping process. The resulting interaction force depends upon the deformations and motions which make the impact more compliant. Depending upon the problem being solved, the equations can be simplified by neglecting many of the deformations and motions.

The equation of motion can be expressed in the alternate form of either impulse-momentum or energy. The impulse-momentum method has not been used for iceberg impacts, but the

energy approach has been used in References 8, 9, 21, and 38. In this method, the initial kinetic energy of the iceberg is transferred to various forms during the impact. For a fixed structure, most of the energy will go into the work of crushing the ice. If the iceberg hits eccentrically with respect to the structure, some of the energy may remain in the iceberg as rotational kinetic energy.

Both horizontal and vertical eccentric hits could occur. For icebergs, the moment arm for horizontal eccentric hits will probably be larger than those for vertical eccentric hits. Bass et al. [4] show that the iceberg shape at the contact and the horizontal eccentricity influence the interaction force significantly. Therefore, a simple approach will be developed to estimate the rotational kinetic energy remaining in an iceberg that hits with a horizontal eccentricity.

Consider an iceberg of mass M and velocity V hitting a structure with a horizontal eccentricity y_0 as shown in Figure 12. The equations for planar motion are

$$F_x = M_x \ddot{x} \quad (35a)$$

$$F_y = M_y \ddot{y} \quad (35b)$$

$$F_y y_0 - F_x x_0 = I \ddot{\theta} \quad (35c)$$

where M_x is the mass including the added mass in the x direction, M_y is the mass including the added mass in the y direction, I is the polar moment of inertia including the added inertia about the center of gravity of the iceberg, and $\ddot{\theta}$ denotes the derivative with respect to time. Substituting Equations (35a) and (35b) into (35c), we obtain

$$M_x x y_0 \ddot{\theta} - M_y y x_0 \ddot{\theta} = I \ddot{\theta} \quad (36)$$

The initial conditions at time t equal zero are $x = Vt$, $y = 0$, and $\theta = 0$. We assume that x_0 and y_0 are constant for small rotation and integrate Equation (36) to obtain

$$M_x (x - vt) y_0 - M_y y x_0 = I \theta \quad (37)$$

We assume that the iceberg rotates through a small angle θ around the hit point and therefore

$$x = \theta y_0 \quad (38a)$$

$$y = \theta x_0 \quad (38b)$$

Substituting Equation (38) into Equation (37) and solving for θ , we obtain

$$\theta = \frac{M_x V y_0}{I + M_x y_0^2 + M_y x_0^2} \quad (39)$$

The rotational kinetic energy E_r of the berg is

$$E_i = \frac{1}{2} M_x (\dot{x})^2 + \frac{1}{2} M_y (\dot{y})^2 + \frac{1}{2} I (\dot{\theta})^2 \quad (40)$$

Substituting Equations (38) and (39) into Equation (40), we obtain the kinetic energy of the iceberg as

$$E_i = \frac{(M_x V y_o)^2}{2 (I + M_x y_o^2 + M_y x_o^2)} \quad (41)$$

If we assume that $M_x = M_y$, then Equation (41) can be expressed as

$$E_i = \frac{M_x V^2}{2} \left[\frac{(y_o/r)^2}{1 + (r_o/r)^2} \right] \quad (42)$$

where $r_o = I/M_x$ and $r^2 = x_o^2 + y_o^2$.

The work done on the structure in crushing and sliding the iceberg is

$$\int F ds + \int T dt \quad (43)$$

where F and T are the normal and tangential forces to the structure, and ds and dt are the normal and tangential incremental displacements. We assume that the slippage displacement $dt = \tan\beta ds$ where β is the structure angle as defined in Figure 12, and the tangential force $T = \mu N$ where μ is the coefficient of friction. Using $F = \sigma A$, Equation (43) becomes

$$(1 + \mu \tan\beta) \sigma Vol \quad (44)$$

where Vol is the volume of crushed ice.

Equating the initial kinetic energy of the iceberg to the work done on the structure and the remaining rotational energy, we have

$$\frac{M_x V^2}{2} = \frac{M_x V^2}{2} \left(\frac{(y_o/r)^2}{1 + (r_o/r)^2} \right) + (1 + \mu \tan\beta) \sigma Vol \quad (45)$$

Equation (45) is solved for the volume of crushed ice. Depending upon the local shape of the structure and iceberg at the contact point, the penetration distance x and contact area A can be found. The local shape can significantly influence the final contact area A and, hence, the force. The force is then determined from $F = \sigma A$.

For an iceberg of spherical shape, $r_o^2/r^2 = 2/5$, and with the maximum eccentricity of $y_o = r$, the energy remaining with the iceberg is 71 percent of the original energy.

STATISTICAL ANALYSIS

The impact force of an iceberg against a structure can be calculated from Equation (45) or from other equations derived from the methods outlined. The engineer must choose the parameters required for design. For Equation (45), these parameters are the iceberg's mass, moment of inertia, initial velocity, eccentricity, strength, and local contact geometry of the structure and the iceberg. The draft of the iceberg is also important since it will limit the size of icebergs that occur in shallow water. The effect of the force on the structure must be evaluated globally for sliding, overturning, and torsion, and locally for wall thickness and framing. Each of the iceberg parameters has a wide range of values. If the engineer selects the extreme for each parameter, the calculated force will be overly conservative. A rational approach is to define the probability of exceedance for each parameter. Then the probability of exceedance for the force can be calculated using these input exceedance distributions. The method used for this calculation is numerical. For each input distribution, a random number between 0 and 1 is generated. This means that any number between 0 and 1 has an equal chance of being chosen. This number is set equal to the probability of exceedance, and the input parameter is determined. This is a valid procedure because the probability of exceedance curves are usually developed with data that are assigned equal probabilities.

After choosing a set of input parameters, a force can be calculated. The process of randomly selecting input parameters is repeated many times, and a force is calculated for each set of input parameters. From these forces a probability of exceedance curve is constructed. An example of a force exceedance curve for a single impact is given in Figure 13[38].

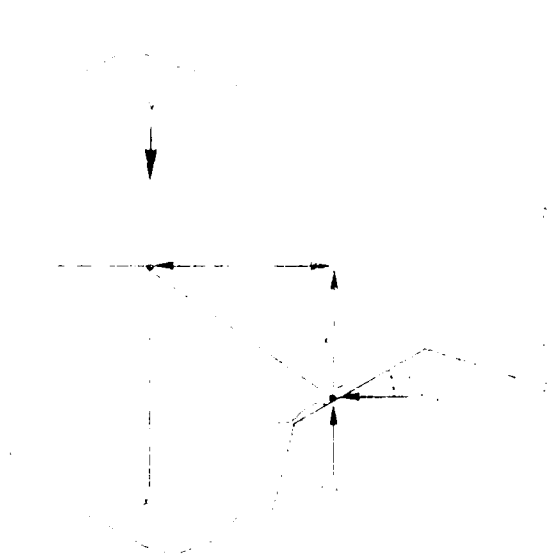


Figure 12. Horizontal Eccentric Hit Geometry

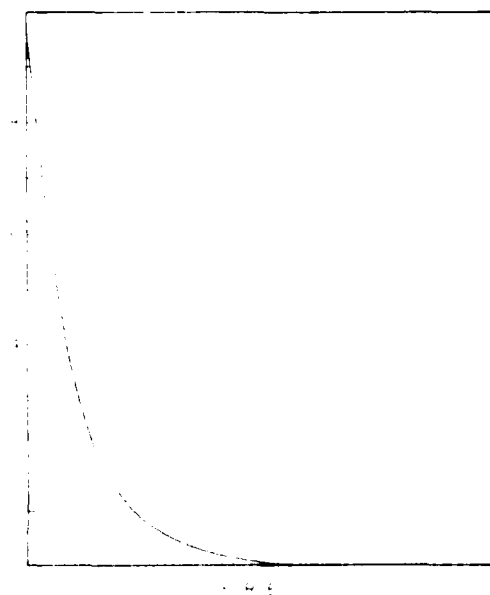


Figure 13. Probability of Exceedance Versus Force

This numerical method is called Monte Carlo distribution sampling. It has been assumed that the input parameter distributions are independent of each other. A modification of this procedure should be used when the input distributions are correlated. There is very little data on iceberg mass and velocity in the literature. There is no data on moment of inertia and local geometry. Benedict and Lewis[5] state that the gamma distribution is valid for iceberg drafts but no data is given. It is known that the oil companies who operate offshore along eastern Canada have been collecting data to calculate the iceberg impact force statistically, but their data is proprietary.

DESIGN CRITERIA

Having established the probability of exceeding the force for an iceberg impacting an offshore structure, we must now choose a reasonable design criteria. Traditionally, design criteria have been selected based upon a return period. The return period is defined as the expected time between obtaining or exceeding the design level. It is equal to the expected number of events to obtain the first exceedance multiplied by the expected time interval between events.

The probability that the first exceedance of the design level occurs on the first, second, third, or nth event is

$$\text{for } n = 1, p \quad (46a)$$

$$\text{for } n = 2, p (1 - p) \quad (46b)$$

$$\text{for } n = 3, p (1 - p)^2 \quad (46c)$$

$$\text{for } n = n, p (1 - p)^{n-1} \quad (46d)$$

The expected or average number of events that will occur before the first exceedance is

$$\sum_{n=1}^{\infty} n p (1 - p)^{n-1} = \frac{1}{p} \quad (47)$$

Hence the return period RP is

$$R P = \frac{1}{p} \Delta T \quad (48)$$

where ΔT is the expected time between events.

A number of references[14,19,36,37,44] have considered the frequency of occurrence of icebergs. In many cases, data from the International Ice Patrol are used. From this data the

average number of iceberg hits per year or its reciprocal, the average time interval between hits must be estimated in order to calculate the return period.

The probability of obtaining n hits in time t can be estimated from Poisson's distribution by

$$p(n|\lambda t) = \frac{(\lambda t)^n e^{-\lambda t}}{n!} \quad (49)$$

where λ is the average rate of hits. Although the probability of receiving n hits in a given time is interesting, more important is the probability of exceeding the force in a given time. This is given by

$$p(F > F_0 | \lambda t) = 1 - (1 - p)^{\lambda t} \quad (50)$$

where p is the probability of exceeding the force F_0 for a single hit.

The selection of the return period has been traditionally accepted as a design criteria in many fields. The specific value has been arbitrary and in some cases adjusted with experience. In principle, it should be some multiple of the expected life of the structure. An alternate design criteria to the return period is Equation (50), the probability of exceeding the force in a given time period. Some structural engineers are uncomfortable with a design force that is not related to a specific event. Dunwoody[13] discusses design events obtained from a return period force.

CONCLUSIONS AND RECOMMENDATIONS

The reason for the size effect on impact ice strength is understood from laboratory and field tests, but reliable strength values are not available in the open literature. The drop ball test was analyzed using both the constant strength and the viscous theory, and the comparison showed little difference. The energy remaining in the iceberg due to its rotation can be calculated without time stepping the dynamic equations of motion. The analytical method for calculating the ice impact force, including its statistical treatment, is known. The required statistical iceberg data of impact velocity, mass, moment of inertia, strength, shape at contact, and expected time between impacts are not available in the open literature. In order to reliably predict impact forces, it is recommended that the following statistical data for icebergs be collected for the location desired: mass, moment of inertia, draft, velocity, local geometry, strength, and frequency of occurrence.

REFERENCES

1. Acton, F., *Numerical Methods That Work*, Harper and Row, 1970.
2. Afanasiev, V., Y. Dolgoplov, L. Shmeleva, N. Khrapaty, and V. Tsuprik, Effect of ice impact forces on the supports of structures in estuaries and shelf zones, International Association of Hydraulic Research Ice Symposium, Luleå, Sweden, 1978, pp. 453-464.
3. Ashby, M., A. Palmer, M. Thouless, D. Goodman, M. Howard, S. Hallam, S. Murrell, N. Jones, T. Sanderson, and A. Ponter, Nonsimultaneous failure and ice loads on Arctic structures, Offshore Technology Conference, 1986, Proceedings Vol. I, pp. 399-404.
4. Bass, D., H. Gaskill, and N. Riggs, Analysis of iceberg impacts with gravity base structures at Hibernia, Fourth International Offshore Mechanics and Arctic Engineering Symposium, Dallas, 1985, Vol. II, pp. 255-259.
5. Benedict, P., and J. Lewis, Iceberg incursion probabilities into subsea structures, Seventh International Conference on Port and Ocean Engineering Under Arctic Conditions, Helsinki, 1983, Vol. I, pp. 273-279.
6. Benoit, J., et al., Medium scale iceberg impact tests, videotape showed at Arctic Offshore Technology Conference, November 1984, Calgary.
7. Butkovich, T., Some physical properties of ice from the TUTO tunnel and ramp, Thule, Greenland, U.S. Army Snow Ice Permafrost Research Establishment RR47, 1959.
8. Cammaert, A., and G. Tsinker, Impact of large ice floes and icebergs on marine structures, The Sixth International Conference on Port and Ocean Engineering Under Arctic Conditions, 1981, Quebec City, Vol. II, pp. 653-662.
9. Cammaert, A., T. Wong, and D. Curtis, Impact of icebergs on offshore gravity and floating platforms, The Seventh International Conference on Port and Ocean Engineering Under Arctic Conditions, 1983, Helsinki, pp. 519-536.
10. Corneau, A., I. Jordan, M. Nessim, and M. Tomin, Ice-structure interaction: a fundamental energy-based approach, International Association of Hydraulic Research Ice Symposium, 1984, Hamburg, Vol. III, pp. 161-174.
11. Croteau, P., M. Rojansky, and B. Gerwick, Summer ice floe impacts against caisson-type exploratory and production platforms, Third International Offshore Mechanics and Arctic Engineering Symposium, New Orleans, 1984, Vol. III, pp. 228-237.
12. Diemand, D., Iceberg temperatures in the North Atlantic — theoretical and measured, Cold Regions Science and Technology, 9 (1984), pp. 171-178.

13. Dunwoody, B., Utilizing design events within risk-based design, *Civil Engineering in the Arctic Offshore*, Proceedings, 1985, pp. 395-402.
14. Ebbesmeyer, C., A. Okubo, and J. Helseth, Description of iceberg probability between Baffin Bay and the Grand Banks using a stochastic model, *Deep-Sea Research*, Vol. 27A, 1980, pp. 975-986.
15. El-Tahan, H., A. Swamidas, and M. Arockiasamy, Impact strength of iceberg and artificial snow ice, *Canadian Coastal Conference*, St. John's, 1985, pp. 365-380.
16. El-Tahan, H., A. Swamidas, M. Arockiasamy, and D. Reddy, Strength of iceberg and artificial snow ice under high strain rates and impact loads, *Third International Symposium on Offshore Mechanics and Arctic Engineering*, New Orleans, 1984, Vol. III, pp. 158-165.
17. Gammon, P., R. Gagnon, W. Bobby, and W. Russell, Physical and mechanical properties of icebergs, *Offshore Technology Conference*, 1983, pp. 143-150.
18. Glen, I., and G. Comfort, Ice impact pressure and load: investigation by laboratory experiments and ship trials, *Seventh International Conference on Port and Ocean Engineering Under Arctic Conditions*, Helsinki, 1983, Vol. I, pp. 516-533.
19. Gustajtis, K. A., Iceberg population distribution study in the Labrador Sea, *C-CORE Report 79-8*, July 1979.
20. Guttman, S., F. Puskar, and R. Bea, Analysis of offshore structures subject to Arctic ice impacts, *Third International Offshore Mechanics and Arctic Engineering Symposium*, New Orleans, 1984, Vol. III, pp. 238-245.
21. Johnson, R., and D. Nevel, Ice impact structural design loads, *Eighth International Conference on Port and Ocean Engineering Under Arctic Conditions*, Greenland, 1985.
22. Kheisin, D. E., and N. V. Cherepanov, *Izmenenie struktury l'da v zone udara tverdogo tela o proverkhnost' ledianogo pokrova*, *Problemy Arktiki i Antarktiki*, Vol. 34, pp. 71-87, 1970. For English translation, see *Change of Ice structure in the zone of impact of a solid body against the ice cover surface*, *Israeli Program for Scientific Translations*, Jerusalem, pp. 239-245, 1973.
23. Kheisin, D. E., and V. A. Likhomanov, *Eksperimental'noe opredelenie udel'noi energii mekhanicheskogo dropleniia l'da pri udare*, *Problemy Arktiki i Antarktiki*, Vol. 41, pp. 55-61, 1973. For English translation, see *Experimental determination of the specific energy of mechanical crushing of ice by impact*, *Problems of the Arctic and Antarctic*, collection of articles Vol. 41, pp. 69-77, 1975.

24. Kheisin, D. E., V. A. Likhomanov, and V. A. Kurdyumov. Opredelenie udelnoi energii razrusheniia i kontaktnykh davlenii pri udare tverdogo tela o led. Arkticheskii i Antarkticheskii nauchno-issledovatel'skii institut. Trudy, Vol. 326, pp. 210-218, 1975. For English translation, see Determination of specific breakup energy and contact pressures produced by the impact of a solid against ice. U.S. Army Cold Regions Research and Engineering Laboratory, TL 539, August 1976.
25. Khrapaty, N., and A. Berezovskii. Laws governing the penetration of a solid body into ice at supercritical impact velocities (Zakonomernosti vnedreniia tverdogo tela v led pri sverkhkriticheskikh skorostiakh soudareniia). Gornyi zhurnal 1980, No. 2, pp. 5-9.
26. Khrapaty, N., and V. Tsuprik. Experimental Study of the Impact of a solid body against ice (Eksperimental'noe issledovanie udara tverdogo tela o led). Trudy koordinatsionnykh soveshchanii po, Gidrotekhnike, vyp. III, Leningrad, Energia, pp. 166-169.
27. Khrapaty, N., and V. Tsuprik. Calculation of the force of impact of ice floes against separate supports (Raschet sily udara i din ob otdel'nuiu oporu). Leningrad Politekhicheskii Institut. Trudy, 1978, No. 361, pp. 81-85.
28. Khrushchov, M., and Y. Berkovich. A study of the hardness of ice. U.S. Army Cold Regions Research and Engineering Laboratory, Technical Translation TL 74, 1970.
29. Kitami, E., K. Fujishima, Y. Taguchi, T. Nawata, T. Kawasaki, and F. Sakai. Iceberg collision with semi-submersible drilling unit. International Association of Hydraulic Research Ice Symposium, 1984, Hamburg, Vol. II, pp. 45-53.
30. Kovacs, A., W. Weeks, and F. Michitti. Variation of some mechanical properties of polar snow, Camp Century, Greenland. U.S. Army Cold Regions Research and Engineering Laboratory, RR 276, 1969.
31. Kurdyumov, V., and D. Kheisin. Hydrodynamic model of solid ice impact (Gidrodinamicheskaya model' udara tverdogo tela o led). Prikladnaya Mekhanika, Tom XII, No. 10, 1976.
32. Lavrov, V., Deformation and strength of ice. Israel Program for Scientific Translations, Jerusalem, 1971.
33. Likhomanov, V. A., and D. E. Kheisin. Eksperimental'noe issledovanie udara tverdogo tela o led. Problemy Arktiki i Antarktiki, Vol. 38, pp. 105-111, 1971. For English translation, see Experimental investigation of solid body impact on ice. Problems of the Arctic and Antarctic, Collection of articles, Vol. 38, Edited by A. F. Treshnikov. New Delhi, American Publishing Co. Pvt. Ltd., pp. 128-136, 1973.

34. Maes, M., and I. Jordaan. Probabilistic analysis of iceberg loads in offshore structures. International Association of Hydraulic Research Ice Symposium, 1984, Hamburg. Vol. II, pp. 175-188.
35. Mansour, A., and A. Seireg. A computer-based simulation of ice-breaking by impact. Second International Symposium on Offshore Mechanics and Arctic Engineering, Houston, 1983, pp. 729-734.
36. Miller, J. D., An assessment of iceberg recurrence intervals in the Grand Banks. First International Symposium on Offshore Mechanics and Arctic Engineering, Houston, 1982, pp. 237-242.
37. Miller, J., and S. Hotzel. Iceberg flux estimation in the Labrador Sea. Third International Offshore Mechanics and Arctic Engineering Symposium, New Orleans, 1984. Vol. III pp. 298-304.
38. Nevel, D., Design ice forces for offshore structures, Ninth International Ship Structures Congress, Geneva, 1985.
39. Pounder, E., and E. Little. Some physical properties of sea ice. Canadian Journal of Physics, Vol. 37, 1959, pp. 443-473.
40. Powell, G., V. Schricker, D. Row, J. Hollings, and R. Sause. Ice-structure interaction of an offshore platform. Civil Engineering in the Arctic Offshore, pp. 230-238, ASCE, 1985.
41. Riska, K., On the role of failure criterion of ice in determining ice loads. Technical Research Centre of Finland, Ship Laboratory Report 7, March 1980.
42. Salvalaggio, M., M. Rojansky, and B. Gerwick. The importance of wave-driven icebergs impacting on offshore structure. Offshore Technology Conference, 1986. Vol. I, pp. 29-38.
43. Slomski, S., and V. Vivatrat. Selection of design ice pressures and application to impact load prediction. Seventh International Conference on Port and Ocean Engineering Under Arctic Conditions, Helsinki, 1983, Vol. II, pp. 909-919.
44. Sutton, J., and D. Mudry. Iceberg distributions in the Labrador sea from SLAR imagery, 1978 to 1980. Seventh International Conference on Port and Ocean Engineering Under Arctic Conditions, Helsinki, 1983, Vol. III, pp. 214-221.
45. Timco, G., and R. Martin. Impact strength tests on Ottawa river ice. National Research Council Canada, Report LTR-LT-97, April 1979.

- 46 Tsurikov, V., and L. Veselova. Dynamic hardness of ice in the Caspian Sea (O dinamicheskoi tverdsti l'da kashniskogo morya). Issledovaniya l'dov yuzhnykh morei SSSR Moscow, Nauka, 1973, pp. 68-81.
- 47 Yen, Y., F. Odar, and L. Bracy. Impact of spheres on ice. American Society of Civil Engineers, Engineering Mechanics Division, October 1970, pp. 641-652.

END

DATE

FILMED

5-88

DTIC